



Gregory, Joseph William (2019) *The selective hydrogenation of alkynyl-substituted aromatic molecules over rhodium/silica*. MSc(R) thesis.

<https://theses.gla.ac.uk/75124/>

Copyright and moral rights for this work are retained by the author

A copy can be downloaded for personal non-commercial research or study, without prior permission or charge

This work cannot be reproduced or quoted extensively from without first obtaining permission in writing from the author

The content must not be changed in any way or sold commercially in any format or medium without the formal permission of the author

When referring to this work, full bibliographic details including the author, title, awarding institution and date of the thesis must be given

Enlighten: Theses

<https://theses.gla.ac.uk/>  
[research-enlighten@glasgow.ac.uk](mailto:research-enlighten@glasgow.ac.uk)



**The Selective Hydrogenation of  
Alkynyl-Substituted Aromatic Molecules  
Over Rhodium/Silica**

**Joseph William Gregory**

**BA (Hons)**

**Thesis submitted for the degree of MSc**

**School of Chemistry**

**College of Science and Engineering**

**University of Glasgow**

**July 2019**

## Abstract

Kinetic studies involving phenylacetylene and 1-phenyl-1-propyne hydrogenation cascades over 2.5% w/w rhodium/silica were carried out to assess aspects of selectivity and catalytic behaviour. The reactions were performed over the temperature range 313 K – 343 K in the liquid phase using 2-propanol (IPA) as a solvent. Typically 0.1g of catalyst was used with 3 barg hydrogen pressure and 10 mmol of aromatic in a stirred tank reactor. Rate constants and activation energies for phenylacetylene, ethylbenzene, 1-phenyl-1-propyne and propylbenzene hydrogenation were calculated and, for molecules with analogous functionality, were found to increase with a decrease in the mass of the substituent.

For the hydrogenation of 1-phenyl-1-propyne, the *cis/trans* ratio of  $\beta$ -methylstyrene was calculated and a kinetic isotope effect observed. The *cis/trans* ratio was typically at its greatest in the initial stages of the reaction and decreased with time. Increasing the temperature increased the *cis/trans* ratio, however this trend was reversed at higher temperatures, suggesting that there was a change in reaction pathway and meaning that the nature of the reaction was temperature-dependent.

Competitive hydrogenation was carried out which showed that, in some instances, aromatic molecules with larger substituents can completely outcompete molecules with smaller substituents. This effect was reflected in an increased selectivity for alkylarenes with shorter-chain substituents when related alkylarenes with longer-chain substituents were present, for example the presence of propylbenzene in a reaction mixture improved ethylbenzene selectivity.

Styrene selectivity during the hydrogenation cascade of phenylacetylene was monitored and found to be largely unaffected by altering the temperature and by changing the reactive hydrogen isotope, however an enhancement was made possible by competition with ethylbenzene and 1-phenyl-1-propyne.

The majority of unsaturated functional groups assessed in this study appeared to undergo hydrogenation at the same active site of the catalyst, however kinetic results suggested the terminal alkyne group of phenylacetylene reacted at a different site. These kinetic results also provided evidence that subsurface hydrogen was the active hydrogen species in some of the hydrogenation processes observed. The findings of

this study have further developed our understanding of the hydrogenation of alkynylaromatics.

## Table of Contents

<b>1</b>	<b>Introduction</b> .....	<b>1</b>
1.1	Chemisorption .....	2
1.2	The Hydrogenation of Double and Triple Bonds .....	5
1.3	The Hydrogenation of Aromatic Rings and Associated Exchange Mechanisms .....	13
1.4	Kinetic Isotope Effect .....	18
<b>2</b>	<b>Aims of the Project</b> .....	<b>22</b>
<b>3</b>	<b>Experimental</b> .....	<b>24</b>
3.1	Instrumentation .....	24
3.1.1	Stirred Tank Reactor .....	24
3.1.2	NMR .....	26
3.1.3	Thermo-Gravimetric Analysis (TGA) .....	26
3.1.4	Gas Chromatography .....	26
3.2	Chemicals .....	28
3.2.1	Styrene .....	29
3.2.2	Catalyst .....	30
3.3	Method .....	31
3.4	Reactions .....	32
3.4.1	Mass Transfer Limitation Analysis .....	32
3.4.2	Analysis of Temperature Dependence .....	32
3.4.3	Reactions with Deuterium and Determination of Kinetic Isotope Effect .....	33

3.4.4	Competitive Reactions .....	34
<b>4</b>	<b>Results .....</b>	<b>35</b>
4.1	Reactions.....	35
4.1.1	Mass Transfer Limitation Analysis.....	35
4.1.2	Temperature Dependence.....	40
4.1.3	Reactions with Deuterium .....	69
4.1.4	Competitive Reactions .....	105
4.2	TGA .....	127
<b>5</b>	<b>Discussion.....</b>	<b>141</b>
5.1	Reactions.....	141
5.1.1	Mass Transfer Limitation.....	141
5.1.2	Temperature Dependence.....	142
5.1.3	Reactions with Deuterium .....	148
5.1.4	Competitive Reactions .....	162
5.2	TGA .....	178
<b>6</b>	<b>Conclusions .....</b>	<b>180</b>
<b>7</b>	<b>Further Work .....</b>	<b>181</b>
<b>8</b>	<b>References .....</b>	<b>182</b>

## List of Tables

Table 1 – The conversion factors and $R^2$ values for the standards in the Focus GC which was used for the duration of the project.....	28
The chemicals used are detailed in Table 2; there were no further purification steps. ....	28
Table 3 – The name, supplier and purity of all chemicals, other than those mentioned in the remainder of Section 3.4, used in the experiments which contributed to this thesis.....	29
Table 4 – A table of properties of the rhodium/silica catalyst used for all experiments which contributed to this thesis. ....	31
Table 5 – The initial rate constants of hydrogen consumption in the hydrogenation of phenylacetylene at different stirrer speeds. ....	39
Table 6 – Phenylacetylene temperature dependence. It was observed that the time taken to reach 100% conversion decreased and the initial rate constant increased with increasing temperature. ....	45
Table 7 – Ethylbenzene temperature dependence with styrene as the reactant. It was observed that the initial rate constant increased with temperature. ....	51
Table 8 – Ethylbenzene temperature dependence. It was observed that the conversion after 180 minutes and the initial rate constant increased with increasing temperature. ....	56
Table 9 – 1-Phenyl-1-propyne temperature dependence. It was observed that the time taken to reach 100% conversion decreased and the initial rate constant increased with increasing temperature. ....	63
Table 10 – Propylbenzene temperature dependence. It was observed that the conversion after 180 minutes and the initial rate constant increased with increasing temperature.....	68
Table 11 – Relative intensities, normalised relative to the smallest peak, of each significant peak in the $^2\text{H}$ NMR spectrum of a sample taken after 10 minutes of phenylacetylene deuteration at $50^\circ\text{C}$ .....	72
Table 12 – Relative intensities, normalised relative to the smallest peak, of each significant peak in the $^2\text{H}$ NMR spectrum of a sample taken after 40 minutes of phenylacetylene deuteration at $50^\circ\text{C}$ .....	73

Table 13 – Relative intensities, normalised relative to the smallest peak, of each significant peak in the $^2\text{H}$ NMR spectrum of a sample taken after 180 minutes of phenylacetylene deuteration at $50^\circ\text{C}$ .....	74
Table 14 – Relative intensities, normalised relative to the smallest peak, of each significant peak in the $^2\text{H}$ NMR spectrum of a sample taken after 10 minutes of phenylacetylene deuteration at $70^\circ\text{C}$ .....	76
Table 15 – Relative intensities, normalised relative to the smallest peak, of each significant peak in the $^2\text{H}$ NMR spectrum of a sample taken after 40 minutes of phenylacetylene deuteration at $70^\circ\text{C}$ .....	78
Table 16 – Relative intensities, normalised relative to the smallest peak, of each significant peak in the $^2\text{H}$ NMR spectrum of a sample taken after 180 minutes of phenylacetylene deuteration at $70^\circ\text{C}$ .....	79
Table 17 – The effect of changing the hydrogen isotope on the hydrogenation of phenylacetylene. At both $50^\circ\text{C}$ and $70^\circ\text{C}$ , $k\text{H}$ is greater than $k\text{D}$ .....	80
Table 18 – Relative intensities, normalised relative to the smallest peak, of each significant peak in the $^2\text{H}$ NMR spectrum of a sample taken after 10 minutes of styrene deuteration at $50^\circ\text{C}$ .....	82
Table 19 – Relative intensities, normalised relative to the smallest peak, of each significant peak in the $^2\text{H}$ NMR spectrum of a sample taken after 40 minutes of styrene deuteration at $50^\circ\text{C}$ .....	83
Table 20 – Relative intensities, normalised relative to the smallest peak, of each significant peak in the $^2\text{H}$ NMR spectrum of a sample taken after 180 minutes of styrene deuteration at $50^\circ\text{C}$ .....	85
Table 21 – Relative intensities, normalised relative to the smallest peak, of each significant peak in the $^2\text{H}$ NMR spectrum of a sample taken after 10 minutes of styrene deuteration at $70^\circ\text{C}$ .....	86
Table 22 – Relative intensities, normalised relative to the smallest peak, of each significant peak in the $^2\text{H}$ NMR spectrum of a sample taken after 40 minutes of styrene deuteration at $70^\circ\text{C}$ .....	88
Table 23 – Relative intensities, normalised relative to the smallest peak, of each significant peak in the $^2\text{H}$ NMR spectrum of a sample taken after 180 minutes of styrene deuteration at $70^\circ\text{C}$ .....	90

Table 24 – Relative intensities, normalised relative to the smallest peak, of each significant peak in the $^2\text{H}$ NMR spectrum of a sample taken after 10 minutes of 1-phenyl-1-propyne deuteration at $50^\circ\text{C}$ . .....	93
Table 25 – Relative intensities, normalised relative to the smallest peak, of each significant peak in the $^2\text{H}$ NMR spectrum of a sample taken after 40 minutes of 1-phenyl-1-propyne deuteration at $50^\circ\text{C}$ . .....	95
Table 26 – Relative intensities, normalised relative to the smallest peak, of each significant peak in the $^2\text{H}$ NMR spectrum of a sample taken after 180 minutes of 1-phenyl-1-propyne deuteration at $50^\circ\text{C}$ . .....	97
Table 27 – Relative intensities, normalised relative to the smallest peak, of each significant peak in the $^2\text{H}$ NMR spectrum of a sample taken after 10 minutes of 1-phenyl-1-propyne deuteration at $70^\circ\text{C}$ . .....	100
Table 28 – Relative intensities, normalised relative to the smallest peak, of each significant peak in the $^2\text{H}$ NMR spectrum of a sample taken after 40 minutes of 1-phenyl-1-propyne deuteration at $70^\circ\text{C}$ . .....	102
Table 29 – Relative intensities, normalised relative to the smallest peak, of each significant peak in the $^2\text{H}$ NMR spectrum of a sample taken after 180 minutes of 1-phenyl-1-propyne deuteration at $70^\circ\text{C}$ . .....	104
Table 30 – The effect of changing the hydrogen isotope on the hydrogenation of 1-phenyl-1-propyne. At $50^\circ\text{C}$ , $k\text{H}$ and $k\text{D}$ were found to be very similar, but at $70^\circ\text{C}$ , $k\text{H}$ was observed to be greater than $k\text{D}$ . .....	104
Table 31 – Relative intensities, normalised relative to the smallest peak, of each significant peak in the $^2\text{H}$ NMR spectrum of a sample taken after 10 minutes of competitive hydrogenation involving toluene- $\text{d}_8$ and phenylacetylene at $50^\circ\text{C}$ . .....	107
Table 32 – Relative intensities, normalised relative to the smallest peak, of each significant peak in the $^2\text{H}$ NMR spectrum of a sample taken after 40 minutes of competitive hydrogenation involving toluene- $\text{d}_8$ and phenylacetylene at $50^\circ\text{C}$ . .....	108
Table 33 – Relative intensities, normalised relative to the smallest peak, of each significant peak in the $^2\text{H}$ NMR spectrum of a sample taken after 180 minutes of competitive hydrogenation involving toluene- $\text{d}_8$ and phenylacetylene at $50^\circ\text{C}$ . .....	109
Table 34 – Relative intensities, normalised relative to the smallest peak, of each significant peak in the $^2\text{H}$ NMR spectrum of a sample taken after 10 minutes of competitive hydrogenation involving toluene- $\text{d}_8$ and 1-phenyl-1-propyne at $50^\circ\text{C}$ . .....	111

Table 35 – Relative intensities, normalised relative to the smallest peak, of each significant peak in the $^2\text{H}$ NMR spectrum of a sample taken after 40 minutes of competitive hydrogenation involving toluene- $\text{d}_8$ and 1-phenyl-1-propyne at $50^\circ\text{C}$ .	112
Table 36 – Relative intensities, normalised relative to the smallest peak, of each significant peak in the $^2\text{H}$ NMR spectrum of a sample taken after 180 minutes of competitive hydrogenation involving toluene- $\text{d}_8$ and 1-phenyl-1-propyne at $50^\circ\text{C}$ .	113
Table 37 – The effect of competition with toluene- $\text{d}_8$ on the initial rate constant of hydrogenation of phenylacetylene and 1-phenyl-1-propyne. For phenylacetylene, the initial rate constant decreased with toluene- $\text{d}_8$ competition, whereas in the case of 1-phenyl-1-propyne, an increase in initial rate constant was observed. ....	114
Table 38 – A comparison of the initial rate constants of hydrogenation of phenylacetylene with no competition, in competition with ethylbenzene, and in competition with 1-phenyl-1-propyne. ....	126
Table 39 – A comparison of the initial rate constants of hydrogenation of 1-phenyl-1-propyne with no competition, in competition with propylbenzene, and in competition with phenylacetylene. ....	126
Table 40 – Calculated activation energies. The column labelled ‘EB (STY)’ denotes the activation energy of ethylbenzene hydrogenation when styrene was the initial reactant. ....	143
Table 41 – A comparison of the relative intensities, normalised relative to the smallest peak, of each significant peak in the $^2\text{H}$ NMR spectrum of a sample taken after 10, 40 and 180 minutes of phenylacetylene deuteration at $50^\circ\text{C}$ and $70^\circ\text{C}$ . ....	159
Table 42 – A comparison of the relative intensities, normalised relative to the smallest peak, of each significant peak in the $^2\text{H}$ NMR spectrum of a sample taken after 10, 40 and 180 minutes of styrene deuteration at $50^\circ\text{C}$ and $70^\circ\text{C}$ . ....	160
Table 43 – A comparison of the relative intensities, normalised relative to the smallest peak, of each significant peak in the $^2\text{H}$ NMR spectrum of a sample taken after 10, 40 and 180 minutes of 1-phenyl-1-propyne deuteration at $50^\circ\text{C}$ and $70^\circ\text{C}$ . The first value for the shift is that given for the spectra of samples taken at $50^\circ\text{C}$ and the second value for the shift is that given for the spectra of samples taken at $70^\circ\text{C}$ . ....	161
Table 44 – A comparison of the relative ion current peaks, normalised relative to the smallest peak in the spectrum, caused by carbon dioxide release from post-reaction catalysts. ....	179

## List of Figures

Figure 1 – Lennard-Jones diagram showing physical adsorption ( $E_p$ ) and chemisorption ( $E_q$ ) <sup>11</sup> . ‘EA’ is the activation energy for the formation of the chemisorbed state.....	3
Figure 2 – Diagrams of chemisorbed hydrocarbons. S represents the surface.....	4
Figure 3 – Horiuti and Polanyi’s mechanism for the behaviour of associatively adsorbed alkenes <sup>13</sup> . ....	7
Figure 4 – The reaction pathway of ethyne adsorbed on a palladium catalyst, according to Margitfalvi et al. <sup>23</sup> . S represents the surface. ....	9
Figure 5 – A diagram showing the positions of surface hydrogen and subsurface hydrogen on a catalytic particle, courtesy of the Fritz-Haber-Institute. ....	10
Figure 6 – The pathway proposed by Horiuti and Polanyi for the exchange of hydrogen with a benzene molecule <sup>13</sup> .....	14
Figure 7 – Sollich-Baumgartner and Garnett’s interpretation of Horiuti and Polanyi’s associative hydrogenation and exchange mechanisms <sup>40</sup> .....	14
Figure 8 – Sollich-Baumgartner and Garnett’s Lennard-Jones style diagram, showing $\pi$ complex adsorption alongside physical adsorption and chemisorption <sup>40</sup> .....	15
Figure 9 – A diagram showing that the difference in energy between the reactant and transition state bond energies for a to a heavier isotope (in this case deuterium) is greater than the difference in energy between the reactant and transition state bond energies for a to a lighter isotope (in this case hydrogen) <sup>57</sup> . This is the reason a normal kinetic isotope effect is observed.....	20
Figure 10 – The reaction scheme for the hydrogenation of phenylacetylene. ....	22
Figure 11 – The reaction scheme for the hydrogenation of 1-phenyl-1-propyne.....	22
Figure 12 – Diagram of the 1 L reactor used. ....	25
Figure 13 – A calibration plot to determine the relationship between the concentration and peak area of the standards in the Focus GC which was used for the duration of the project.....	27
Figure 14 – A representation of the vacuum distillation setup used to obtain pure styrene. ....	30
Figure 15 – Hydrogen consumption profile for the hydrogenation of phenylacetylene at 500 rpm.....	35

Figure 16 – A zero order plot of hydrogen consumption against time at 500 rpm for the hydrogenation of phenylacetylene. ....	36
Figure 17 – Hydrogen consumption profile for the hydrogenation of phenylacetylene at 750 rpm.....	36
Figure 18 – A zero order plot of hydrogen consumption against time at 750 rpm for the hydrogenation of phenylacetylene. ....	37
Figure 19 – Hydrogen consumption profile for the hydrogenation of phenylacetylene at 1000 rpm.....	37
Figure 20 – A zero order plot of hydrogen consumption against time at 1000 rpm for the hydrogenation of phenylacetylene. ....	38
Figure 21 – Hydrogen consumption profile for the hydrogenation of phenylacetylene at 1500 rpm.....	38
Figure 22 – A zero order plot of hydrogen consumption against time at 1500 rpm for the hydrogenation of phenylacetylene. ....	39
Figure 23 – Reaction profile for the hydrogenation of phenylacetylene. Conditions: 3 barg H <sub>2</sub> , 10 mmol phenylacetylene, 40°C. ....	41
Figure 24 – Zero order plot to determine the initial rate constant of phenylacetylene hydrogenation at 40°C.....	41
Figure 25 – Reaction profile for the hydrogenation of phenylacetylene. Conditions: 3 barg H <sub>2</sub> , 10 mmol phenylacetylene, 50°C. ....	42
Figure 26 – Zero order plot to determine the initial rate constant of phenylacetylene hydrogenation at 50°C.....	42
Figure 27 – Reaction profile for the hydrogenation of phenylacetylene. Conditions: 3 barg H <sub>2</sub> , 10 mmol phenylacetylene, 60°C. ....	43
Figure 28 – Zero order plot to determine the initial rate constant of phenylacetylene hydrogenation at 60°C.....	43
Figure 29 – Reaction profile for the hydrogenation of phenylacetylene. Conditions: 3 barg H <sub>2</sub> , 10 mmol phenylacetylene, 70°C. ....	44
Figure 30 – Zero order plot to determine the initial rate constant of phenylacetylene hydrogenation at 70°C.....	44
Figure 31 – Arrhenius plot for the hydrogenation of phenylacetylene using the rate constants calculated from the zero order plots shown in Figures 24, 26, 28 and 30. ....	46
Figure 32 – Reaction profile for the hydrogenation of styrene. Conditions: 3 barg H <sub>2</sub> , 10 mmol styrene, 40°C.....	47

Figure 33 – Zero order plot to determine the initial rate constant of ethylbenzene hydrogenation at 40°C with styrene as the reactant. ....	47
Figure 34 – Reaction profile for the hydrogenation of styrene. Conditions: 3 barg H <sub>2</sub> , 10 mmol styrene, 50°C. ....	48
Figure 35 – Zero order plot to determine the initial rate constant of ethylbenzene hydrogenation at 50°C with styrene as the reactant. ....	48
Figure 36 – Reaction profile for the hydrogenation of styrene. Conditions: 3 barg H <sub>2</sub> , 10 mmol styrene, 60°C. ....	49
Figure 37 – Zero order plot to determine the initial rate constant of ethylbenzene hydrogenation at 60°C with styrene as the reactant. ....	49
Figure 38 – Reaction profile for the hydrogenation of styrene. Conditions: 3 barg H <sub>2</sub> , 10 mmol styrene, 70°C. ....	50
Figure 39 – Zero order plot to determine the initial rate constant of ethylbenzene hydrogenation at 60°C with styrene as the reactant. ....	50
Figure 40 – Arrhenius plot for the hydrogenation of ethylbenzene with styrene as the reactant using the rate constants calculated from the zero order plots shown in Figures 33, 35, 37 and 39. ....	51
Figure 41 – Reaction profile for the hydrogenation of ethylbenzene. Conditions: 3 barg H <sub>2</sub> , 10 mmol ethylbenzene, 50°C. ....	52
Figure 42 – Zero order plot to determine the initial rate constant of ethylbenzene hydrogenation at 50°C. ....	53
Figure 43 – Reaction profile for the hydrogenation of ethylbenzene. Conditions: 3 barg H <sub>2</sub> , 10 mmol ethylbenzene, 60°C. ....	53
Figure 44 – Zero order plot to determine the initial rate constant of ethylbenzene hydrogenation at 60°C. ....	54
Figure 45 – Reaction profile for the hydrogenation of ethylbenzene. Conditions: 3 barg H <sub>2</sub> , 10 mmol ethylbenzene, 70°C. ....	54
Figure 46 – Zero order plot to determine the initial rate constant of ethylbenzene hydrogenation at 70°C. ....	55
Figure 47 – Arrhenius plot for the hydrogenation of ethylbenzene using the rate constants calculated from the zero order plots shown in Figures 42, 44 and 46. ....	57
Figure 48 – Reaction profile for the hydrogenation of 1-phenyl-1-propyne. Conditions: 3 barg H <sub>2</sub> , 10 mmol 1-phenyl-1-propyne, 40°C. ....	58

Figure 49 – Zero order plot to determine the initial rate constant of 1-phenyl-1-propyne hydrogenation at 40°C.....	59
Figure 50 – Reaction profile for the hydrogenation of 1-phenyl-1-propyne. Conditions: 3 barg H <sub>2</sub> , 10 mmol 1-phenyl-1-propyne, 50°C.....	59
Figure 51 – Zero order plot to determine the initial rate constant of 1-phenyl-1-propyne hydrogenation at 50°C.....	60
Figure 52 – Reaction profile for the hydrogenation of 1-phenyl-1-propyne. Conditions: 3 barg H <sub>2</sub> , 10 mmol 1-phenyl-1-propyne, 60°C.....	60
Figure 53 – Zero order plot to determine the initial rate constant of 1-phenyl-1-propyne hydrogenation at 60°C.....	61
Figure 54 – Reaction profile for the hydrogenation of 1-phenyl-1-propyne. Conditions: 3 barg H <sub>2</sub> , 10 mmol 1-phenyl-1-propyne, 70°C.....	61
Figure 55 – Zero order plot to determine the initial rate constant of 1-phenyl-1-propyne hydrogenation at 70°C.....	62
Figure 56 – Arrhenius plot for the hydrogenation of 1-phenyl-1-propyne using the rate constants calculated from the zero order plots shown in Figures 49, 51, 53 and 55.	64
Figure 57 – Reaction profile for the hydrogenation of propylbenzene. Conditions: 3 barg H <sub>2</sub> , 10 mmol propylbenzene, 50°C.....	65
Figure 58 – Zero order plot to determine the initial rate constant of propylbenzene hydrogenation at 40°C.....	65
Figure 59 – Reaction profile for the hydrogenation of propylbenzene. Conditions: 3 barg H <sub>2</sub> , 10 mmol propylbenzene, 60°C.....	66
Figure 60 – Zero order plot to determine the initial rate constant of propylbenzene hydrogenation at 60°C.....	66
Figure 61 – Reaction profile for the hydrogenation of propylbenzene. Conditions: 3 barg H <sub>2</sub> , 10 mmol propylbenzene, 70°C.....	67
Figure 62 – Zero order plot to determine the initial rate constant of propylbenzene hydrogenation at 70°C.....	67
Figure 63 – Arrhenius plot for the hydrogenation of propylbenzene using the rate constants calculated from the zero order plots shown Figures 58, 60 and 62.....	69
Figure 64 – Reaction profile for the deuteration of phenylacetylene. Conditions: 3 barg D <sub>2</sub> , 10 mmol phenylacetylene, 50°C.....	70
Figure 65 – Zero order plot to determine the initial rate constant of phenylacetylene deuteration at 50°C.....	71

Figure 66 – $^2\text{H}$ NMR spectrum of a sample taken after 10 minutes of phenylacetylene deuteriation at $50^\circ\text{C}$ .....	71
Figure 67 – $^2\text{H}$ NMR spectrum of a sample taken after 40 minutes of phenylacetylene deuteriation at $50^\circ\text{C}$ .....	72
Figure 68 – $^2\text{H}$ NMR spectrum of a sample taken after 180 minutes of phenylacetylene deuteriation at $50^\circ\text{C}$ .....	74
Figure 69 – Reaction profile for the deuteriation of phenylacetylene. Conditions: 3 barg $\text{D}_2$ , 10 mmol phenylacetylene, $70^\circ\text{C}$ . ....	75
Figure 70 – Zero order plot to determine the initial rate constant of phenylacetylene deuteriation at $70^\circ\text{C}$ .....	75
Figure 71 – $^2\text{H}$ NMR spectrum of a sample taken after 10 minutes of phenylacetylene deuteriation at $70^\circ\text{C}$ .....	76
Figure 72 – $^2\text{H}$ NMR spectrum of a sample taken after 40 minutes of phenylacetylene deuteriation at $70^\circ\text{C}$ .....	77
Figure 73 – $^2\text{H}$ NMR spectrum of a sample taken after 180 minutes of phenylacetylene deuteriation at $70^\circ\text{C}$ .....	79
Figure 74 – Reaction profile for the deuteriation of styrene. Conditions: 3 barg $\text{D}_2$ , 10 mmol styrene, $50^\circ\text{C}$ .....	81
Figure 75 – $^2\text{H}$ NMR spectrum of a sample taken after 10 minutes of styrene deuteriation at $50^\circ\text{C}$ .....	81
Figure 76 – $^2\text{H}$ NMR spectrum of a sample taken after 40 minutes of styrene deuteriation at $50^\circ\text{C}$ .....	82
Figure 77 – $^2\text{H}$ NMR spectrum of a sample taken after 180 minutes of styrene deuteriation at $50^\circ\text{C}$ .....	84
Figure 78 – Reaction profile for the deuteriation of styrene. Conditions: 3 barg $\text{D}_2$ , 10 mmol styrene, $70^\circ\text{C}$ .....	85
Figure 79 – $^2\text{H}$ NMR spectrum of a sample taken after 10 minutes of styrene deuteriation at $70^\circ\text{C}$ .....	86
Figure 80 – $^2\text{H}$ NMR spectrum of a sample taken after 40 minutes of styrene deuteriation at $70^\circ\text{C}$ .....	87
Figure 81 – $^2\text{H}$ NMR spectrum of a sample taken after 180 minutes of styrene deuteriation at $70^\circ\text{C}$ .....	89
Figure 82 – Reaction profile for the deuteriation of 1-phenyl-1-propyne. Conditions: 3 barg $\text{D}_2$ , 10 mmol 1-phenyl-1-propyne, $50^\circ\text{C}$ . ....	91

Figure 83 – Zero order plot to determine the initial rate constant of 1-phenyl-1-propyne deuteration at 50°C.....	91
Figure 84 – <sup>2</sup> H NMR spectrum of a sample taken after 80 minutes of 1-phenyl-1-propyne deuteration at 50°C. ....	92
Figure 85 – <sup>2</sup> H NMR spectrum of a sample taken after 40 minutes of 1-phenyl-1-propyne deuteration at 50°C. ....	94
Figure 86 – <sup>2</sup> H NMR spectrum of a sample taken after 180 minutes of 1-phenyl-1-propyne deuteration at 50°C. ....	96
Figure 87 – Reaction profile for the deuteration of 1-phenyl-1-propyne. Conditions: 3 barg D <sub>2</sub> , 10 mmol 1-phenyl-1-propyne, 70°C. ....	98
Figure 88 – Zero order plot to determine the initial rate constant of 1-phenyl-1-propyne deuteration at 70°C.....	98
Figure 89 – <sup>2</sup> H NMR spectrum of a sample taken after 10 minutes of 1-phenyl-1-propyne deuteration at 70°C. ....	99
Figure 90 – <sup>2</sup> H NMR spectrum of a sample taken after 40 minutes of 1-phenyl-1-propyne deuteration at 70°C. ....	101
Figure 91 – <sup>2</sup> H NMR spectrum of a sample taken after 180 minutes of 1-phenyl-1-propyne deuteration at 70°C. ....	103
Figure 92 – Reaction profile for the competitive hydrogenation of phenylacetylene and toluene-d <sub>8</sub> . Conditions: 3 barg H <sub>2</sub> , 10 mmol phenylacetylene, 10 mmol toluene-d <sub>8</sub> , 50°C.....	106
Figure 93 – Zero order plot to determine the initial rate constant of phenylacetylene hydrogenation in the presence of toluene-d <sub>8</sub> at 50°C.....	106
Figure 94 – <sup>2</sup> H NMR spectrum of a sample taken after 10 minutes of competitive hydrogenation involving toluene-d <sub>8</sub> and phenylacetylene at 50°C.....	107
Figure 95 – <sup>2</sup> H NMR spectrum of a sample taken after 40 minutes of competitive hydrogenation involving toluene-d <sub>8</sub> and phenylacetylene at 50°C.....	108
Figure 96 – <sup>2</sup> H NMR spectrum of a sample taken after 180 minutes of competitive hydrogenation involving toluene-d <sub>8</sub> and phenylacetylene at 50°C.....	109
Figure 97 – Reaction profile for the competitive hydrogenation of 1-phenyl-1-propyne and toluene-d <sub>8</sub> . Conditions: 3 barg H <sub>2</sub> , 10 mmol 1-phenyl-1-propyne, 10 mmol toluene-d <sub>8</sub> , 50°C.....	110
Figure 98 – Zero order plot to determine the initial rate constant of 1-phenyl-1-propyne hydrogenation in the presence of toluene-d <sub>8</sub> at 50°C.....	110

Figure 99 – $^2\text{H}$ NMR spectrum of a sample taken after 10 minutes of competitive hydrogenation involving toluene- $\text{d}_8$ and 1-phenyl-1-propyne at $50^\circ\text{C}$ . .....	111
Figure 100 – $^2\text{H}$ NMR spectrum of a sample taken after 40 minutes of competitive hydrogenation involving toluene- $\text{d}_8$ and 1-phenyl-1-propyne at $50^\circ\text{C}$ . .....	112
Figure 101 – $^2\text{H}$ NMR spectrum of a sample taken after 180 minutes of competitive hydrogenation involving toluene- $\text{d}_8$ and 1-phenyl-1-propyne at $50^\circ\text{C}$ . .....	113
Figure 102 – Reaction profile for the competitive hydrogenation of phenylacetylene and ethylbenzene. Conditions: 3 barg $\text{H}_2$ , 10 mmol phenylacetylene, 10 mmol ethylbenzene, $50^\circ\text{C}$ . .....	115
Figure 103 – Zero order plot to determine the initial rate constant of phenylacetylene hydrogenation in the presence of ethylbenzene at $50^\circ\text{C}$ . .....	115
Figure 104 – Reaction profile for the competitive hydrogenation of phenylacetylene and ethylbenzene. Conditions: 3 barg $\text{H}_2$ , 10 mmol phenylacetylene, 10 mmol ethylbenzene, $70^\circ\text{C}$ . .....	116
Figure 105 – Zero order plot to determine the initial rate constant of phenylacetylene hydrogenation in the presence of ethylbenzene at $70^\circ\text{C}$ . .....	116
Figure 106 – Reaction profile for the competitive hydrogenation of phenylacetylene and styrene. Conditions: 3 barg $\text{H}_2$ , 10 mmol phenylacetylene, 10 mmol styrene, $50^\circ\text{C}$ . .....	117
Figure 107 – Zero order plot to determine the initial rate constant of phenylacetylene hydrogenation in the presence of styrene at $50^\circ\text{C}$ . .....	118
Figure 108 – Reaction profile for the competitive hydrogenation of phenylacetylene and styrene. Conditions: 3 barg $\text{H}_2$ , 10 mmol phenylacetylene, 10 mmol styrene, $70^\circ\text{C}$ . .....	118
Figure 109 – Zero order plot to determine the initial rate constant of phenylacetylene hydrogenation in the presence of styrene at $70^\circ\text{C}$ . .....	119
Figure 110 – Reaction profile for the competitive hydrogenation of 1-phenyl-1-propyne and propylbenzene. Conditions: 3 barg $\text{H}_2$ , 10 mmol 1-phenyl-1-propyne, 10 mmol propylbenzene, $50^\circ\text{C}$ . .....	120
Figure 111 – Zero order plot to determine the initial rate constant of 1-phenyl-1-propyne hydrogenation in the presence of propylbenzene at $50^\circ\text{C}$ . .....	120
Figure 112 – Reaction profile for the competitive hydrogenation of 1-phenyl-1-propyne and propylbenzene. Conditions: 3 barg $\text{H}_2$ , 10 mmol 1-phenyl-1-propyne, 10 mmol propylbenzene, $70^\circ\text{C}$ . .....	121

Figure 113 – Zero order plot to determine the initial rate constant of 1-phenyl-1-propyne hydrogenation in the presence of propylbenzene at 70°C. ....	121
Figure 114 – Reaction profile for the competitive hydrogenation of phenylacetylene and 1-phenyl-1-propyne. Conditions: 3 barg H <sub>2</sub> , 10 mmol phenylacetylene, 10 mmol 1-phenyl-1-propyne, 50°C. ....	122
Figure 115 – Zero order plot to determine the initial rate constant of phenylacetylene hydrogenation in the presence of 1-phenyl-1-propyne at 50°C. ....	123
Figure 116 – Zero order plot to determine the initial rate constant of 1-phenyl-1-propyne hydrogenation in the presence of phenylacetylene at 50°C. ....	123
Figure 117 – Reaction profile for the competitive hydrogenation of phenylacetylene and 1-phenyl-1-propyne. Conditions: 3 barg H <sub>2</sub> , 10 mmol phenylacetylene, 10 mmol 1-phenyl-1-propyne, 70°C. ....	124
Figure 118 – Zero order plot to determine the initial rate constant of phenylacetylene hydrogenation in the presence of 1-phenyl-1-propyne at 70°C. ....	124
Figure 119 – Zero order plot to determine the initial rate constant of 1-phenyl-1-propyne hydrogenation in the presence of phenylacetylene at 70°C. ....	125
Figure 120 – Temperature profiles of the weight as a percentage and the derivative weight loss for the post-reaction catalyst after the hydrogenation of phenylacetylene at 50°C. ....	127
Figure 121 – Temperature profiles of the derivative weight and ion current corresponding to the loss of ions with a mass of 44 m/e (CO <sub>2</sub> ) for the post-reaction catalyst after the hydrogenation of phenylacetylene at 50°C. ....	128
Figure 122 – Temperature profiles of the weight as a percentage and the derivative weight loss for the post-reaction catalyst after the hydrogenation of phenylacetylene at 70°C. ....	128
Figure 123 – Temperature profiles of the derivative weight and ion current corresponding to the loss of ions with a mass of 44 m/e (CO <sub>2</sub> ) for the post-reaction catalyst after the hydrogenation of phenylacetylene at 70°C. ....	129
Figure 124 – Temperature profiles of the weight as a percentage and the derivative weight loss for the post-reaction catalyst after the deuteration of phenylacetylene at 50°C. ....	129
Figure 125 – Temperature profiles of the derivative weight and ion current corresponding to the loss of ions with a mass of 44 m/e (CO <sub>2</sub> ) for the post-reaction catalyst after the deuteration of phenylacetylene at 50°C. ....	130

Figure 126 – Temperature profiles of the weight as a percentage and the derivative weight loss for the post-reaction catalyst after the deuteration of phenylacetylene at 70°C. ....	130
Figure 127 – Temperature profiles of the derivative weight and ion current corresponding to the loss of ions with a mass of 44 m/e (CO <sub>2</sub> ) for the post-reaction catalyst after the deuteration of phenylacetylene at 70°C.....	131
Figure 128 – Temperature profiles of the weight as a percentage and the derivative weight loss for the post-reaction catalyst after the hydrogenation of styrene at 50°C. ....	132
Figure 129 – Temperature profiles of the derivative weight and ion current corresponding to the loss of ions with a mass of 44 m/e (CO <sub>2</sub> ) for the post-reaction catalyst after the hydrogenation of styrene at 50°C.....	132
Figure 130 – Temperature profiles of the weight as a percentage and the derivative weight loss for the post-reaction catalyst after the hydrogenation of styrene at 70°C. ....	133
Figure 131 – Temperature profiles of the derivative weight and ion current corresponding to the loss of ions with a mass of 44 m/e (CO <sub>2</sub> ) for the post-reaction catalyst after the hydrogenation of styrene at 70°C.....	133
Figure 132 – Temperature profiles of the weight as a percentage and the derivative weight loss for the post-reaction catalyst after the deuteration of styrene at 50°C. ....	134
Figure 133 – Temperature profiles of the derivative weight and ion current corresponding to the loss of ions with a mass of 44 m/e (CO <sub>2</sub> ) for the post-reaction catalyst after the deuteration of styrene at 50°C.....	134
Figure 134 – Temperature profiles of the weight as a percentage and the derivative weight loss for the post-reaction catalyst after the deuteration of styrene at 70°C. ....	135
Figure 135 – Temperature profiles of the derivative weight and ion current corresponding to the loss of ions with a mass of 44 m/e (CO <sub>2</sub> ) for the post-reaction catalyst after the deuteration of styrene at 70°C.....	135
Figure 136 – Temperature profiles of the weight as a percentage and the derivative weight loss for the post-reaction catalyst after the hydrogenation of 1-phenyl-1-propyne at 50°C.....	136
Figure 137 – Temperature profiles of the derivative weight and ion current corresponding to the loss of ions with a mass of 44 m/e (CO <sub>2</sub> ) for the post-reaction catalyst after the hydrogenation of 1-phenyl-1-propyne at 50°C. ....	137

Figure 138 – Temperature profiles of the weight as a percentage and the derivative weight loss for the post-reaction catalyst after the hydrogenation of 1-phenyl-1-propyne at 70°C.....	137
Figure 139 – Temperature profiles of the derivative weight and ion current corresponding to the loss of ions with a mass of 44 m/e (CO <sub>2</sub> ) for the post-reaction catalyst after the hydrogenation of 1-phenyl-1-propyne at 70°C. ....	138
Figure 140 – Temperature profiles of the weight as a percentage and the derivative weight loss for the post-reaction catalyst after the deuteration of 1-phenyl-1-propyne at 50°C.....	138
Figure 141 – Temperature profiles of the derivative weight and ion current corresponding to the loss of ions with a mass of 44 m/e (CO <sub>2</sub> ) for the post-reaction catalyst after the deuteration of 1-phenyl-1-propyne at 50°C. ....	139
Figure 142 – Temperature profiles of the weight as a percentage and the derivative weight loss for the post-reaction catalyst after the deuteration of 1-phenyl-1-propyne at 70°C.....	139
Figure 143 – Temperature profiles of the derivative weight and ion current corresponding to the loss of ions with a mass of 44 m/e (CO <sub>2</sub> ) for the post-reaction catalyst after the deuteration of 1-phenyl-1-propyne at 70°C. ....	140
Figure 144 – A plot of hydrogen consumption against time at different stirrer speeds for the hydrogenation of phenylacetylene.....	141
Figure 145 – A plot of the initial rate constant against different stirrer speeds for the hydrogenation of phenylacetylene. ....	142
Figure 146 – Styrene mole fraction profiles at different temperatures during the hydrogenation of phenylacetylene.....	145
Figure 147 – <i>cis</i> -β-Methylstyrene mole fraction profiles at different temperatures during the hydrogenation of 1-phenyl-1-propyne.....	145
Figure 148 – <i>trans</i> -β-Methylstyrene mole fraction profiles at different temperatures during the hydrogenation of 1-phenyl-1-propyne.....	146
Figure 149 – <i>cis/trans</i> ratio of β-methylstyrene during the hydrogenation of 1-phenyl-1-propyne at different temperatures.....	147
Figure 150 – A comparison of the ethylcyclohexane mole fraction profiles during the hydrogenation of phenylacetylene with hydrogen and deuterium at 50°C. ....	149
Figure 151 – A comparison of the ethylcyclohexane mole fraction profiles during the hydrogenation of phenylacetylene with hydrogen and deuterium at 70°C. ....	149

Figure 152 – A comparison of the propylcyclohexane mole fraction profiles during the hydrogenation of 1-phenyl-1-propyne with hydrogen and deuterium at 50°C.....	150
Figure 153 – A comparison of the propylcyclohexane mole fraction profiles during the hydrogenation of 1-phenyl-1-propyne with hydrogen and deuterium at 70°C.....	151
Figure 154 – A comparison of the conversion of styrene to (ethylbenzene to) ethylcyclohexane at 50°C and 70°C with 3 barg D <sub>2</sub> .....	152
Figure 155 – A comparison of the styrene mole fraction profiles during the hydrogenation of phenylacetylene with hydrogen and deuterium at 50°C. ....	154
Figure 156 – A comparison of the styrene mole fraction profiles during the hydrogenation of phenylacetylene with hydrogen and deuterium at 70°C. ....	154
Figure 157 – A comparison of the <i>cis</i> -β-methylstyrene mole fraction profiles during the hydrogenation of 1-phenyl-1-propyne with hydrogen and deuterium at 50°C..	155
Figure 158 – A comparison of the <i>cis</i> -β-methylstyrene mole fraction profiles during the hydrogenation of 1-phenyl-1-propyne with hydrogen and deuterium at 70°C..	155
Figure 159 – A comparison of the <i>trans</i> -β-methylstyrene mole fraction profiles during the hydrogenation of 1-phenyl-1-propyne with hydrogen and deuterium at 50°C..	156
Figure 160 – A comparison of the <i>trans</i> -β-methylstyrene mole fraction profiles during the hydrogenation of 1-phenyl-1-propyne with hydrogen and deuterium at 70°C..	156
Figure 161 – <i>cis/trans</i> ratio of β-methylstyrene during the hydrogenation and deuteration of 1-phenyl-1-propyne at 50°C.....	158
Figure 162 – <i>cis/trans</i> ratio of β-methylstyrene during the hydrogenation and deuteration of 1-phenyl-1-propyne at 70°C.....	158
Figure 163 – A graph showing phenylacetylene conversion with no competition, in competition with styrene, in competition with ethylbenzene, and in competition with 1-phenyl-1-propyne, all at 50°C. ....	163
Figure 164 – A graph showing phenylacetylene conversion with no competition, in competition with styrene, in competition with ethylbenzene, and in competition with 1-phenyl-1-propyne, all at 70°C. ....	164
Figure 165 – A graph showing ethylcyclohexane mole fraction from reactions of only phenylacetylene, only ethylbenzene, phenylacetylene and styrene, phenylacetylene and ethylbenzene, and phenylacetylene and 1-phenyl-1-propyne, all at 50°C. It should be noted that 100% ethylcyclohexane mole fraction in the competitive reactions would represent twice the number of moles of ethylcyclohexane as a 100% mole fraction in the other reactions. ....	165

Figure 166 – A graph showing ethylcyclohexane mole fraction from reactions of only phenylacetylene, only ethylbenzene, phenylacetylene and styrene, phenylacetylene and ethylbenzene, and phenylacetylene and 1-phenyl-1-propyne, all at 70°C. It should be noted that 100% ethylcyclohexane mole fraction in the competitive reactions would represent twice the number of moles of ethylcyclohexane as a 100% mole fraction in the other reactions. ....	166
Figure 167 – A graph showing propylcyclohexane mole fraction from reactions of only 1-phenyl-1-propyne, only propylbenzene, 1-phenyl-1-propyne and propylbenzene, and 1-phenyl-1-propyne and phenylacetylene, all at 50°C. It should be noted that 100% propylcyclohexane mole fraction in the competitive reactions would represent twice the number of moles of propylcyclohexane as a 100% mole fraction in the other reactions. ....	167
Figure 168 – A graph showing propylcyclohexane mole fraction from reactions of only 1-phenyl-1-propyne, only propylbenzene, 1-phenyl-1-propyne and propylbenzene, and 1-phenyl-1-propyne and phenylacetylene, all at 70°C. It should be noted that 100% propylcyclohexane mole fraction in the competitive reactions would represent twice the number of moles of propylcyclohexane as a 100% mole fraction in the other reactions. ....	168
Figure 169 - A graph showing 1-phenyl-1-propyne conversion with no competition, in competition with propylbenzene, and in competition with phenylacetylene, all at 50°C.....	169
Figure 170 - A graph showing 1-phenyl-1-propyne conversion with no competition, in competition with propylbenzene, and in competition with phenylacetylene, all at 70°C.....	170
Figure 171 – A mole fraction profile for the competitive hydrogenation of phenylacetylene and 1-phenyl-1-propyne at 50°C.....	171
Figure 172 – A mole fraction profile for the competitive hydrogenation of phenylacetylene and 1-phenyl-1-propyne at 70°C.....	171
Figure 173 – A comparison of the styrene mole fraction profiles during the hydrogenation of phenylacetylene alone and of phenylacetylene in competition with styrene, ethylbenzene, and 1-phenyl-1-propyne at 50°C. ....	172
Figure 174 – A comparison of the styrene mole fraction profiles during the hydrogenation of phenylacetylene alone and of phenylacetylene in competition with styrene, ethylbenzene, and 1-phenyl-1-propyne at 70°C. ....	173

Figure 175 – A comparison of the <i>cis</i> - $\beta$ -methylstyrene mole fraction profiles during the hydrogenation of 1-phenyl-1-propyne alone and of 1-phenyl-1-propyne in competition with propylbenzene, and phenylacetylene at 50°C.....	173
Figure 176 – A comparison of the <i>cis</i> - $\beta$ -methylstyrene mole fraction profiles during the hydrogenation of 1-phenyl-1-propyne alone and of 1-phenyl-1-propyne in competition with propylbenzene, and phenylacetylene at 70°C.....	174
Figure 177 – A comparison of the <i>trans</i> - $\beta$ -methylstyrene mole fraction profiles during the hydrogenation of 1-phenyl-1-propyne alone and of 1-phenyl-1-propyne in competition with propylbenzene, and phenylacetylene at 50°C.....	174
Figure 178 – A comparison of the <i>trans</i> - $\beta$ -methylstyrene mole fraction profiles during the hydrogenation of 1-phenyl-1-propyne alone and of 1-phenyl-1-propyne in competition with propylbenzene, and phenylacetylene at 70°C.....	175
Figure 179 – <i>cis/trans</i> ratio of $\beta$ -methylstyrene during the hydrogenation of 1-phenyl-1-propyne without competition, in competition with propylbenzene and in competition with phenylacetylene, at 50°C. ....	177
Figure 180 – <i>cis/trans</i> ratio of $\beta$ -methylstyrene during the hydrogenation of 1-phenyl-1-propyne without competition, in competition with propylbenzene and in competition with phenylacetylene, at 70°C. ....	177

## **Acknowledgements**

I would like to thank Professor Jackson for offering me the opportunity to undertake this research in his group, as well as for his advice and support throughout.

I am particularly indebted to Kathleen Kirkwood, who took time to demonstrate many of the practical aspects of this research. She was also a most important source of moral support in moments of need.

My thanks are directed towards Andrew Monaghan, whose technical expertise enabled this project to reach its completion.

Finally, I would like to thank all members of the catalysis section at the University of Glasgow for welcoming me into the team and for sharing their knowledge with me.

## **Author's Declaration**

I declare that this thesis contains only my own work, except where reference is made to other authors. This thesis has not been submitted for any other degree or qualification.

---

Joseph William Gregory, BA (Hons)

# 1 Introduction

Catalysts are a fundamental aspect of modern chemical industry, being involved in an estimated 90% of industrial chemical processes<sup>1</sup>, and have been observed since the first half of the 19<sup>th</sup> century<sup>2</sup>, when Berzelius coined the term '*katalys*'. Catalysts work by providing an alternative route for the reaction they are catalysing and are not used up in the overall reaction. This route has a lower activation energy, meaning that the process can proceed at lower temperatures and pressures. This is useful for chemists because it means that reactions which would otherwise occur very slowly or not at all at lower temperatures can be caused to occur rapidly with just a small input of energy. With sustainability and energy usage minimisation being priorities in these times of environmental uncertainty, catalysis is providing a more acceptable, as well as cost effective, method of producing a large variety of molecules on an industrial scale.

This project will focus on the catalysis of the hydrogenation cascades of alkynylarenes over rhodium/silica, assessing aspects of selectivity and kinetics.

Heterogeneous and homogeneous are the terms used to describe the two branches of catalysis, with heterogeneous catalysis involving a substrate and catalyst in different physical phases, while homogeneous catalysis involves a substrate and catalyst which exist in the same physical phase. Heterogeneous catalysis is the most popular type of catalysis in industry, making up around 80% of all catalysed reactions<sup>3</sup>, and is the focus of this thesis, specifically organic molecules reacting on metal surfaces.

Hydrogenation is a widespread process in the chemical industry, being used in a number of sectors from oil refining to fine chemical production. The reaction is particularly versatile and has a high atom efficiency<sup>4</sup>. The hydrogenation of benzene was first achieved in 1901 by Sabatier and Senderens using a nickel catalyst<sup>5</sup>, with Sabatier's work on hydrogenation reactions of organic molecules eventually winning him the Nobel Prize in 1912. Since then, there has been a steady stream of research into the heterogeneous catalysis of the reduction of aromatic compounds.

Selective hydrogenation is of significance to the chemical industry<sup>6</sup>. The ability to select a molecule and optimise its production has obvious benefits and this is the principle which will be investigated here. Recent research in our laboratory has focused on the hydrogenation of complex molecules over rhodium/silica catalysts,

working towards the improvement of rates and selectivities. This thesis will focus on the hydrogenation of molecules with multiple unsaturated functionalities, which may proceed as a cascade reaction, meaning the reaction scheme can be represented as one molecule reacting to make the next along the chain of products until the final product is reached ( $A \rightarrow B \rightarrow C \rightarrow D$  etc.). This is, however, a simplified model of what can be a complex chemical process, especially when a catalyst is involved. The products will build up and decline at different rates and may compete for sites on the catalyst. The binding and reacting of some molecules can change the active sites or poison the catalyst, altering its behaviour, and thus affect other steps. These factors can be a hindrance when attempting to selectively produce one product, but with careful study, it is possible to find conditions which optimise productivity and selectivity.

There has been some research on the topic of phenylacetylene and styrene hydrogenation over rhodium<sup>7,8</sup>, but research into the hydrogenation of these molecules has largely been carried out, with low concentrations of phenylacetylene in order to replicate industrial conditions<sup>9</sup>. To gain a more complete understanding of the process such that it might be applicable in a broader sense, it is necessary to study competitive reactions under more general conditions. The literature on the hydrogenation of 1-phenyl-1-propyne, especially in a competitive sense, is rather sparse. This thesis will compare the nature of the hydrogenation of these aromatics and assess the difference between the hydrogenation of the terminal and internal alkynes. Moreover, it will explore the behaviour of phenylacetylene, 1-phenyl-1-propyne, and their hydrogenation products under competitive conditions with a view to utilising these competitive reactions to improve understanding.

## 1.1 Chemisorption

Chemisorption is a type of adsorption which involves the chemical bonding of a substrate to a surface. The energetics of this process can be described by a Lennard-Jones diagram<sup>10</sup> (Figure 1), which shows the favourability of both physical adsorption and chemisorption by plotting energy as a function of the distance between the surface and the adsorbing molecule. Physical adsorption, in contrast to chemisorption, does

not involve the breaking of chemical bonds, but is rather a van der Waals interaction between the surface and the molecule. The relevance of this concept lies in the way in which it governs the interactions between the metal surface and the reactants. Different types of adsorption allow molecules, or different groups within a molecule, to react in different ways and the impact of this becomes apparent when one considers the catalysed reactions of hydrogen with alkynes, alkenes and aromatics.

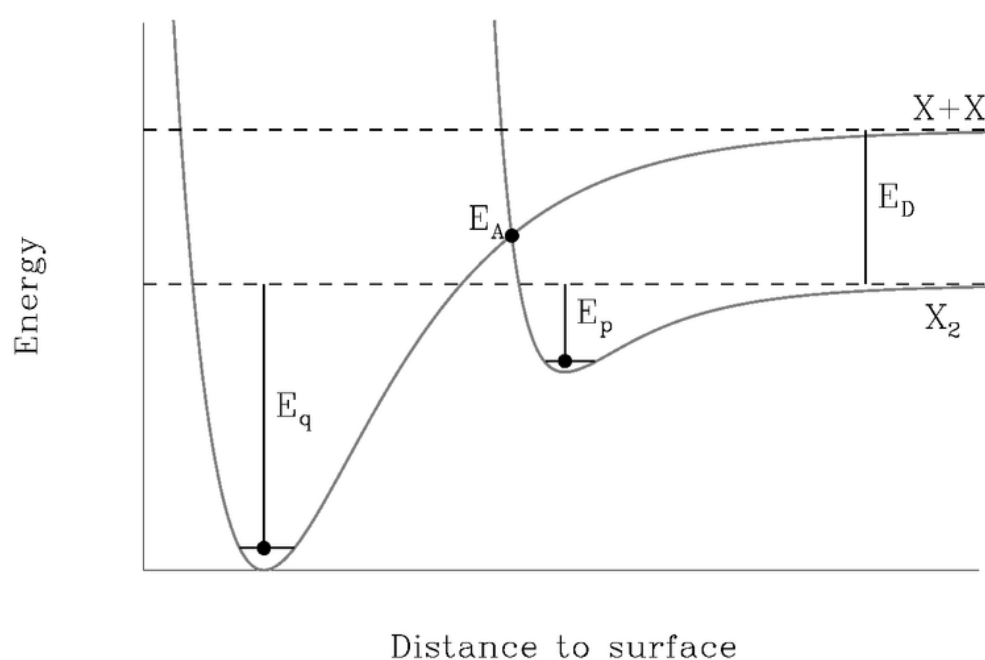


**Figure 1 – Lennard-Jones diagram showing physical adsorption ( $E_p$ ) and chemisorption ( $E_q$ )<sup>11</sup>. ‘EA’ is the activation energy for the formation of the chemisorbed state.**

Diatomic hydrogen, a key reactant in hydrogenation reactions, is dissociatively chemisorbed by many transition metals<sup>12</sup>. By this, it is meant that the original molecule is broken into more than one fragment. In this case, the hydrogen atoms each form a bond to the metal surface and the  $\sigma$  bond which held the molecule together is broken. In contrast, associative chemisorption is defined as the adsorption of a molecule to a

surface without the molecule being broken into fragments. This can happen, for example, with the breaking of a  $\pi$  bond within the molecule to form two  $\sigma$  bonds to a surface. These are the two classical modes of chemisorption which are considered when molecules interact chemically with a surface.

The chemisorption of hydrocarbons is significantly more complex than that of hydrogen, with many possible geometries and bonding arrangements (Figure 2). The way in which a molecule adsorbs to a surface can be highly influential in determining the reaction it undergoes, however it is difficult to make definitive conclusions surrounding this type of chemical behaviour from kinetic studies and often requires further analysis.

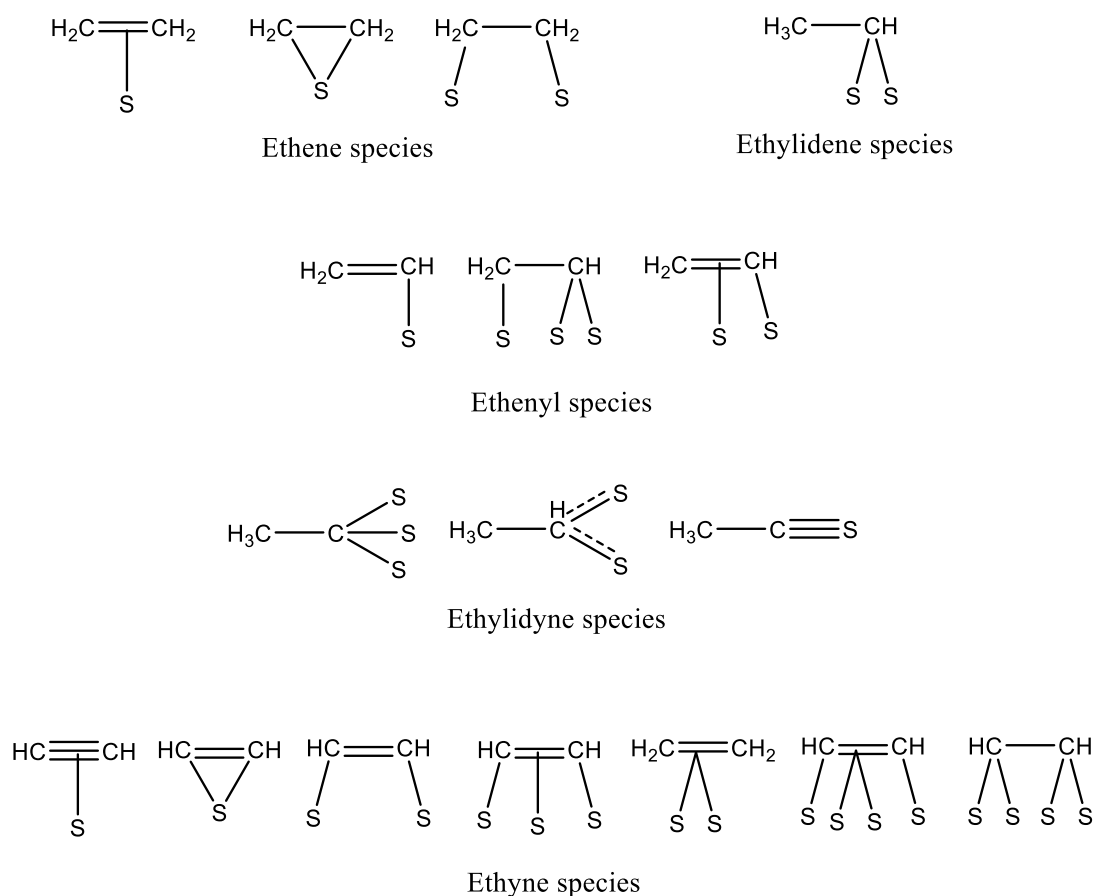


**Figure 2 – Diagrams of chemisorbed hydrocarbons. S represents the surface.**

Chemisorption is commonly seen in mechanisms associated with heterogeneous catalysis, as it provides a more reactive species for the subsequent step and allows for a pathway involving a lower activation energy, with the adsorption of the substrate to the surface being more favourable than unsupported fission of the bond. The adsorption of reactants on a metal surface also has the advantage of bringing them into close proximity without the need to rely on collisions, hence increasing the rate of reaction.

Overall, chemisorption is a fundamental process in heterogeneous catalytic hydrogenation. It breaks the bond of diatomic hydrogen, providing two reactive hydrogen species, and influences the kinetics of hydrocarbon reactivity, meaning reactions can happen more readily than uncatalysed processes.

## 1.2 The Hydrogenation of Double and Triple Bonds

The questions posed when assessing the mechanism of the hydrogenation of unsaturated organic compounds on a surface go further than what is usually considered when probing uncatalysed reactions. Which molecules are adsorbed at which stages and the nature of this adsorption are key factors in the mechanism and these can cloud the analysis of the data gathered when studying these reactions. Early theories about a stepwise pathway of the adsorption, bond formation and bond breaking processes have given rise to insights about structure sensitivity, the sites involved in hydrogenation, the effects of carbonaceous deposits on the catalyst surface and the roles of different types of hydrogen. Larger alkynes and alkenes have also been studied in more recent times, providing insights into how the structure of the whole molecule affects the reactivity of the  $\pi$ -bond. Understanding the catalytic hydrogenation of alkynes and alkenes requires a consideration of a number of factors relating to the catalyst and the mechanistic pathway.

Horiuti and Polanyi's famous mechanism<sup>13</sup> (Figure 3) is generally accepted as a good explanation of the behaviour of simple alkenes when interacting with dissociatively-adsorbed hydrogen on a surface and provides a simple outline of each step of the

exchange and hydrogenation reactions. In their mechanism, the  $\pi$ -bond breaks and the carbon atoms which were part of the alkene group form  $\sigma$ -bonds with the surface. One of the carbon atoms then forms a bond with an atom of surface hydrogen, producing a half-hydrogenated state before the mechanism diverges, giving pathways for both exchange and hydrogenation.

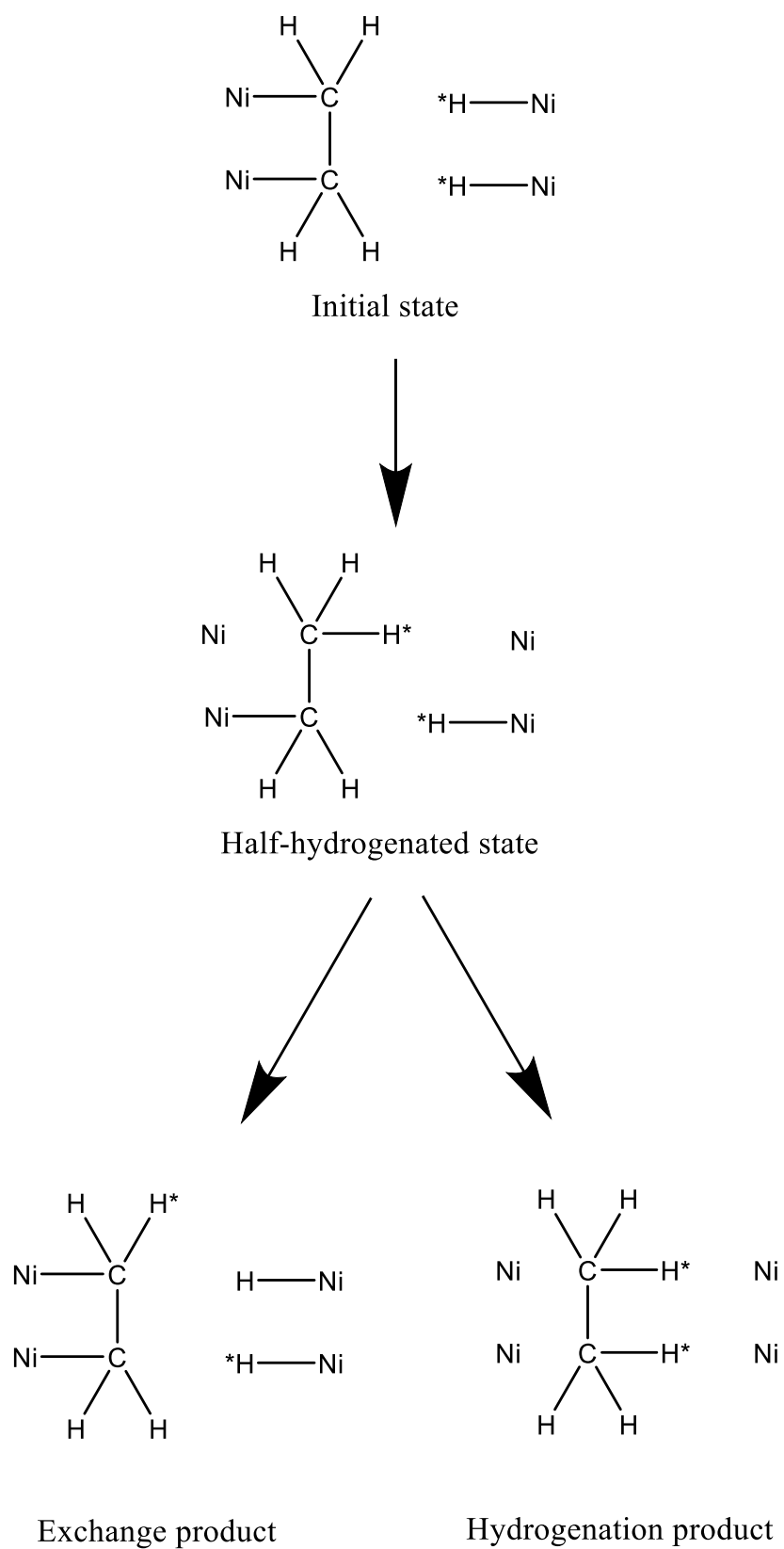


**Figure 3 – Horiuti and Polanyi's mechanism for the behaviour of associatively adsorbed alkenes<sup>13</sup>.**

Adding to this work, Twigg proposed that the rate-determining step in the hydrogenation of ethene was the second half-hydrogenation step between a chemisorbed hydrogen atom and the half-hydrogenated ethene which produces non-adsorbed ethane<sup>14</sup>. Later work by Mohsin *et al.* investigated the form of adsorbed species on Pt(111) faces<sup>15</sup>. This research showed di- $\sigma$ -bonded species,  $\pi$ -bonded species and ethylidyne to be present, with ethylidyne known to be a spectator species<sup>16</sup>. Cremer *et al.* then showed that the active species in hydrogenation was the  $\pi$ -bonded species<sup>17</sup>, thus bringing understanding of the mechanism for ethene hydrogenation to a point of seeming completion.

At first glance, the hydrogenation of ethyne on a metal surface may seem to follow that of ethene, simply repeating the hydrogenation process once the molecule is adsorbed to produce ethane via a vinyl radical (co-hydrogenation). Nakatsuji *et al.*<sup>18</sup> suggested that a Langmuir-Hinshelwood model was sufficient to describe the process. Studies by McGown *et al.*<sup>19</sup> and LeViness *et al.*<sup>20</sup>, however, presented a more complex reaction scheme, whereby an alternative pathway exists in some cases, including that of rhodium<sup>21</sup>, alongside the ethane co-hydrogenation process. This alternative direct hydrogenation process does not proceed via the vinyl radical, but rather via an ethylidyne (or other strongly adsorbed) species, meaning that there are no doubly-bonded intermediates. It should be noted, though, that the co-hydrogenation pathway is the dominant route of ethyne hydrogenation, accounting for over 90% of the ethane formed. These studies also showed that, in spite of ethyne adsorbing more strongly than ethene<sup>22</sup>, at high ethyne concentrations ethene is still hydrogenated, meaning ethyne and ethene are hydrogenated at different sites in the co-hydrogenation pathway. A commonly accepted reaction pathway is shown in Figure 4. These findings provided a starting point for more in depth considerations about the catalyst's role in alkyne hydrogenation and are also useful when investigating competitive hydrogenation.

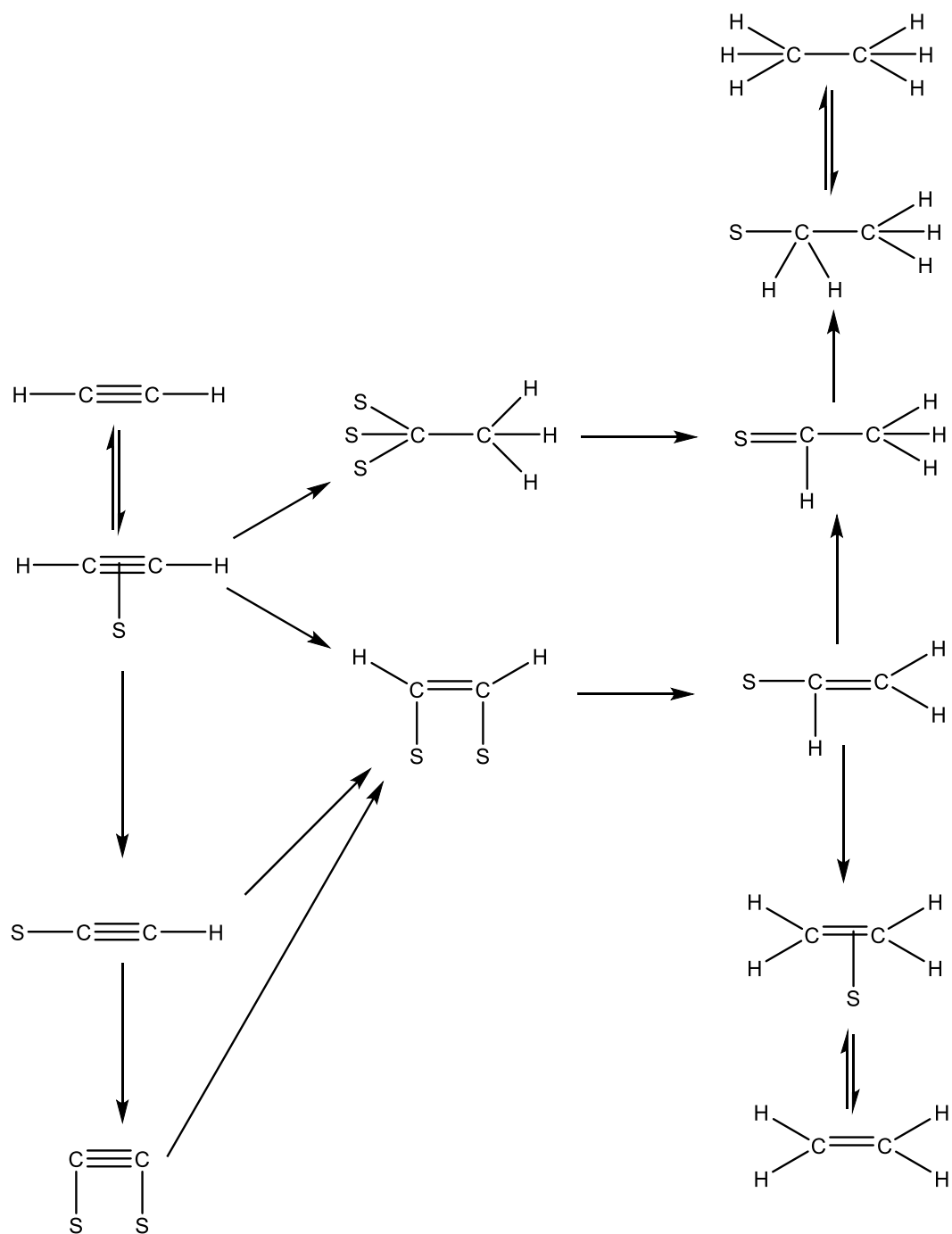


**Figure 4 – The reaction pathway of ethyne adsorbed on a palladium catalyst, according to Margitfalvi et al.<sup>23</sup>. S represents the surface.**

It had long been asserted that ethene hydrogenation is structure-insensitive and the effects of particle structure on the hydrogenation of ethyne have historically proven difficult to investigate<sup>12</sup>. The work of Al-Ammar and Webb introduced the ideas that ethene and ethyne could hydrogenate at different sites and that ethyne could react to directly produce ethane with no ethene intermediate on palladium, rhodium and iridium<sup>24, 25</sup>. It has since been suggested by Borodziński and Gołębiowski, based on a study which used a palladium catalyst, that there are two highly active sites for ethyne hydrogenation and there is a less active site where adsorption is competitive on the palladium catalyst which was examined<sup>26</sup>. More recent studies have shown that carbonaceous deposits have the effect of increasing the rate of hydrogenation of alkenes and alkynes<sup>12</sup> and it has been suggested, using a palladium catalyst for the research, that this is due to the deposit's ability to facilitate the diffusion of hydrogen into subsurface layers of metal particles through corner and edge sites<sup>27</sup>, as is shown in Figure 5; palladium's ability to absorb hydrogen into the subsurface region is supported by neutron spectroscopy analysis<sup>28</sup> and was thought to be a unique property<sup>29</sup>. There is evidence that rhodium exhibits a similar propensity to absorb hydrogen<sup>30</sup>, however there is little in the literature examining whether this property has similar effects on rhodium's catalytic behaviour. This subsurface hydrogen is necessary for the hydrogenation of double bonds and is thought to be key in selective hydrogenation<sup>31</sup>.

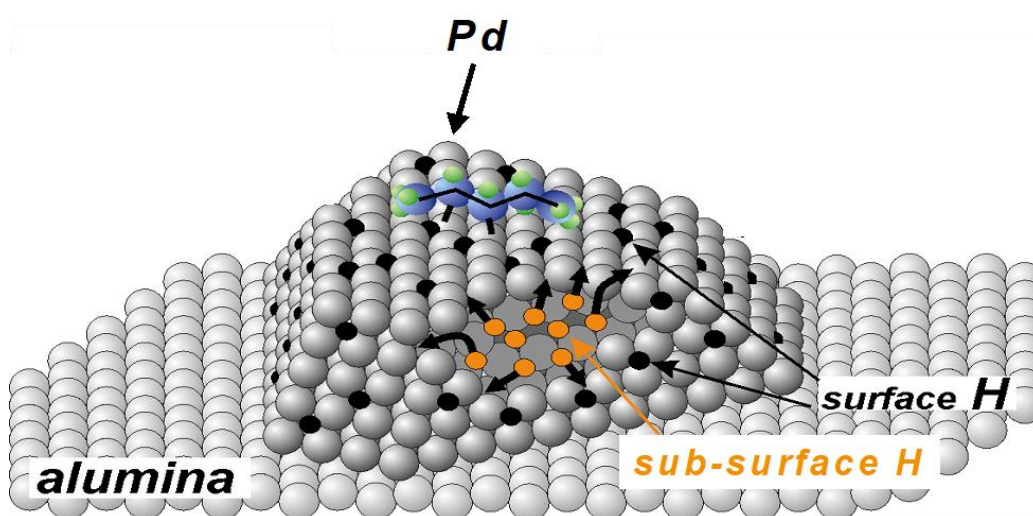


**Figure 5 – A diagram showing the positions of surface hydrogen and subsurface hydrogen on a catalytic particle, courtesy of the Fritz-Haber-Institute.**

The hydrogenation of longer-chain alkenes and alkanes has been studied, showing that mechanism and kinetics of their reduction is not always exactly the same as that of two-carbon molecules<sup>32</sup>. Despite this, they are still a good model to work from when considering reactions of larger molecules. In a study of the surface chemistry of three-carbon molecules on platinum, Zaera and Chrysostomou observed a slow half-hydrogenation step to a 1-propyl species as the dominant pathway, indicating that the central carbon is preferentially hydrogenated<sup>33</sup>. The propylidyne species observed on the surface of the catalyst is analogous to the ethylidyne species observed during the hydrogenation of ethyne and shows that the two molecules demonstrate similar surface chemistry. Further studies by Zaera have shown that Pt(111) surfaces favour *cis-trans* isomerisation of but-2-ene<sup>34</sup>, while Pt(557) stepped surfaces are not involved in isomerisation, but rather play a role in the full hydrogenation of alkynes<sup>35</sup>. Isomerisation and exchange processes for but-2-ene on platinum were shown to follow the Horiuti-Polanyi mechanism<sup>36</sup>, providing another analogy between two-carbon systems and three- and four-carbon systems. These reactions, being performed using a platinum catalyst, give an idea of how surface processes involving unsaturated molecules develops as the chain is lengthened, however these molecules are still relatively small and further complications could arise. It should be noted that this behaviour is observed in the absence of subsurface hydrogen, which could mean that the chemistry is altered when rhodium is introduced.

The behaviour of five- and six-carbon systems on palladium have been studied, opening up kinetic insights into how longer unsaturated molecules behave when interacting with both surface and subsurface hydrogen. Teschner *et al.* showed that 1-pentyne underwent rapid deposition onto the palladium catalyst, preventing significant quantities of hydrogen from adsorbing on the surface<sup>37</sup>. The same study concluded that higher hydrogen : pentyne ratios favoured pentane production, while decreasing the hydrogen : pentyne ratio provided a method for increasing the selectivity towards the alkene. McGregor and Gladden also showed that carbon quickly became incorporated into the surface of a palladium catalyst when 1-pentyne was added and concluded that this resulted in the formation of a catalytically-active layer, as well as

suggesting that pentenes' capacities to isomerise and exchange protons decreased with increasing adsorption strength<sup>38</sup>. As well as these conclusions regarding palladium catalysts, they found that carbon laydown from *cis*-2-pentene on nickel catalysts formed a layer which was particularly active for the hydrogenation of *trans*-2-pentene and that carbon laydown from *trans*-2-pentene on nickel catalysts formed a layer which was particularly active for the hydrogenation of *cis*-2-pentene. This research shows that, in the case of longer-chain unsaturated molecules, conditions can decide the selectivity of hydrogenation through their impact on the formation of carbonaceous deposits and their ability to influence, in cases where palladium catalysts are used, the quantity and type of hydrogen available.

In a study involving six-carbon systems and a palladium catalyst, Anderson *et al.* observed that terminal alkynes underwent double-bond shift at step and edge sites, while 2-pentene isomerised on terraced surfaces<sup>39</sup>. This study starts to highlight the importance of the position of the functional group, with terminal groups seemingly interacting with different catalytic sites to internal groups. This is a particularly prominent consideration when both surface and subsurface hydrogen are present, as edge sites must be considered in the context of both hydrogenation and hydrogen entering the subsurface region.

To summarise, the associative mechanism of Horiuti and Polanyi laid the foundations for an understanding of how alkenes and alkynes are hydrogenated on metal surfaces. Further studies revealed that carbonaceous deposits on the metal surface enhance the rate of hydrogenation and it has been suggested that this is due to subsurface hydrogen being involved in the reaction. This may be a property which is unique to palladium, however rhodium's capacity to allow hydrogen diffusion into its subsurface region may allow for a replication of this catalytic activity. There is evidence that ethene and ethyne react at different sites and research on the hydrogenation of higher alkynes has found that terminal alkynes likely hydrogenate on corner and edge sites, with internal alkynes hydrogenating on terraced faces. These factors must all be taken into account when assessing the kinetics of the reactions in this study and will be used to draw conclusions regarding the nature of the reactions.

### 1.3 The Hydrogenation of Aromatic Rings and Associated Exchange Mechanisms

Benzene and its derivatives are interesting chemically due to their delocalised  $\pi$  systems. The electron density above and below the ring stabilises the molecules and they are thus more difficult to saturate than three localised double bonds. This aromaticity, along with the planar nature of the ring, makes the study of hydrogenation reactions on a surface distinct from the behaviour of other hydrocarbons. With many early suggestions regarding the mechanism of aromatic hydrogenation failing to explain experimental results, a new, less conventional pathway was needed in order to understand the results being observed. Structure sensitivity, the effect of carbonaceous deposits, probable sites of hydrogenation, and the roles of different types of hydrogen are prominent considerations when understanding the nature of aromatic hydrogenation and allow for a more complete understanding of the process. The hydrogenation of substituted aromatics have been studied to a lesser extent than benzene, but the research which has been done provides a framework to which this study aims to contribute.

Following the initial hydrogenation of benzene by Sabatier and Senderens<sup>5</sup>, early investigations regarding the behaviour of aromatics adsorbed to metal surfaces were carried out by a number of researchers. Horiuti and Polanyi's earlier paper suggested that their mechanism was applicable to benzene (Figures 6-7) and, thus, that hydrogen exchange could take place via the chemisorption of two carbon atoms from the ring to the metal surface, breaking the aromaticity of the ring and forming an adsorbed cyclic diene<sup>13</sup>. This species reacts with dissociatively chemisorbed hydrogen to produce the half-hydrogenated state, as with the alkene mechanism. The problem that is faced when using the same model as with alkenes is that interfering with aromaticity requires much more energy than breaking a regular  $\pi$ -bond, such as those found in alkenes. This does not necessitate a different mechanism, but does mean that it cannot simply be assumed that hydrogenation and exchange processes in alkenes and arenes are analogous.

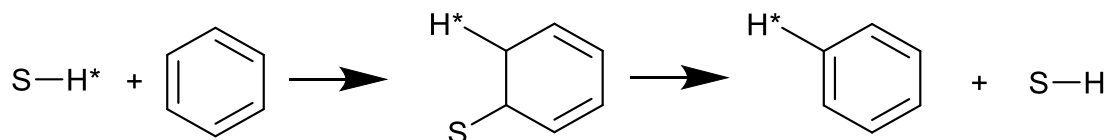


**Figure 6 – The pathway proposed by Horiuti and Polanyi for the exchange of hydrogen with a benzene molecule<sup>13</sup>.**

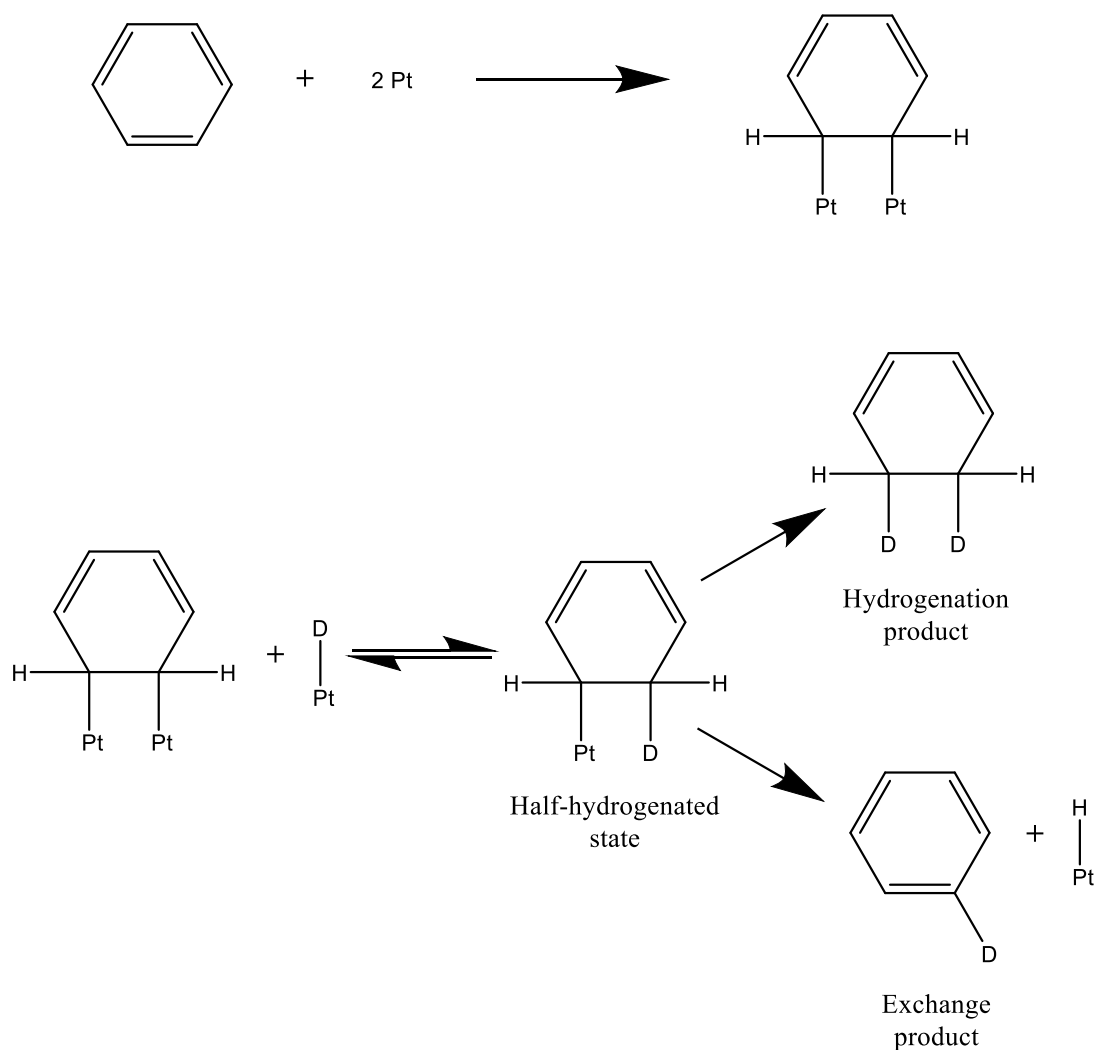


**Figure 7 – Sollich-Baumgartner and Garnett's interpretation of Horiuti and Polanyi's associative hydrogenation and exchange mechanisms<sup>40</sup>.**

Garnett and Sollich-Baumgartner advanced understanding on the matter with their presentation of a different type of adsorption, which they termed  $\pi$  complex adsorption, as a generalised model for group VIII metals<sup>40</sup>. The theory combines theoretical understanding of hybridised orbitals with experimental observation to explain the role of the  $\pi$  system in aromatic adsorption and the data gathered surrounding exchange and hydrogenation reactions. The potential energy curve, plotted against the molecule's distance from the metal, sits between the potential energy curves associated with van der Waals (physical) adsorption and chemisorption, providing a middle ground to satisfy the concerns raised with the previously documented mechanisms, as can be seen in Figure 8.

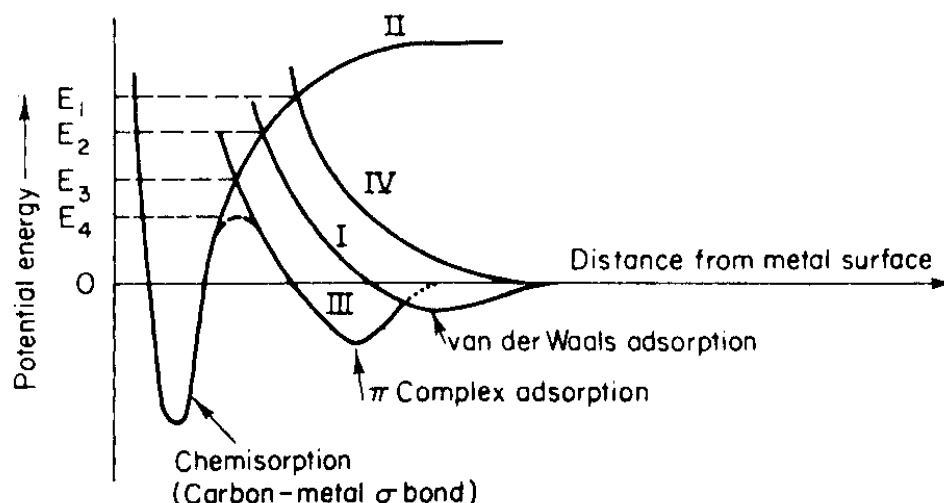


**Figure 8 – Sollich-Baumgartner and Garnett's Lennard-Jones style diagram, showing  $\pi$  complex adsorption alongside physical adsorption and chemisorption<sup>40</sup>.**

The  $\pi$  complex adsorption model used by Garnett and Sollich-Baumgartner<sup>40</sup> is a formalisation of a concept already alluded to in an exchange mechanism by Crawford and Kemball<sup>41</sup>, and a mechanism for both exchange<sup>41</sup> and hydrogenation as exemplified by Rooney<sup>42</sup>. The exchange mechanisms are described as being associative and dissociative by Garnett and Sollich-Baumgartner, but are different to the 'classical' associative and dissociative mechanisms, as they rely on  $\pi$  complex adsorption. In a

recent review of the field, Bond (like many others) favours Rooney's mechanism for hydrogenation as a probable explanation of the evidence provided, but concedes that the mechanism for hydrogen exchange is still far from definitive, citing the associative and dissociative mechanisms based on  $\pi$  complex adsorption<sup>12</sup>.

More precise details of the process have since been investigated, with Schönmaker-Stolk *et al.*<sup>43</sup> proposing a mechanism for hydrogenation on ruthenium which involves a 1,4-cyclohexadiene intermediate. This mechanism is accepted by Stanislaus and Cooper<sup>44</sup>, but Garnett suggests that the observed kinetics may be the result of a number of mechanisms occurring simultaneously<sup>45</sup>. More recent studies by Su *et al.* show that the dominant pathway on platinum is one which includes a 1,3-cyclohexadiene intermediate<sup>46</sup>.

It has been shown that the most active catalysts for benzene hydrogenation are ruthenium/carbon and rhodium/carbon<sup>12</sup>; they adsorb aromatic molecules strongly enough that a reaction can take place, but not so strongly that the surface becomes effectively poisoned by the substrate. The hydrogenation is known to take place on surfaces of trigonal symmetry, most notably the fcc(111) plane, which is the same face reportedly active for alkene and alkyne hydrogenation.

The influence of the catalyst is a factor which has been more carefully investigated since the mechanistic pathway was determined. For the hydrogenation of benzene, the turnover frequency had long appeared to be independent of particle dispersion under most industrial conditions, however more recent studies have concluded that that decreasing the temperature at which the catalyst is reduced below 50°C and having dispersions over 50% can significantly reduce the turnover frequency<sup>12</sup>. This could be the result of higher temperature reduction effecting a structural reorganisation during the reduction, however many now believe that there is a degree of structure sensitivity associated with benzene hydrogenation and that this was not initially realised due to the small proportion of edge and corner sites on many catalysts. It has been shown using a ruthenium catalyst that carbonaceous deposits, in contrast to their promoting role in the hydrogenation of alkenes and alkynes, act as a poison in benzene hydrogenation<sup>47</sup>. This strongly suggests that the dominant form of hydrogen involved in this process is surface hydrogen and, unlike in the case of alkene and alkyne hydrogenation, subsurface hydrogen does not play a significant role. These catalytic

properties influence the hydrogenation process and are reflected in the observed kinetics, something which will be discussed in relation to the results obtained in this thesis.

In a similar fashion to ethyne and ethene being good models for alkyne and alkene hydrogenation, but not always having exactly the same mechanism and kinetics as larger molecules, benzene hydrogenation is complicated by the addition of substituents and it is largely these complications which this thesis will investigate. The system requires further considerations, as there can be interactions between aromatic systems, sometimes known as  $\pi$ -stacking<sup>48</sup>, which can have unpredictable effects on the kinetics of reactions.

Substituents have a significant impact on hydrogenation activity. Minot and Gallezot showed that toluene adsorbs more strongly than benzene<sup>49</sup>. Adding, to this, it was demonstrated that more branching and longer branching leading to slower hydrogenation due to greater adsorption strengths<sup>50</sup>. This was explained as being due to the enhancement of  $\pi$  complex adsorption by the donation of electron density from the alkyl groups<sup>51</sup>, with longer chains donating more electron density. The nature of the substituents contributes to the adsorption of the molecule and, in a competitive reaction, this will affect the way in which molecules are able to interact with a catalyst.

There have been some rudimentary studies regarding the hydrogenation of phenylacetylene. Basic kinetic analysis of phenylacetylene hydrogenation has been carried out on palladium<sup>52,53</sup>, which shows that styrene selectivity can be improved by increasing the catalyst particle dispersion and decreasing the hydrogen pressure, however these studies stop short of linking palladium's ability to absorb hydrogen into the subsurface region to the kinetics observed and none of the authors report observing ring hydrogenation. A similar kinetic study was carried out using rhodium nanoparticles<sup>54</sup>, but no conclusions were drawn about the nature of the hydrogen involved and, again, no ring hydrogenation was observed.

In a competitive study carried out on palladium catalysts, it was found that phenylacetylene inhibited internal alkyne hydrogenation to a greater extent than internal alkynes inhibited the hydrogenation of other internal alkynes<sup>55</sup>. This suggests that phenylacetylene is adsorbing at sites which are not on the faces of the palladium particles. A study of the hydrogenation of allylbenzene, *cis*- $\beta$ -methylstyrene and *trans*-

$\beta$ -methylstyrene produced evidence that a rhodium catalyst did behave in the way which would be expected of a palladium catalyst, facilitated by kinetics which suggest that the terminal and internal alkenes are hydrogenating at different sites<sup>56</sup>.

The matter of aromatic hydrogenation is more complicated than that of alkenes and alkynes.  $\pi$  Complex adsorption provides a satisfactory explanation to the mechanistic questions posed and further research has built a more complete picture of the overall process. Particle size appears to have little effect on the rate of aromatic hydrogenation, which is postulated to occur on trigonal faces such as the fcc(111) plane. Carbonaceous deposits have been shown to decrease the rate of the reaction and surface hydrogen is accepted to be the only active hydrogen species in the process. This thesis will look at how the interplay between the hydrogenation of multiple unsaturated functionalities affects kinetics and the results will be considered in conjunction with the work which has already been carried out.

## 1.4 Kinetic Isotope Effect

The kinetic isotope effect shows the role of a particular bond in the mechanism of a reaction and is observed by a rate difference between reactions involving isotopically substituted analogues of the same molecule. In the case of catalytic hydrogenation, it is a technique which can be used to probe the rate determining step and will be used in this investigation to assess the involvement of hydrogen in the rate determining step of the hydrogenation process.

From the following relationship:

$$\omega \propto \sqrt{\frac{k_f}{\mu}}$$

where  $\omega$  is the vibrational frequency of a bond,  $k_f$  is the force constant, and  $\mu$  is the reduced mass, it can be shown that bonds to heavier isotopes require more energy to break. This is where the difference in reaction rates stems from – if a bond to, for example, hydrogen is formed or broken in the rate determining step of a reaction, then

that reaction will proceed faster than the same reaction involving deuterium in place of hydrogen. In this particular case, a normal primary kinetic isotope effect is observed and a value of greater than one for  $\frac{k_H}{k_D}$  is measured, where  $k_H$  is the rate constant of the reaction involving the molecule which involves the lower mass isotope, in this case hydrogen, and  $k_D$  is the reaction involving the molecule which involves the higher mass isotope, in this case deuterium.

Secondary kinetic isotope effects are observed when the hybridisation (or in some cases, conjugation) of an atom which is bonded to the isotopically-substituted atom changes. This change is more subtle than a primary kinetic isotope effect and the  $\frac{k_H}{k_D}$  value will generally be closer to one; this effect is usually only observable when studying isotopes of hydrogen due to the large relative difference between their masses. A normal secondary kinetic isotope effect ( $\frac{k_H}{k_D} > 1$ ) indicates a change between a stiffer (greater difference between vibrational energy levels) and a less stiff (smaller difference between vibrational energy levels) bond, for example a change between  $sp^3$  C-H and  $sp^2$  C-H, where hydrogen is the atom being isotopically substituted.

A potential energy profile explaining how normal kinetic isotope effects arise is shown in Figure 9.

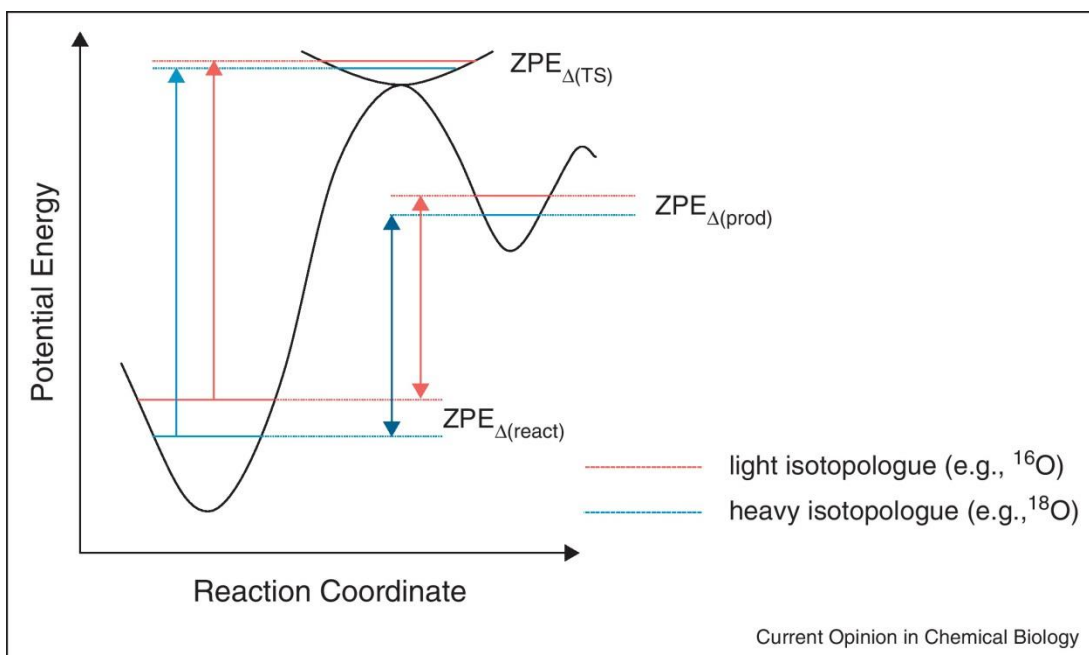


**Figure 9** – A diagram showing that the difference in energy between the reactant and transition state bond energies for a to a heavier isotope (in this case deuterium) is greater than the difference in energy between the reactant and transition state bond energies for a to a lighter isotope (in this case hydrogen)<sup>57</sup>. This is the reason a normal kinetic isotope effect is observed.

Inverse kinetic isotope effects exist, where  $\frac{k_H}{k_D} < 1$ , in a small number of cases. Rapid pre-equilibria, for example specific acid catalysis, see a greater equilibrium constant for the heavier isotope ( $D_3O^+$  is a stronger acid than  $H_3O^+$ ) and this effect is more significant than the normal kinetic isotope effect, meaning that the reaction involving the heavier isotope is the faster one<sup>58</sup>. Various other explanations have been considered for specific cases.

It is uncommon for kinetic isotope effects to be discussed in the context of hydrogenation over a heterogeneous catalyst. One study showed a small inverse kinetic isotope effect for the hydrogenation of benzene over nickel<sup>59</sup>, with a more recent investigation suggesting that the inverse kinetic isotope effect for ring hydrogenation becomes more significant with increasing alkyl chain length<sup>60</sup>, with

toluene, ethylbenzene and *n*-propylbenzene hydrogenation producing  $k_{\text{H}}/k_{\text{D}}$  values of 0.57, 0.51 and 0.39 respectively.

This thesis will draw on the present understanding of the mechanisms and kinetics of hydrogenation for different unsaturated functionalities, as well as the studies carried out with regard to the kinetic isotope effect. It will combine these with results from a number of reactions, some involving deuterium and some competitive, and aims to build on a body of knowledge which is beginning to take account of molecules which have multiple functionalities.

## 2 Aims of the Project

Overall, the aim of the project is to work towards understanding the selectivity found in hydrogenation of molecules which have unsaturated functionality through the optimisation of conditions and the use of competitive species.

In order to assess such reactions, the change in concentration of each molecule over time will be monitored under different conditions. The data gathered will be used to calculate kinetic and thermodynamic parameters which will provide an insight into the individual processes which contribute to the overall reaction.

The two reaction schemes to be investigated are given in Figures 10-11.

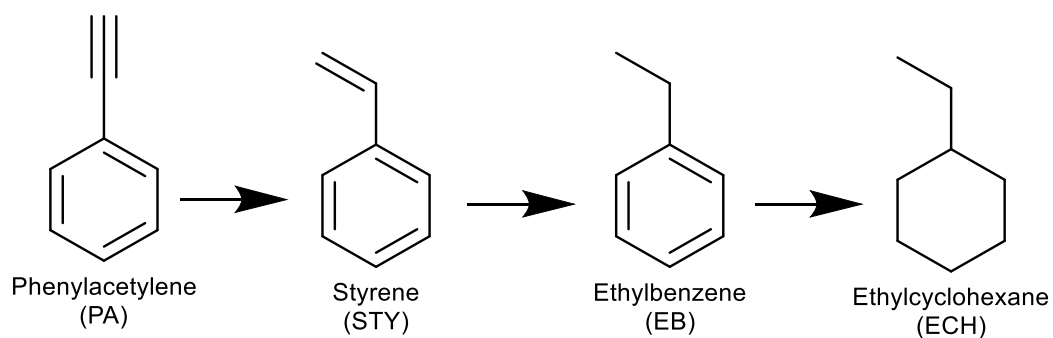


**Figure 10 – The reaction scheme for the hydrogenation of phenylacetylene.**

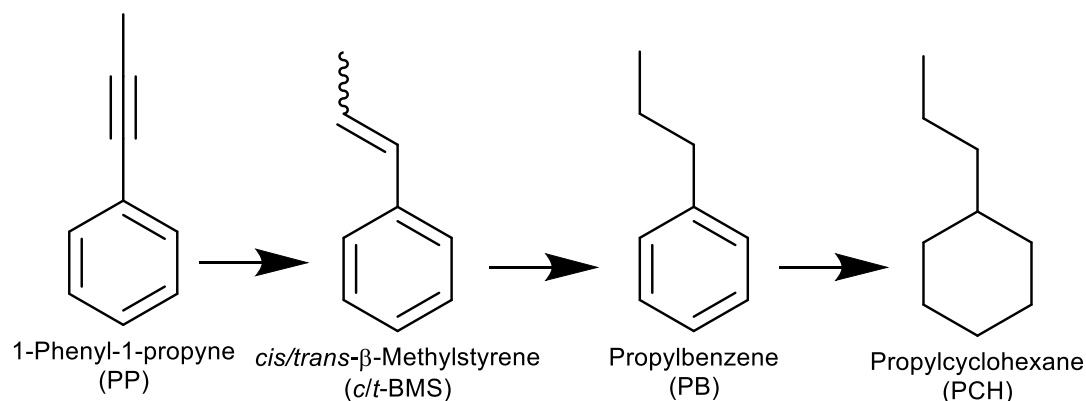


**Figure 11 – The reaction scheme for the hydrogenation of 1-phenyl-1-propyne.**

Competitive reactions will make up part of the project and will be used to assess the interplay of different molecules within the same reaction scheme as well as looking at how reaction schemes change when they proceed alongside other reactions.

## 3 Experimental

This section will cover the practical aspects of the investigation and includes a description of how the experiments were carried out as well as information regarding the instrumentation used.

### 3.1 Instrumentation

This section details the instrumentation used in experiments, the results of which are presented in Section 4.

#### 3.1.1 Stirred Tank Reactor

The reactor used was a Büchi stirred autoclave with an oil jacket and a hydrogen-on-demand system. This consisted of a 1L Büchi stirred tank reactor, a Büchi pressflow gas controller and a Julabo heating circulator for temperature control; a thermocouple connected to the heating circulator was used to monitor the temperature. The reactant gas used was H<sub>2</sub> and the inert gas was N<sub>2</sub>. An injection port existed for the introduction of the reactant to the reactor and a scavenge tap provided a means for releasing pressure. A testo 460 control was used to set the speed of the stirrer. Figure 12 shows a diagram of the reactor.

Typically, the mass balance of the reactions was 100±5%.

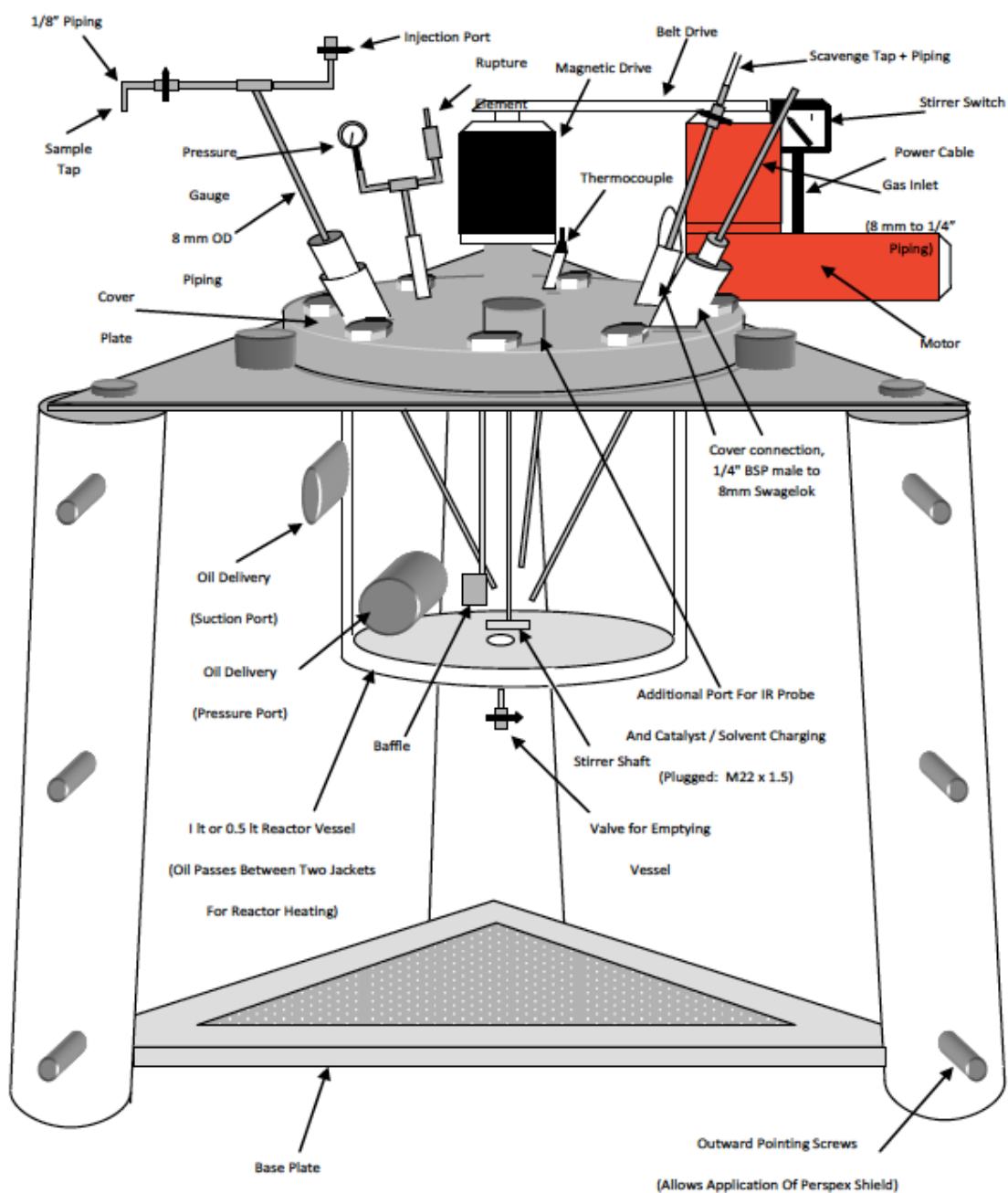


Figure 12 – Diagram of the 1 L reactor used.

### 3.1.2 NMR

$^2\text{H}$  NMR Spectroscopy was performed on samples from selected experiments. The instrument used was a Bruker AVIII 500 MHz Spectrometer. Samples were taken at 10, 40 and 180 minutes of appropriate reactions for analysis.

### 3.1.3 Thermo-Gravimetric Analysis (TGA)

TGA was performed on post-reaction catalysts that had been used for the hydrogenation of phenylacetylene, styrene and 1-phenyl-1-propyne at 50°C and 70°C. The instrument used was a TGA/DSC SDT Q600 thermal analyser coupled with an ESS mass spectrometer following m/z peaks at 2, 14, 15, 16, 17, 18, 28, 30, 32, 44 and 46 AMU. The TGA of samples with a typical weight of 10 mg was carried out under 2%  $\text{O}_2/\text{Ar}$  (100 mL  $\text{min}^{-1}$ ) with the temperature increasing by 10°C  $\text{min}^{-1}$  until it reached 1000°C.

### 3.1.4 Gas Chromatography

A Focus GC with HP 1701, 30 m long, 0.25 mm diameter, 1.0  $\mu\text{m}$  film thickness column was used to analyse the samples taken. The settings were 1  $\mu\text{L}$  injection volume, 230°C injector temperature, helium carrier gas with a flow rate of 1 mL  $\text{min}^{-1}$  and 300°C detector temperature.

Calibrations of reactants and expected products were taken prior to the reactions using 10%, 30%, 50%, 70% and 100% standards of a 0.04 mol  $\text{L}^{-1}$  solution in isopropyl alcohol. The peak areas were used to produce a calibration plot to allow for unknown concentrations to be calculated from chromatograms. The calibration plots are given in Figure 13 and the results are displayed in Table 1. A calibration plot of *cis*- $\beta$ -methylstyrene could not be produced, as the *cis*- $\beta$ -methylstyrene is commercially unavailable, so the relationship between peak area and concentration was assumed to

be the same as that of *trans*- $\beta$ -methylstyrene, as both molecules have identical masses and functionality, as well as similar structures.

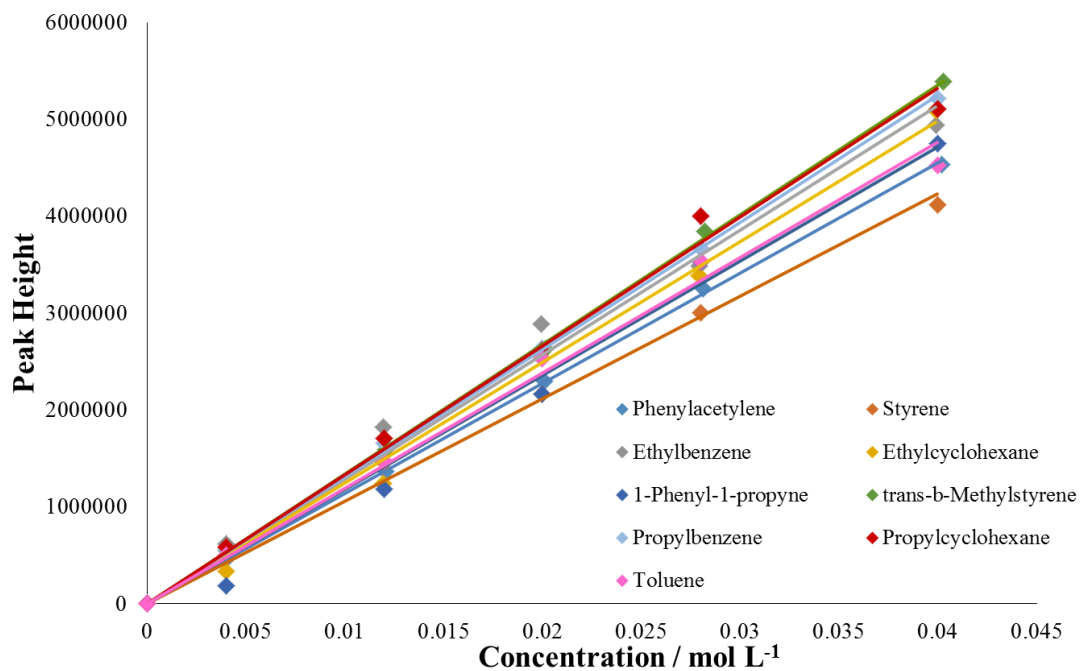


**Figure 13 – A calibration plot to determine the relationship between the concentration and peak area of the standards in the Focus GC which was used for the duration of the project.**

**Table 1 – The conversion factors and R<sup>2</sup> values for the standards in the Focus GC which was used for the duration of the project.**

<b>Molecule</b>	<b>Peak Area ÷ Concentration / L mol<sup>-1</sup></b>	<b>R<sup>2</sup></b>
Phenylacetylene	113758624.00	1.00
Styrene	1057906731.91	0.99
Ethylbenzene	128402833.17	0.99
Ethylcyclohexane	124482400.29	0.99
1-Phenyl-1-propyne	117842203.80	0.99
<i>trans</i> -β-Methylstyrene	133749282.55	1.00
Propylbenzene	131121421.20	1.00
Propylcyclohexane	132951240.49	0.99
Toluene	118976843.75	0.99

### 3.2 Chemicals

The chemicals used are detailed in Table 2; there were no further purification steps.

**Table 3 – The name, supplier and purity of all chemicals, other than those mentioned in the remainder of Section 3.4, used in the experiments which contributed to this thesis.**

<b>Name</b>	<b>Supplier</b>	<b>Purity (%)</b>
Ethynylbenzene (Phenylacetylene)	Sigma Aldrich	98
1-Phenyl-1-propyne	Sigma Aldrich	99
<i>trans</i> -Propenylbenzene ( <i>trans</i> - $\beta$ -Methylstyrene)	Sigma Aldrich	99
Ethylbenzene	Sigma Aldrich	$\geq 99.5$
Ethylcyclohexane	Sigma Aldrich	$\geq 99$
Propylbenzene	Sigma Aldrich	98
Propylcyclohexane	Sigma Aldrich	99
2-Propanol (Isopropyl alcohol)	Sigma Aldrich	$\geq 99.5$
Toluene-d <sub>8</sub>	Sigma Aldrich	$\geq 99$ (chemical) 99 (isotope)

### 3.2.1 Styrene

Styrene (Sigma Aldrich,  $\geq 99.5\%$ ) is stored as a mixture with a stabiliser (4-*tert*-butylcatechol) due to its tendency to polymerise when stored as a pure liquid. The stabiliser has the potential to poison the catalyst and, for this reason, it was necessary to distil the styrene shortly before use. This was done using a standard vacuum distillation setup as depicted in Figure 14.

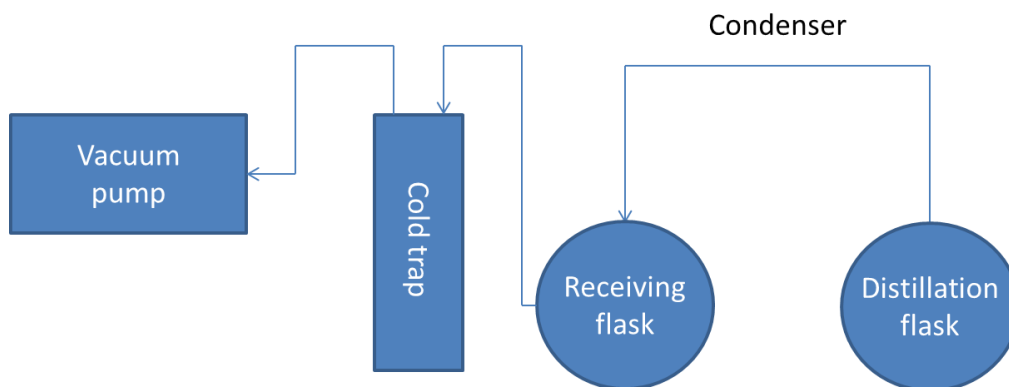


**Figure 14 – A representation of the vacuum distillation setup used to obtain pure styrene.**

### **3.2.2 Catalyst**

A rhodium/silica catalyst supplied by Johnson Matthey was used in all reactions. Its properties are given in Table 4.

**Table 4 – A table of properties of the rhodium/silica catalyst used for all experiments which contributed to this thesis.**

<b>Batch number</b>	M01078
<b>Pore size / nm</b>	13.2
<b>Average metal crystallite size / nm</b>	2.2
<b>Surface area / m<sup>2</sup> g<sup>-1</sup></b>	321
<b>Rhodium dispersion / %</b>	50
<b>Rhodium surface area / m<sup>2</sup> g<sup>-1</sup></b>	5.5
<b>Total pore length / m g<sup>-1</sup></b>	7740
<b>Weight loading of rhodium / %</b>	2.5

### 3.3 Method

Rhodium/SiO<sub>2</sub> catalyst (0.1 g) suspended in isopropyl alcohol (310 mL) was reduced under hydrogen (0.5 barg, 100 mL min<sup>-1</sup>) in the Büchi stirred autoclave at 70°C for 30 minutes with stirring at 1000 rpm. The pressure was then released through the scavenge tap and the reaction vessel temperature adjusted to the appropriate temperature for the reaction. The reactant (10 mmol), dissolved in isopropyl alcohol (40 mL) by sonication for 15 minutes and degassed with argon for 25 minutes, was injected into the reaction vessel and the reaction mixture was stirred at 1000 rpm for 15 seconds. Stirring was ceased and nitrogen was then used to pressurise the reaction vessel to 0.5 barg. The sample for time = 0 minutes was taken. The pressure was released and stirring at 1000 rpm (unless otherwise stated) resumed before the reaction vessel was pressurised with hydrogen (3 barg). Samples were taken at 5, 10, 15, 20, 25, 30, 40, 50, 60, 80, 100, 120, 140, 160 and 180 minutes and difference in hydrogen

moles over the sampling period was recorded; stirring was ceased during the sampling period.

## 3.4 Reactions

### 3.4.1 Mass Transfer Limitation Analysis

The effect of stirrer speed on the rate of reaction was analysed in order to determine whether the rate of reaction was being influenced by mass transfer. If so, it would show that the catalysts surface is not demonstrating maximum saturation and thus the kinetics would not be governed solely by the behaviour of the molecules on the catalyst surfaces.

The reactant used in temperature analysis reactions was phenylacetylene. The reactions were carried out at 50° with stirrer speeds of 500 rpm, 750 rpm, 1000 rpm and 1500 rpm.

For these reactions, no samples were taken, but hydrogen consumption (mol) was recorded from a display on the hydrogen-on-demand system at 5 minute intervals. The reaction was stopped when no hydrogen was consumed over a 20 minute period.

### 3.4.2 Analysis of Temperature Dependence

The dependence of the initial rate of a reaction on temperature can be used to determine the activation energy.

If the initial rate is approximated to be zero order in a reactant, then the rate at which the concentration of reactant ( $[R]$ ) depletes is equal to the zero order rate constant ( $k_0$ ):

$$\frac{d[R]}{d[t]} = -k_0$$
$$-\int d[R] = \int k_0 dt$$

$$-[R] = k_0 t$$

Thus, a plot of  $[R]_0 - [R]$  against time ( $t$ ), where  $[R]_0$  is the initial concentration of reactant, gives a gradient  $k_0$ .

The rate constants at different temperatures can then be used to determine the activation energy through the manipulation of the Arrhenius equation:

$$k = A e^{-\frac{E_a}{RT}}$$

$$\ln k = -\frac{E_a}{RT} + \ln A$$

where  $A$  is the pre-exponential factor,  $E_a$  is the activation energy,  $R$  is the gas constant and  $T$  is the temperature.

Thus, a plot of  $\ln k$  against  $\frac{1}{T}$  gives a gradient of  $-\frac{E_a}{R}$ , from which the activation energy can be calculated.

The reactants used in temperature analysis reactions were ethylbenzene, styrene, phenylacetylene, propylbenzene and 1-phenyl-1-propyne. The reactions were carried out at 40°C, where appropriate, 50°C, 60°C and 70°C.

### 3.4.3 Reactions with Deuterium and Determination of Kinetic Isotope Effect

The kinetic isotope effect was calculated using rate constants for the hydrogenation of the appropriate molecules under hydrogen ( $k_H$ ) and deuterium ( $k_D$ ).

The reactants used in temperature analysis reactions were styrene, phenylacetylene and 1-phenyl-1-propyne. The reactions were carried out at 50° and 70°C.

### 3.4.4 Competitive Reactions

Competitive reactions were used to assess the simultaneous interaction of different molecules with the catalyst.

The combinations of reactants used in competitive reactions were ethylbenzene and phenylacetylene, styrene and phenylacetylene, propylbenzene and 1-phenyl-1-propyne, phenylacetylene and 1-phenyl-1-propyne, toluene-d<sub>8</sub> and phenylacetylene, and toluene-d<sub>8</sub> and 1-phenyl-1-propyne. The reactions were carried out at 50°C and, where appropriate, 70°C.

It should be noted that 10 mmol of each reactant was used in these reactions in order that comparisons can be made with previous reactions.

## 4 Results

### 4.1 Reactions

The rate constants for the reported reactions were determined using zero order plots; first order plots also provided a good fit for some experiments, but after consideration of rate plots at different temperatures, a zero order plot was deemed most appropriate for all molecules studied.

#### 4.1.1 Mass Transfer Limitation Analysis

Reactions were carried out at different stirrer speeds to determine at which stirrer speed no mass transfer effects limited the rate of hydrogenation. To determine which speed was required hydrogen consumption was plotted against time, shown in Figures 15, 17, 19 and 21. Zero order rate constants were also calculated in Figures 16, 18, 20 and 22.

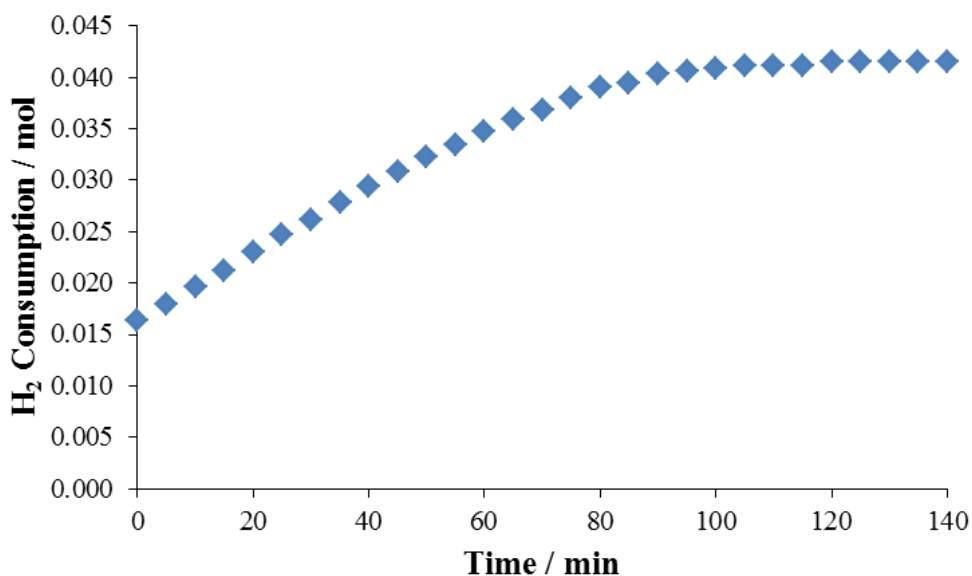


**Figure 15 – Hydrogen consumption profile for the hydrogenation of phenylacetylene at 500 rpm.**

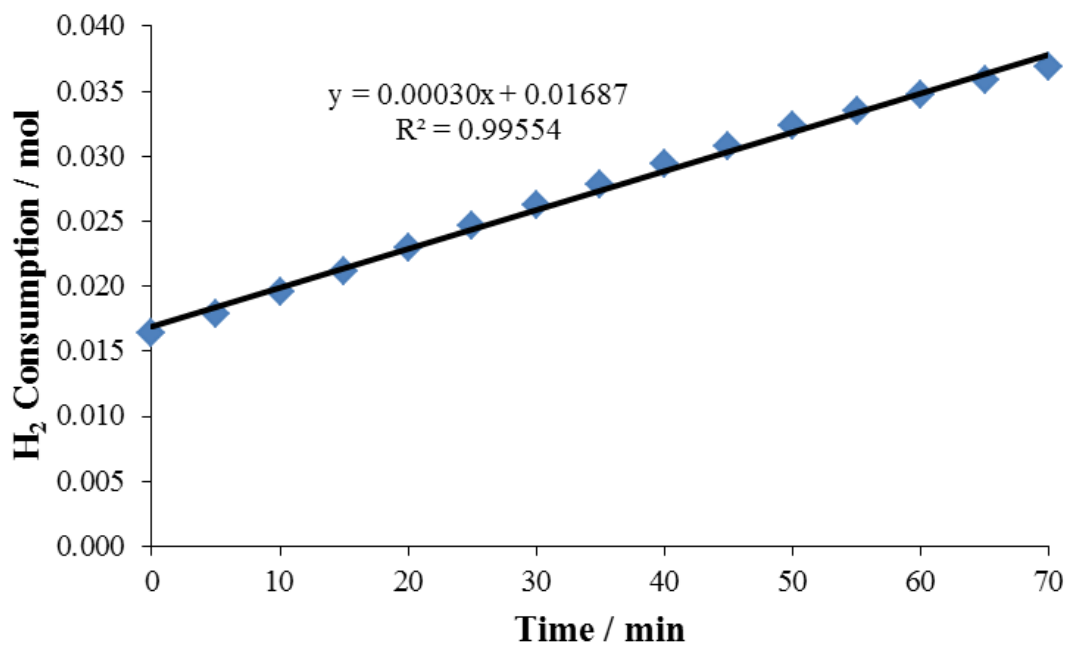


Figure 16 – A zero order plot of hydrogen consumption against time at 500 rpm for the hydrogenation of phenylacetylene.

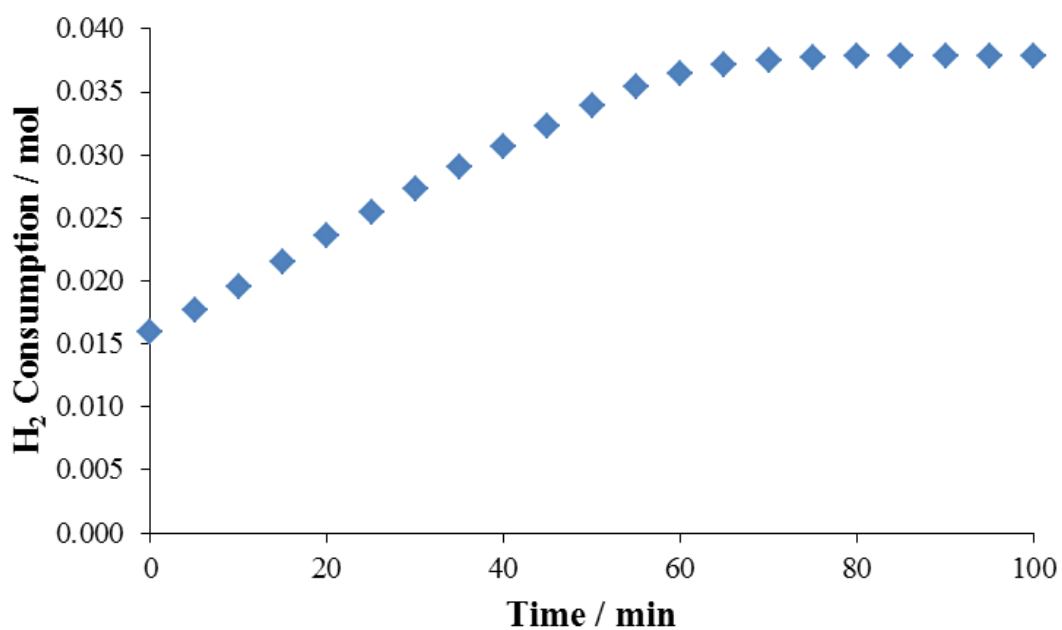


Figure 17 – Hydrogen consumption profile for the hydrogenation of phenylacetylene at 750 rpm.

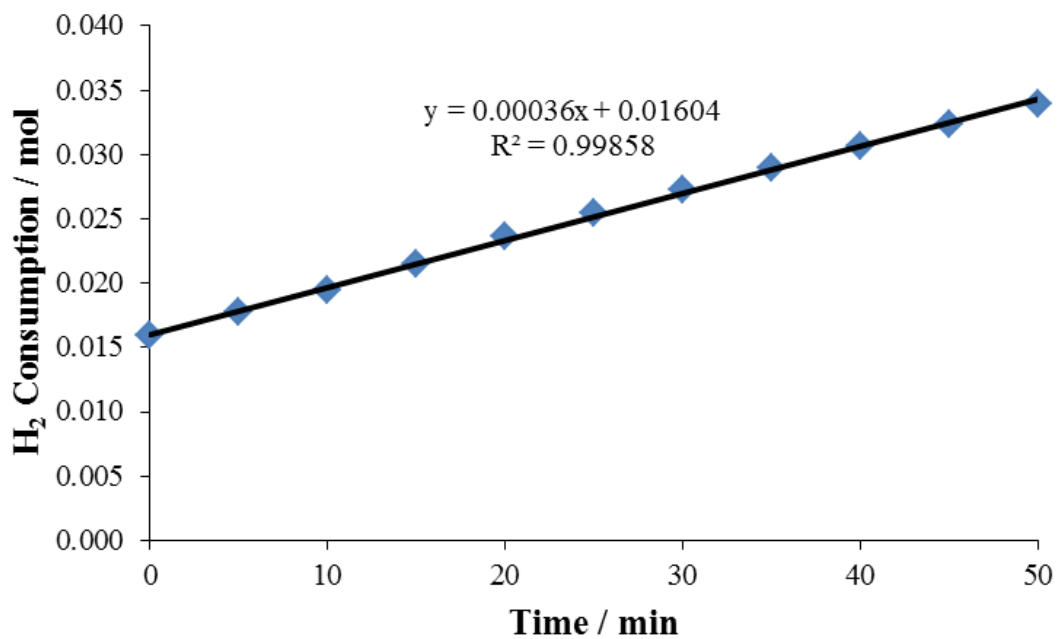


Figure 18 – A zero order plot of hydrogen consumption against time at 750 rpm for the hydrogenation of phenylacetylene.

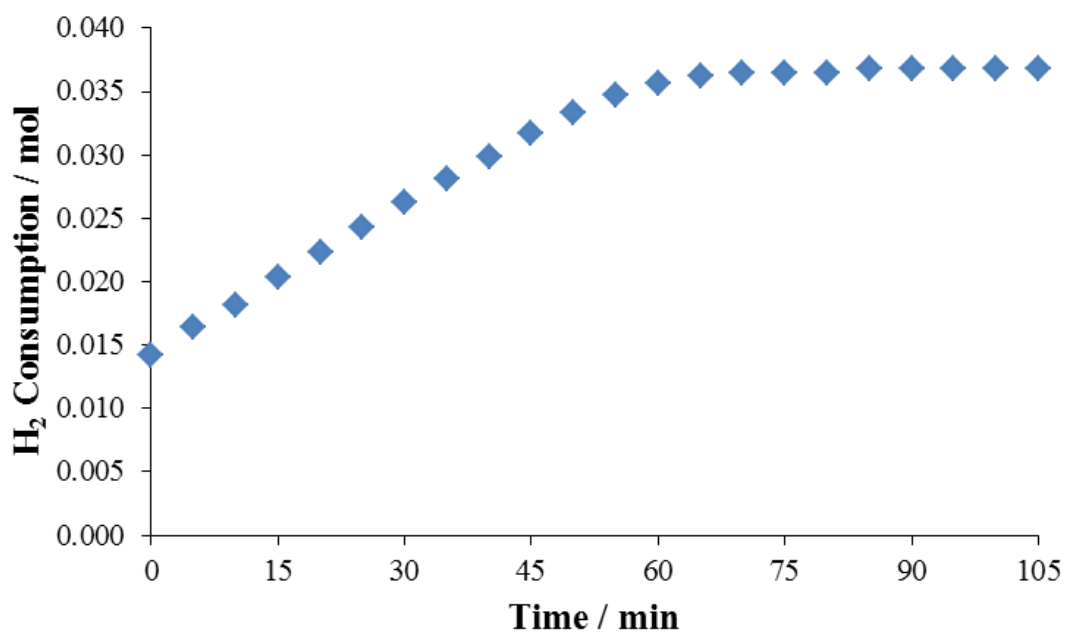


Figure 19 – Hydrogen consumption profile for the hydrogenation of phenylacetylene at 1000 rpm.

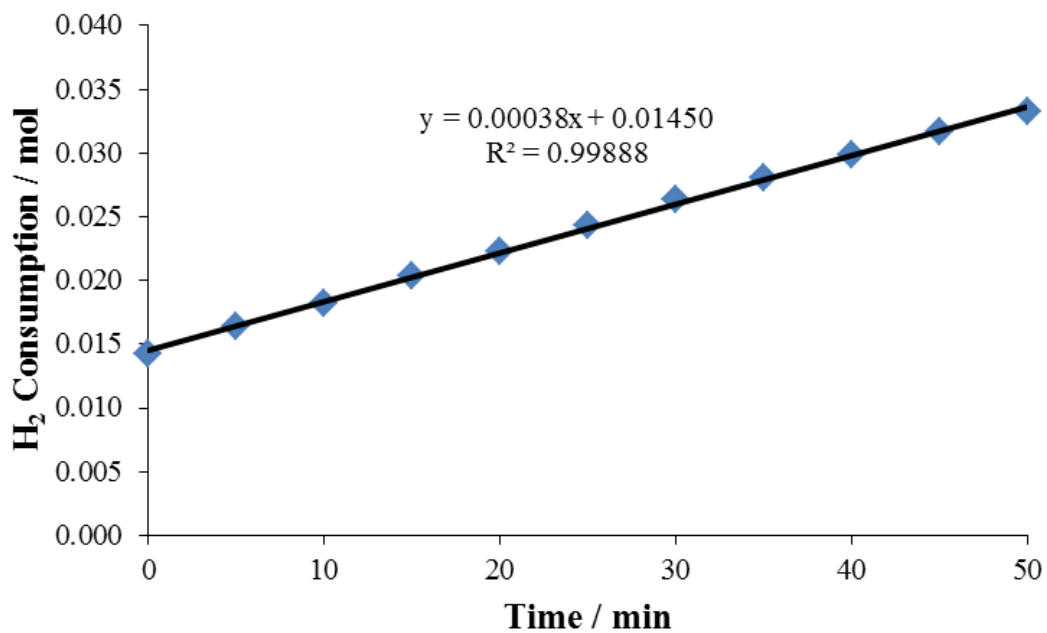


Figure 20 – A zero order plot of hydrogen consumption against time at 1000 rpm for the hydrogenation of phenylacetylene.

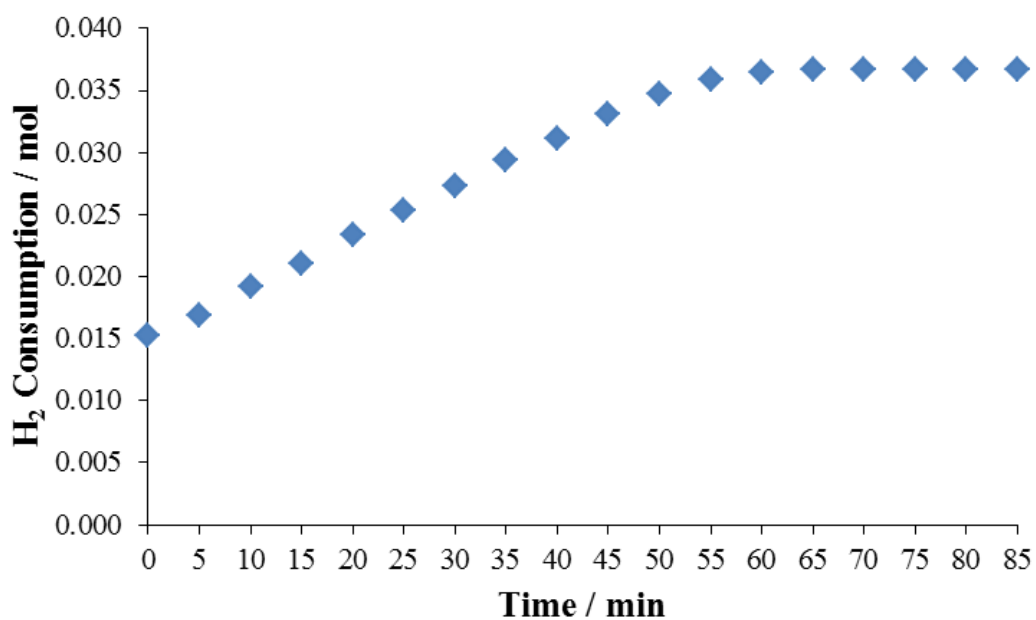
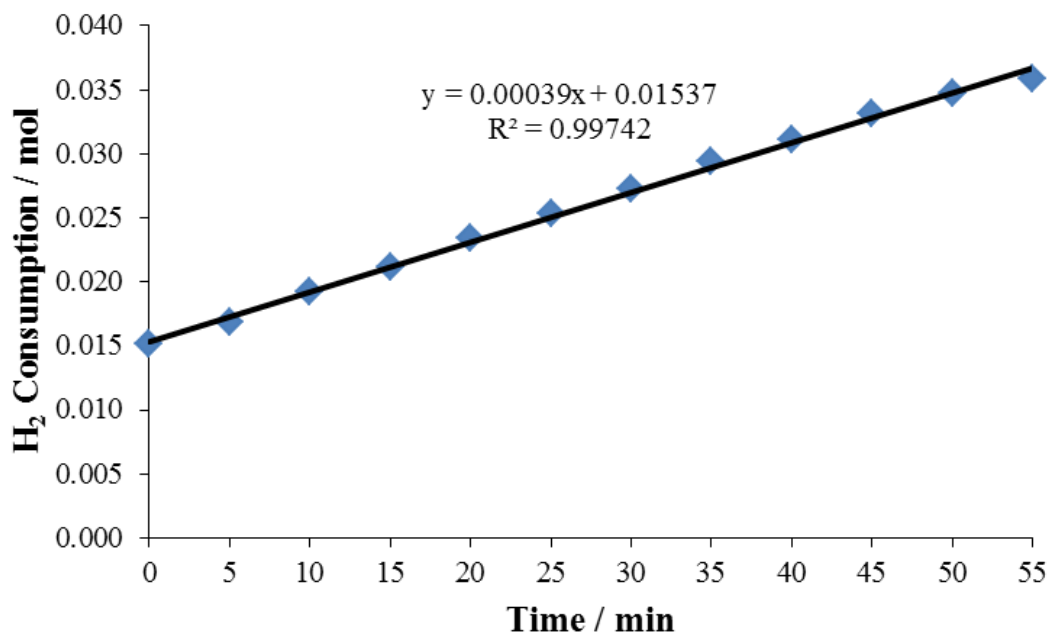


Figure 21 – Hydrogen consumption profile for the hydrogenation of phenylacetylene at 1500 rpm.



**Figure 22 – A zero order plot of hydrogen consumption against time at 1500 rpm for the hydrogenation of phenylacetylene.**

The initial rate constants at each stirrer speed are given in Table 5.

**Table 5 – The initial rate constants of hydrogen consumption in the hydrogenation of phenylacetylene at different stirrer speeds.**

Stirrer Speed / rpm	Initial Rate Constant, $k_0$ / mol min <sup>-1</sup>
500	0.00030
750	0.00036
1000	0.00038
1500	0.00039

Therefore a stirrer speed of 1000 rpm was used throughout this work.

#### 4.1.2 Temperature Dependence

The temperature dependence of the rates of hydrogenation was assessed in order to calculate the activation energy of each molecule, as set out in Section 3.2.1. The following results show the reaction profiles and the zero order plots to determine the rate constants for hydrogenation of phenylacetylene, ethylbenzene, 1-phenyl-1-propyne, and propylbenzene under the conditions described in Section 3.2.1 and the activation energies calculated from them according to the method described in Section 3.2.1, with an Arrhenius plot of  $\ln k$  against  $\frac{1}{T}$ . The observed rates of reaction for the alkene-substituted molecules were too high to accurately report, but hydrogenation reactions of styrene were carried out.

A reaction profile for each reaction was plotted using the mole fractions calculated from the chromatograms.

The reaction profiles for phenylacetylene over the temperature range 40-70°C are shown in Figures 23, 25, 27 and 29. Zero order plots were also constructed and are shown in Figures 24, 26, 28 and 30. Initially, the phenylacetylene mole fraction decreased and the styrene mole fraction increased moderately. As the styrene mole fraction approached 50%, its increase slowed until it reached a maximum. The styrene mole fraction then rapidly decayed as the phenylacetylene mole fraction reached zero. The ethylbenzene mole fraction increased slowly throughout the first phase of the reaction, then more rapidly once the styrene mole fraction started to decay, until it neared 100%. Ethylcyclohexane was then produced in quantities which were significantly increased by an increase in temperature. Small quantities of ethylcyclohexene were occasionally observed. All aspects of the reaction increased in rate when the temperature was increased.

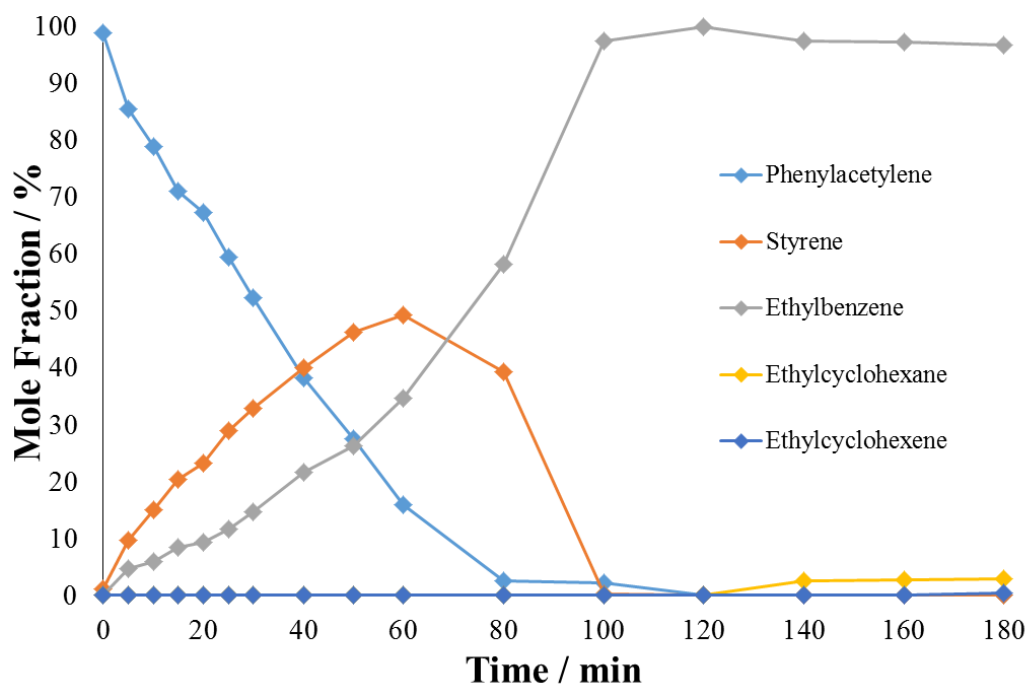


Figure 23 – Reaction profile for the hydrogenation of phenylacetylene. Conditions: 3 barg  $H_2$ , 10 mmol phenylacetylene, 40°C.

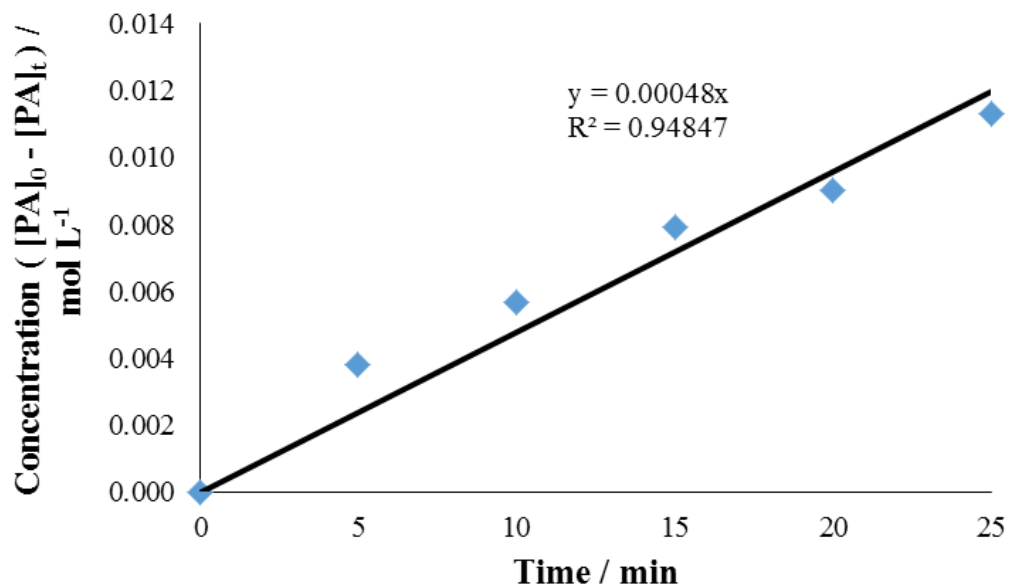


Figure 24 – Zero order plot to determine the initial rate constant of phenylacetylene hydrogenation at 40°C.

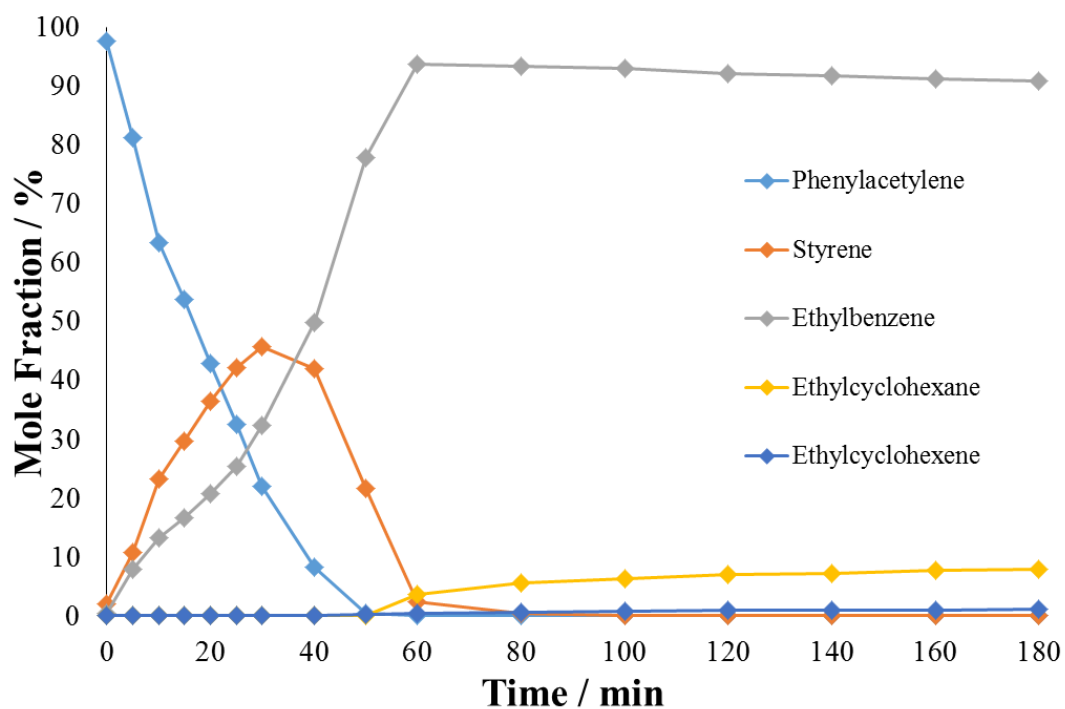


Figure 25 – Reaction profile for the hydrogenation of phenylacetylene. Conditions: 3 barg  $H_2$ , 10 mmol phenylacetylene, 50°C.

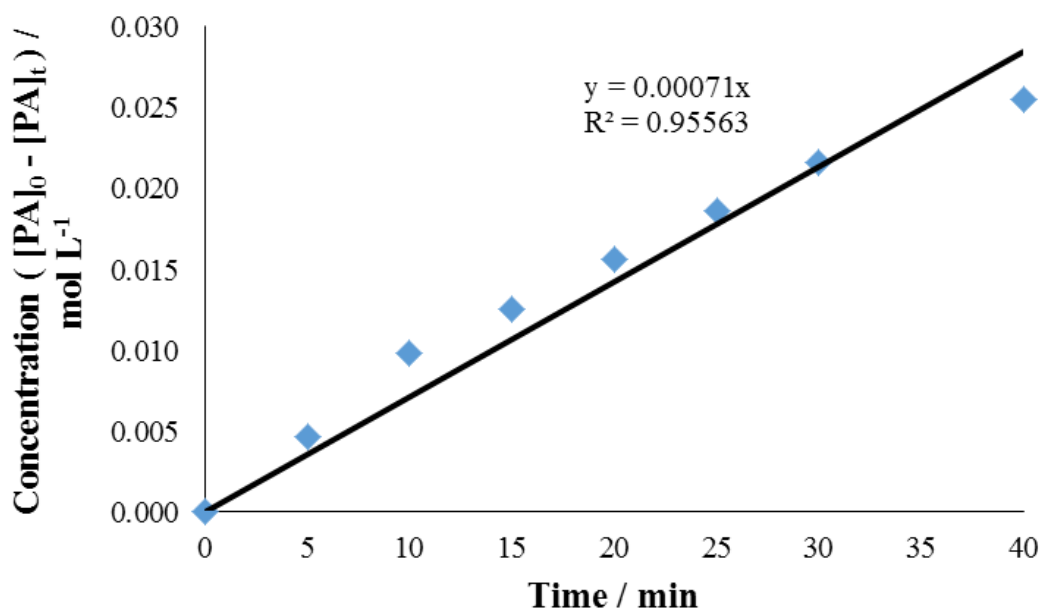


Figure 26 – Zero order plot to determine the initial rate constant of phenylacetylene hydrogenation at 50°C.

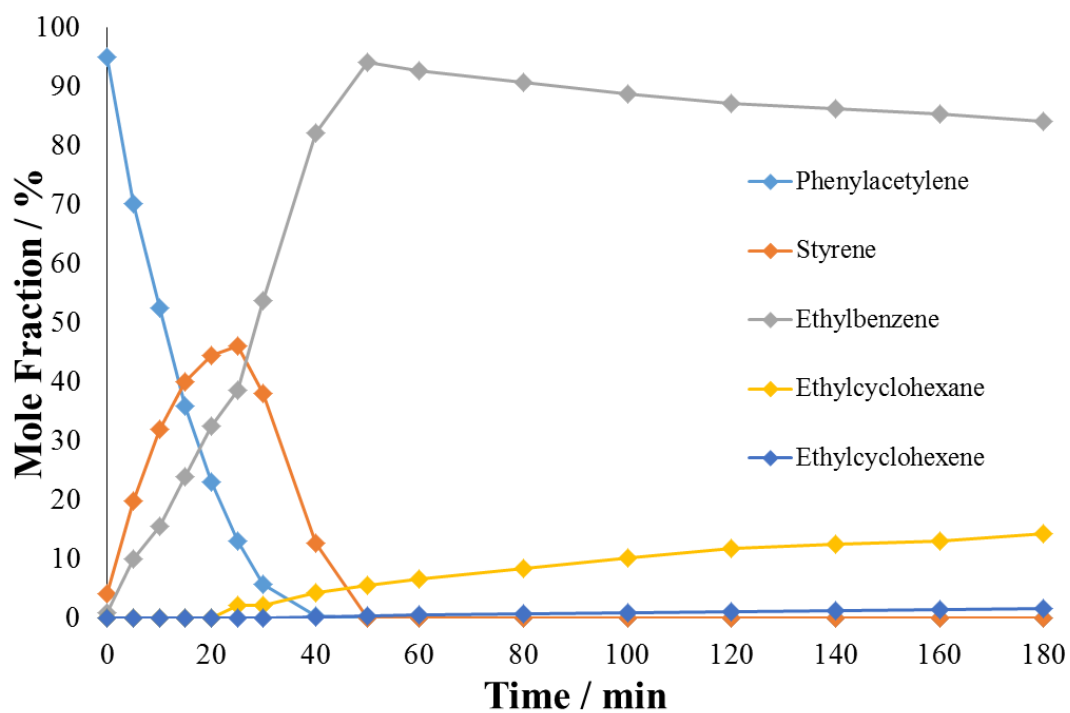


Figure 27 – Reaction profile for the hydrogenation of phenylacetylene. Conditions: 3 barg  $H_2$ , 10 mmol phenylacetylene, 60°C.

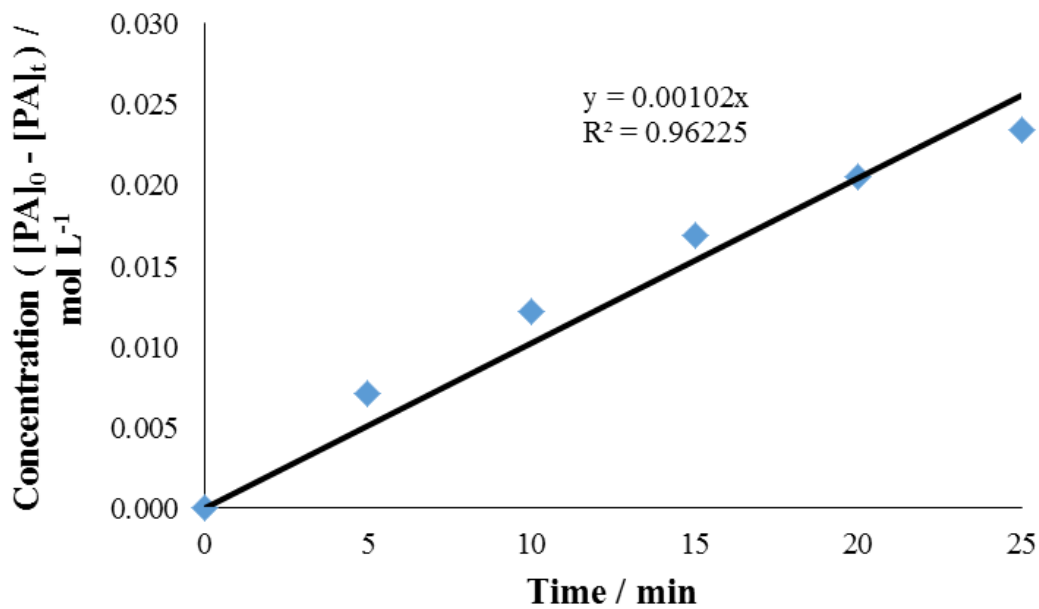


Figure 28 – Zero order plot to determine the initial rate constant of phenylacetylene hydrogenation at 60°C.

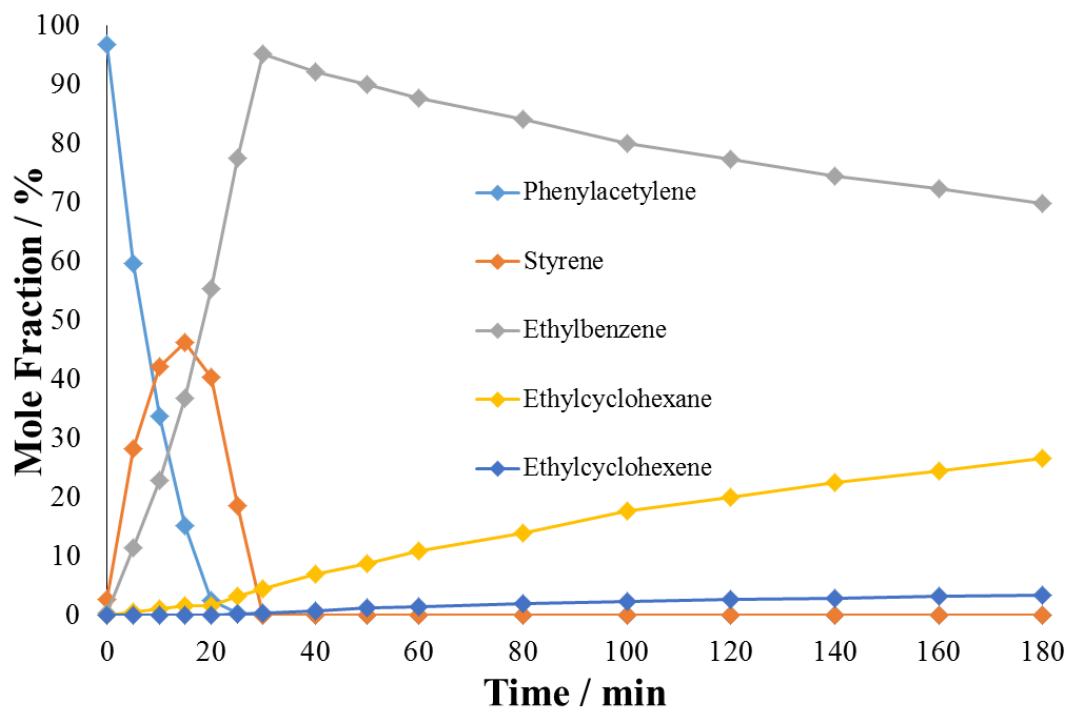


Figure 29 – Reaction profile for the hydrogenation of phenylacetylene. Conditions: 3 barg  $H_2$ , 10 mmol phenylacetylene, 70°C.

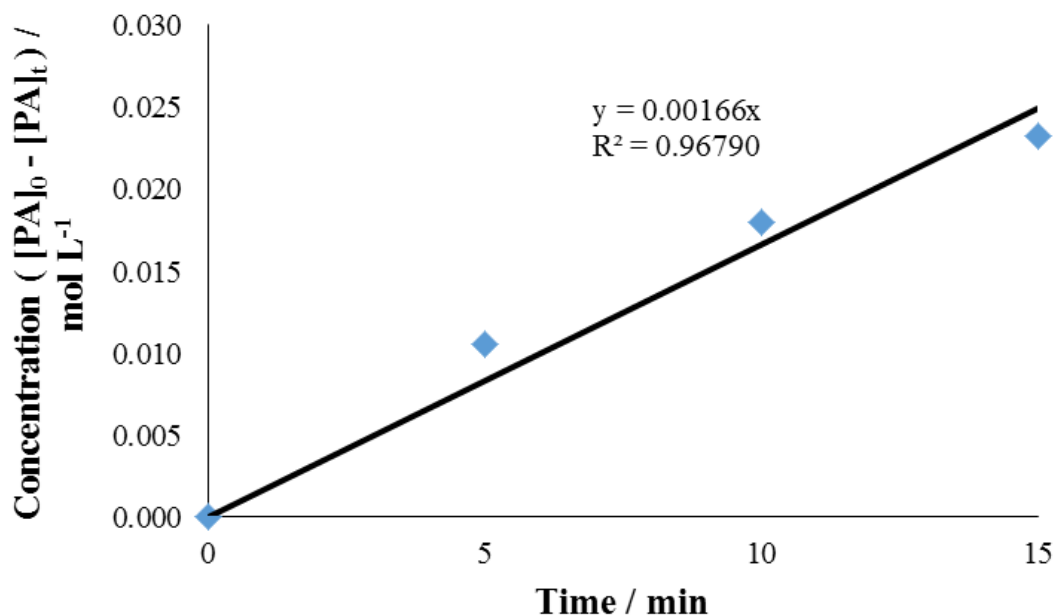
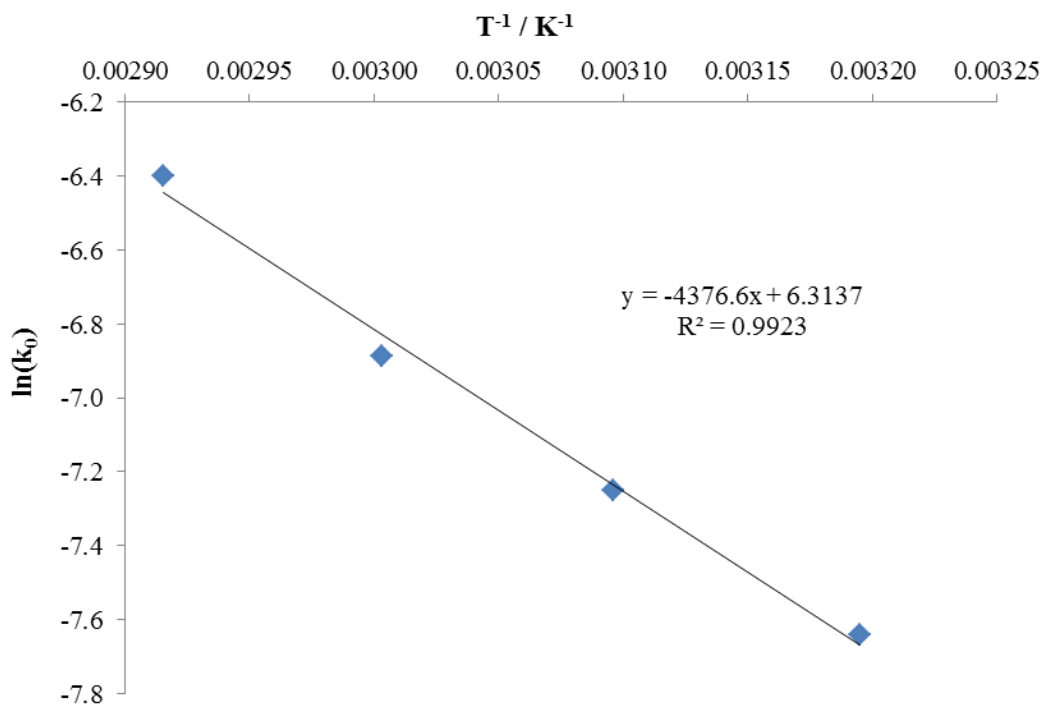


Figure 30 – Zero order plot to determine the initial rate constant of phenylacetylene hydrogenation at 70°C.

Kinetic data from the hydrogenation of phenylacetylene is displayed in Table 6.

**Table 6 – Phenylacetylene temperature dependence. It was observed that the time taken to reach 100% conversion decreased and the initial rate constant increased with increasing temperature.**

<b>Temperature / K</b>	313	323	343	353
<b>Time for complete conversion / min</b>	120	60	50	30
<b>Initial rate constant, <math>k_0 \times 10^4 / \text{mol L}^{-1} \text{min}^{-1}</math></b>	4.8	7.1	10.2	16.6



**Figure 31 – Arrhenius plot for the hydrogenation of phenylacetylene using the rate constants calculated from the zero order plots shown in Figures 24, 26, 28 and 30.**

From Figure 31 with gradient  $-4376.6$ , the activation energy of phenylacetylene hydrogenation was calculated to be  $36.4 \text{ kJ mol}^{-1}$ .

The reaction profiles for styrene over the temperature range  $40\text{-}70^\circ\text{C}$  are shown in Figures 32, 34, 36 and 38. Zero order plots were also constructed for the hydrogenation of ethylbenzene within the cascade and are shown in Figures 33, 35, 37 and 39. These zero order plots did not exhibit a straight line relationship for styrene hydrogenation, as the reaction was too rapid and, thus, there were insufficient data points. Initially, the styrene mole fraction decreased rapidly, as the ethylbenzene mole fraction increased at a similar rate. After nearing 100%, the ethylbenzene mole fraction started to decay at a rate which increased with temperature. Ethylcyclohexane was then produced in quantities which were significantly increased by an increase in temperature.

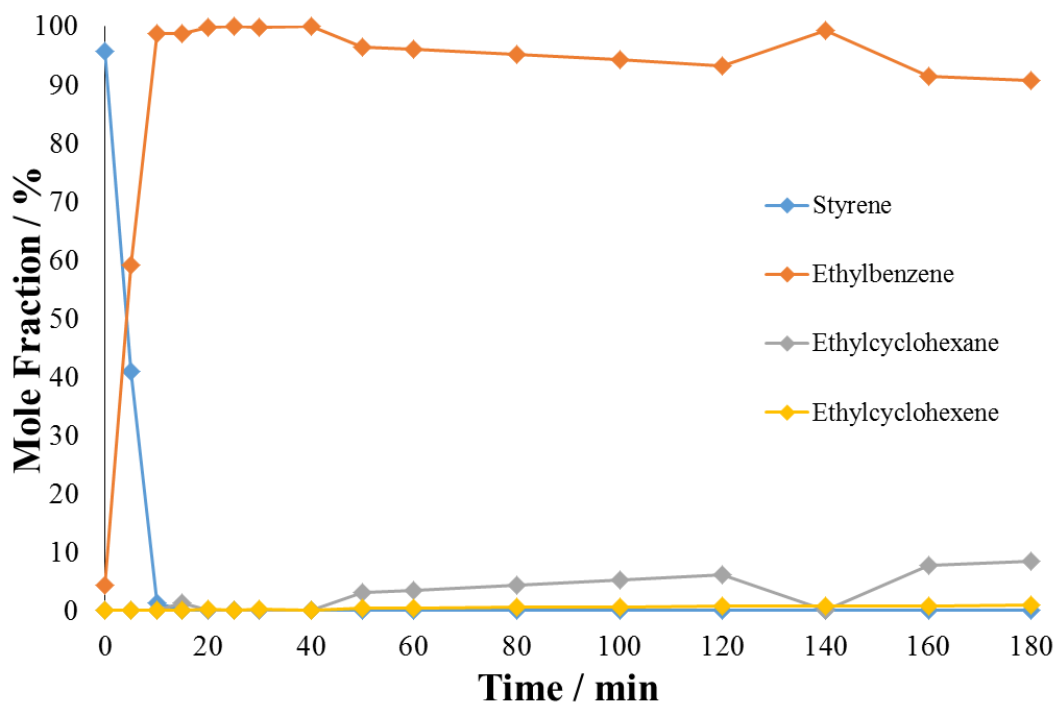


Figure 32 – Reaction profile for the hydrogenation of styrene. Conditions: 3 barg H<sub>2</sub>, 10 mmol styrene, 40°C.

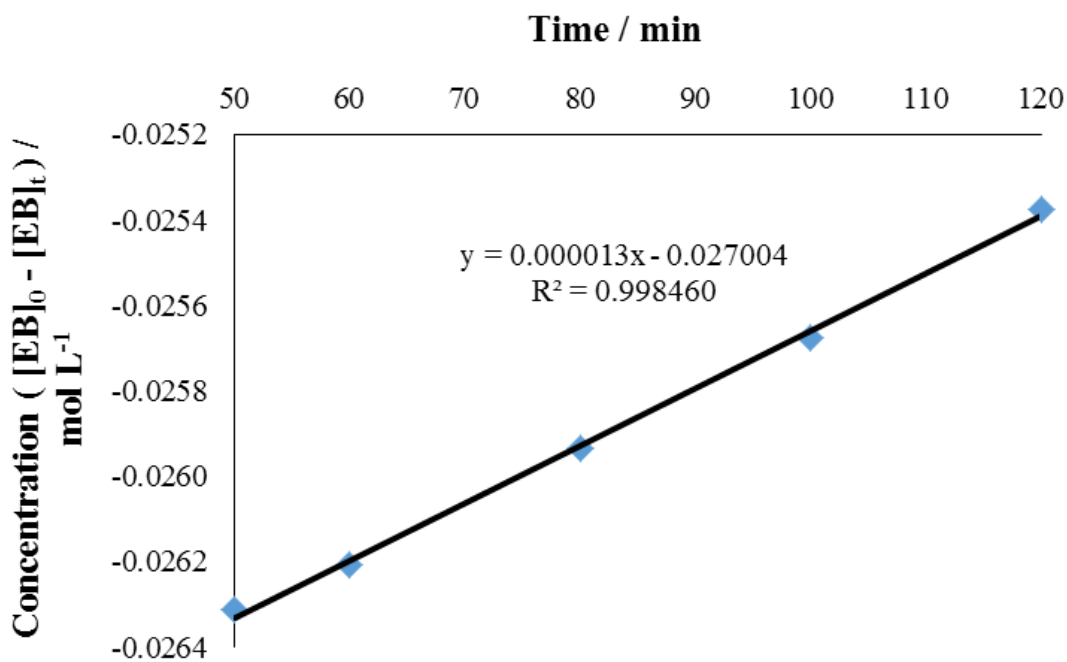


Figure 33 – Zero order plot to determine the initial rate constant of ethylbenzene hydrogenation at 40°C with styrene as the reactant.

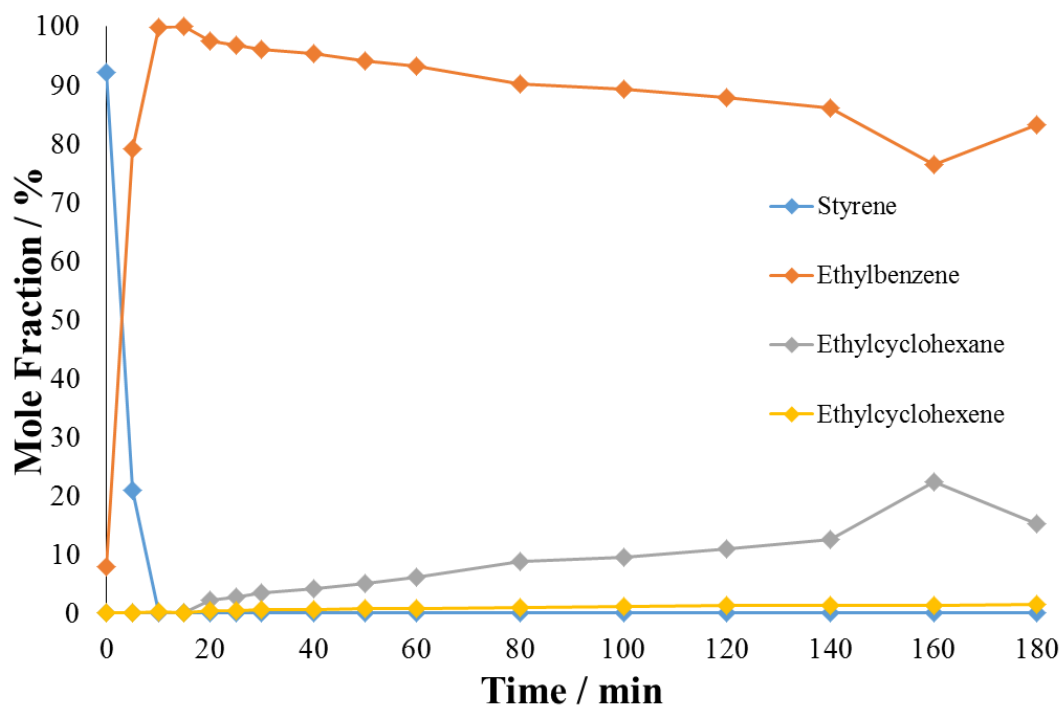


Figure 34 – Reaction profile for the hydrogenation of styrene. Conditions: 3 barg  $H_2$ , 10 mmol styrene, 50°C.

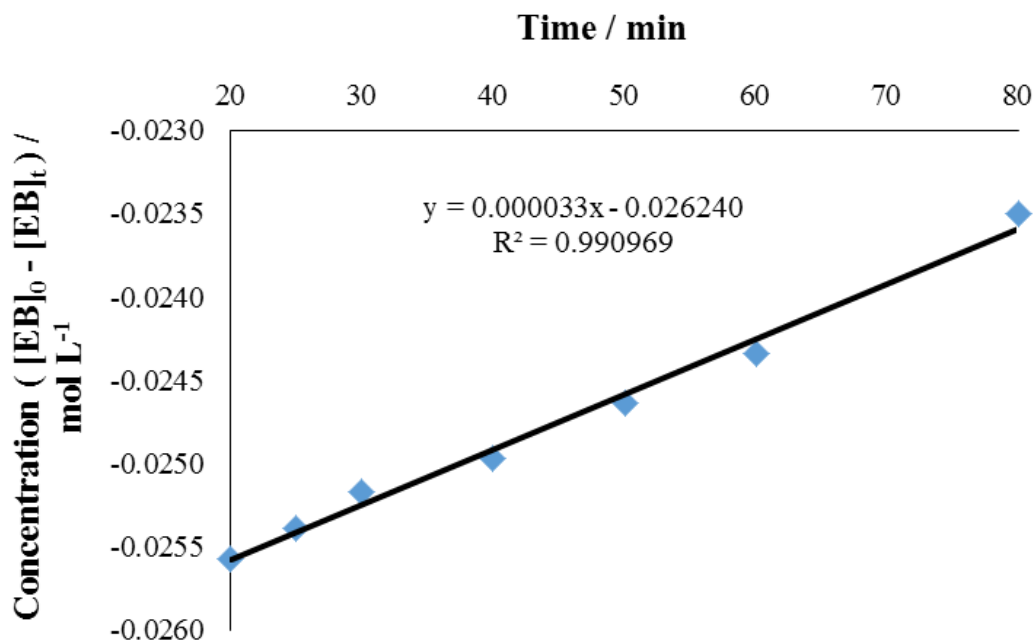


Figure 35 – Zero order plot to determine the initial rate constant of ethylbenzene hydrogenation at 50°C with styrene as the reactant.

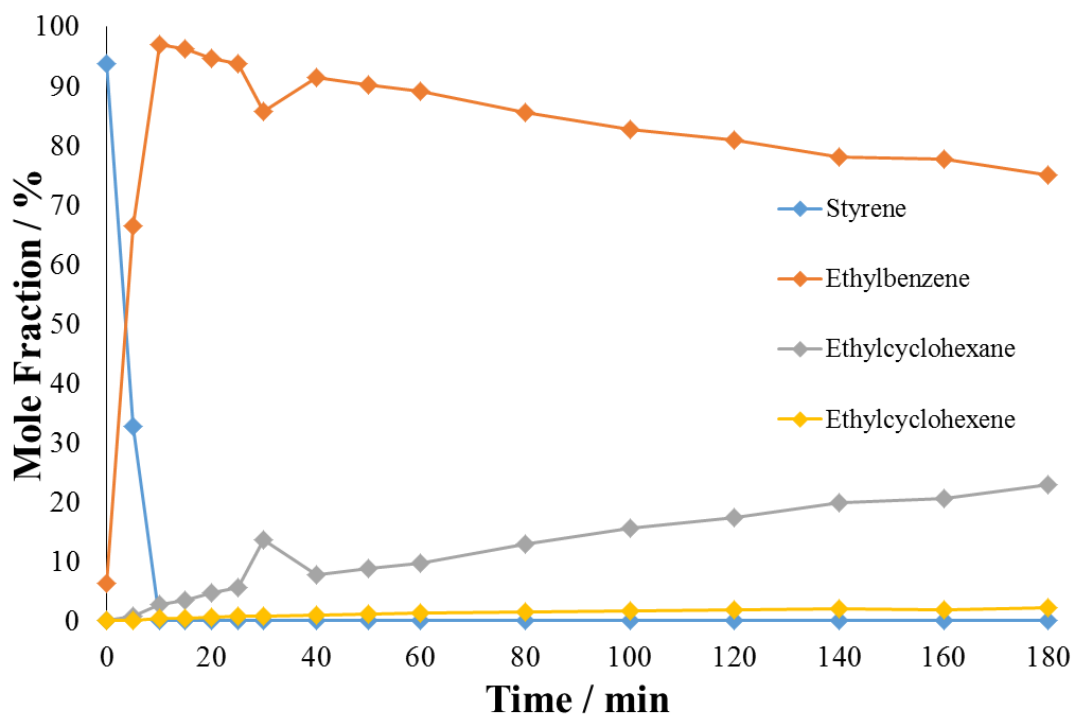


Figure 36 – Reaction profile for the hydrogenation of styrene. Conditions: 3 barg  $H_2$ , 10 mmol styrene, 60°C.

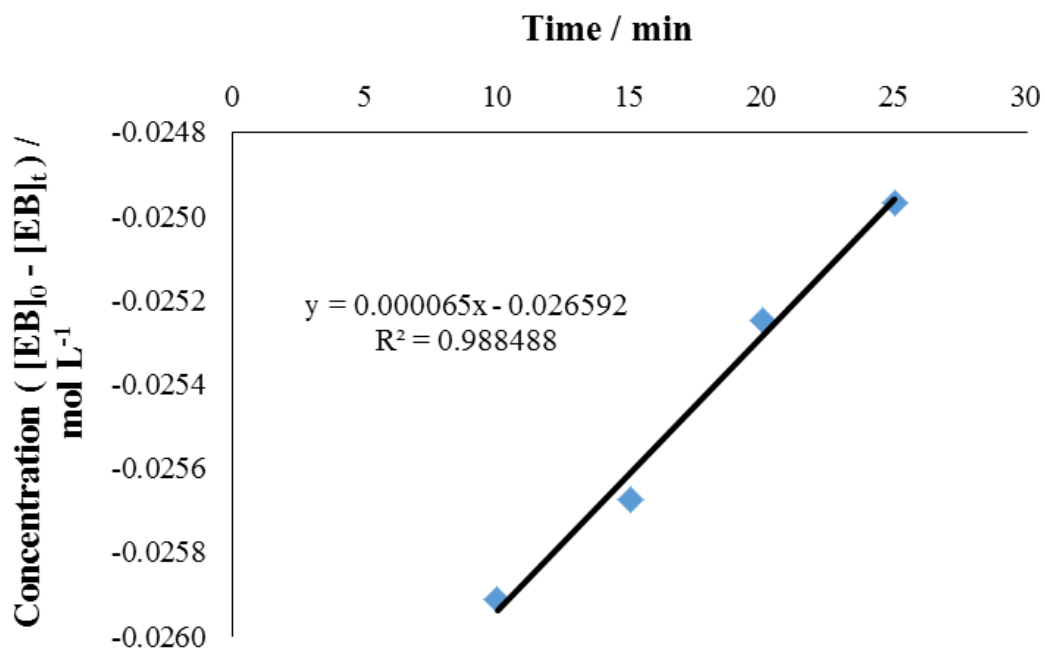


Figure 37 – Zero order plot to determine the initial rate constant of ethylbenzene hydrogenation at 60°C with styrene as the reactant.

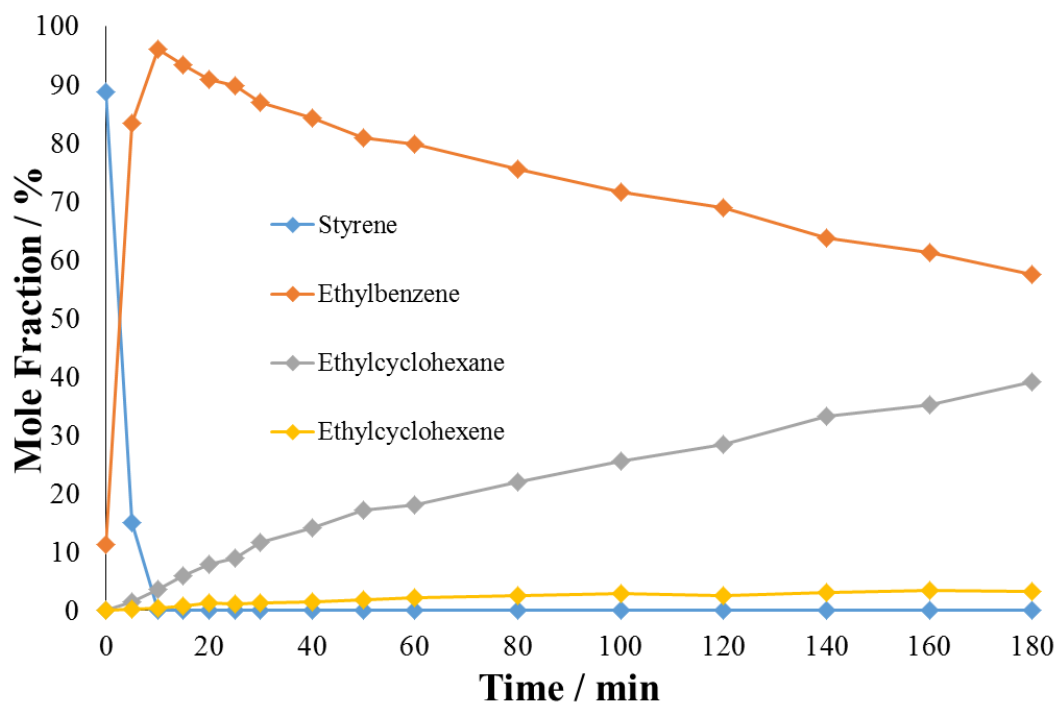


Figure 38 – Reaction profile for the hydrogenation of styrene. Conditions: 3 barg H<sub>2</sub>, 10 mmol styrene, 70°C.

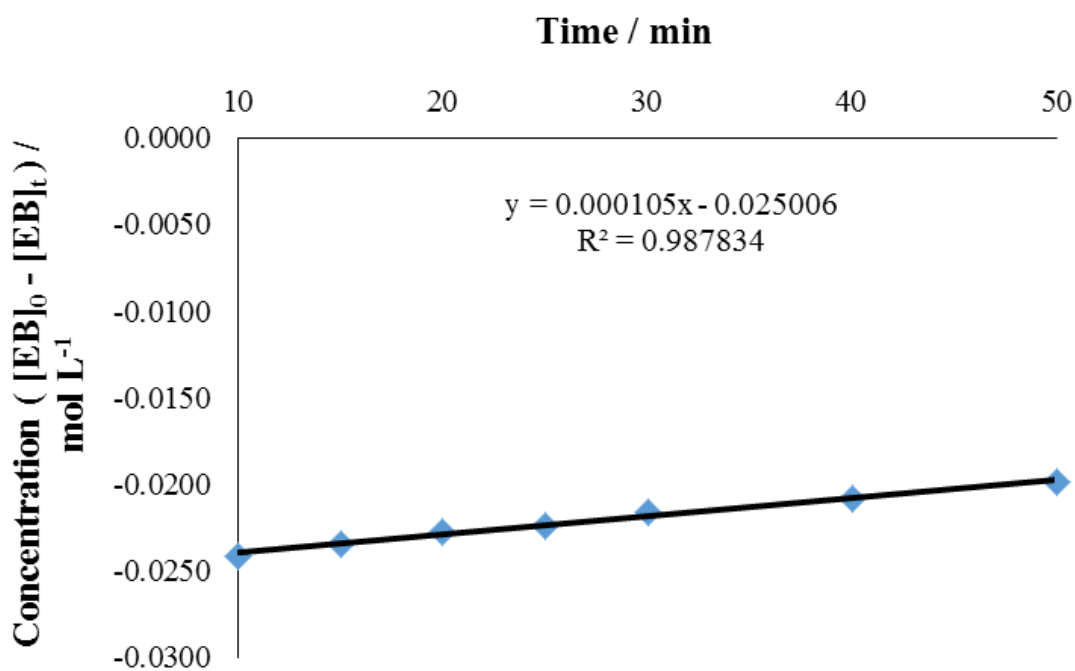
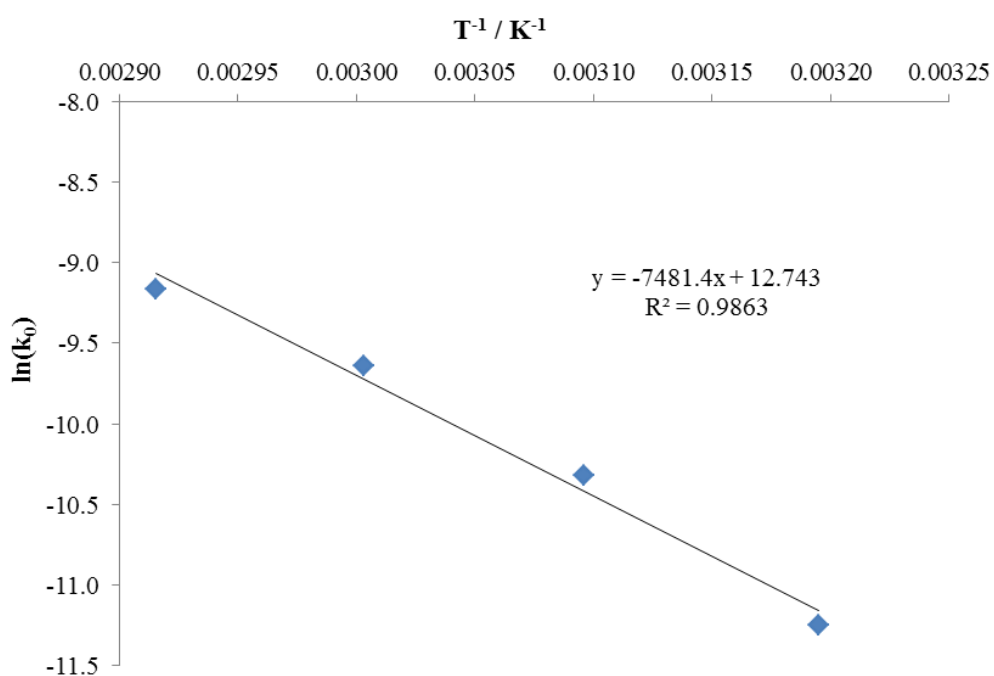


Figure 39 – Zero order plot to determine the initial rate constant of ethylbenzene hydrogenation at 60°C with styrene as the reactant.

Kinetic data relating to the hydrogenation of ethylbenzene with styrene as the reactant is displayed in Table 7.

**Table 7 – Ethylbenzene temperature dependence with styrene as the reactant. It was observed that the initial rate constant increased with temperature.**

<b>Temperature / K</b>	313	323	333	343
<b>Initial rate constant, <math>k_0 \times 10^5</math> / mol L<sup>-1</sup> min<sup>-1</sup></b>	1.3	3.3	6.5	10.5



**Figure 40 – Arrhenius plot for the hydrogenation of ethylbenzene with styrene as the reactant using the rate constants calculated from the zero order plots shown in Figures 33, 35, 37 and 39.**

From Figure 40 with gradient  $-7481.4$ , the activation energy of ethylbenzene hydrogenation with styrene as the reactant was calculated to be  $62.2 \text{ kJ mol}^{-1}$ .

The reaction profiles for ethylbenzene over the temperature range  $50\text{-}70^\circ\text{C}$  are shown in Figures 41, 43 and 45. Zero order plots were also constructed and are shown in Figures 42, 44 and 46. The general trend of the reactions was the slowly decreasing mole fraction of ethylbenzene with the similarly slow increasing ethylcyclohexane mole fraction. Both of these processes increased in rate as temperature was increased. Small quantities of ethylcyclohexene were observed.

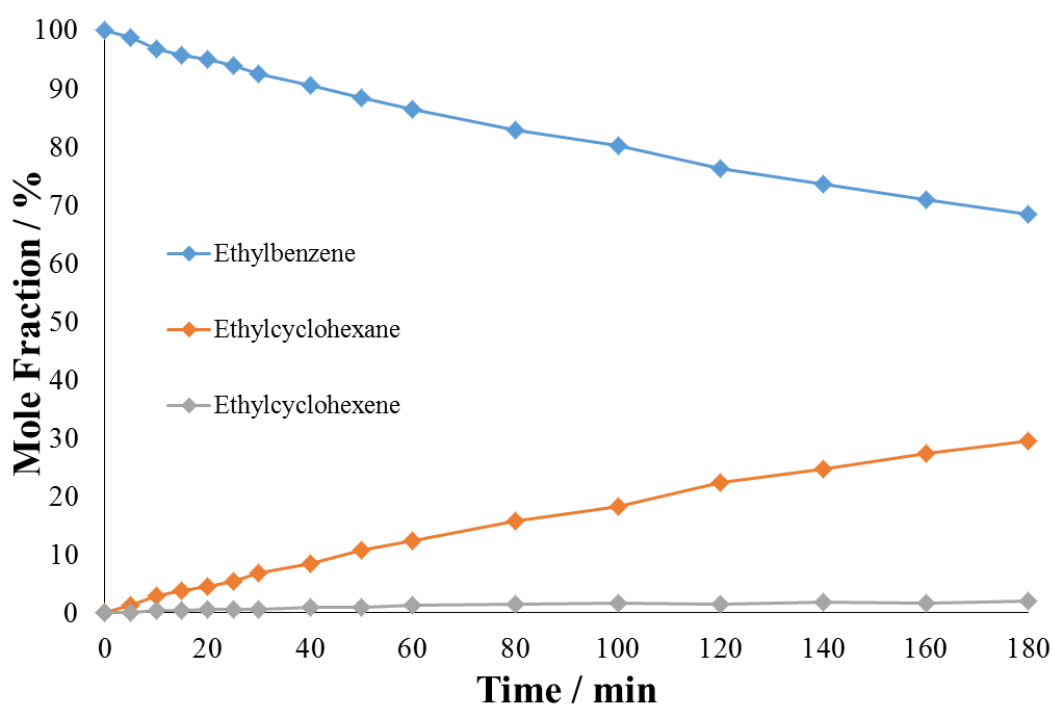


**Figure 41 – Reaction profile for the hydrogenation of ethylbenzene. Conditions: 3 barg  $\text{H}_2$ , 10 mmol ethylbenzene,  $50^\circ\text{C}$ .**

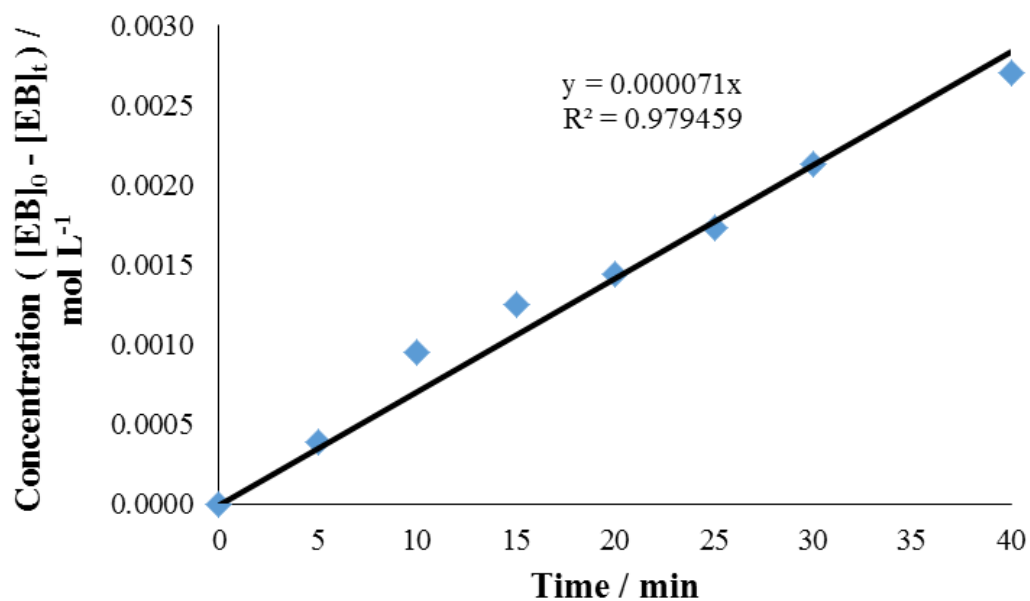


Figure 42 – Zero order plot to determine the initial rate constant of ethylbenzene hydrogenation at 50°C.

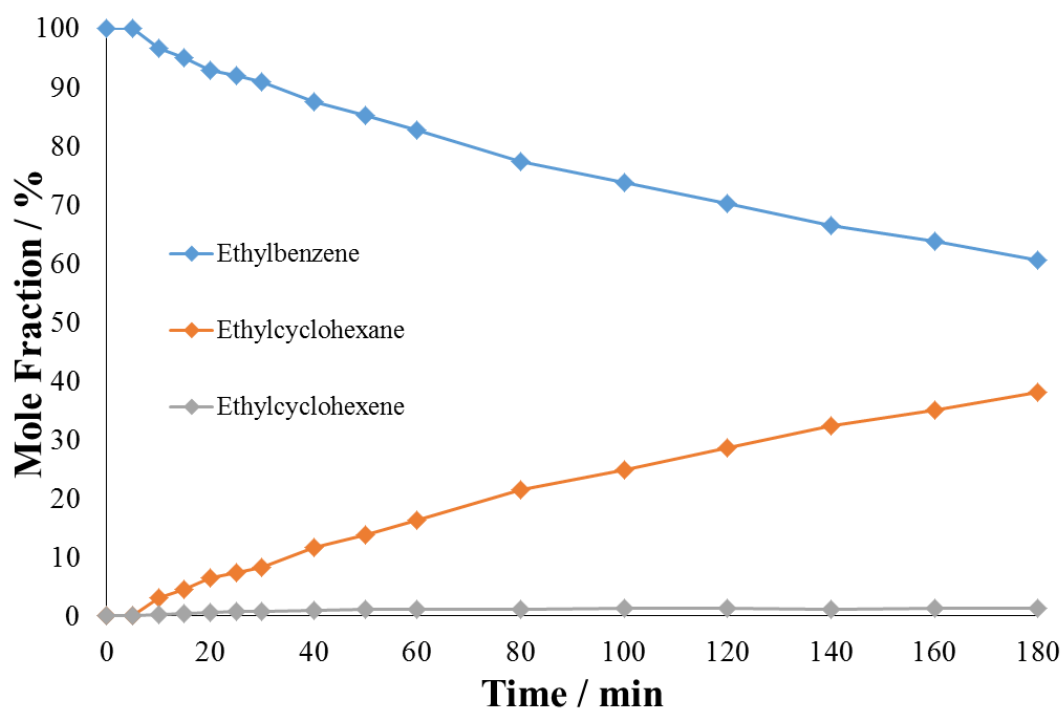


Figure 43 – Reaction profile for the hydrogenation of ethylbenzene. Conditions: 3 barg  $\text{H}_2$ , 10 mmol ethylbenzene, 60°C.

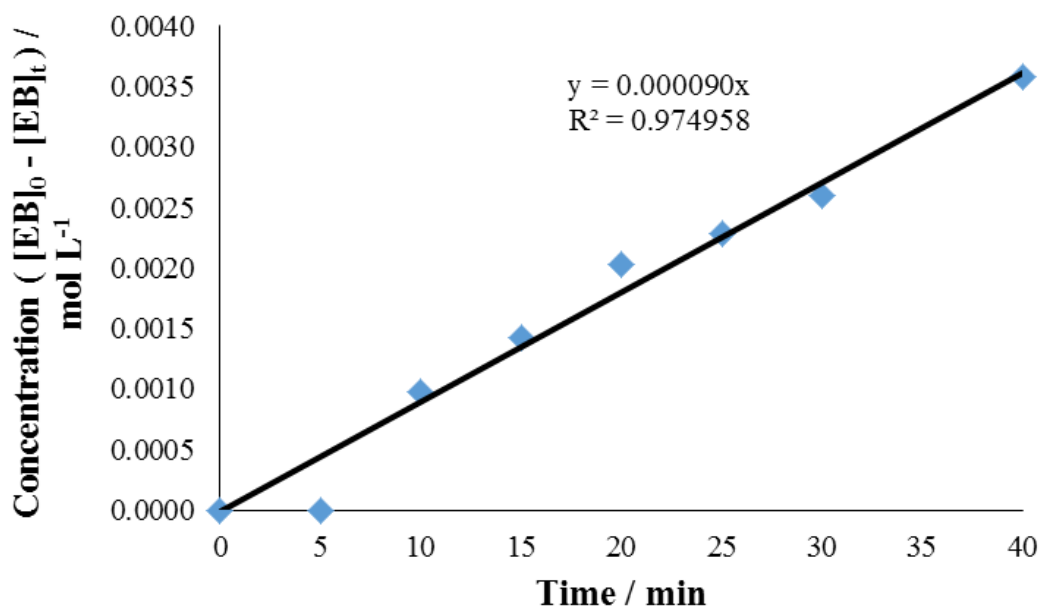


Figure 44 – Zero order plot to determine the initial rate constant of ethylbenzene hydrogenation at 60°C.

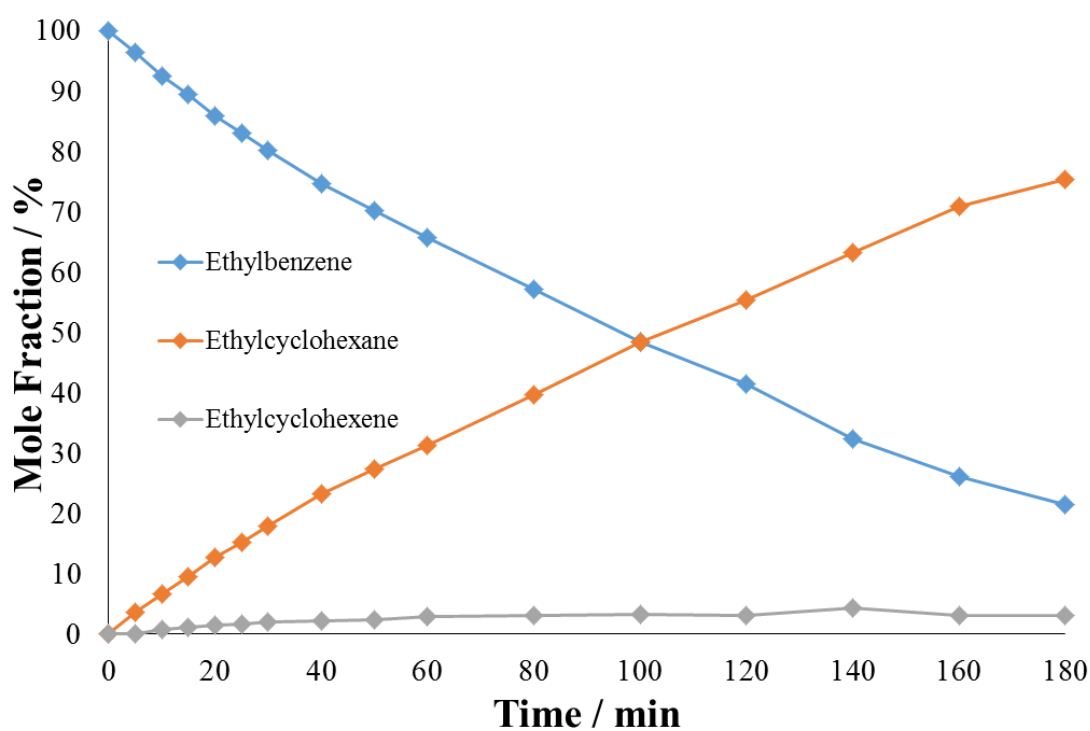
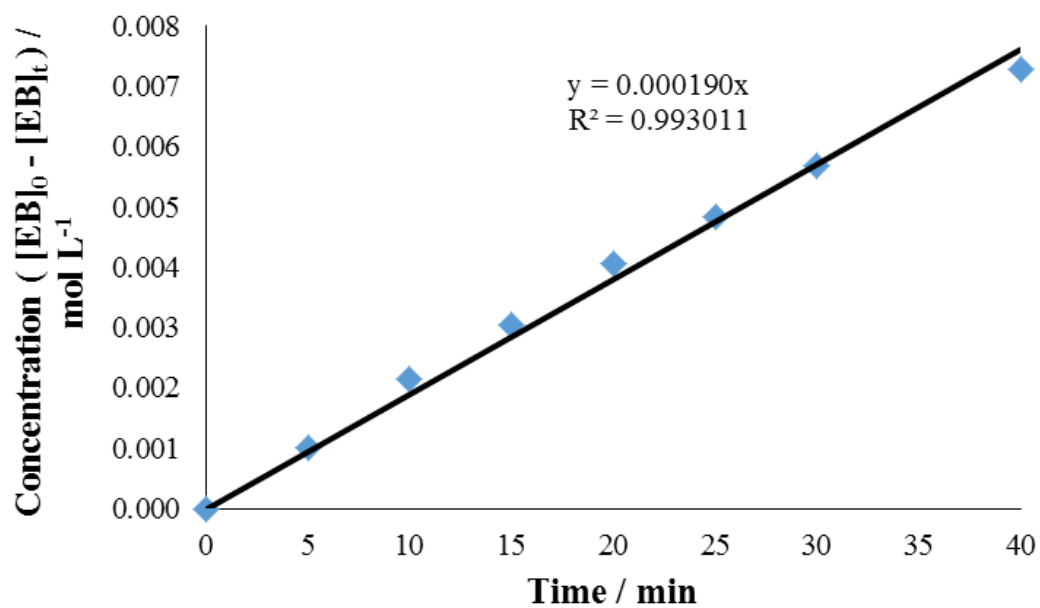


Figure 45 – Reaction profile for the hydrogenation of ethylbenzene. Conditions: 3 barg H<sub>2</sub>, 10 mmol ethylbenzene, 70°C.



**Figure 46 – Zero order plot to determine the initial rate constant of ethylbenzene hydrogenation at 70°C.**

Kinetic data from the hydrogenation of ethylbenzene is displayed in Table 8.

**Table 8 – Ethylbenzene temperature dependence. It was observed that the conversion after 180 minutes and the initial rate constant increased with increasing temperature.**

<b>Temperature / K</b>	323	343	353
<b>Conversion after 180 mins / %</b>	32	39	78
<b>Initial rate constant, <math>k_0 \times 10^5 / \text{mol L}^{-1} \text{min}^{-1}</math></b>	7.1	9.6	19.0

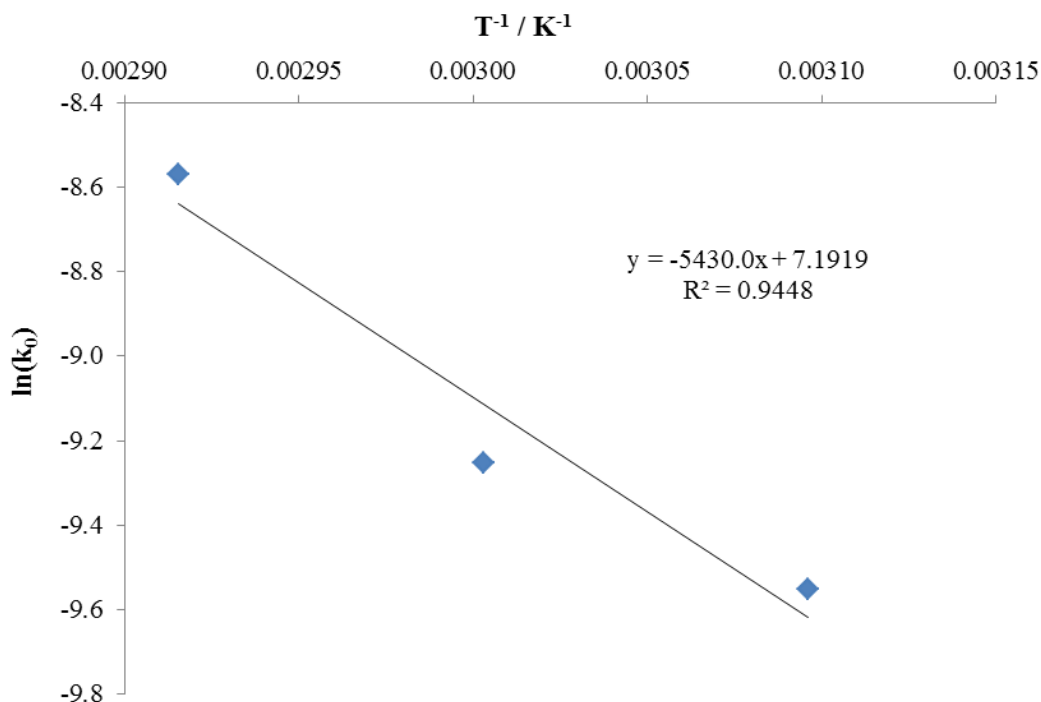


**Figure 47 – Arrhenius plot for the hydrogenation of ethylbenzene using the rate constants calculated from the zero order plots shown in Figures 42, 44 and 46.**

From Figure 47 with gradient -5430.0, the activation energy of ethylbenzene hydrogenation was calculated to be 45.1 kJ mol<sup>-1</sup>.

The reaction profiles for 1-phenyl-1-propyne over the temperature range 40-70°C are shown in Figures 48, 50, 52 and 54. Zero order plots were also constructed and are shown in Figures 49, 51, 53 and 55. Initially, the 1-phenyl-1-propyne mole fraction decreased, the *cis*- $\beta$ -methylstyrene and propylbenzene mole fractions increased moderately and there was a slow increase in the *trans*- $\beta$ -methylstyrene mole fraction. The *cis*- $\beta$ -methylstyrene mole fraction typically reached a maximum at around 30% and then decayed slowly, whilst the propylbenzene mole fraction tended towards 100%. The *trans*- $\beta$ -methylstyrene mole fraction reached a maximum later in the reaction than the *cis*- $\beta$ -methylstyrene, typically at around 10%, then slowly decayed. The propylbenzene mole fraction increased gradually throughout the reaction, but this was one of the slowest observed processes. Small quantities of propylcyclohexene

were occasionally observed. All aspects of the reaction increased in rate when the temperature was increased.

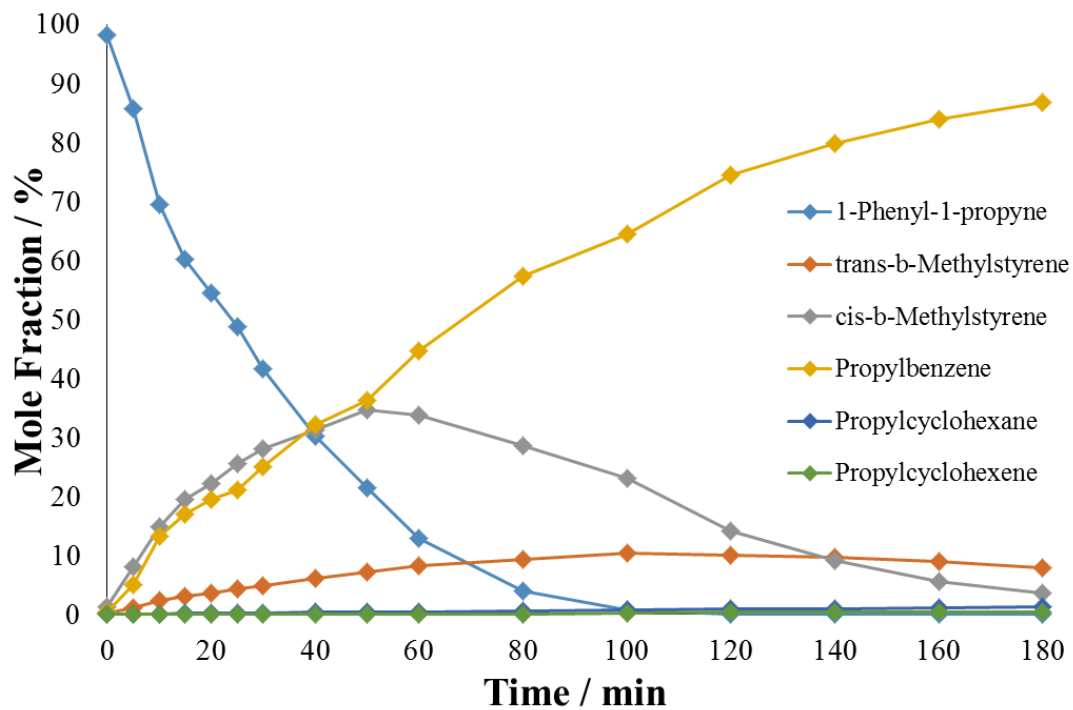


**Figure 48 – Reaction profile for the hydrogenation of 1-phenyl-1-propyne. Conditions: 3 barg  $H_2$ , 10 mmol 1-phenyl-1-propyne, 40°C.**

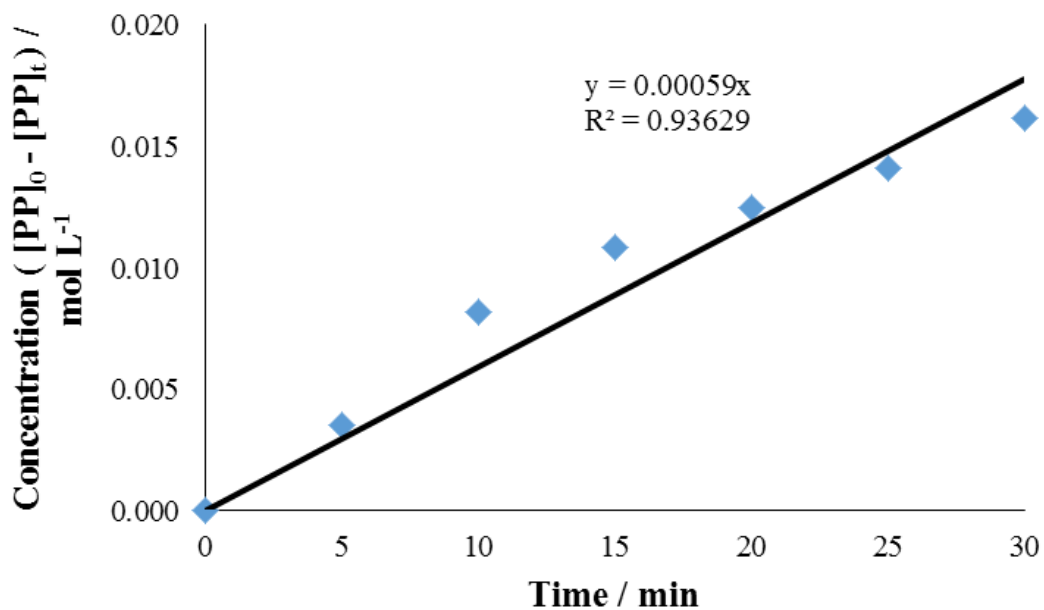


Figure 49 – Zero order plot to determine the initial rate constant of 1-phenyl-1-propyne hydrogenation at 40°C.

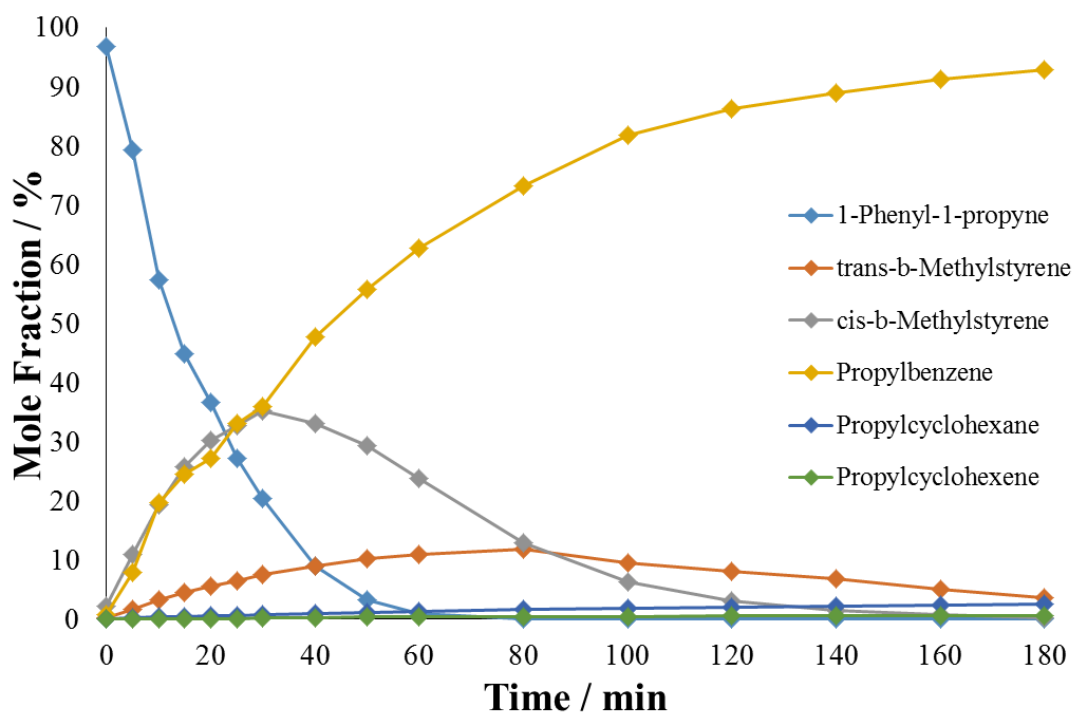


Figure 50 – Reaction profile for the hydrogenation of 1-phenyl-1-propyne. Conditions: 3 barg H<sub>2</sub>, 10 mmol 1-phenyl-1-propyne, 50°C.

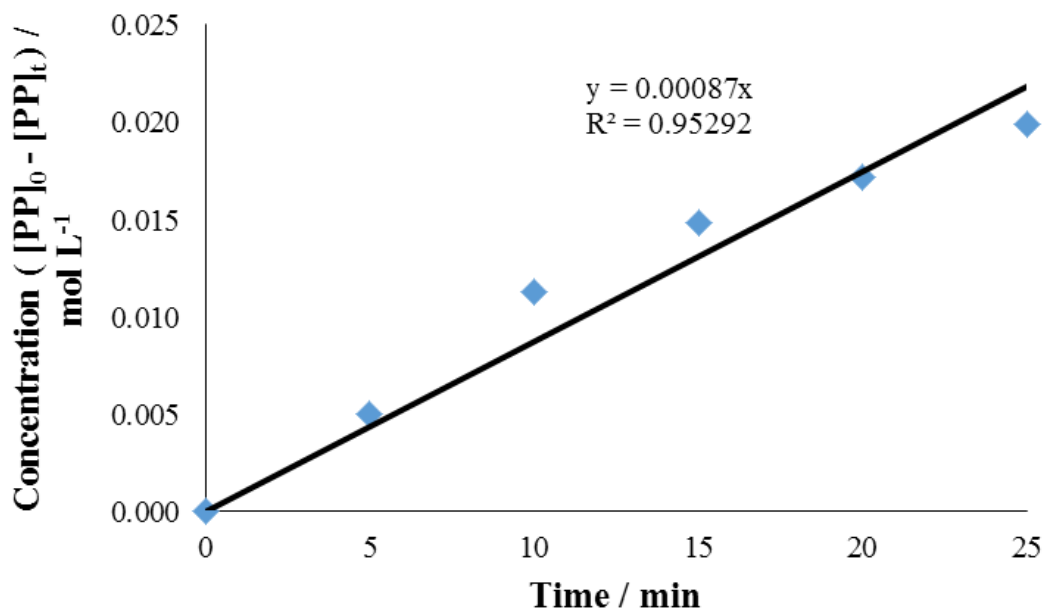


Figure 51 – Zero order plot to determine the initial rate constant of 1-phenyl-1-propyne hydrogenation at 50°C.

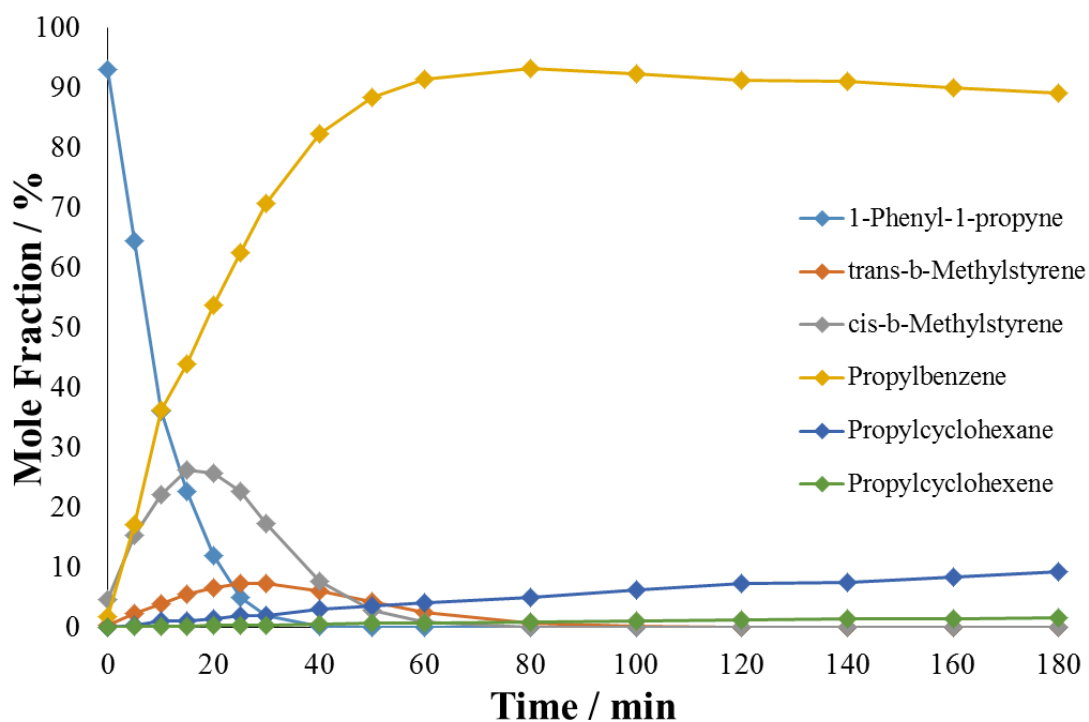


Figure 52 – Reaction profile for the hydrogenation of 1-phenyl-1-propyne. Conditions: 3 barg H<sub>2</sub>, 10 mmol 1-phenyl-1-propyne, 60°C.

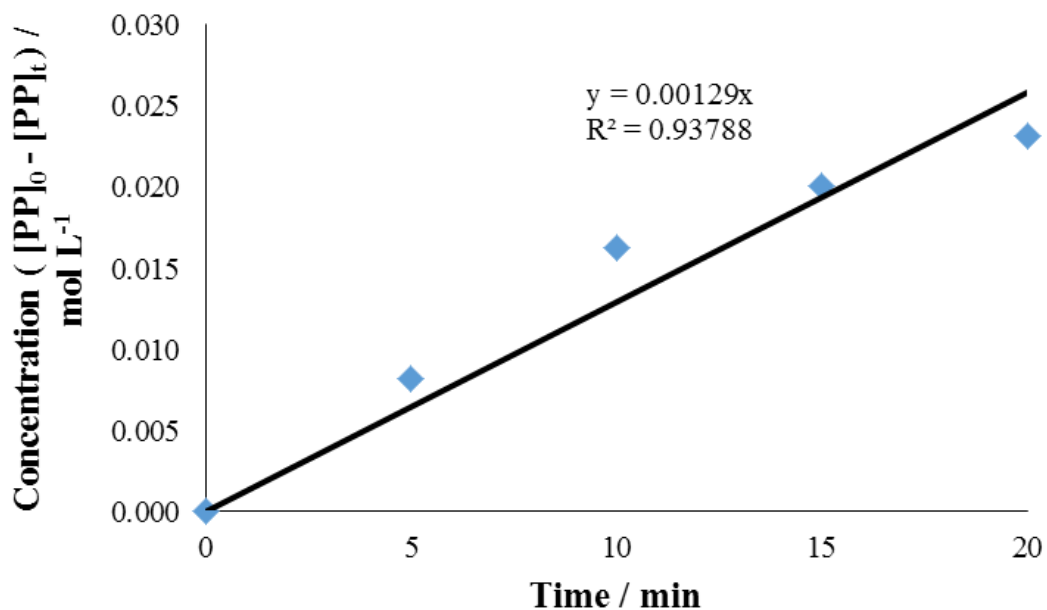


Figure 53 – Zero order plot to determine the initial rate constant of 1-phenyl-1-propyne hydrogenation at 60°C.

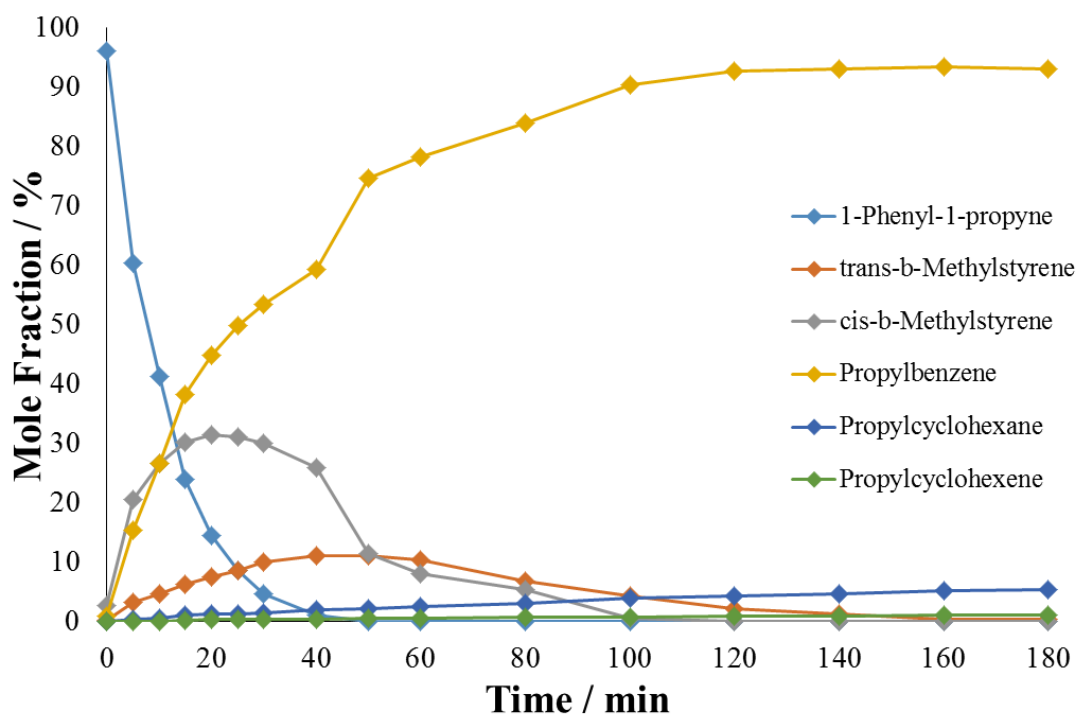
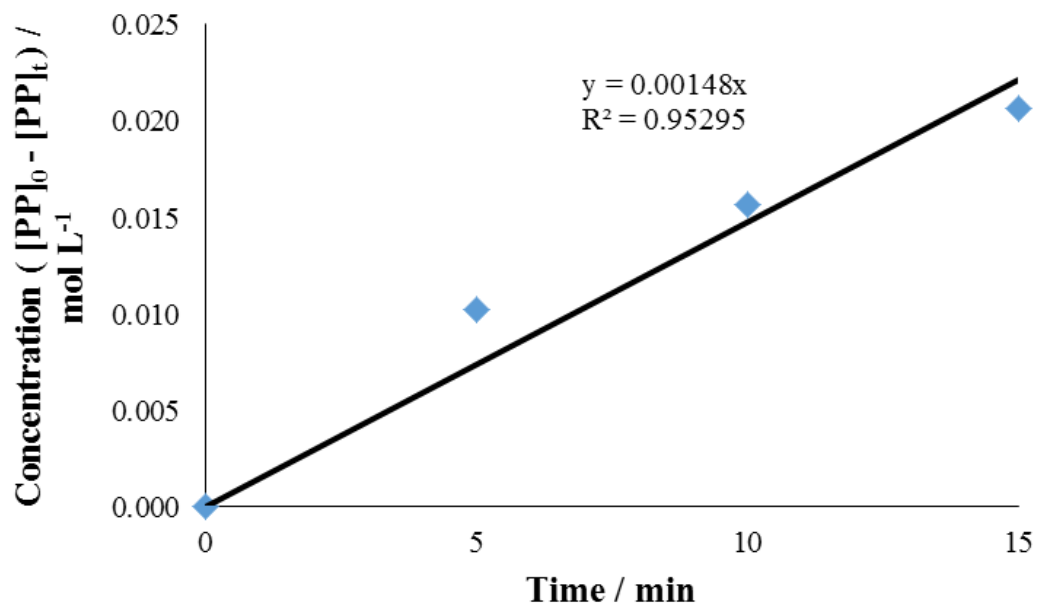


Figure 54 – Reaction profile for the hydrogenation of 1-phenyl-1-propyne. Conditions: 3 barg H<sub>2</sub>, 10 mmol 1-phenyl-1-propyne, 70°C.



**Figure 55 – Zero order plot to determine the initial rate constant of 1-phenyl-1-propyne hydrogenation at 70°C.**

Kinetic data from the hydrogenation of 1-phenyl-1-propyne is displayed in Table 9.

**Table 9 – 1-Phenyl-1-propyne temperature dependence. It was observed that the time taken to reach 100% conversion decreased and the initial rate constant increased with increasing temperature.**

<b>Temperature / K</b>	313	323	343	353
<b>Time for complete conversion / min</b>	120	80	50	50
<b>Initial rate constant, <math>k_0 \times 10^4 / \text{mol L}^{-1} \text{min}^{-1}</math></b>	5.9	8.7	12.9	14.8

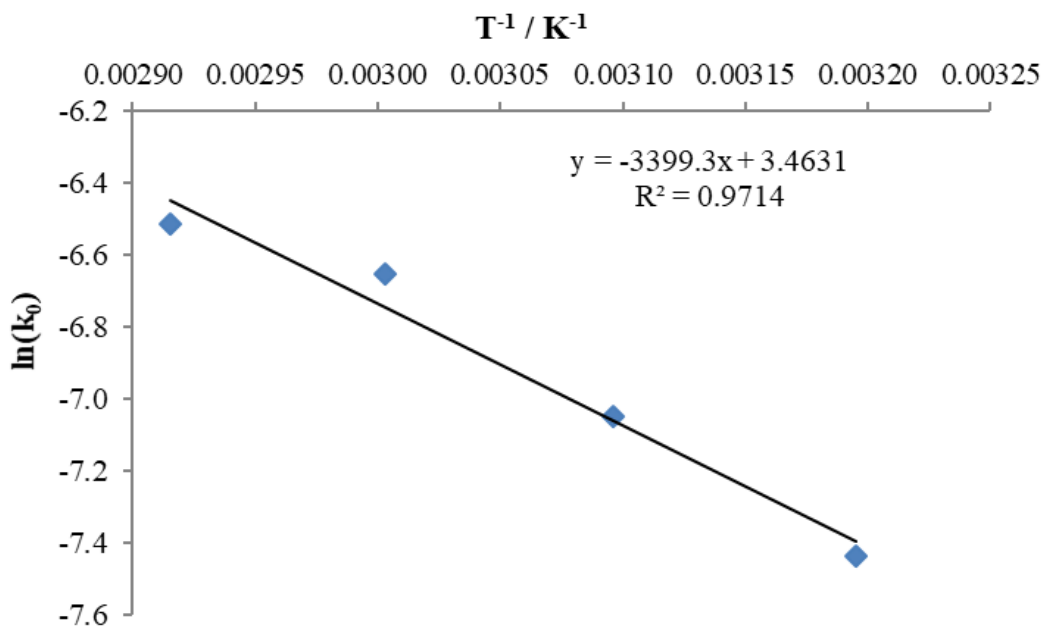


**Figure 56 – Arrhenius plot for the hydrogenation of 1-phenyl-1-propyne using the rate constants calculated from the zero order plots shown in Figures 49, 51, 53 and 55.**

From Figure 56 with gradient -3399.3, the activation energy of 1-phenyl-1-propyne hydrogenation was calculated to be  $26.3 \text{ kJ mol}^{-1}$ .

The reaction profiles for propylbenzene over the temperature range 50-70°C are shown in Figures 57, 59 and 61. Zero order plots were also constructed and are shown in Figures 58, 60 and 62. The trends observed were a decrease in the propylbenzene mole fraction and an increase in the propylcyclohexane throughout. Small quantities of propylcyclohexene were occasionally observed. All aspects of the reaction increased in rate when the temperature was increased.

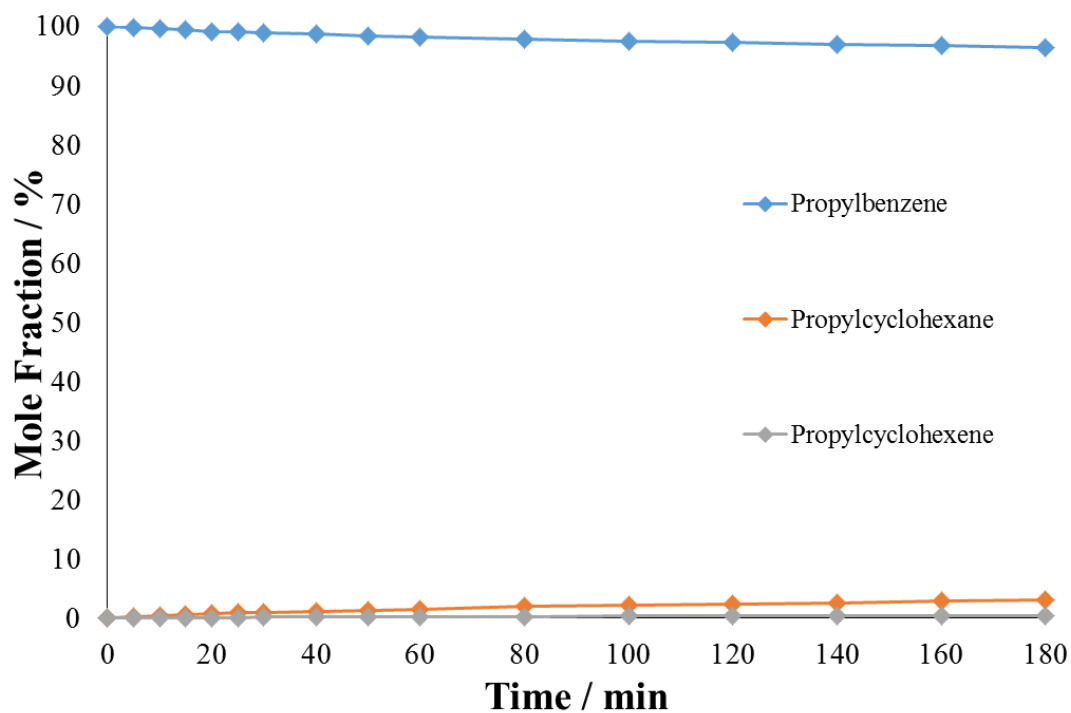


Figure 57 – Reaction profile for the hydrogenation of propylbenzene. Conditions: 3 barg  $H_2$ , 10 mmol propylbenzene, 50°C.

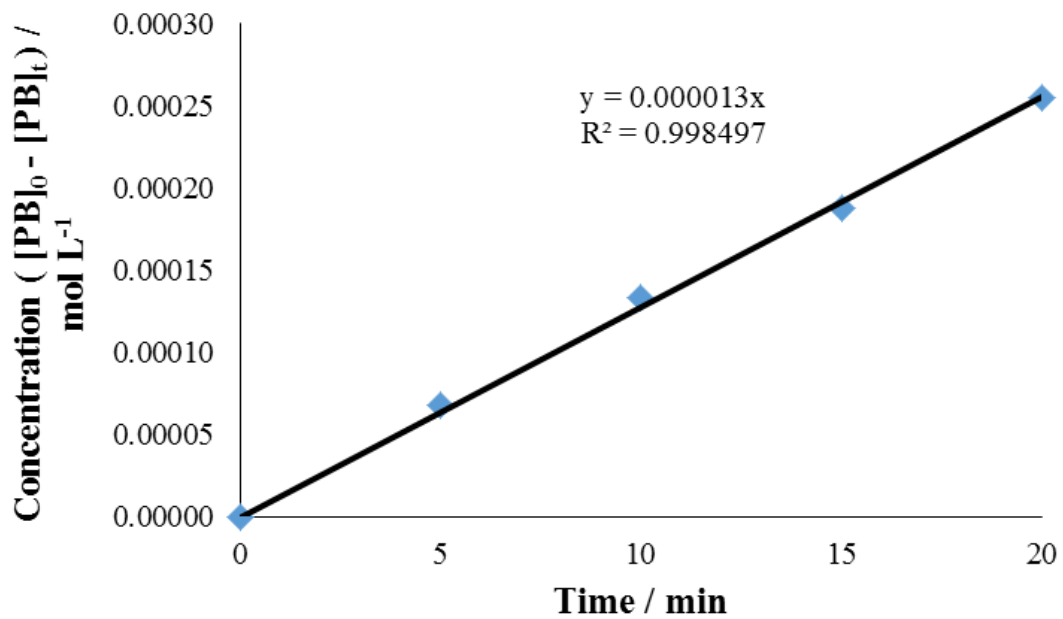


Figure 58 – Zero order plot to determine the initial rate constant of propylbenzene hydrogenation at 40°C.

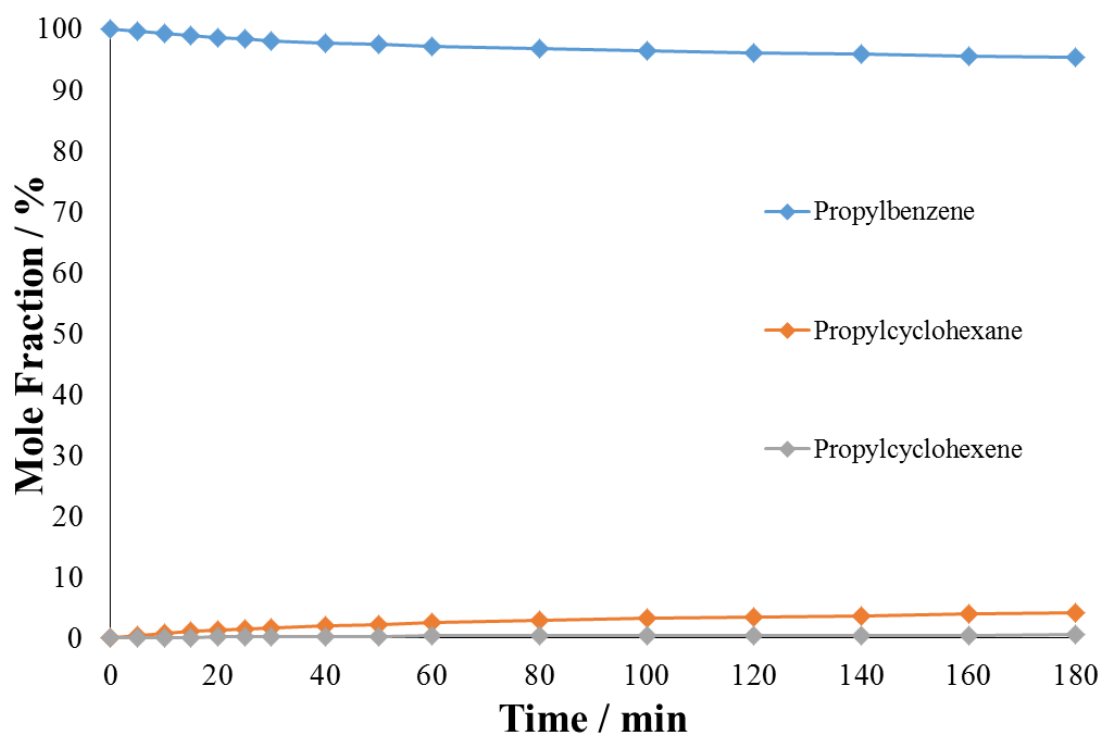


Figure 59 – Reaction profile for the hydrogenation of propylbenzene. Conditions: 3 barg  $H_2$ , 10 mmol propylbenzene, 60°C.

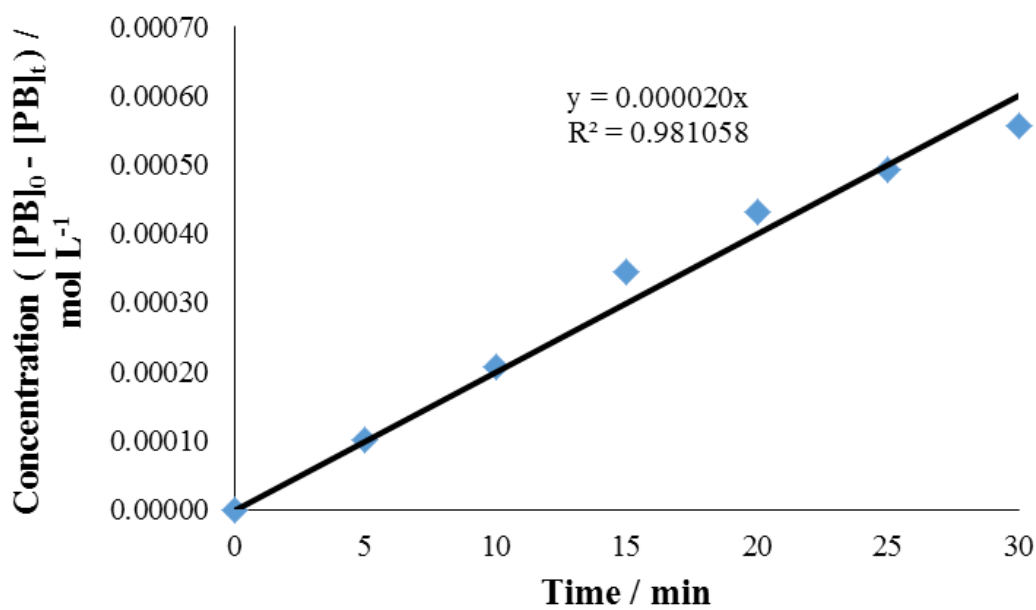


Figure 60 – Zero order plot to determine the initial rate constant of propylbenzene hydrogenation at 60°C.

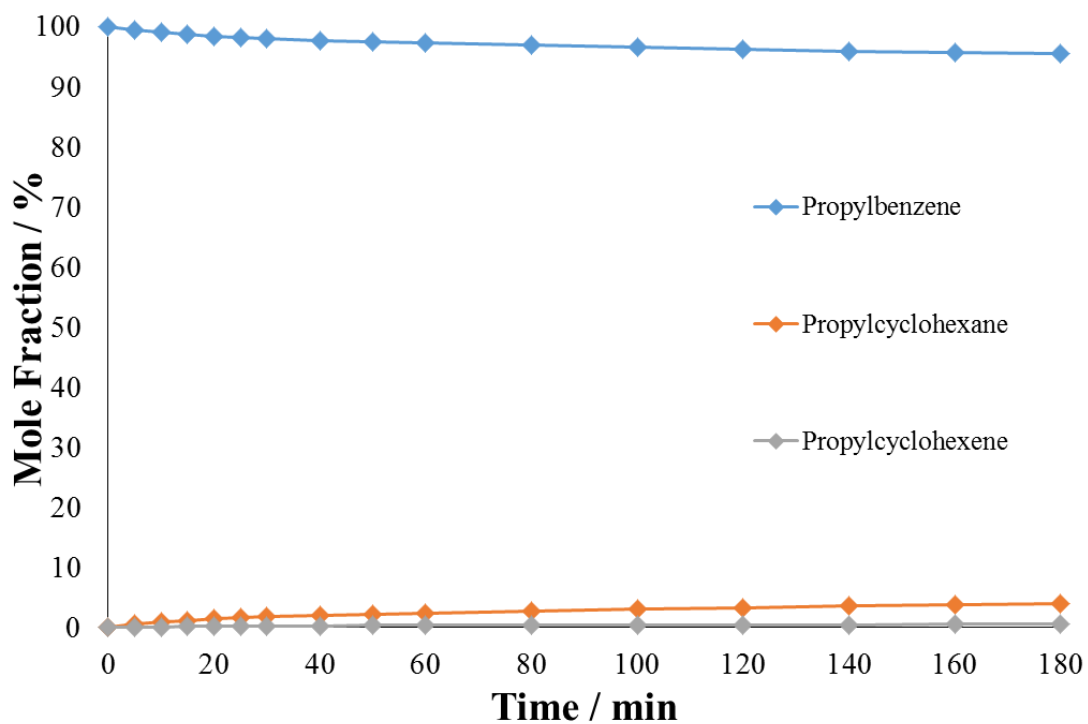


Figure 61 – Reaction profile for the hydrogenation of propylbenzene. Conditions: 3 barg  $H_2$ , 10 mmol propylbenzene, 70°C.

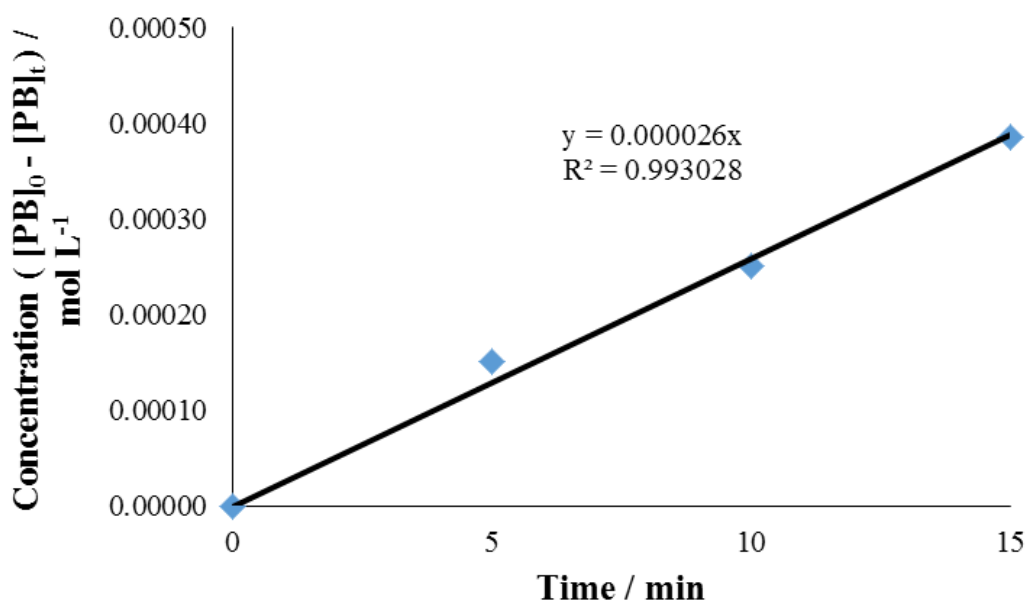
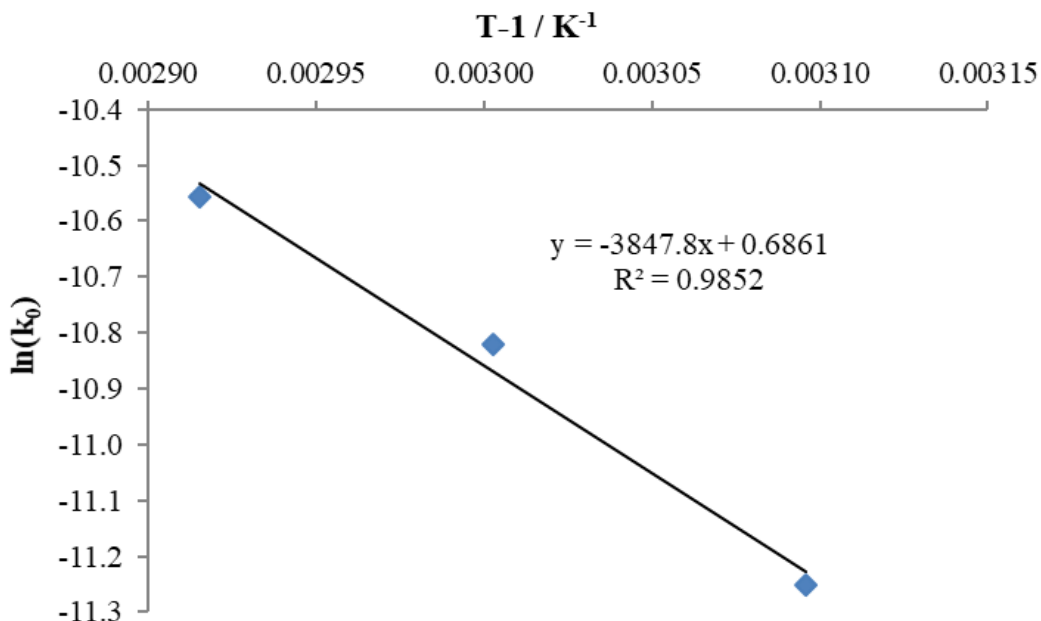


Figure 62 – Zero order plot to determine the initial rate constant of propylbenzene hydrogenation at 70°C.

Kinetic data from the hydrogenation of propylbenzene is displayed in Table 10.

**Table 10 – Propylbenzene temperature dependence. It was observed that the conversion after 180 minutes and the initial rate constant increased with increasing temperature.**

<b>Temperature / K</b>	323	343	353
<b>Conversion after 180 mins / %</b>	3.56	4.60	4.70
<b>Initial rate constant, <math>k_0 \times 10^4 / \text{mol L}^{-1} \text{min}^{-1}</math></b>	1.3	2.0	2.6



**Figure 63** – Arrhenius plot for the hydrogenation of propylbenzene using the rate constants calculated from the zero order plots shown Figures 58, 60 and 62.

From Figure 63 with gradient  $-3847.8$ , the activation energy of propylbenzene hydrogenation was calculated to be  $32.0 \text{ kJ mol}^{-1}$ .

#### 4.1.3 Reactions with Deuterium

Deuteration reactions of phenylacetylene, styrene and 1-phenyl-1-propyne were carried out to determine the kinetic isotope effects on their hydrogenation (except in the case of styrene, which reacts too fast to calculate a reliable rate constant), as explained in Section 3.2.2, and to assess aspects of exchange.  $^2\text{H}$  NMR spectra of samples were taken at 10, 40 and 180 minutes and the peak intensities were compared – integration was difficult to perform, as the concentration of molecules was low, meaning the baseline contained a significant amount of noise.

A reaction profile for each reaction was plotted using the mole fractions calculated from the chromatograms.

The reaction profiles for phenylacetylene deuteration at temperatures of  $50^\circ\text{C}$  and  $70^\circ\text{C}$  are shown in Figures 64 and 69. Zero order plots were also constructed and are shown in Figures 65 and 70.  $^2\text{H}$  NMR spectra are presented in Figures 66-68 and 71-

73, with the corresponding data shown in Tables 11-16. The reaction profiles from the deuteration of phenylacetylene were similar to those produced when phenylacetylene was hydrogenated. The notable differences were that the rates of the individual processes are typically decreased and there was an absence of ethylcyclohexane. All aspects of the reaction, aside from the ring hydrogenation processes, increased in rate when the temperature was increased.

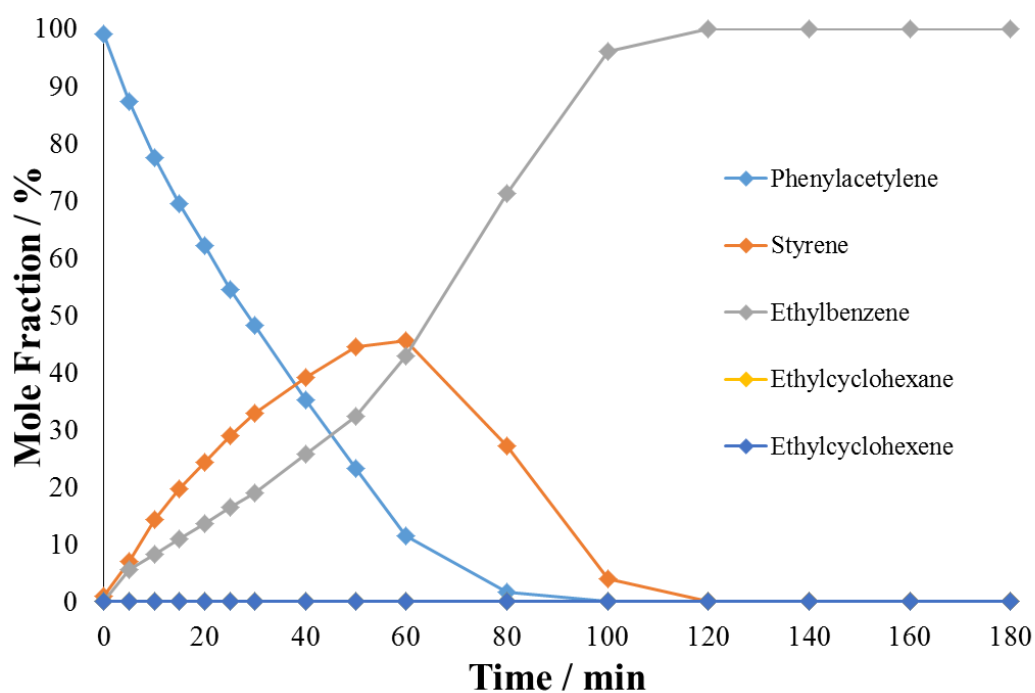


**Figure 64 – Reaction profile for the deuteration of phenylacetylene. Conditions: 3 barg  $D_2$ , 10 mmol phenylacetylene, 50°C.**

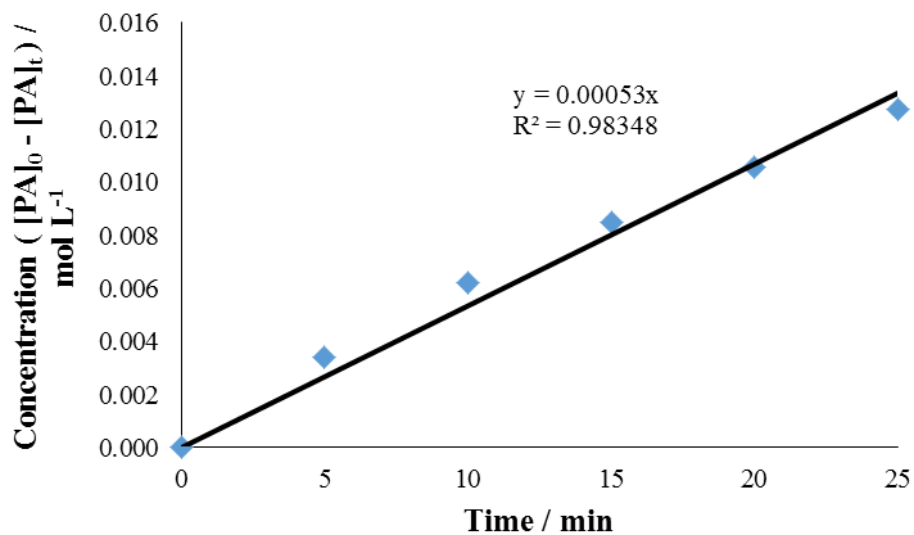


Figure 65 – Zero order plot to determine the initial rate constant of phenylacetylene deuteration at 50°C.

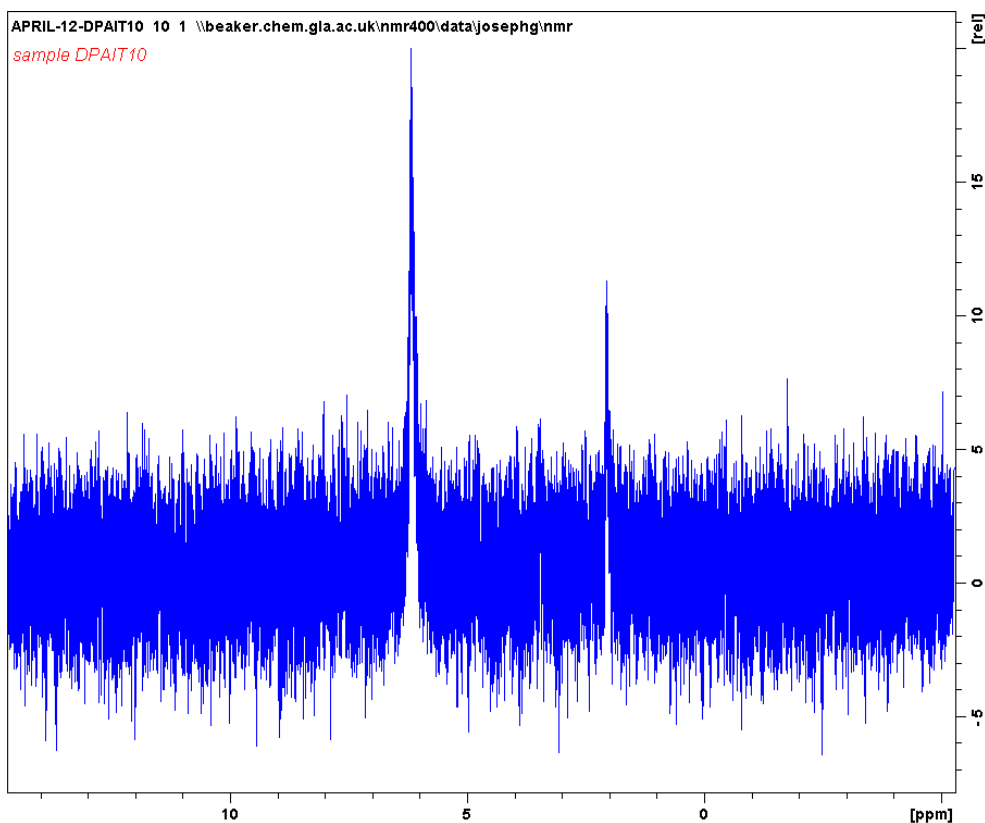


Figure 66 – <sup>2</sup>H NMR spectrum of a sample taken after 10 minutes of phenylacetylene deuteration at 50°C.

Table 11 – Relative intensities, normalised relative to the smallest peak, of each significant peak in the  $^2\text{H}$  NMR spectrum of a sample taken after 10 minutes of phenylacetylene deuteration at  $50^\circ\text{C}$ .

Shift, $\delta$ / ppm	Relative intensity
6.18	1.8
2.06	1.0

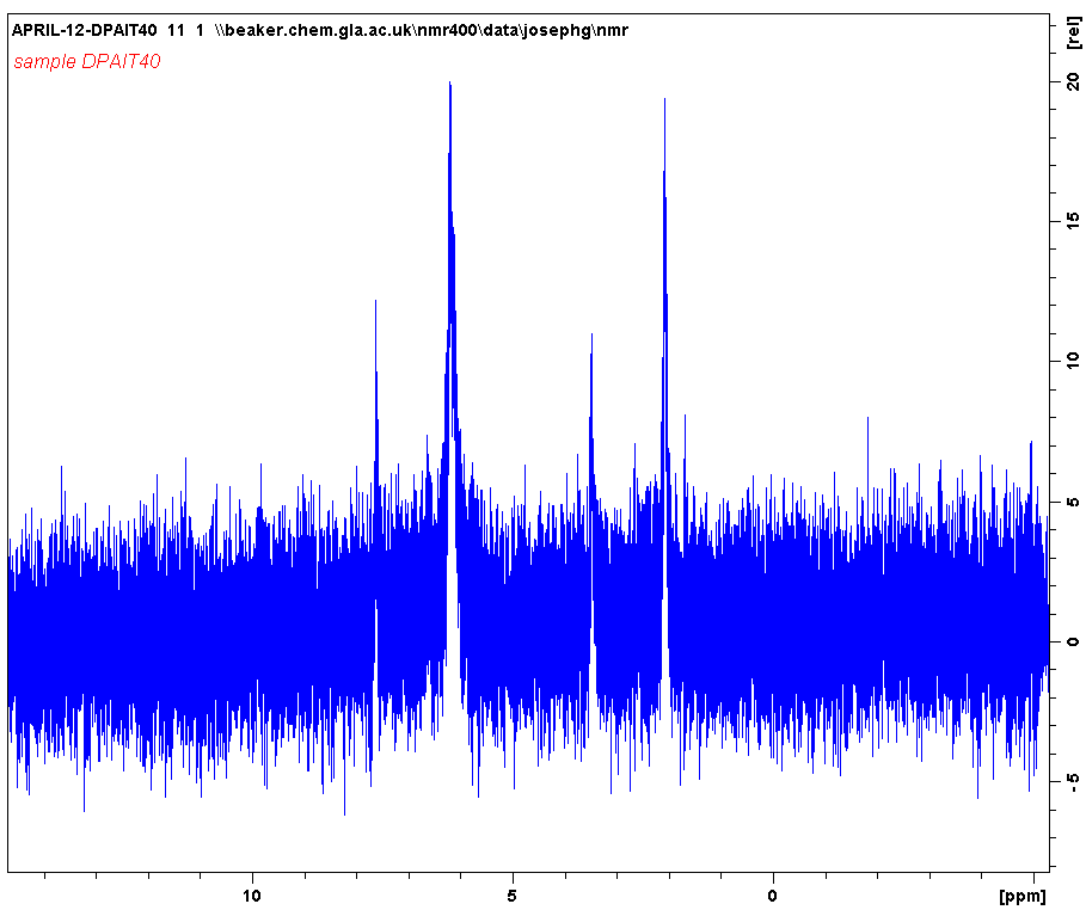
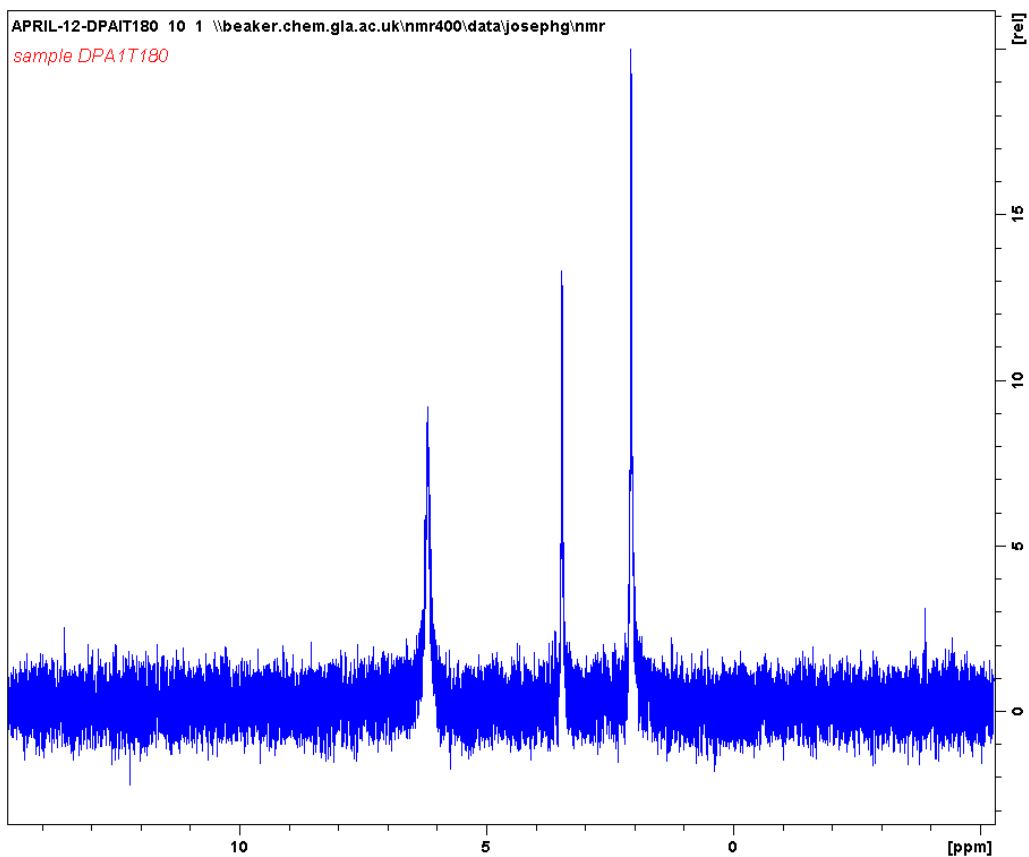


Figure 67 –  $^2\text{H}$  NMR spectrum of a sample taken after 40 minutes of phenylacetylene deuteration at  $50^\circ\text{C}$ .

**Table 12 – Relative intensities, normalised relative to the smallest peak, of each significant peak in the  $^2\text{H}$  NMR spectrum of a sample taken after 40 minutes of phenylacetylene deuteration at 50°C.**

<b>Shift, <math>\delta</math> / ppm</b>	<b>Relative intensity</b>
7.61	1.1
6.20	1.8
3.48	1.0
2.08	1.8



**Figure 68** –  $^2\text{H}$  NMR spectrum of a sample taken after 180 minutes of phenylacetylene deuteration at  $50^\circ\text{C}$ .

**Table 13** – Relative intensities, normalised relative to the smallest peak, of each significant peak in the  $^2\text{H}$  NMR spectrum of a sample taken after 180 minutes of phenylacetylene deuteration at  $50^\circ\text{C}$ .

Shift, $\delta$ / ppm	Relative intensity
6.18	1.0
3.46	1.4
2.06	2.2

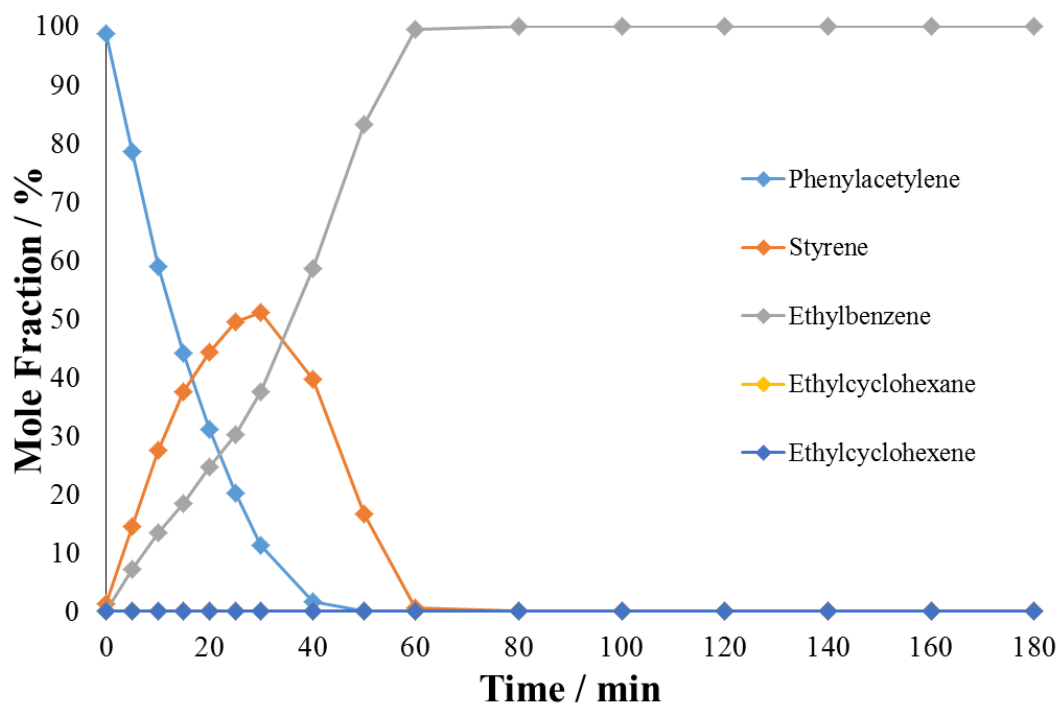


Figure 69 – Reaction profile for the deuteration of phenylacetylene. Conditions: 3 barg  $D_2$ , 10 mmol phenylacetylene, 70°C.

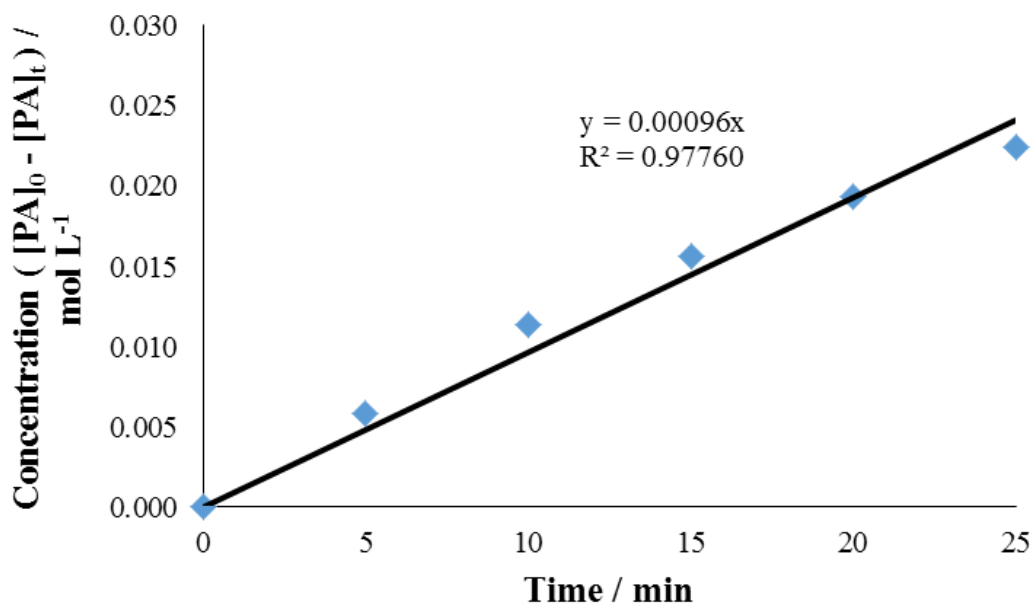
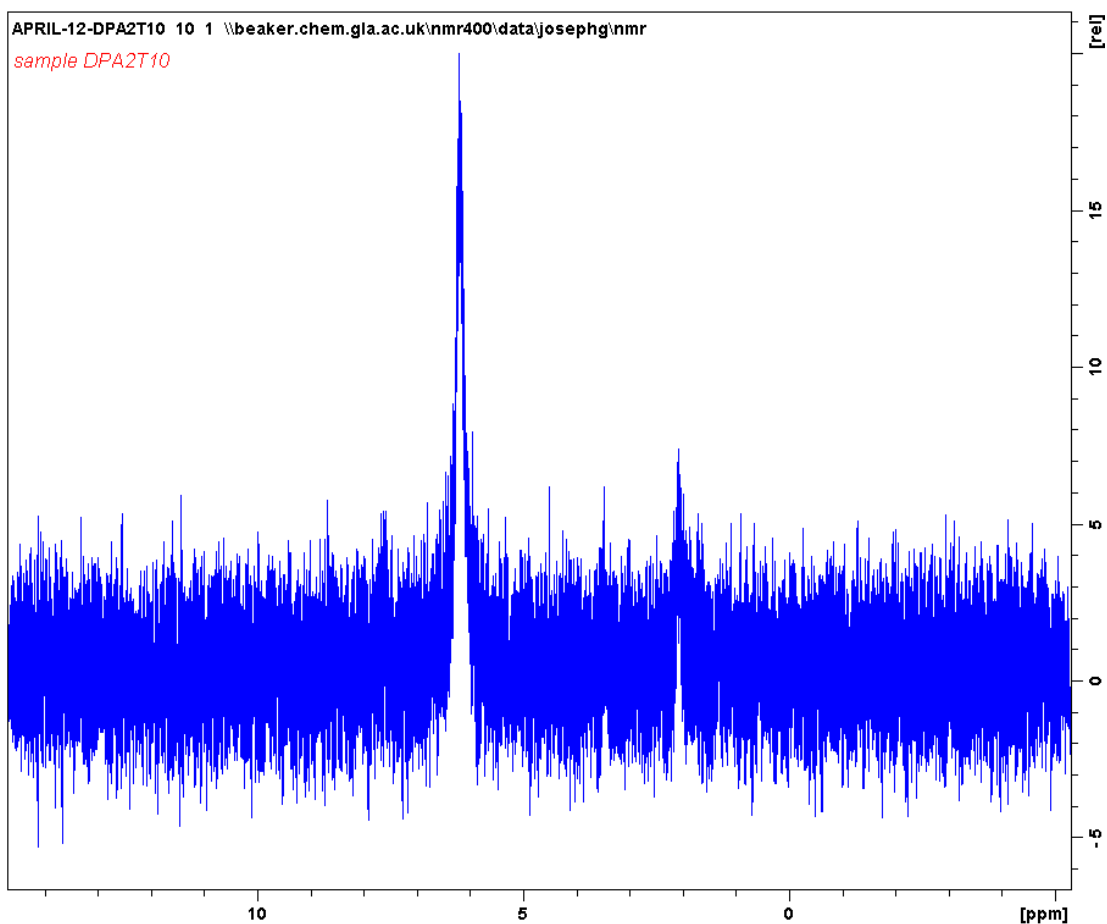


Figure 70 – Zero order plot to determine the initial rate constant of phenylacetylene deuteration at 70°C.



**Figure 71 –  $^2\text{H}$  NMR spectrum of a sample taken after 10 minutes of phenylacetylene deuteration at  $70^\circ\text{C}$ .**

**Table 14 – Relative intensities, normalised relative to the smallest peak, of each significant peak in the  $^2\text{H}$  NMR spectrum of a sample taken after 10 minutes of phenylacetylene deuteration at  $70^\circ\text{C}$ .**

Shift, $\delta$ / ppm	Relative intensity
6.19	2.7
2.08	1.0

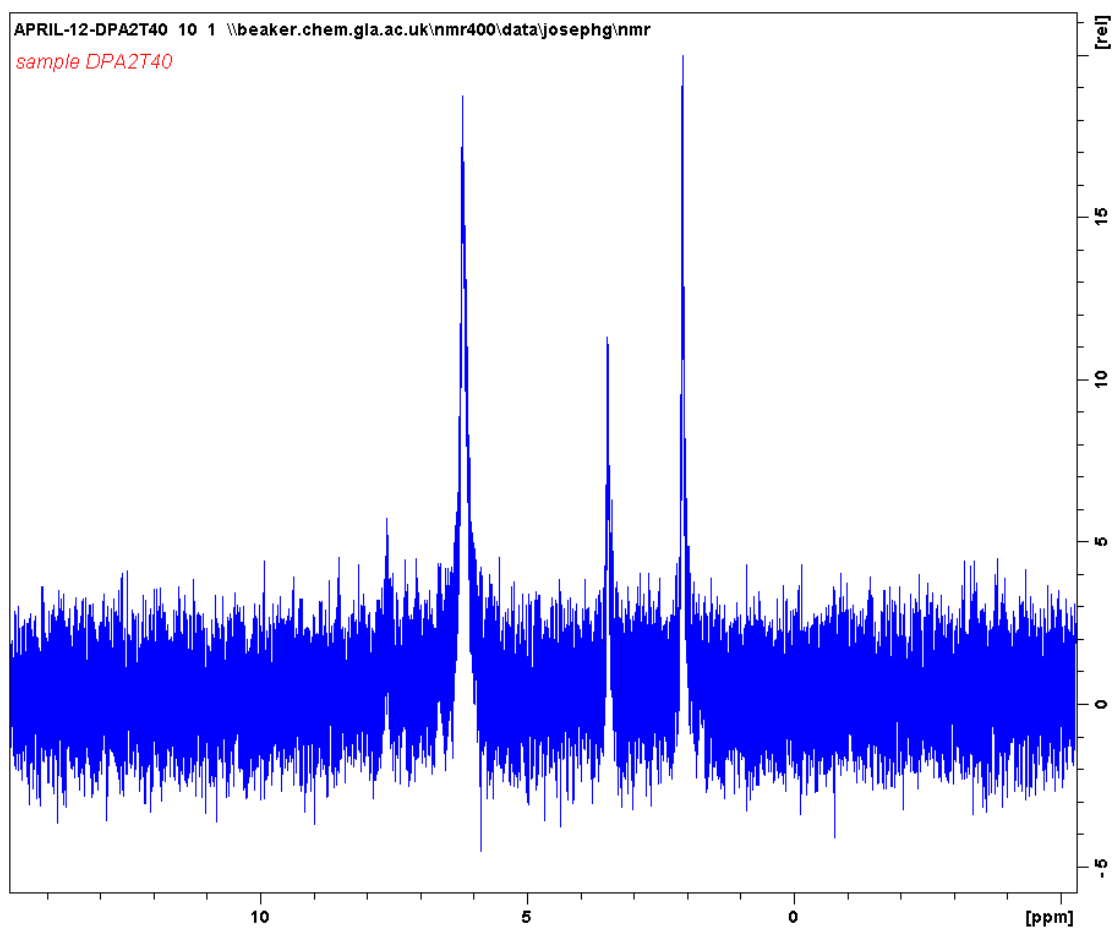
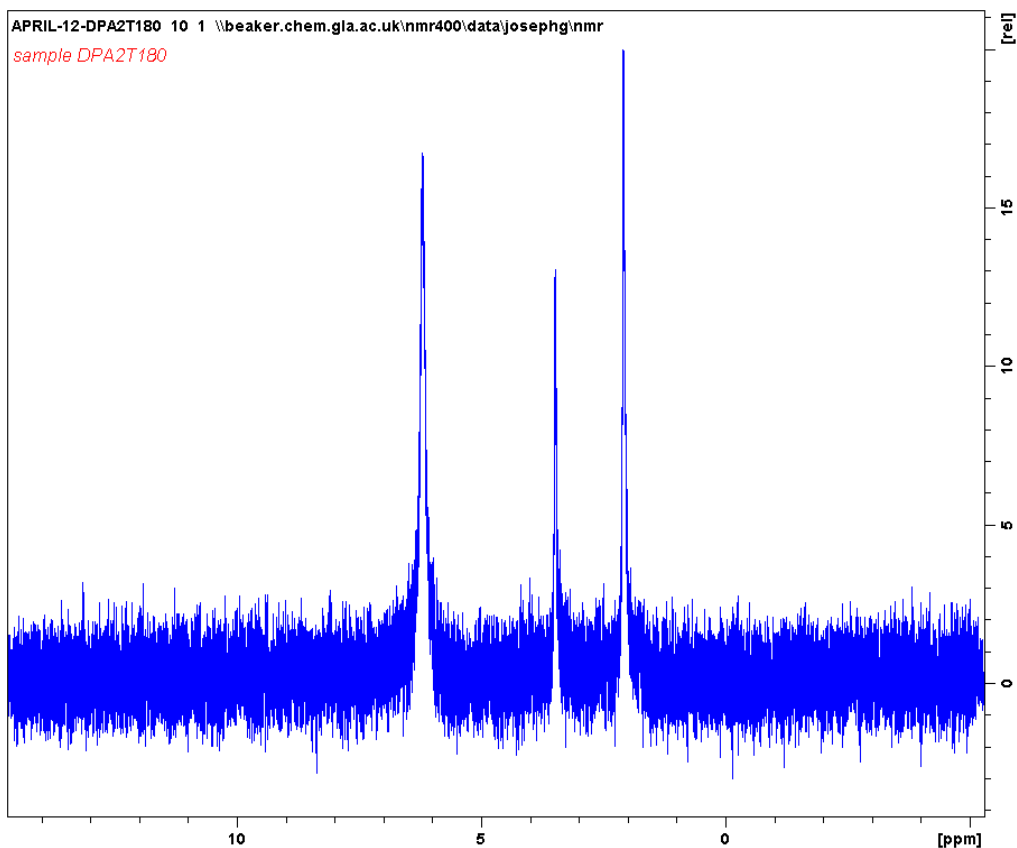


Figure 72 –  $^2\text{H}$  NMR spectrum of a sample taken after 40 minutes of phenylacetylene deuteration at  $70^\circ\text{C}$ .

**Table 15 – Relative intensities, normalised relative to the smallest peak, of each significant peak in the  $^2\text{H}$  NMR spectrum of a sample taken after 40 minutes of phenylacetylene deuteration at 70°C.**

<b>Shift, <math>\delta</math> / ppm</b>	<b>Relative intensity</b>
7.62	1.0
6.21	3.3
3.49	2.0
2.08	3.5



**Figure 73 –  $^2\text{H}$  NMR spectrum of a sample taken after 180 minutes of phenylacetylene deuteration at  $70^\circ\text{C}$ .**

**Table 16 – Relative intensities, normalised relative to the smallest peak, of each significant peak in the  $^2\text{H}$  NMR spectrum of a sample taken after 180 minutes of phenylacetylene deuteration at  $70^\circ\text{C}$ .**

Shift, $\delta$ / ppm	Relative intensity
6.19	1.3
3.48	1.0
2.09	1.5

The initial rates of reaction and kinetic isotope effects calculated are given in Table 17.

**Table 17 – The effect of changing the hydrogen isotope on the hydrogenation of phenylacetylene. At both 50°C and 70°C,  $k_H$  is greater than  $k_D$ .**

		$k_H \times 10^4 / \text{min}^{-1}$	$k_D \times 10^4 / \text{min}^{-1}$	$k_H/k_D$
<b>Temperature</b> / °C	50	7.1	5.3	1.3
	70	14.9	9.6	1.6

The reaction profiles for styrene deuteration at temperatures of 50°C and 70°C are shown in Figures 74 and 78.  $^2\text{H}$  NMR spectra are presented in Figures 75-77 and 79-81, with the corresponding data shown in Tables 18-23. An initial rapid decrease in the styrene mole fraction and increase in ethylbenzene mole fraction was observed; the temperature dependence of this stage of the reaction could not be determined due to the lack of data points. The following decrease in ethylbenzene mole fraction and increase in ethylcyclohexane mole fraction occurred at a faster rate at 50°C than at 70°C.

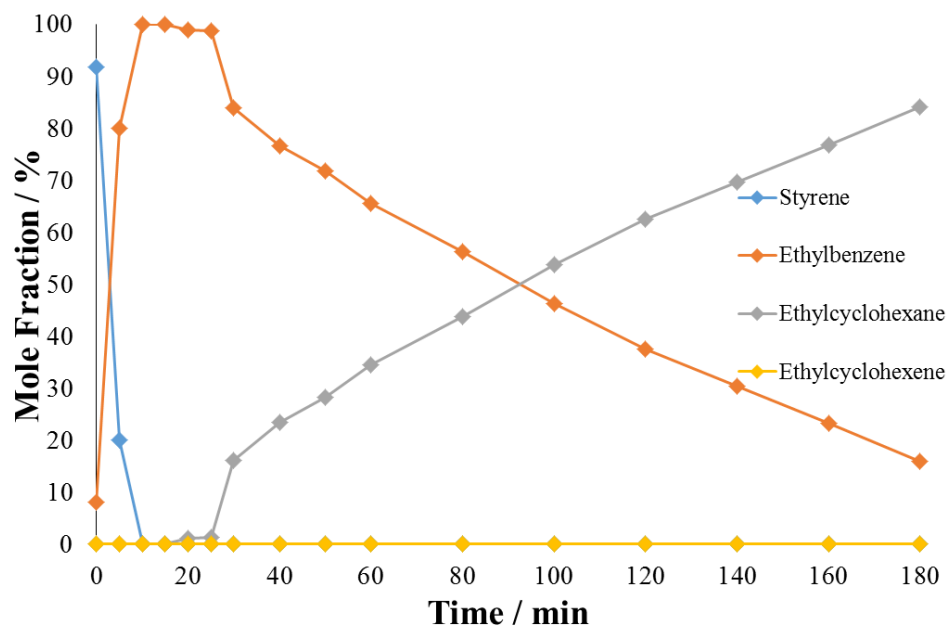


Figure 74 – Reaction profile for the deuteration of styrene. Conditions: 3 barg  $D_2$ , 10 mmol styrene, 50°C.

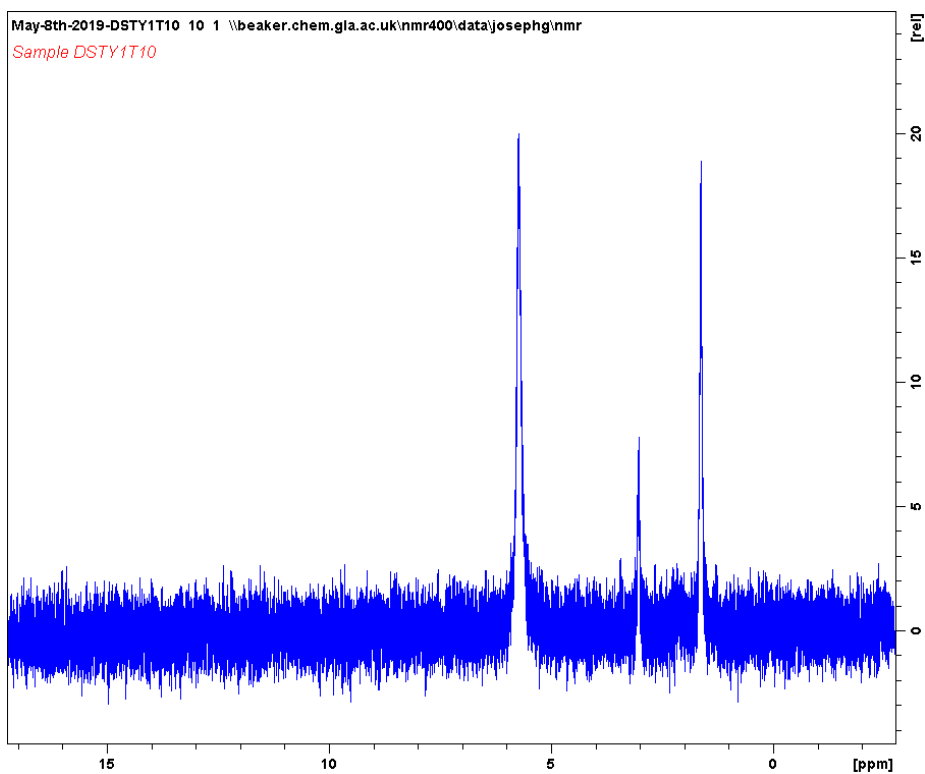
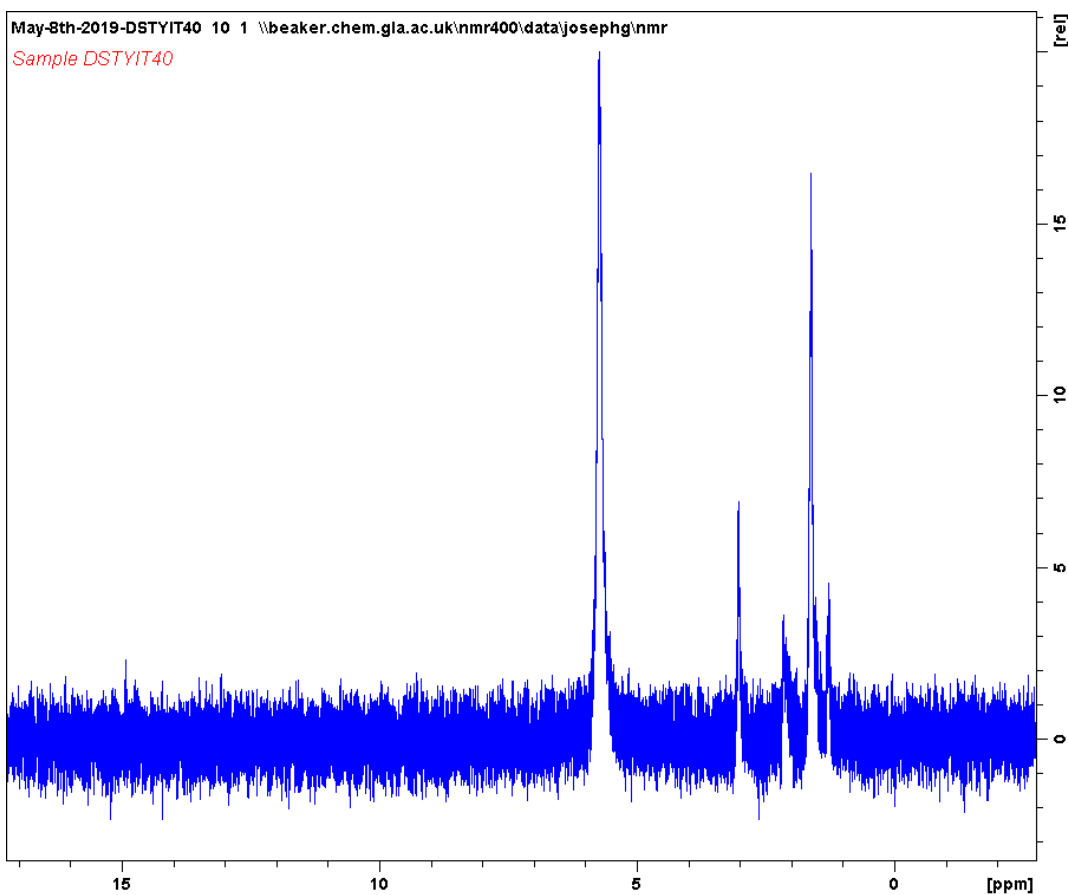


Figure 75 –  $^2H$  NMR spectrum of a sample taken after 10 minutes of styrene deuteration at 50°C.

**Table 18 – Relative intensities, normalised relative to the smallest peak, of each significant peak in the  $^2\text{H}$  NMR spectrum of a sample taken after 10 minutes of styrene deuteration at  $50^\circ\text{C}$ .**

Shift, $\delta$ / ppm	Relative intensity
5.73	2.6
3.01	1.0
1.61	2.4



**Figure 76 –  $^2\text{H}$  NMR spectrum of a sample taken after 40 minutes of styrene deuteration at  $50^\circ\text{C}$ .**

**Table 19 – Relative intensities, normalised relative to the smallest peak, of each significant peak in the  $^2\text{H}$  NMR spectrum of a sample taken after 40 minutes of styrene deuteration at 50°C.**

<b>Shift, <math>\delta</math> / ppm</b>	<b>Relative intensity</b>
5.72	5.6
3.01	1.9
2.14	1.0
1.61	4.6
1.26	1.3

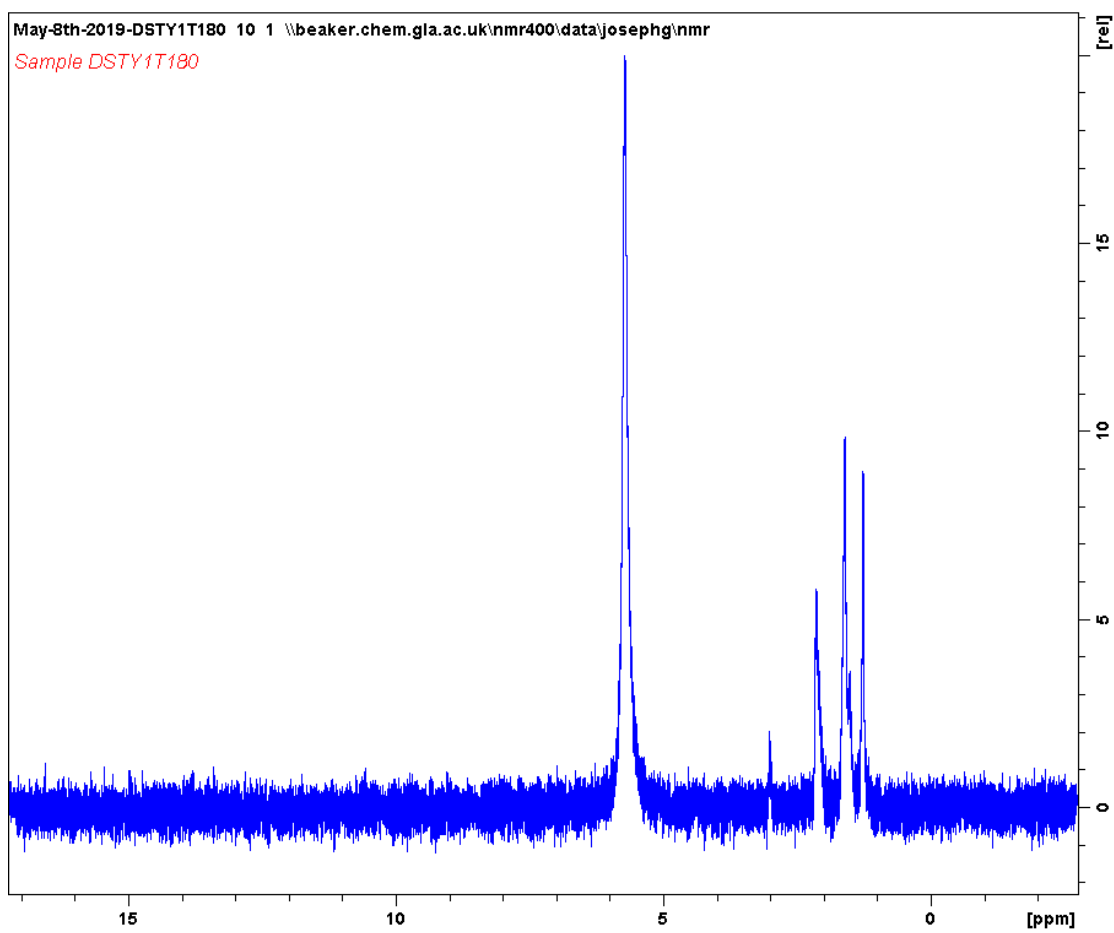


**Figure 77** –  $^2\text{H}$  NMR spectrum of a sample taken after 180 minutes of styrene deuteration at 50°C.

**Table 20 – Relative intensities, normalised relative to the smallest peak, of each significant peak in the  $^2\text{H}$  NMR spectrum of a sample taken after 180 minutes of styrene deuteration at 50°C.**

Shift, $\delta$ / ppm	Relative intensity
5.71	9.9
3.00	1.0
2.13	2.9
1.59	4.9
1.25	4.4

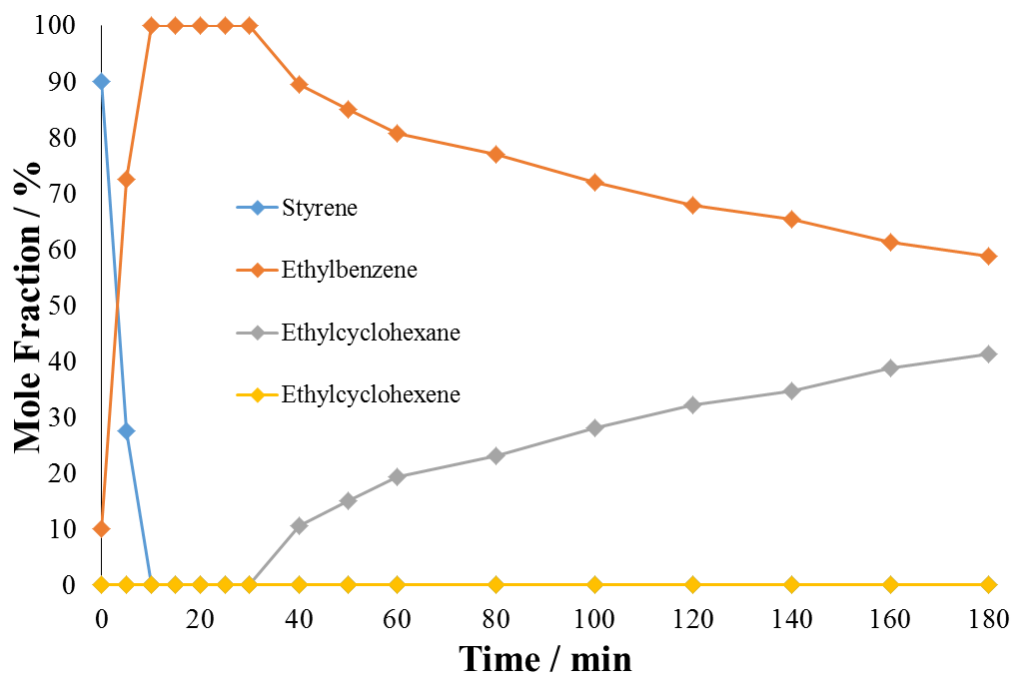


**Figure 78 – Reaction profile for the deuteration of styrene. Conditions: 3 barg  $\text{D}_2$ , 10 mmol styrene, 70°C.**

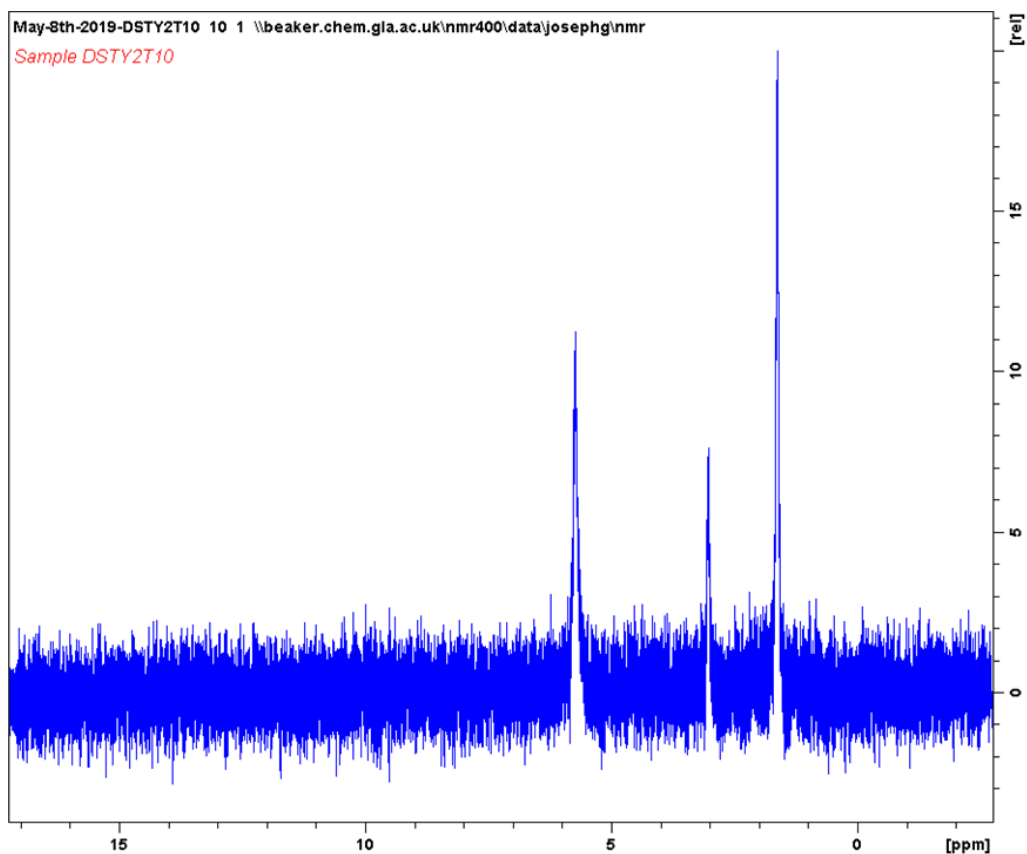


**Figure 79** –  $^2\text{H}$  NMR spectrum of a sample taken after 10 minutes of styrene deuteration at  $70^\circ\text{C}$ .

**Table 21** – Relative intensities, normalised relative to the smallest peak, of each significant peak in the  $^2\text{H}$  NMR spectrum of a sample taken after 10 minutes of styrene deuteration at  $70^\circ\text{C}$ .

Shift, $\delta$ / ppm	Relative intensity
5.72	1.5
3.01	1.0
1.61	2.6

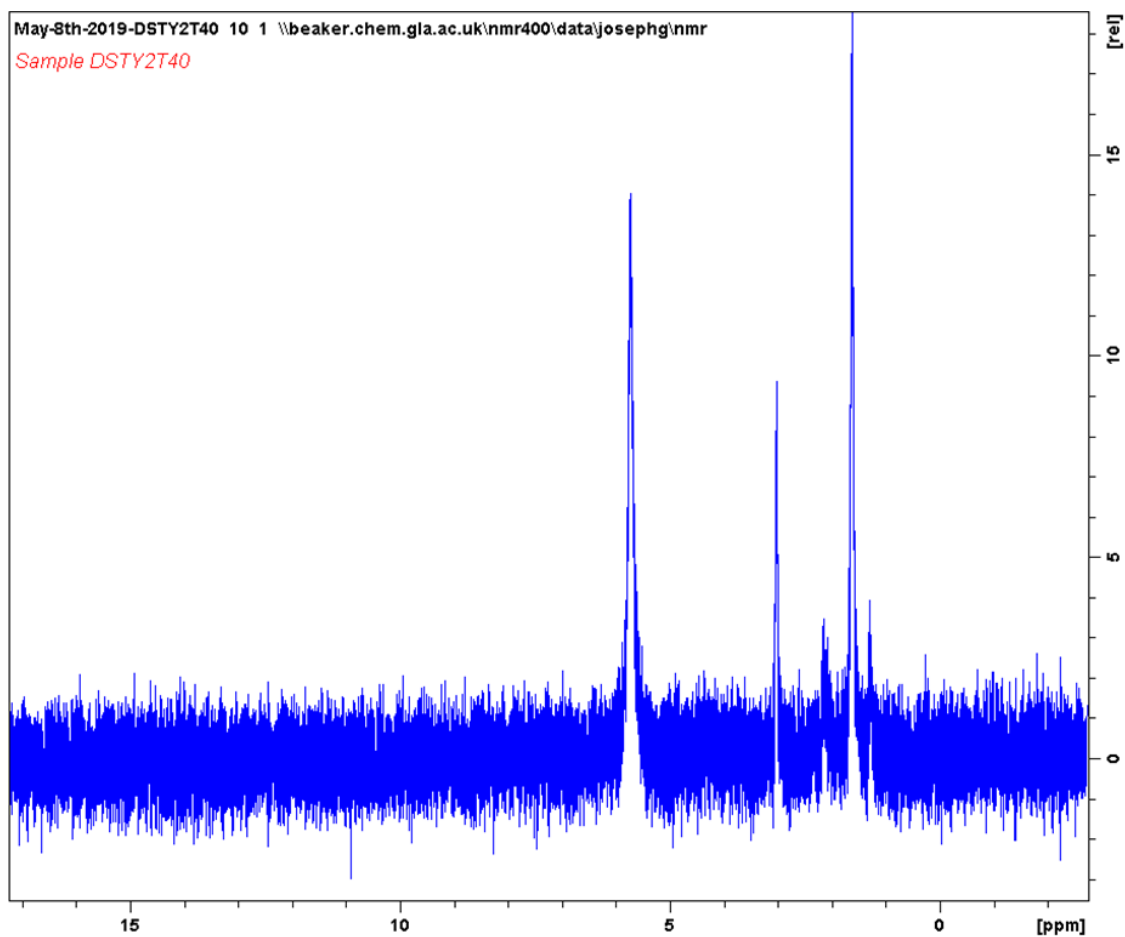


**Figure 80 –  $^2\text{H}$  NMR spectrum of a sample taken after 40 minutes of styrene deuteration at 70°C.**

**Table 22 – Relative intensities, normalised relative to the smallest peak, of each significant peak in the  $^2\text{H}$  NMR spectrum of a sample taken after 40 minutes of styrene deuteration at 70°C.**

<b>Shift, <math>\delta</math> / ppm</b>	<b>Relative intensity</b>
5.72	4.0
3.01	2.7
2.13	1.0
1.61	5.7
1.29	1.1

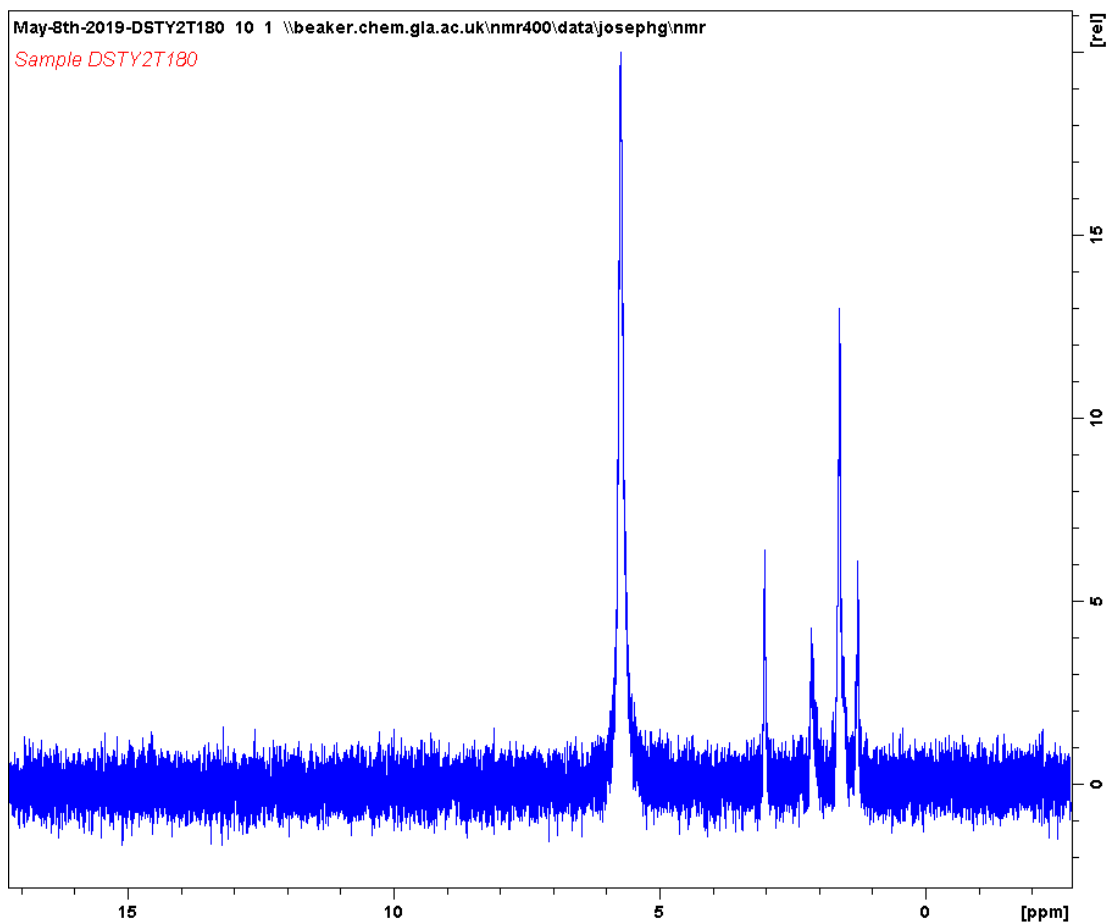


**Figure 81 –  $^2\text{H}$  NMR spectrum of a sample taken after 180 minutes of styrene deuteration at 70°C.**

**Table 23 – Relative intensities, normalised relative to the smallest peak, of each significant peak in the  $^2\text{H}$  NMR spectrum of a sample taken after 180 minutes of styrene deuteration at 70°C.**

Shift, $\delta$ / ppm	Relative intensity
5.72	4.7
3.01	1.5
2.14	1.0
1.61	3.0
1.26	1.4

The reaction profiles for 1-phenyl-1-propyne deuteration at temperatures of 50°C and 70°C are shown in Figures 82 and 87. Zero order plots were also constructed and are shown in Figures 83 and 88.  $^2\text{H}$  NMR spectra are presented in Figures 84-86 and 89-91, with the corresponding data shown in Tables 24-29. The reaction profile from the deuteration of 1-phenyl-1-propyne at 50°C was similar to the reaction profile of 1-phenyl-1-propyne hydrogenation, however at 70°C, the rate of most processes appeared to have increased with the use of deuterium. The exceptions were the products of ring hydrogenation, the mole fractions of which increased at a slower rate with deuterium use. All aspects of the reaction increased in rate when the temperature was increased.

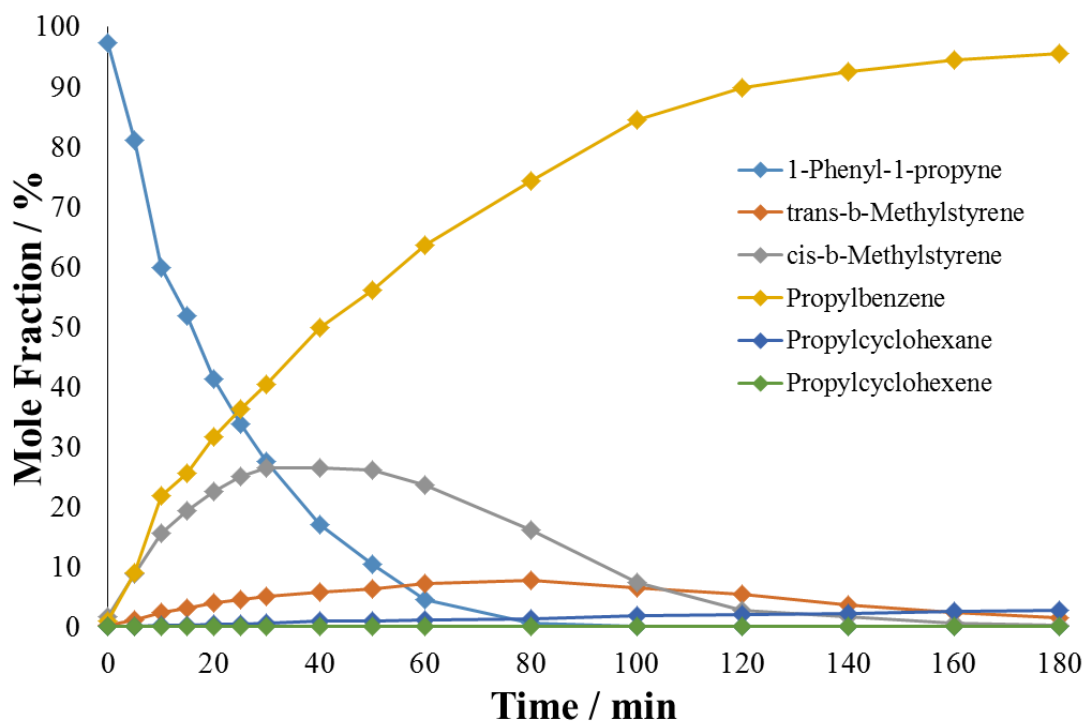


Figure 82 – Reaction profile for the deuteration of 1-phenyl-1-propyne. Conditions: 3 barg  $D_2$ , 10 mmol 1-phenyl-1-propyne, 50°C.

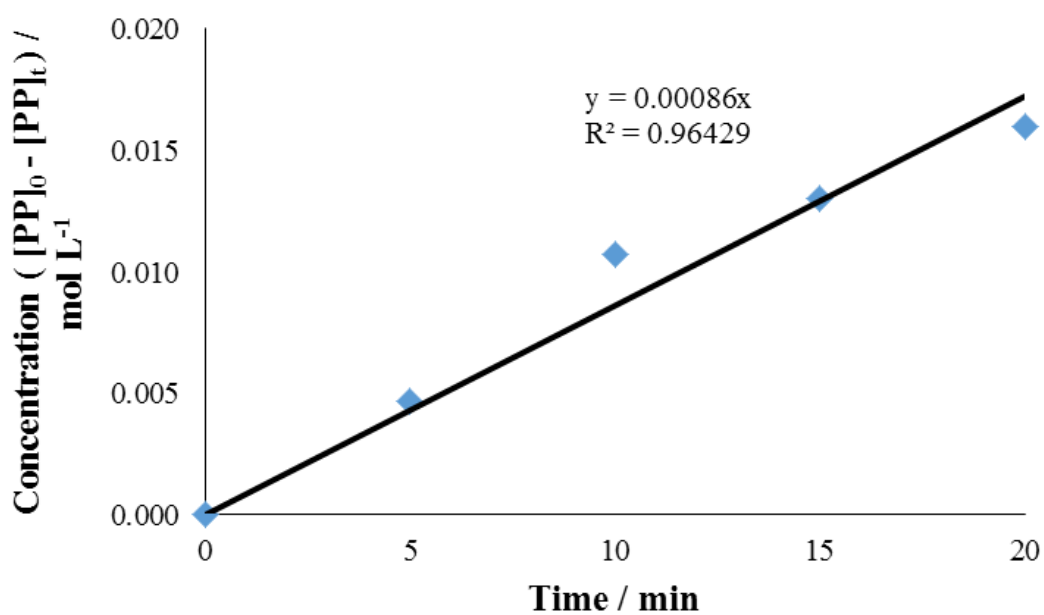
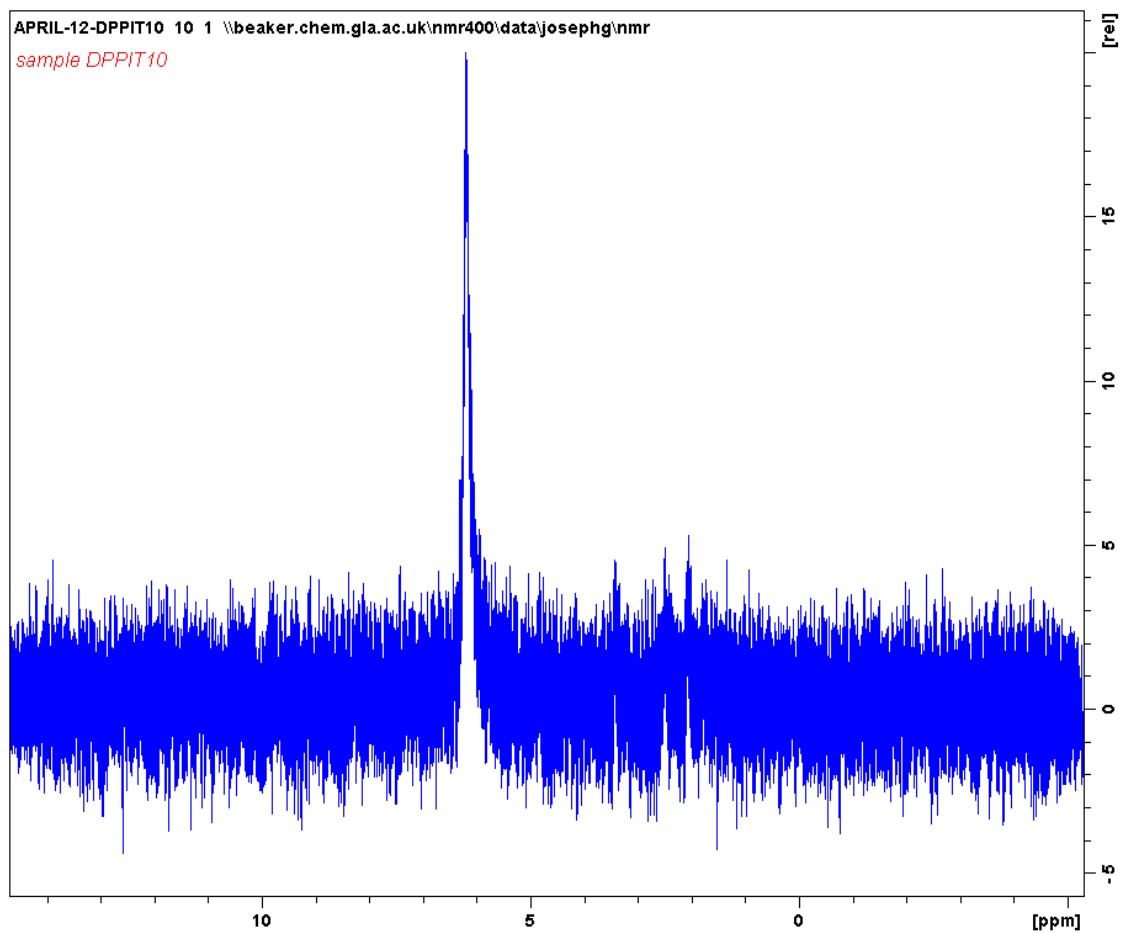


Figure 83 – Zero order plot to determine the initial rate constant of 1-phenyl-1-propyne deuteration at 50°C.



**Figure 84** –  $^2\text{H}$  NMR spectrum of a sample taken after 80 minutes of 1-phenyl-1-propyne deuteration at  $50^\circ\text{C}$ .

**Table 24 – Relative intensities, normalised relative to the smallest peak, of each significant peak in the  $^2\text{H}$  NMR spectrum of a sample taken after 10 minutes of 1-phenyl-1-propyne deuteration at 50°C.**

<b>Shift, <math>\delta</math> / ppm</b>	<b>Relative intensity</b>
6.19	6.8
3.43	1.0
2.49	1.0
2.07	1.0

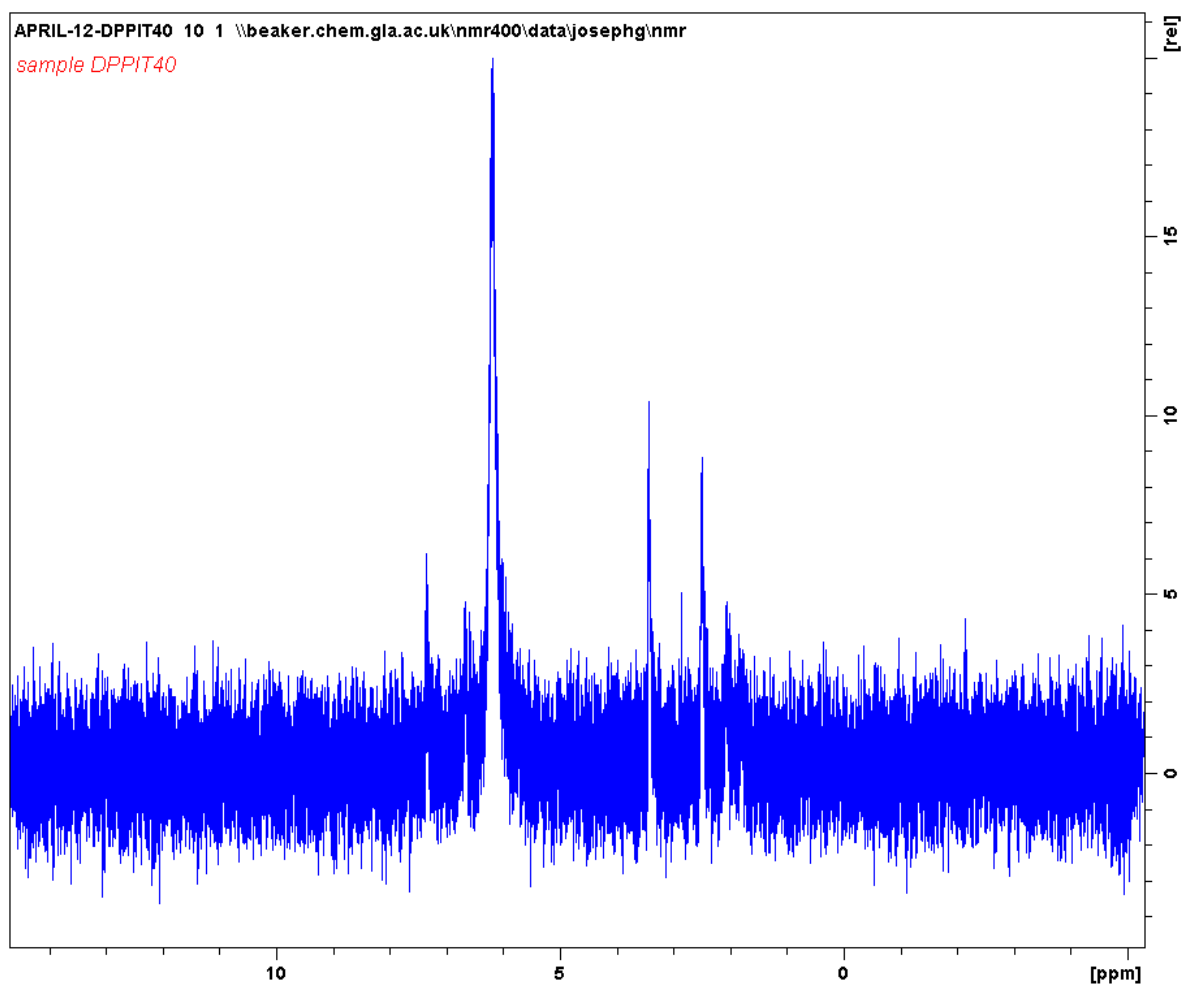


**Figure 85 –  $^2\text{H}$  NMR spectrum of a sample taken after 40 minutes of 1-phenyl-1-propyne deuteration at 50°C.**

**Table 25 – Relative intensities, normalised relative to the smallest peak, of each significant peak in the  $^2\text{H}$  NMR spectrum of a sample taken after 40 minutes of 1-phenyl-1-propyne deuteration at 50°C.**

<b>Shift, <math>\delta</math> / ppm</b>	<b>Relative intensity</b>
7.34	1.6
6.65	1.2
6.18	5.1
3.43	2.7
2.49	2.3
2.05	1.2
1.85	1.0

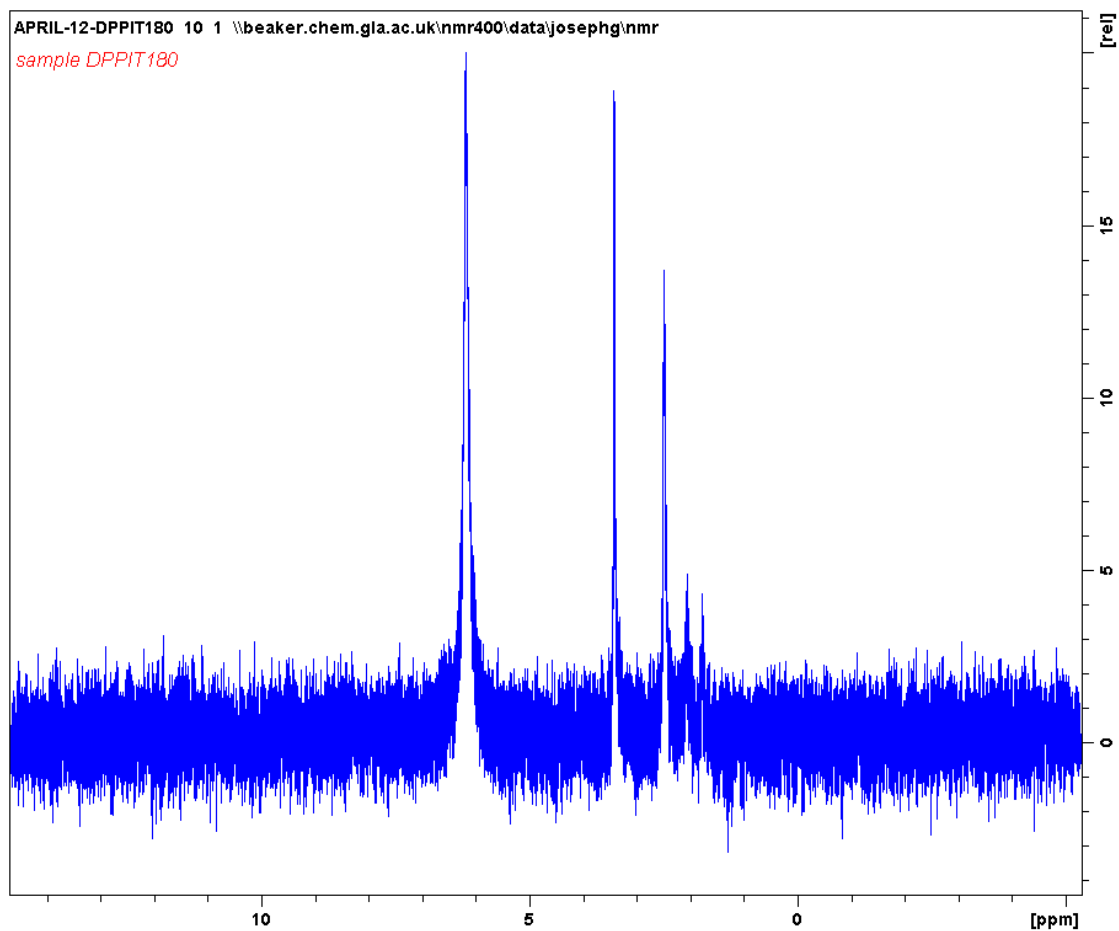


Figure 86 –  $^2\text{H}$  NMR spectrum of a sample taken after 180 minutes of 1-phenyl-1-propyne deuteration at 50°C.

**Table 26 – Relative intensities, normalised relative to the smallest peak, of each significant peak in the  $^2\text{H}$  NMR spectrum of a sample taken after 180 minutes of 1-phenyl-1-propyne deuteration at 50°C.**

<b>Shift, <math>\delta</math> / ppm</b>	<b>Relative intensity</b>
6.18	4.6
3.42	4.4
2.48	3.2
2.06	1.1
1.77	1.0

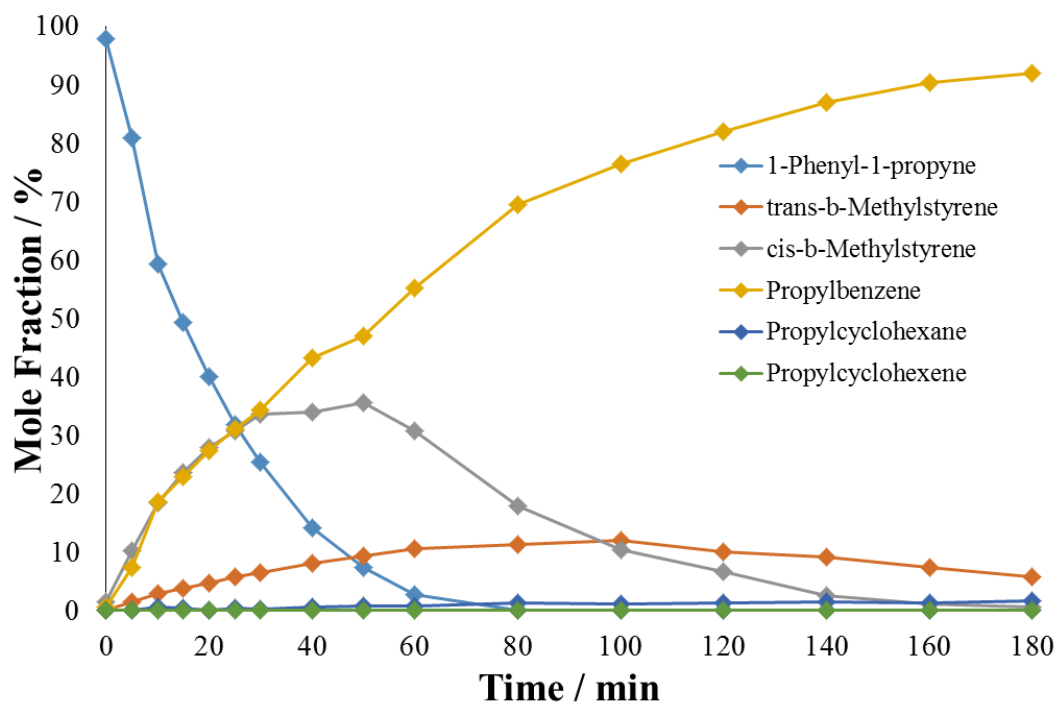


Figure 87 – Reaction profile for the deuteration of 1-phenyl-1-propyne. Conditions: 3 barg  $D_2$ , 10 mmol 1-phenyl-1-propyne, 70°C.

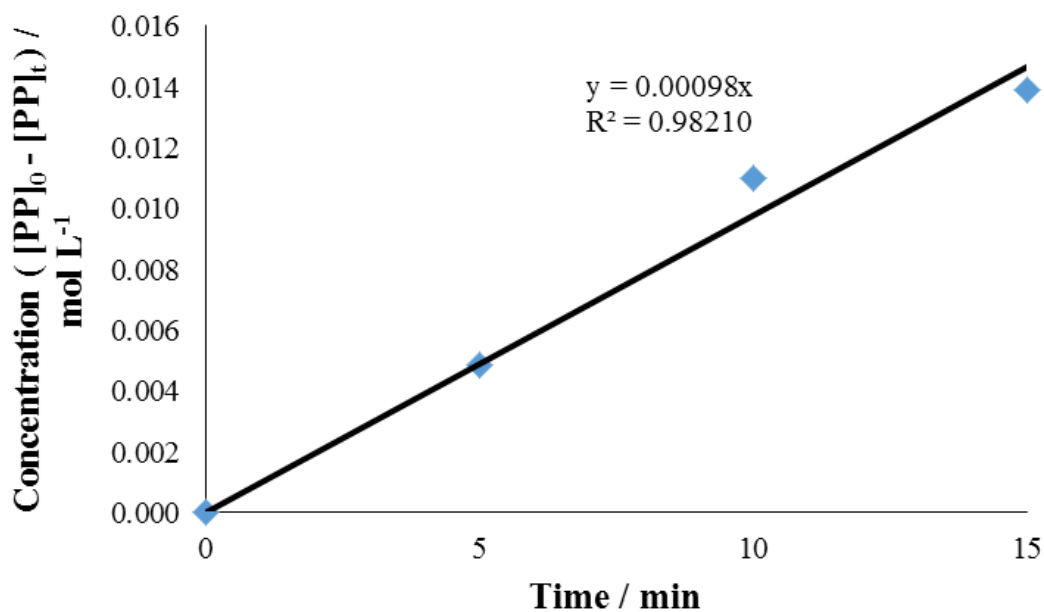
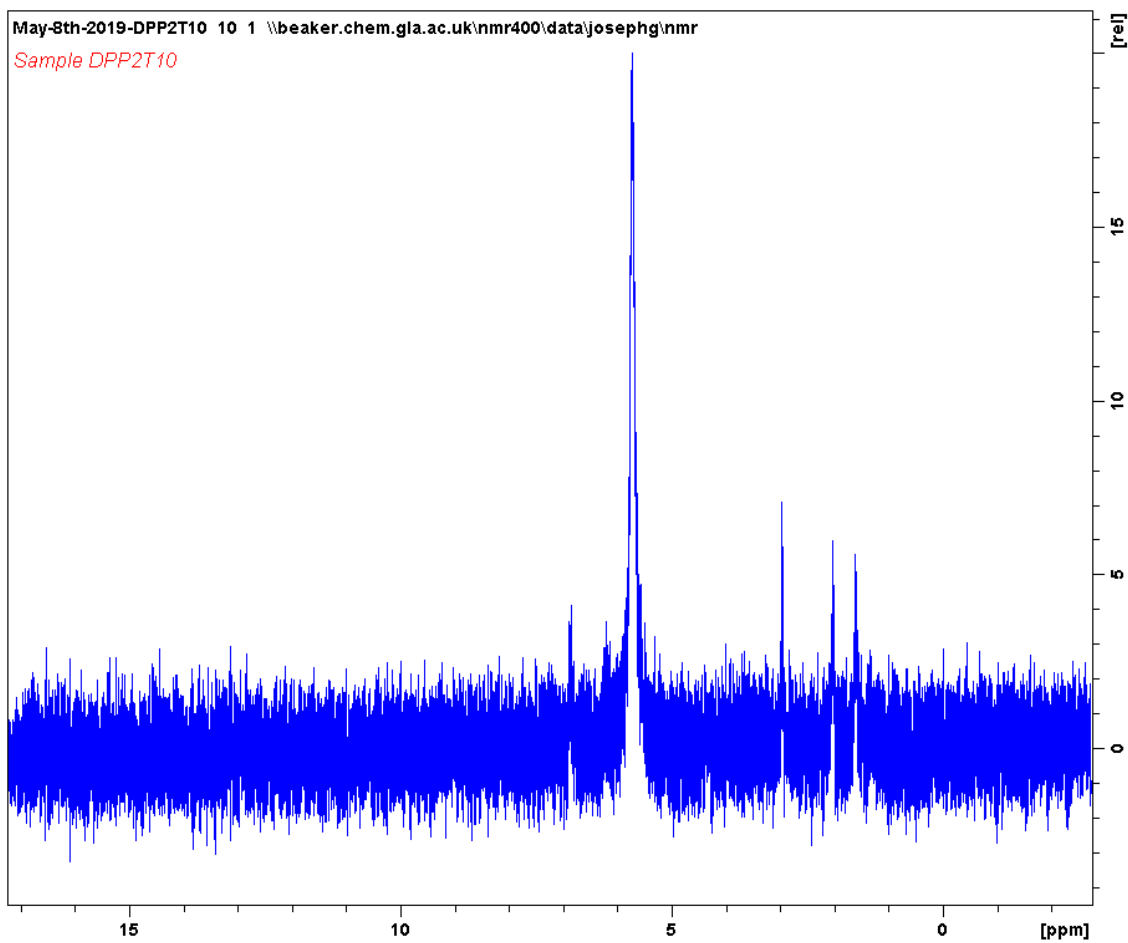


Figure 88 – Zero order plot to determine the initial rate constant of 1-phenyl-1-propyne deuteration at 70°C.



**Figure 89** –  $^2\text{H}$  NMR spectrum of a sample taken after 10 minutes of 1-phenyl-1-propyne deuteration at 70°C.

**Table 27 – Relative intensities, normalised relative to the smallest peak, of each significant peak in the  $^2\text{H}$  NMR spectrum of a sample taken after 10 minutes of 1-phenyl-1-propyne deuteration at 70°C.**

<b>Shift, <math>\delta</math> / ppm</b>	<b>Relative intensity</b>
6.85	1.0
5.72	4.9
2.96	1.7
2.03	1.5
1.61	1.4

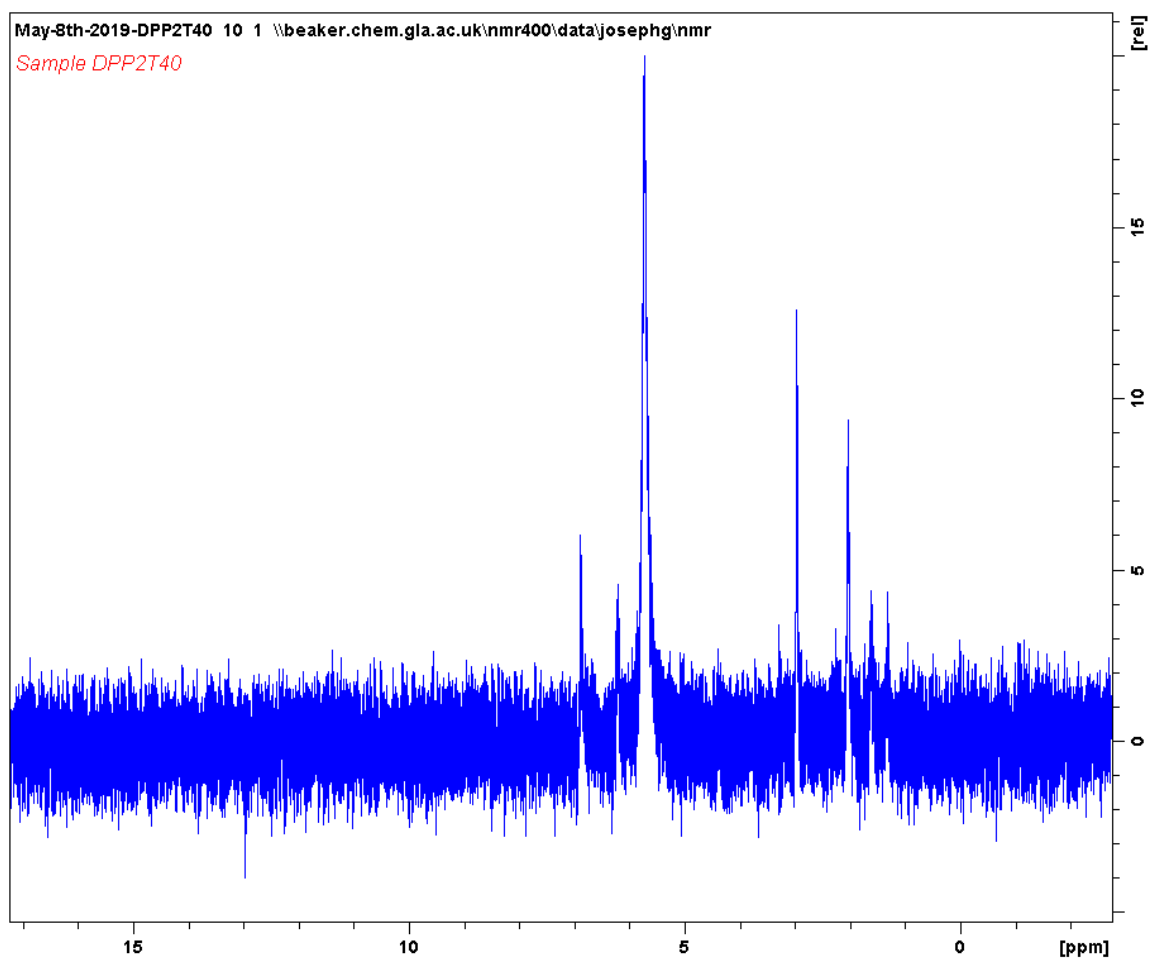


**Figure 90 –  $^2\text{H}$  NMR spectrum of a sample taken after 40 minutes of 1-phenyl-1-propyne deuteration at 70°C.**

**Table 28 – Relative intensities, normalised relative to the smallest peak, of each significant peak in the  $^2\text{H}$  NMR spectrum of a sample taken after 40 minutes of 1-phenyl-1-propyne deuteration at 70°C.**

<b>Shift, <math>\delta</math> / ppm</b>	<b>Relative intensity</b>
6.88	1.4
6.20	1.1
5.72	4.6
2.96	2.9
2.03	2.2
1.62	1.0
1.31	1.0

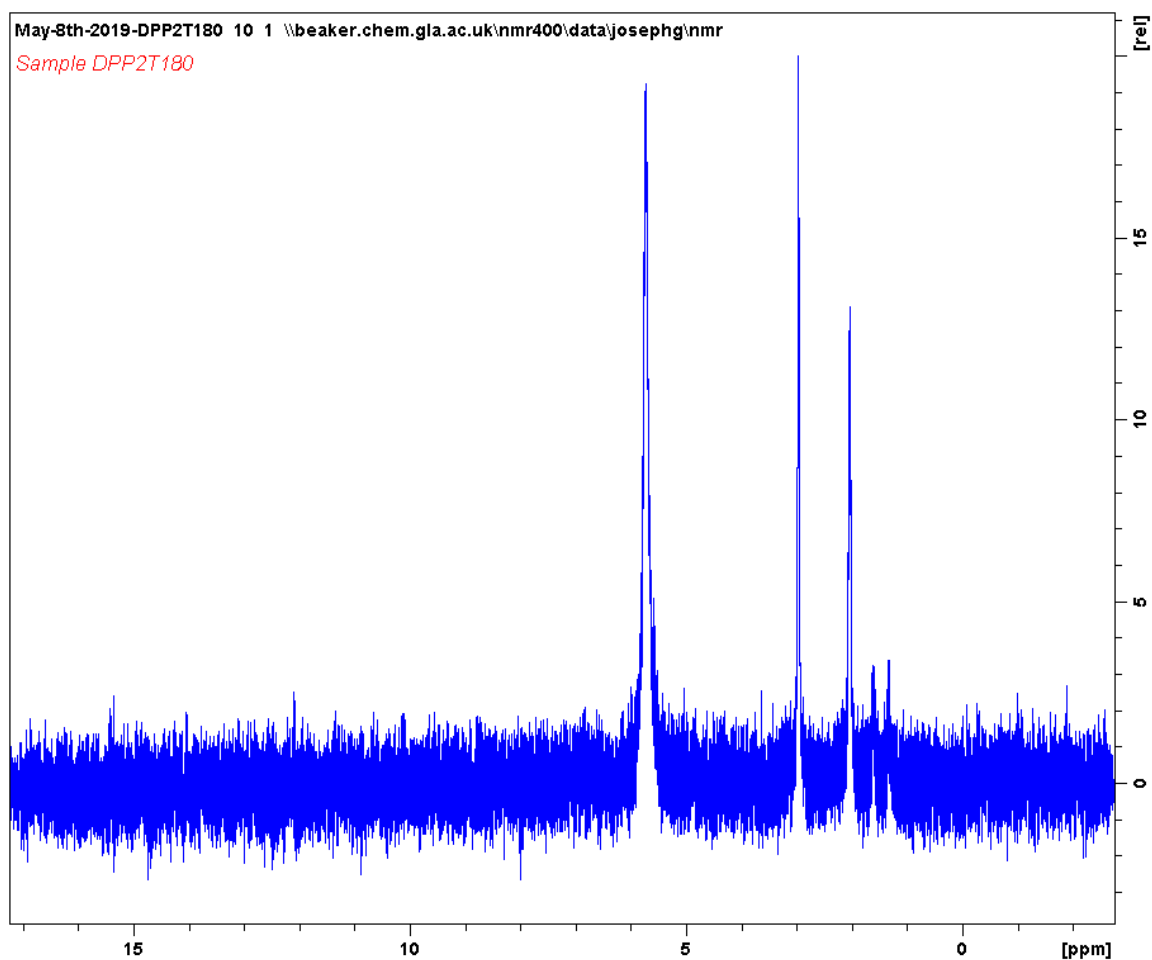


Figure 91 –  $^2\text{H}$  NMR spectrum of a sample taken after 180 minutes of 1-phenyl-1-propyne deuteration at  $70^\circ\text{C}$ .

**Table 29 – Relative intensities, normalised relative to the smallest peak, of each significant peak in the  $^2\text{H}$  NMR spectrum of a sample taken after 180 minutes of 1-phenyl-1-propyne deuteration at 70°C.**

Shift, $\delta$ / ppm	Relative intensity
5.72	6.0
2.96	6.2
2.03	4.1
1.61	1.0
1.32	1.0

The initial rates of reaction and kinetic isotope effects calculate are given in Table 30.

**Table 30 – The effect of changing the hydrogen isotope on the hydrogenation of 1-phenyl-1-propyne. At 50°C,  $k_{\text{H}}$  and  $k_{\text{D}}$  were found to be very similar, but at 70°C,  $k_{\text{H}}$  was observed to be greater than  $k_{\text{D}}$ .**

		$k_{\text{H}} \times 10^4 / \text{min}^{-1}$	$k_{\text{D}} \times 10^4 / \text{min}^{-1}$	$k_{\text{H}}/k_{\text{D}}$
<b>Temperature</b> / °C	50	8.7	8.6	1.0
	70	14.8	9.8	1.5

#### 4.1.4 Competitive Reactions

Competition can influence the kinetics of reactions through a number of processes, including direct competition for sites, indirect competition for reactants and alterations made to the catalyst.

The hydrogenation of toluene- $d_8$  in competition with phenylacetylene and with 1-phenyl-1-propyne was used to assess aspects of adsorption and exchange. The reaction profiles from reactions carried out at 50°C are shown in Figures 92 and 97. Zero order plots were also constructed and are shown in Figures 93 and 98.  $^2\text{H}$  NMR spectra are presented in Figures 94-96 and 99-101, with the corresponding data shown in Tables 31-36. It can be seen that in both reactions, the toluene- $d_8$  concentration did not change and that the  $^2\text{H}$  NMR spectra did not change over the course of the reaction. The mole fractions of molecules in the phenylacetylene and 1-phenyl-1-propyne cascades followed the same trends as when hydrogenated without competition. The rate of phenylacetylene hydrogenation decreases by a small amount when competition with toluene- $d_8$  is introduced, however the introduction of toluene- $d_8$  had the opposite effect on the rate of 1-phenyl-1-propyne hydrogenation, which increased by almost 20%.

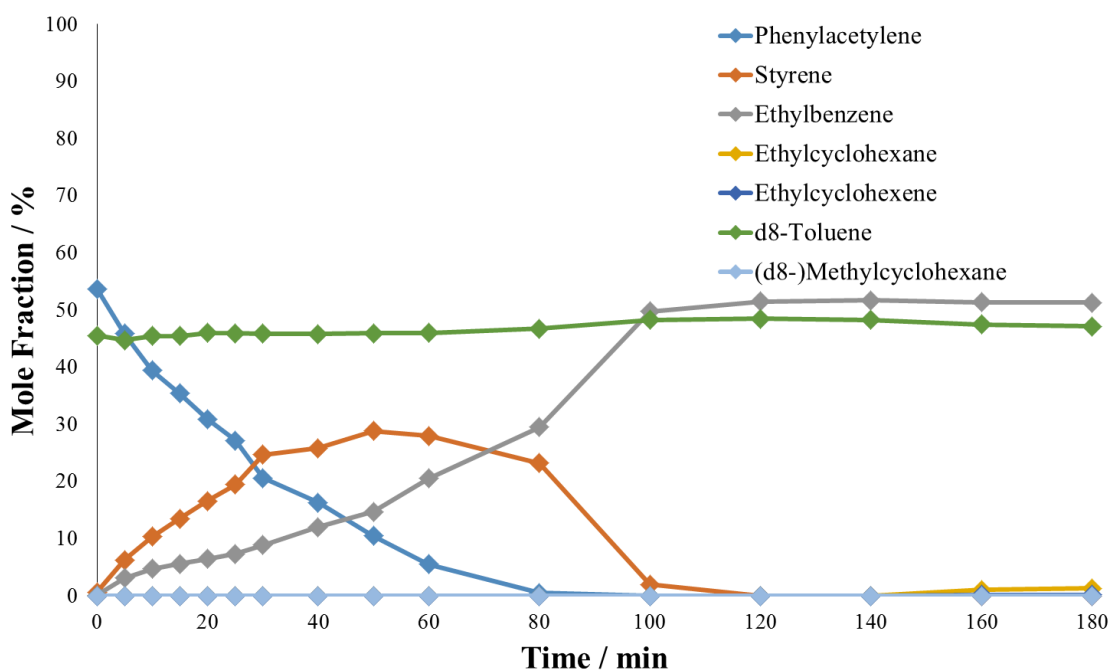


Figure 92 – Reaction profile for the competitive hydrogenation of phenylacetylene and toluene-d<sub>8</sub>. Conditions: 3 barg H<sub>2</sub>, 10 mmol phenylacetylene, 10 mmol toluene-d<sub>8</sub>, 50°C.

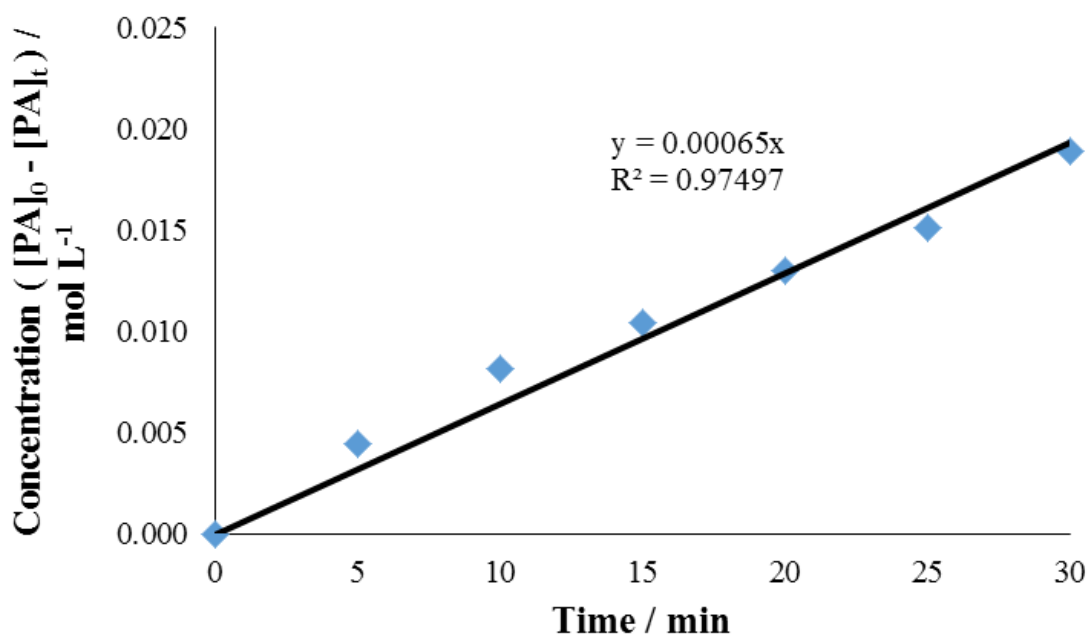
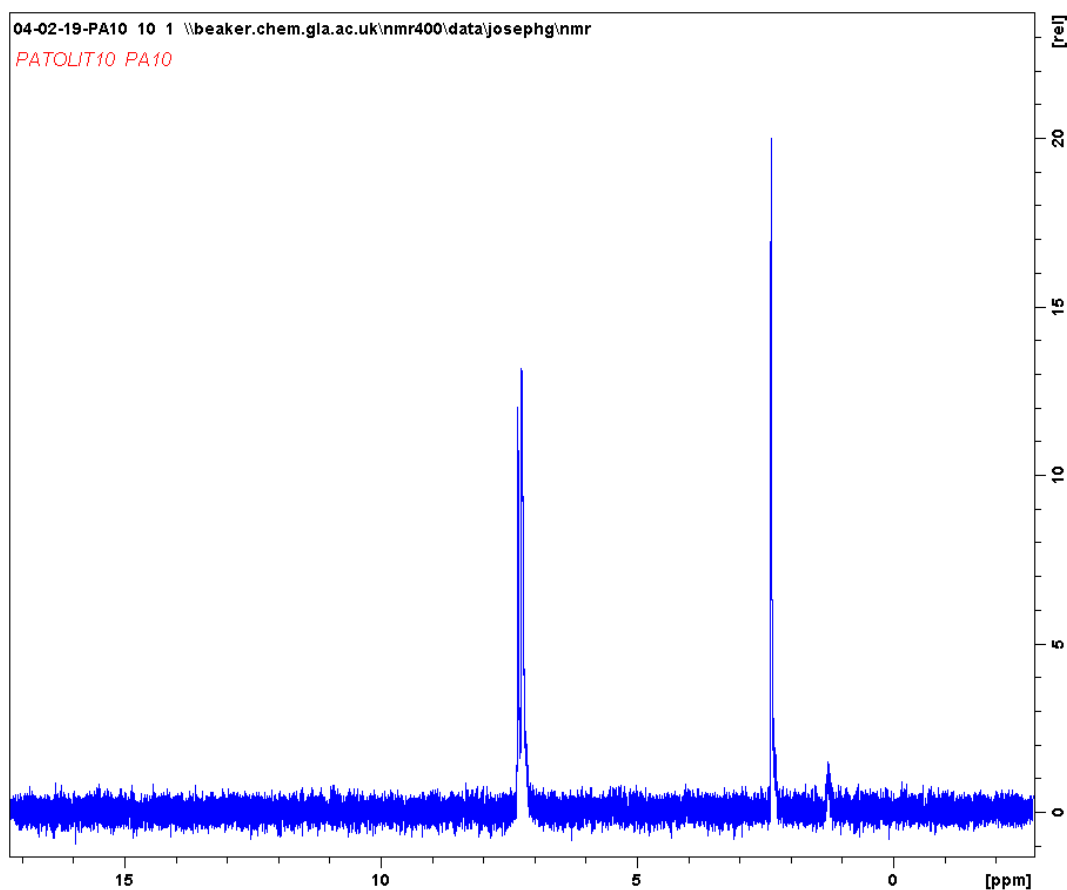


Figure 93 – Zero order plot to determine the initial rate constant of phenylacetylene hydrogenation in the presence of toluene-d<sub>8</sub> at 50°C.



**Figure 94** –  $^2\text{H}$  NMR spectrum of a sample taken after 10 minutes of competitive hydrogenation involving toluene- $\text{d}_8$  and phenylacetylene at  $50^\circ\text{C}$ .

**Table 31** – Relative intensities, normalised relative to the smallest peak, of each significant peak in the  $^2\text{H}$  NMR spectrum of a sample taken after 10 minutes of competitive hydrogenation involving toluene- $\text{d}_8$  and phenylacetylene at  $50^\circ\text{C}$ .

Shift, $\delta$ / ppm	Relative intensity
7.24	8.8
2.37	13.3
1.26	1.0

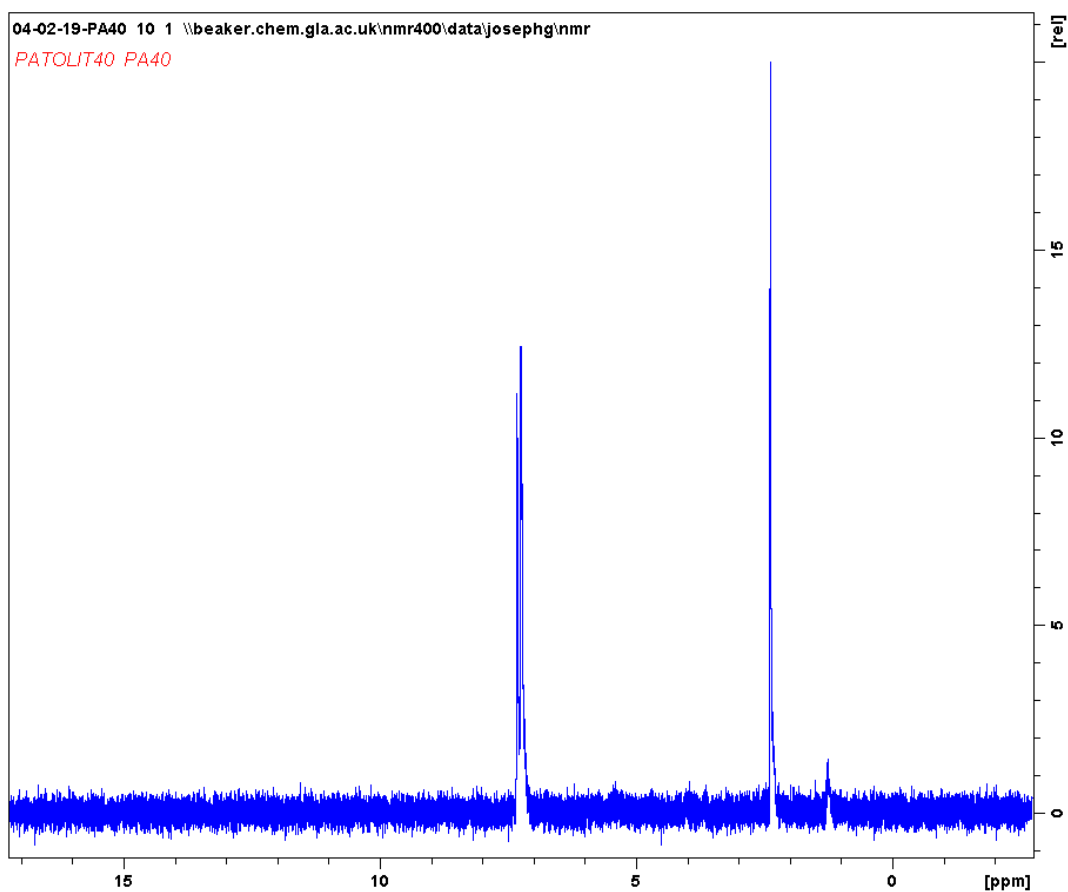


**Figure 95** –  $^2\text{H}$  NMR spectrum of a sample taken after 40 minutes of competitive hydrogenation involving toluene- $\text{d}_8$  and phenylacetylene at  $50^\circ\text{C}$ .

**Table 32** – Relative intensities, normalised relative to the smallest peak, of each significant peak in the  $^2\text{H}$  NMR spectrum of a sample taken after 40 minutes of competitive hydrogenation involving toluene- $\text{d}_8$  and phenylacetylene at  $50^\circ\text{C}$ .

Shift, $\delta$ / ppm	Relative intensity
7.24	8.6
2.37	13.8
1.24	1.0

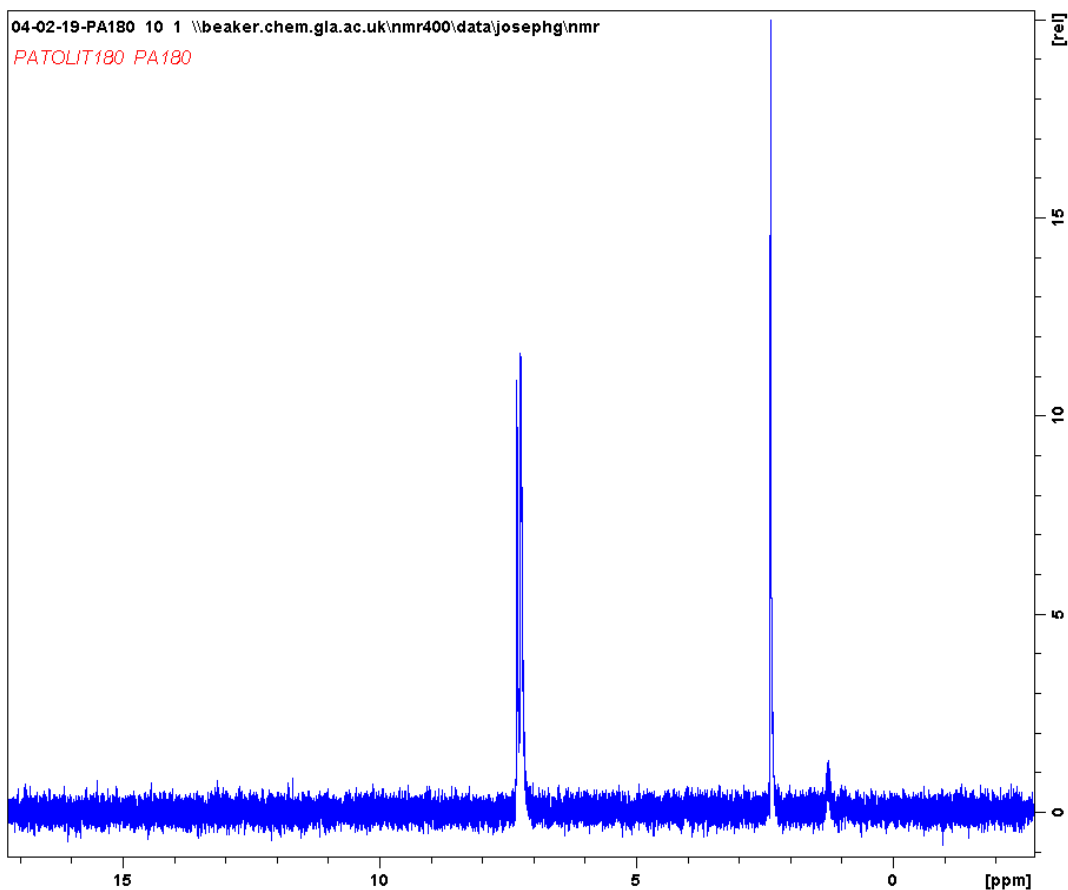


**Figure 96** –  $^2\text{H}$  NMR spectrum of a sample taken after 180 minutes of competitive hydrogenation involving toluene- $\text{d}_8$  and phenylacetylene at  $50^\circ\text{C}$ .

**Table 33** – Relative intensities, normalised relative to the smallest peak, of each significant peak in the  $^2\text{H}$  NMR spectrum of a sample taken after 180 minutes of competitive hydrogenation involving toluene- $\text{d}_8$  and phenylacetylene at  $50^\circ\text{C}$ .

Shift, $\delta$ / ppm	Relative intensity
7.24	8.8
2.37	15.2
1.24	1.0

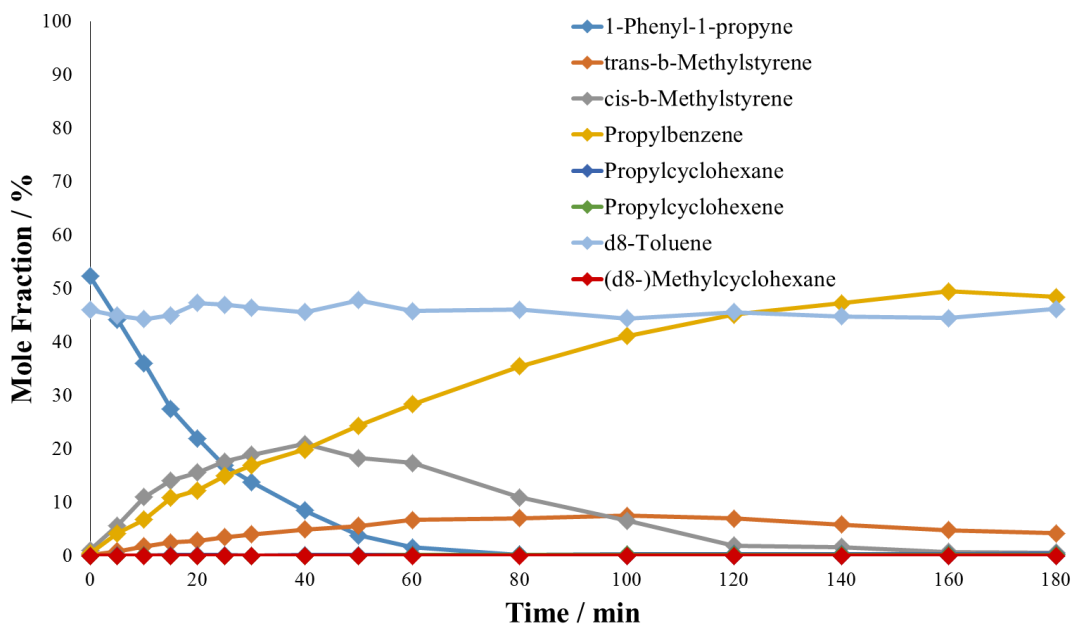


Figure 97 – Reaction profile for the competitive hydrogenation of 1-phenyl-1-propyne and toluene-d<sub>8</sub>. Conditions: 3 barg H<sub>2</sub>, 10 mmol 1-phenyl-1-propyne, 10 mmol toluene-d<sub>8</sub>, 50°C.

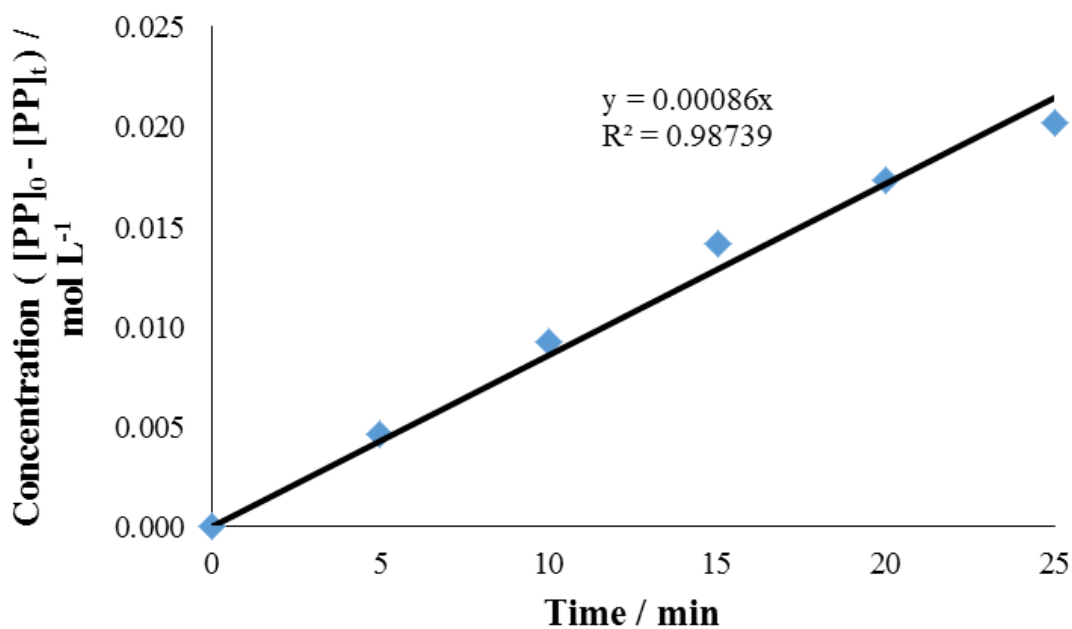
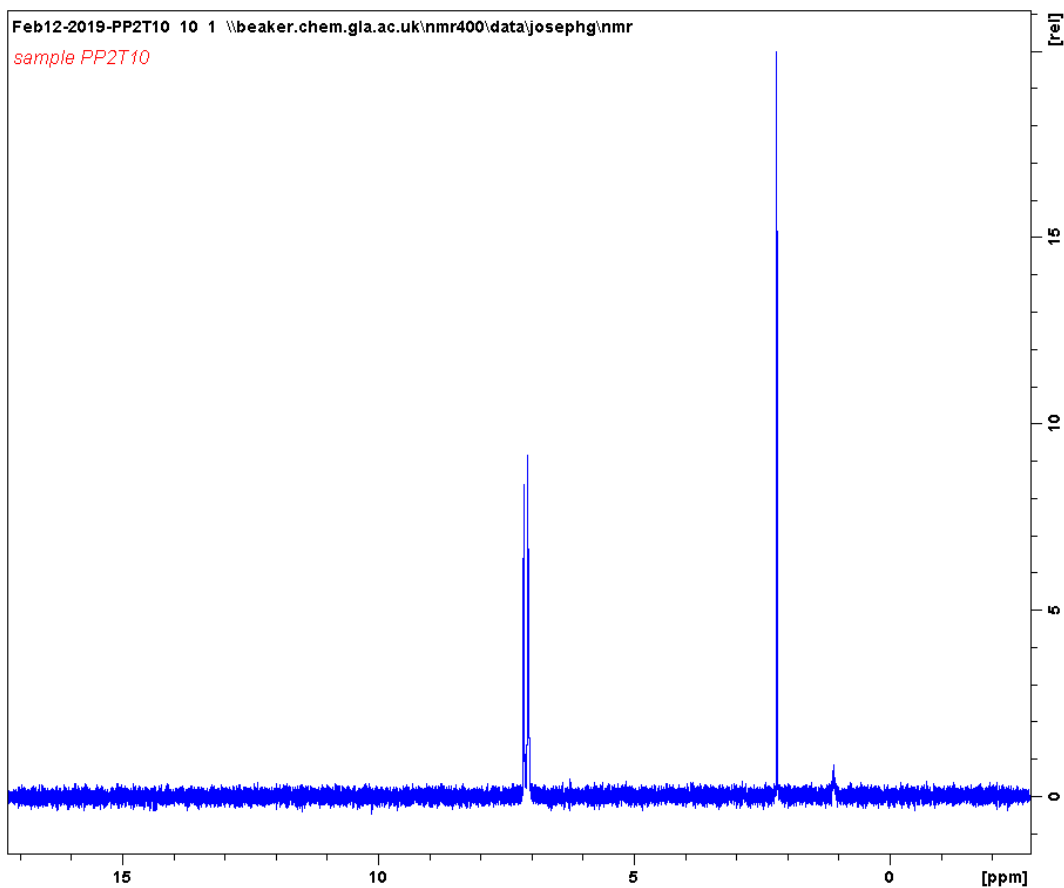


Figure 98 – Zero order plot to determine the initial rate constant of 1-phenyl-1-propyne hydrogenation in the presence of toluene-d<sub>8</sub> at 50°C.



**Figure 99** –  $^2\text{H}$  NMR spectrum of a sample taken after 10 minutes of competitive hydrogenation involving toluene- $\text{d}_8$  and 1-phenyl-1-propyne at  $50^\circ\text{C}$ .

**Table 34** – Relative intensities, normalised relative to the smallest peak, of each significant peak in the  $^2\text{H}$  NMR spectrum of a sample taken after 10 minutes of competitive hydrogenation involving toluene- $\text{d}_8$  and 1-phenyl-1-propyne at  $50^\circ\text{C}$ .

Shift, $\delta$ / ppm	Relative intensity
7.06	10.9
2.20	23.7
1.09	1.0

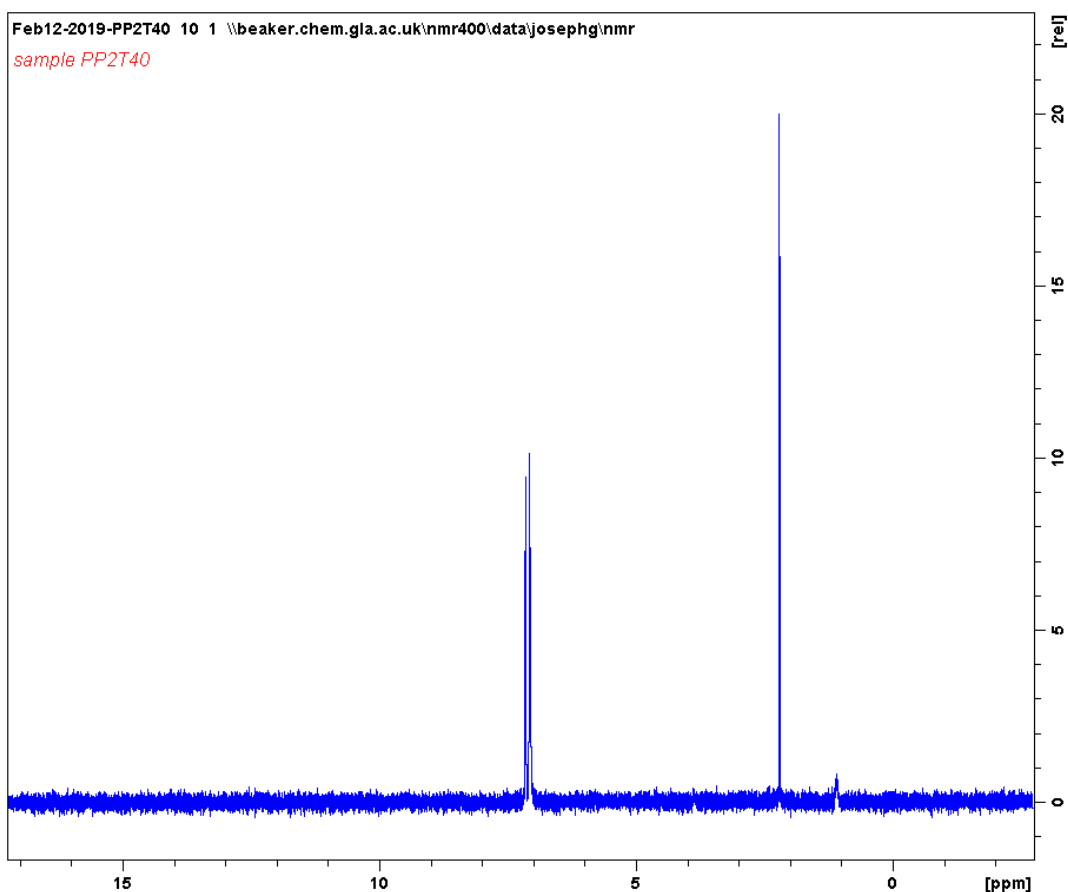


**Figure 100** –  $^2\text{H}$  NMR spectrum of a sample taken after 40 minutes of competitive hydrogenation involving toluene- $\text{d}_8$  and 1-phenyl-1-propyne at  $50^\circ\text{C}$ .

**Table 35** – Relative intensities, normalised relative to the smallest peak, of each significant peak in the  $^2\text{H}$  NMR spectrum of a sample taken after 40 minutes of competitive hydrogenation involving toluene- $\text{d}_8$  and 1-phenyl-1-propyne at  $50^\circ\text{C}$ .

Shift, $\delta$ / ppm	Relative intensity
7.07	12.2
2.20	24.1
1.08	1.0

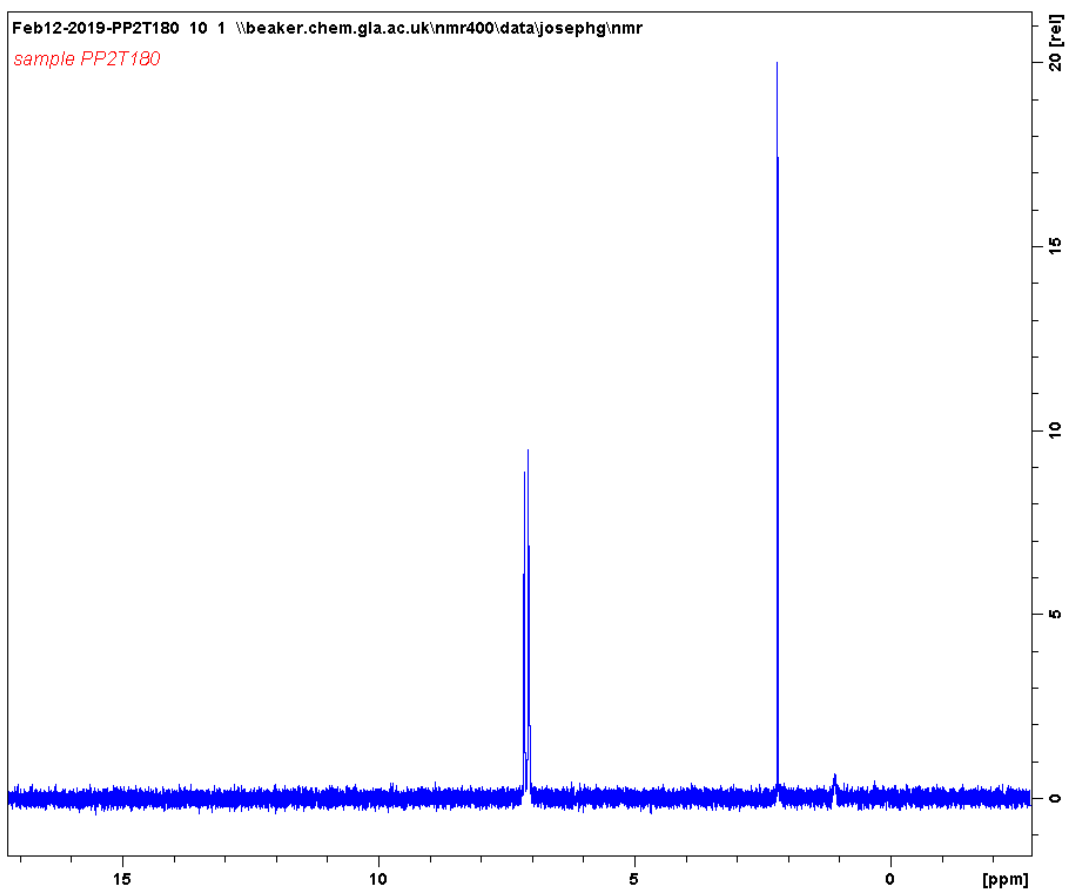


**Figure 101** –  $^2\text{H}$  NMR spectrum of a sample taken after 180 minutes of competitive hydrogenation involving toluene- $d_8$  and 1-phenyl-1-propyne at  $50^\circ\text{C}$ .

**Table 36** – Relative intensities, normalised relative to the smallest peak, of each significant peak in the  $^2\text{H}$  NMR spectrum of a sample taken after 180 minutes of competitive hydrogenation involving toluene- $d_8$  and 1-phenyl-1-propyne at  $50^\circ\text{C}$ .

Shift, $\delta$ / ppm	Relative intensity
7.06	14.3
2.20	30.1
1.08	1.0

Kinetic data from the competitive hydrogenation reactions of phenylacetylene and 1-phenyl-1-propyne with toluene-d<sub>8</sub> is reported in Table 37.

**Table 37 – The effect of competition with toluene-d<sub>8</sub> on the initial rate constant of hydrogenation of phenylacetylene and 1-phenyl-1-propyne. For phenylacetylene, the initial rate constant decreased with toluene-d<sub>8</sub> competition, whereas in the case of 1-phenyl-1-propyne, an increase in initial rate constant was observed.**

	<b>Initial rate constant, <math>k_0 \times 10^4 / \text{mol L}^{-1} \text{min}^{-1}</math></b>	
	<b>Phenylacetylene</b>	<b>1-Phenyl-1-propyne</b>
<b>Non-competitive</b>	7.3	7.2
<b>Competition with Toluene-d<sub>8</sub></b>	6.5	8.6

Adding ethylbenzene minimally decreased the rate of hydrogenation of phenylacetylene, but drastically reduced the rate of ring hydrogenation. The reaction profiles for the competitive hydrogenation of phenylacetylene and ethylbenzene at temperatures of 50°C and 70°C are shown in Figures 102 and 104. Zero order plots were also constructed and are shown in Figures 103 and 105. Initially, the phenylacetylene mole fraction decreased and the styrene and ethylbenzene mole fractions increased moderately. As the phenylacetylene mole fraction approached 0%, the styrene mole fraction reached a maximum. Subsequently, the styrene mole fraction started to decrease and the ethylbenzene neared 100%. Ethylcyclohexane was then produced in smaller quantities than it was in the absence of competition: the yield increased with an increase in temperature. All aspects of the reaction increased in rate when the temperature was increased.

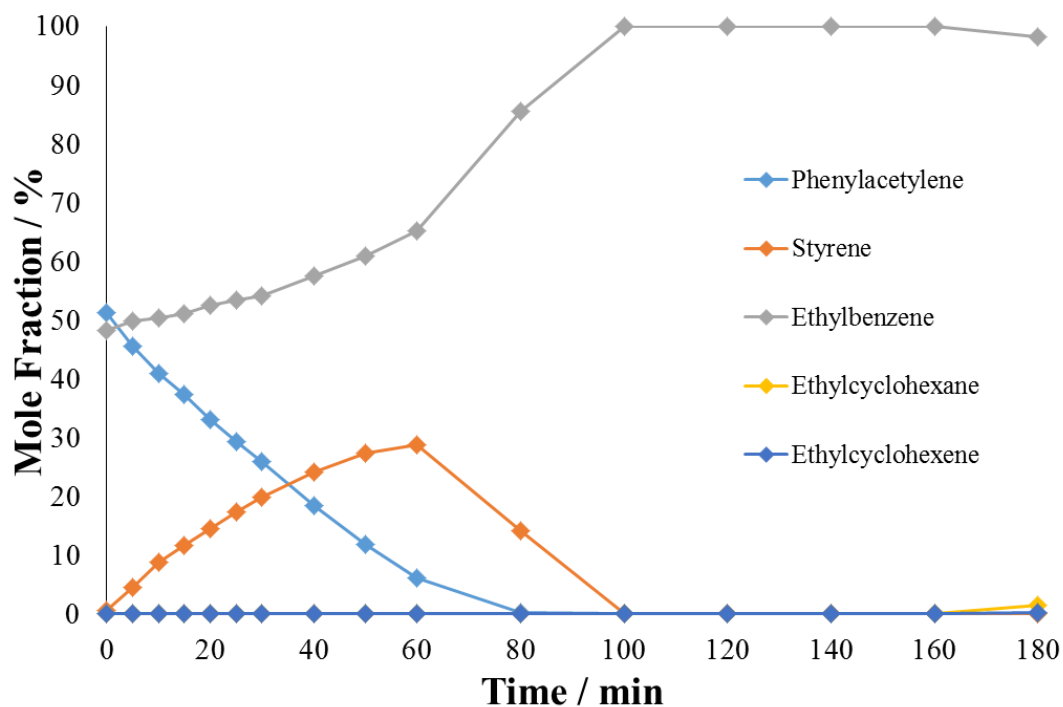


Figure 102 – Reaction profile for the competitive hydrogenation of phenylacetylene and ethylbenzene. Conditions: 3 barg  $H_2$ , 10 mmol phenylacetylene, 10 mmol ethylbenzene, 50°C.

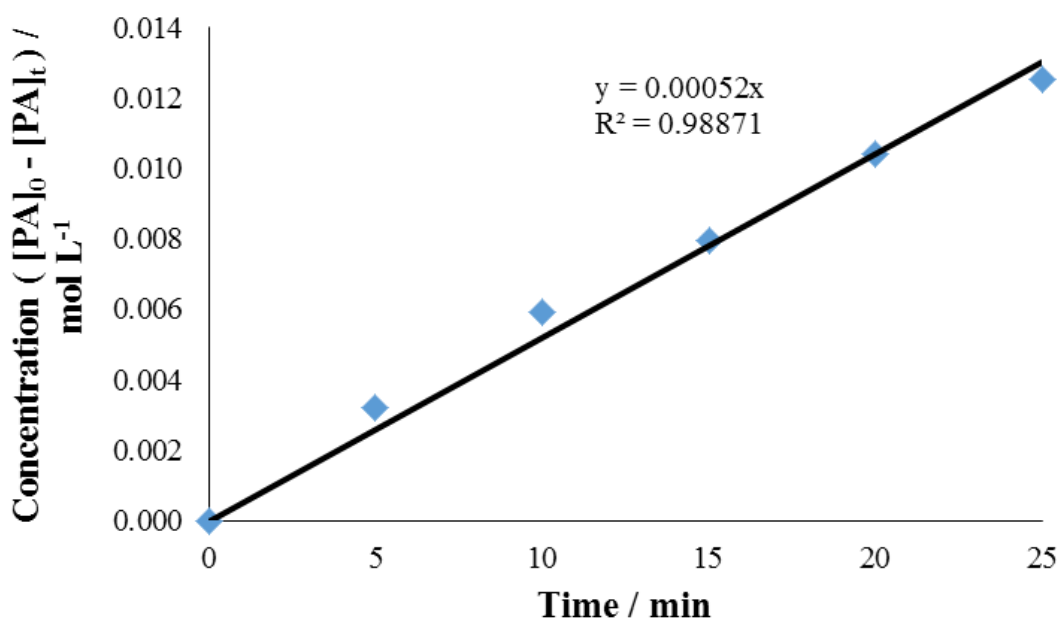


Figure 103 – Zero order plot to determine the initial rate constant of phenylacetylene hydrogenation in the presence of ethylbenzene at 50°C.

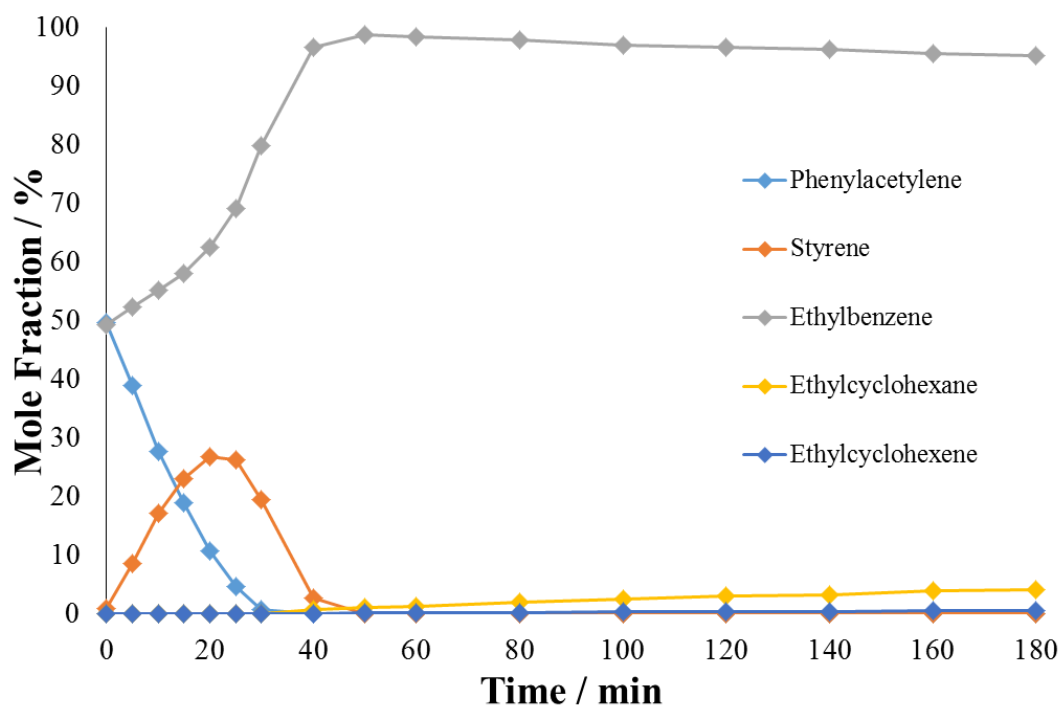


Figure 104 – Reaction profile for the competitive hydrogenation of phenylacetylene and ethylbenzene. Conditions: 3 barg  $H_2$ , 10 mmol phenylacetylene, 10 mmol ethylbenzene, 70°C.

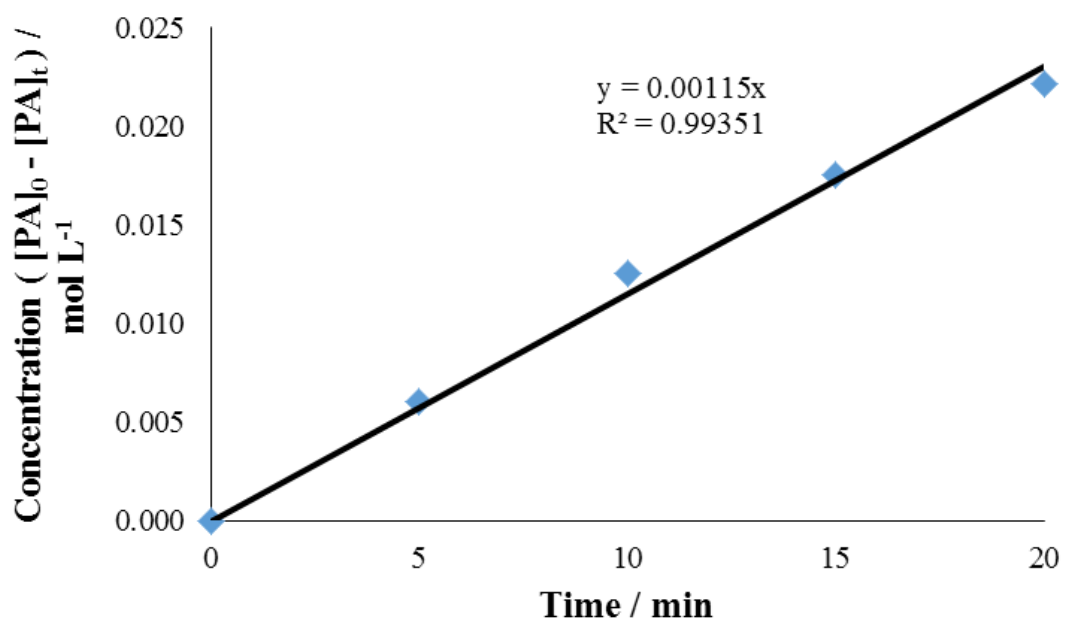
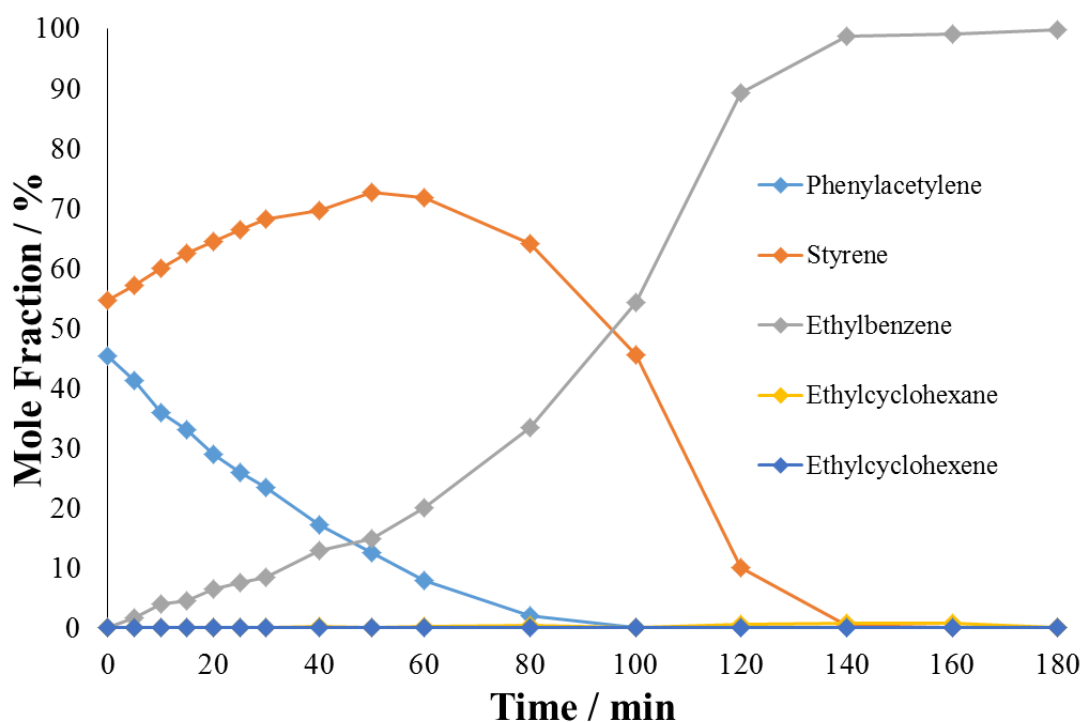


Figure 105 – Zero order plot to determine the initial rate constant of phenylacetylene hydrogenation in the presence of ethylbenzene at 70°C.

Styrene has a similar effect to ethylbenzene on phenylacetylene hydrogenation, as can be seen in the following results. The reaction profiles for the competitive hydrogenation of phenylacetylene and styrene at temperatures of 50°C and 70°C are shown in Figures 106 and 108. Zero order plots were also constructed and are shown in Figures 107 and 109. Initially, the phenylacetylene mole fraction decreased and the styrene and ethylbenzene mole fractions increased moderately. As the phenylacetylene mole fraction approached 0%, the styrene mole fraction reached a maximum. Subsequently, the styrene mole fraction started to decrease and the ethylbenzene neared 100%. Ethylcyclohexane was then produced in smaller quantities than it was in the absence of competition which were increased by an increase in temperature. All aspects of the reaction increased in rate when the temperature was increased.



**Figure 106 – Reaction profile for the competitive hydrogenation of phenylacetylene and styrene. Conditions: 3 barg H<sub>2</sub>, 10 mmol phenylacetylene, 10 mmol styrene, 50°C.**

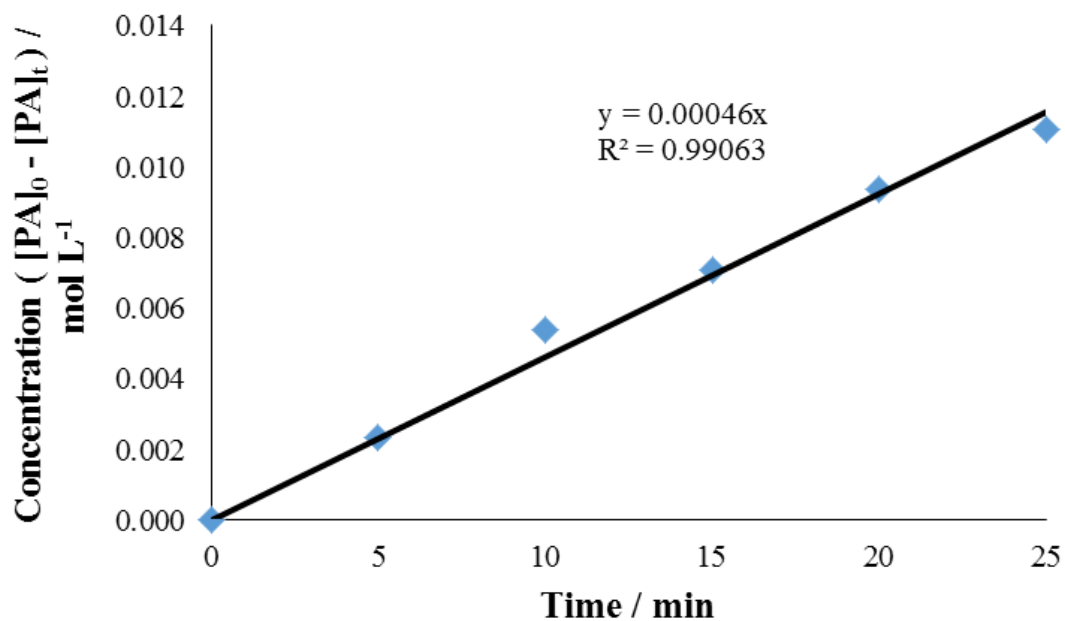


Figure 107 – Zero order plot to determine the initial rate constant of phenylacetylene hydrogenation in the presence of styrene at 50°C.

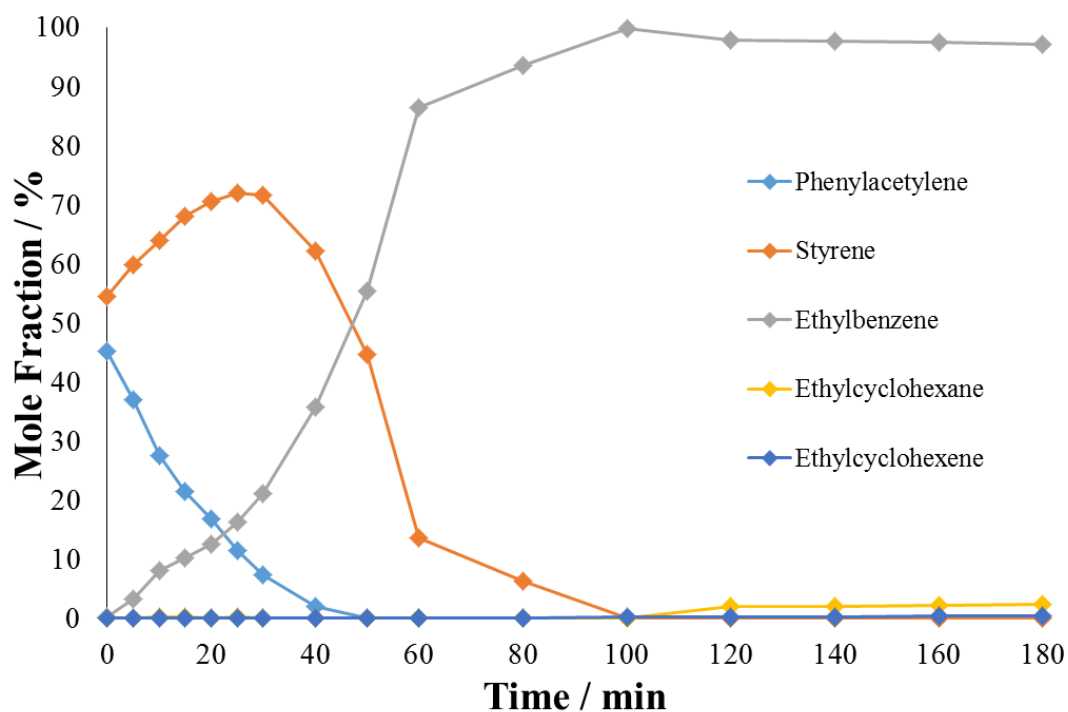
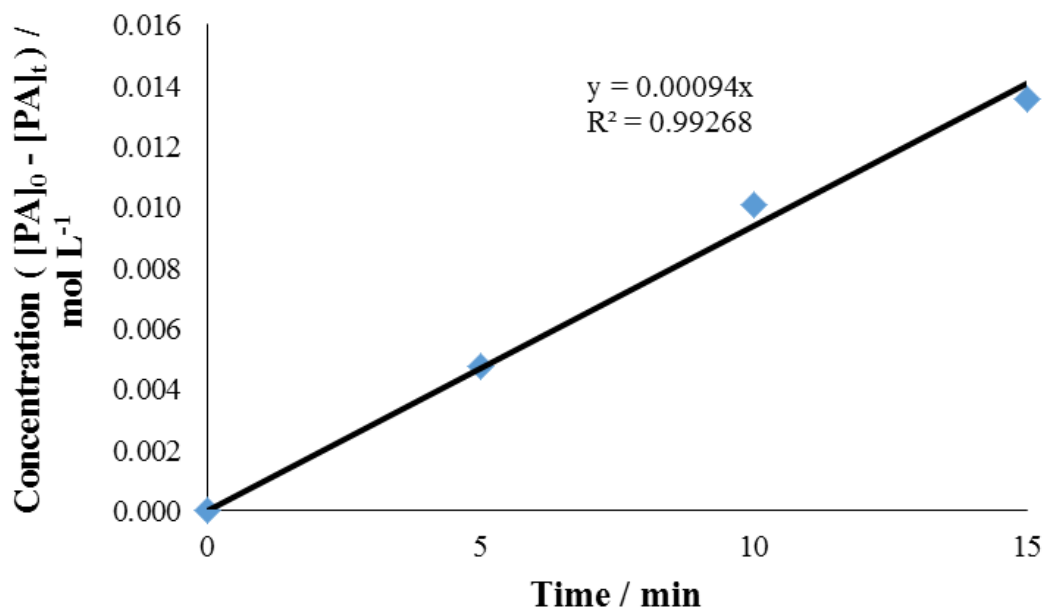


Figure 108 – Reaction profile for the competitive hydrogenation of phenylacetylene and styrene. Conditions: 3 barg H<sub>2</sub>, 10 mmol phenylacetylene, 10 mmol styrene, 70°C.



**Figure 109 – Zero order plot to determine the initial rate constant of phenylacetylene hydrogenation in the presence of styrene at 70°C.**

The effect of competition between 1-phenyl-1-propyne and propylbenzene produced similar results to those observed when phenylacetylene and ethylbenzene were hydrogenated together. The reaction profiles for the competitive hydrogenation of 1-phenyl-1-propyne and propylbenzene at temperatures of 50°C and 70°C are shown in Figures 110 and 112. Zero order plots were also constructed and are shown in Figures 111 and 113. The processes are generally slowed by the presence of the competitive species and the rate of increase of the ring hydrogenation products falls close to zero. All aspects of the reaction increased in rate when the temperature was increased.

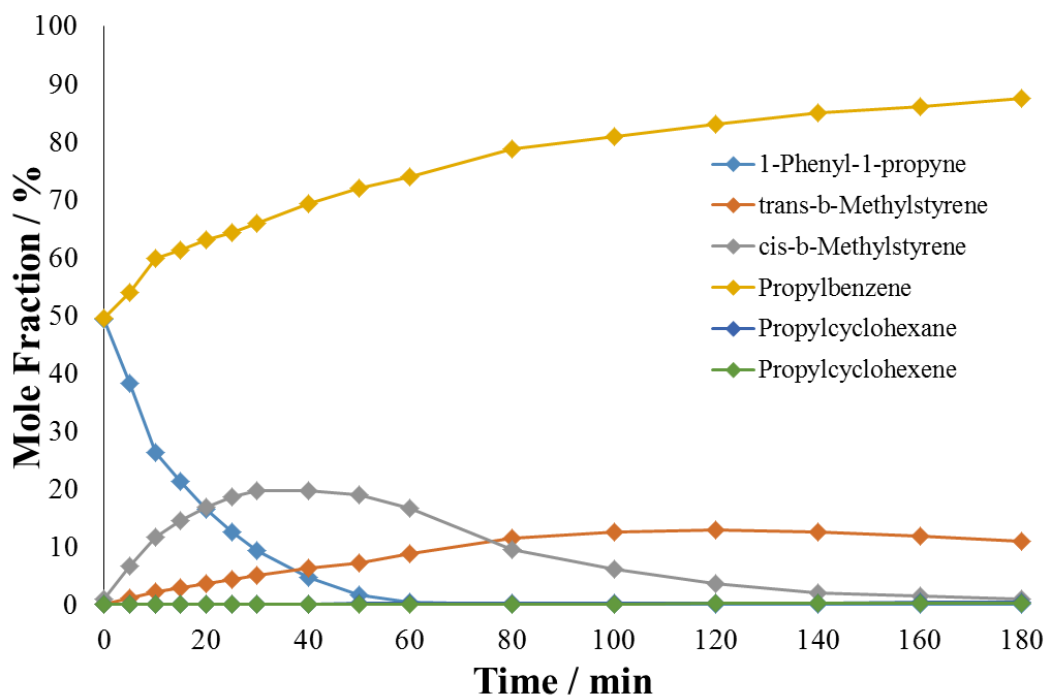


Figure 110 – Reaction profile for the competitive hydrogenation of 1-phenyl-1-propyne and propylbenzene. Conditions: 3 barg  $H_2$ , 10 mmol 1-phenyl-1-propyne, 10 mmol propylbenzene, 50°C.

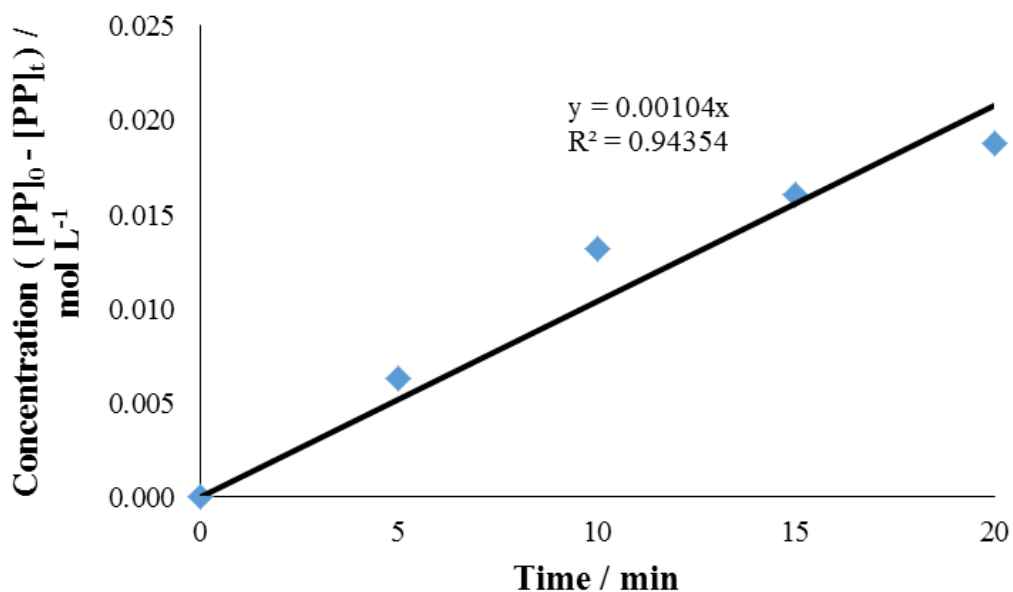


Figure 111 – Zero order plot to determine the initial rate constant of 1-phenyl-1-propyne hydrogenation in the presence of propylbenzene at 50°C.

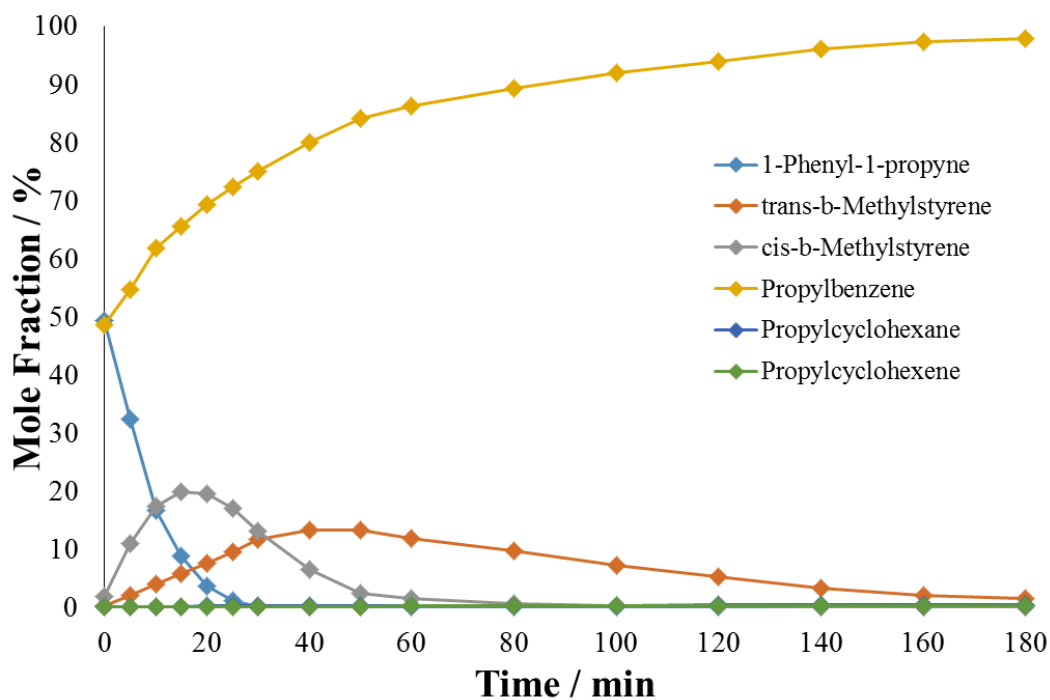


Figure 112 – Reaction profile for the competitive hydrogenation of 1-phenyl-1-propyne and propylbenzene. Conditions: 3 barg  $H_2$ , 10 mmol 1-phenyl-1-propyne, 10 mmol propylbenzene, 70°C.

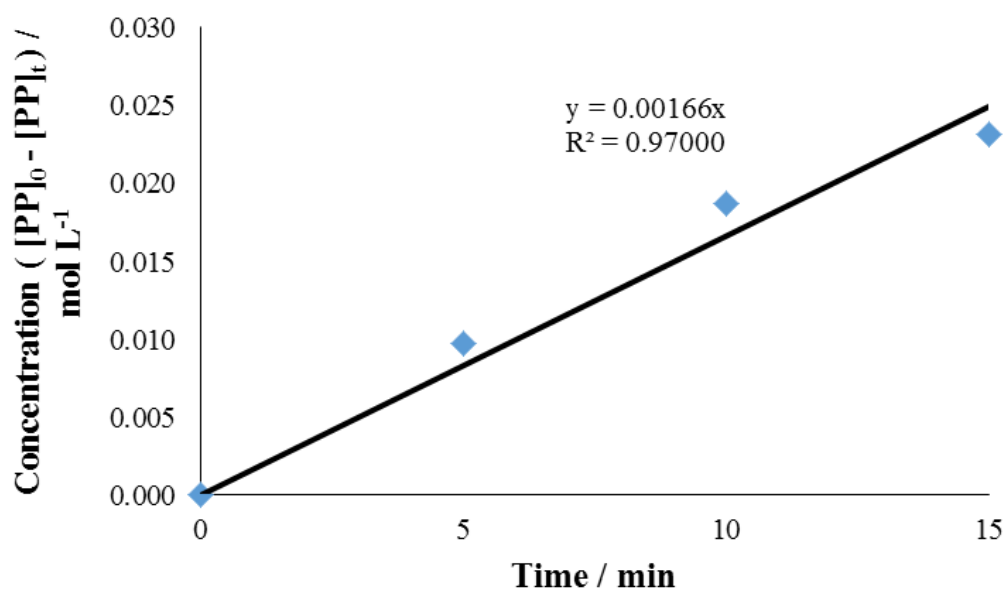
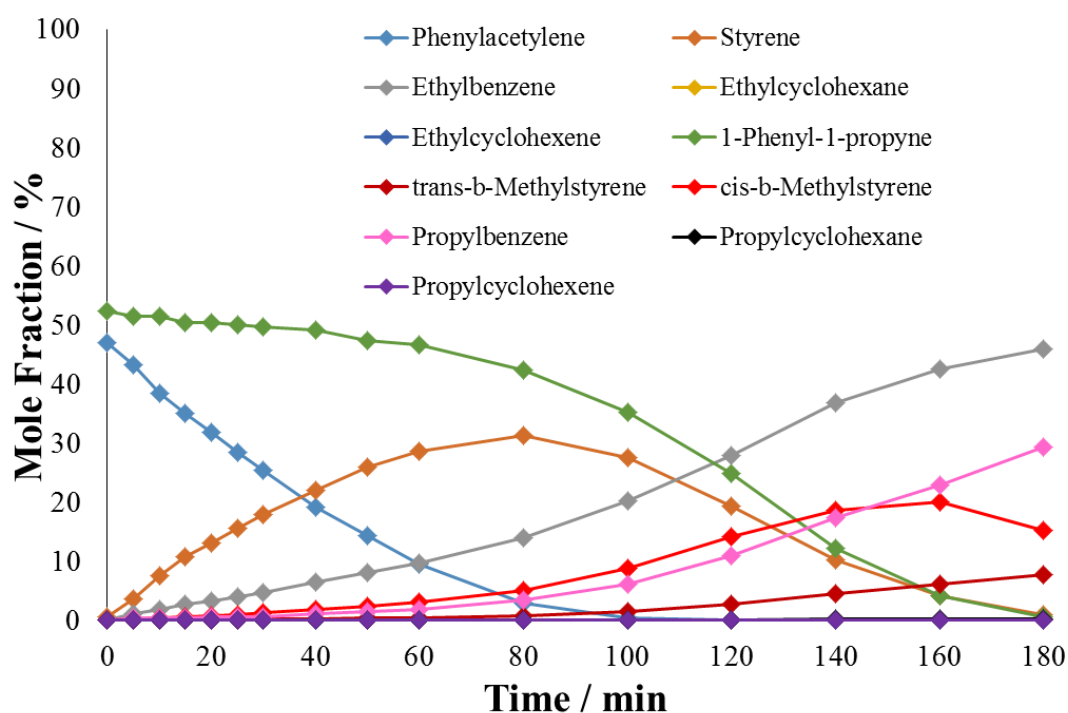


Figure 113 – Zero order plot to determine the initial rate constant of 1-phenyl-1-propyne hydrogenation in the presence of propylbenzene at 70°C.

Competition between phenylacetylene and 1-phenyl-1-propyne has a much more pronounced effect on the hydrogenation of 1-phenyl-1-propyne relative to its non-competitive hydrogenation than it did on phenylacetylene hydrogenation. The reaction profiles for the competitive hydrogenation of phenylacetylene and 1-phenyl-1-propyne at temperatures of 50°C and 70°C are shown in Figures 114 and 117. Zero order plots were also constructed and are shown in Figures 115-116 and 118-119. Initially, the phenylacetylene mole fraction decreased and the styrene and ethylbenzene mole fractions increased moderately. The change in mole fractions of molecules in the phenylacetylene cascade was slowed minimally by competition, but the changes in mole fractions of molecules in the 1-phenyl-1-propyne cascade were delayed until the phenylacetylene mole fraction neared 0%. All aspects of the reaction increased in rate when the temperature was increased.



**Figure 114 – Reaction profile for the competitive hydrogenation of phenylacetylene and 1-phenyl-1-propyne. Conditions: 3 barg H<sub>2</sub>, 10 mmol phenylacetylene, 10 mmol 1-phenyl-1-propyne, 50°C.**

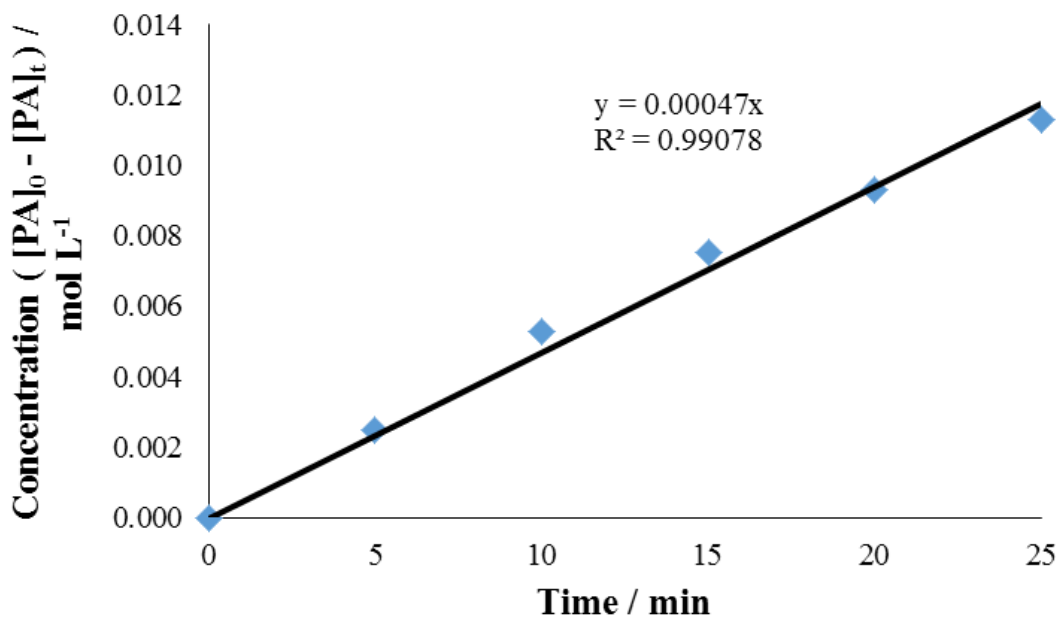


Figure 115 – Zero order plot to determine the initial rate constant of phenylacetylene hydrogenation in the presence of 1-phenyl-1-propyne at 50°C.

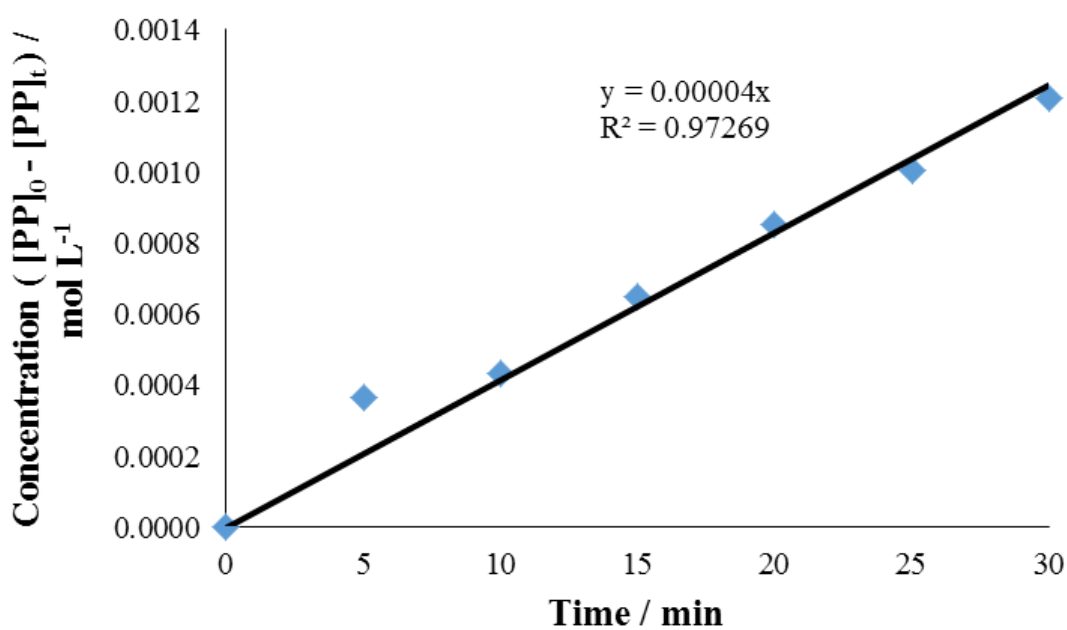


Figure 116 – Zero order plot to determine the initial rate constant of 1-phenyl-1-propyne hydrogenation in the presence of phenylacetylene at 50°C.

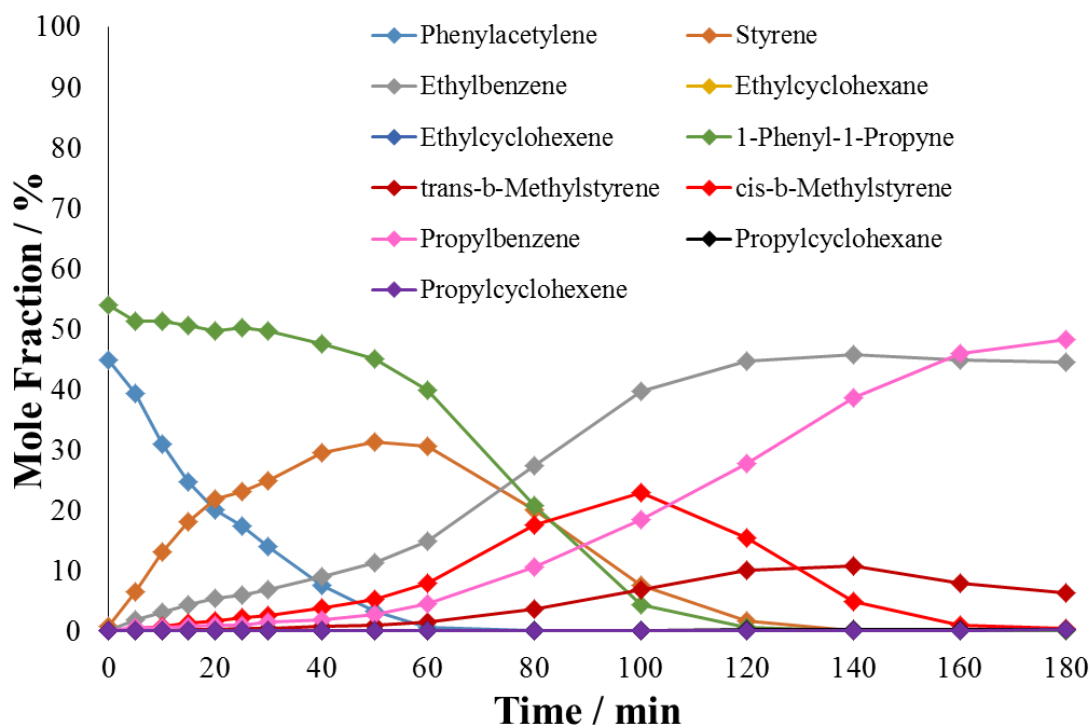


Figure 117 – Reaction profile for the competitive hydrogenation of phenylacetylene and 1-phenyl-1-propyne. Conditions: 3 barg  $H_2$ , 10 mmol phenylacetylene, 10 mmol 1-phenyl-1-propyne, 70°C.

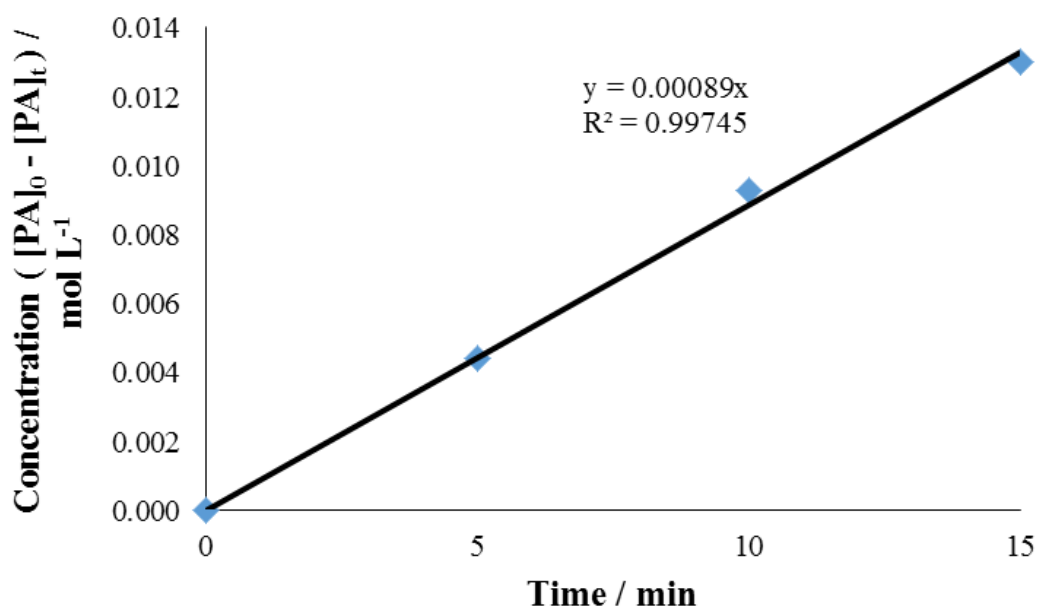
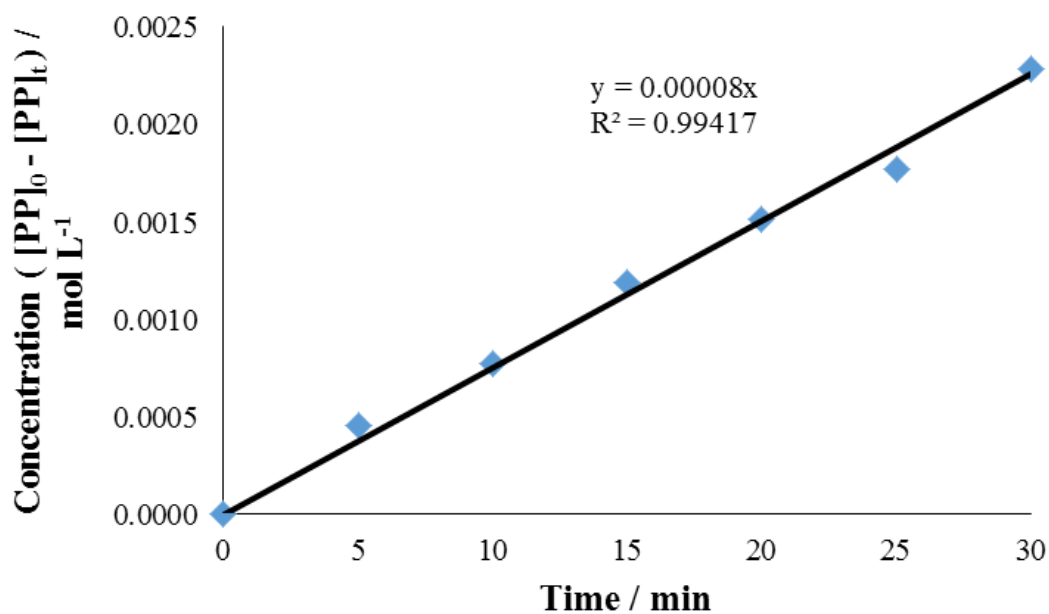


Figure 118 – Zero order plot to determine the initial rate constant of phenylacetylene hydrogenation in the presence of 1-phenyl-1-propyne at 70°C.



**Figure 119 – Zero order plot to determine the initial rate constant of 1-phenyl-1-propyne hydrogenation in the presence of phenylacetylene at 70°C.**

The initial rates of hydrogenation of phenylacetylene under the discussed competitive conditions are given in Table 38. The initial rate constant was generally decreased by competition and increases with an increase in temperature.

**Table 38 – A comparison of the initial rate constants of hydrogenation of phenylacetylene with no competition, in competition with ethylbenzene, and in competition with 1-phenyl-1-propyne.**

	<b>Initial rate constant, <math>k_0 \times 10^4 / \text{mol L}^{-1} \text{min}^{-1}</math></b>			
<b>Temperature / °C</b>	PA	PA + EB	PA + STY	PA + PP
50	7.1	5.2	4.6	4.7
70	14.9	11.5	9.4	8.9

Upon closer inspection of the data, it can be noted that the presence of propylbenzene enhances the rate of 1-phenyl-1-propyne hydrogenation. The initial rates of hydrogenation of 1-phenyl-1-propyne under the discussed competitive conditions are given in Table 39. The initial rate constants for competitive hydrogenation with propylbenzene were observed to be greater than those for non-competitive reactions, however the initial rate constants for competitive hydrogenation with phenylacetylene were significantly smaller than those for non-competitive reactions. An increase in temperature increased the rate of reaction.

**Table 39 – A comparison of the initial rate constants of hydrogenation of 1-phenyl-1-propyne with no competition, in competition with propylbenzene, and in competition with phenylacetylene.**

	<b>Initial rate constant, <math>k_0 \times 10^4 / \text{mol L}^{-1} \text{min}^{-1}</math></b>		
<b>Temperature / °C</b>	PP	PP + PB	PP + PA
50	8.7	10.4	0.4
70	14.8	16.6	0.8

## 4.2 TGA

Thermogravimetric analysis of the post-reaction catalyst was carried out following the hydrogenation and deuteration of phenylacetylene, styrene and 1-phenyl-1-propyne. The weight loss was compared to the derivative weight, and weight loss due to CO<sub>2</sub> was analysed.

The results for catalysts after reactions involving phenylacetylene showed that the weight loss of the post-reaction catalyst was in the range of 5-6%, as can be seen in Figures 120, 122, 124 and 126, and three peaks were generally observed on the 44 m/e ion current plot, shown in Figures 121, 123, 125 and 127.

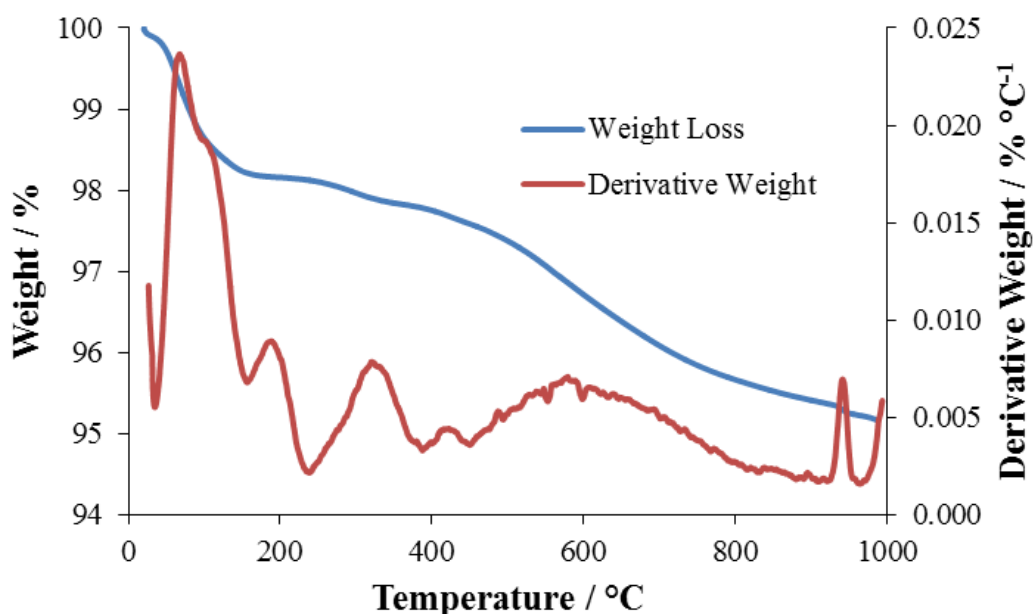


**Figure 120** – Temperature profiles of the weight as a percentage and the derivative weight loss for the post-reaction catalyst after the hydrogenation of phenylacetylene at 50°C.

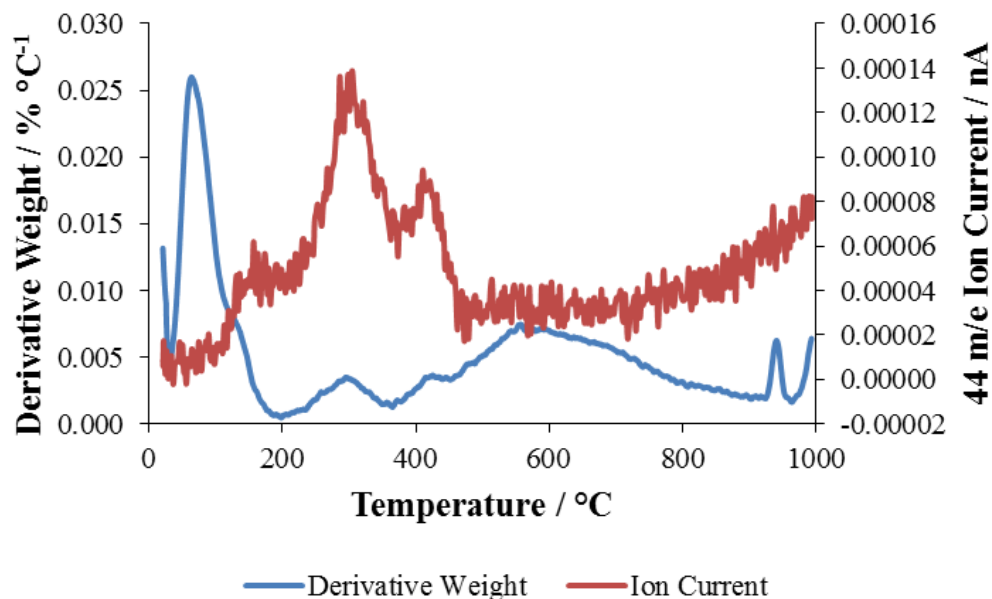


Figure 121 – Temperature profiles of the derivative weight and ion current corresponding to the loss of ions with a mass of 44 m/e (CO<sub>2</sub>) for the post-reaction catalyst after the hydrogenation of phenylacetylene at 50°C.

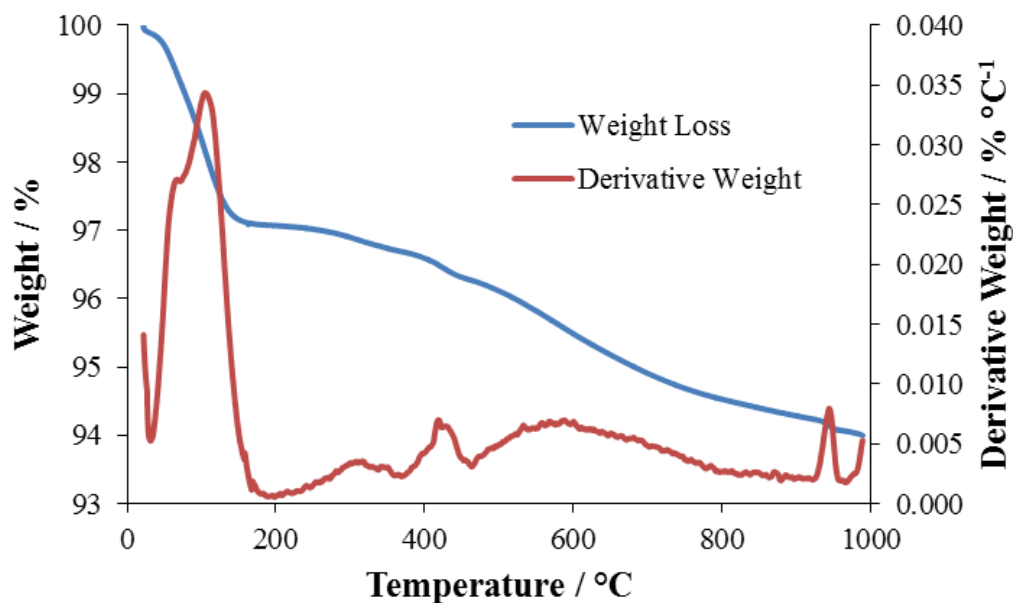


Figure 122 – Temperature profiles of the weight as a percentage and the derivative weight loss for the post-reaction catalyst after the hydrogenation of phenylacetylene at 70°C.

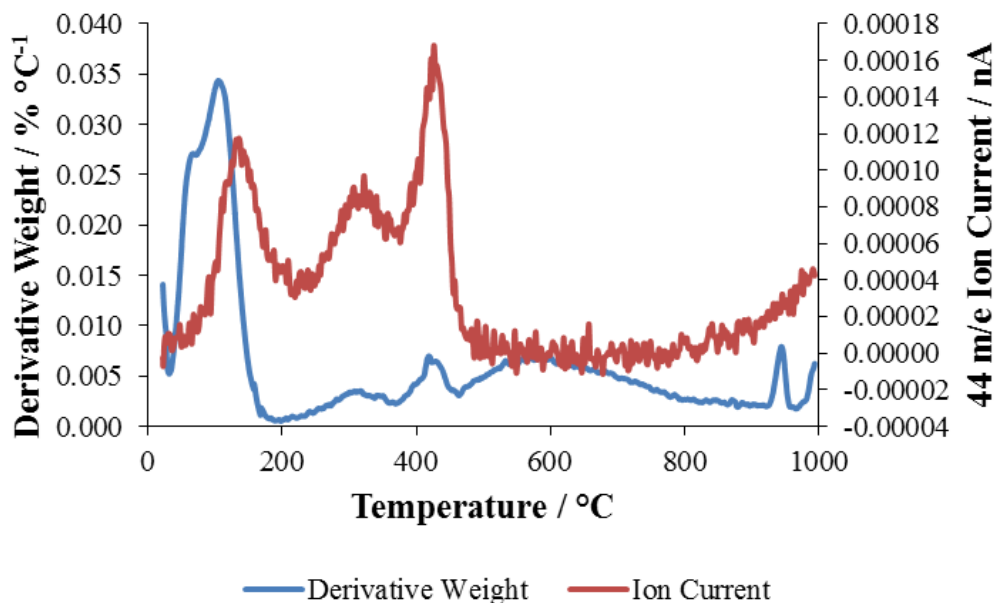


Figure 123 – Temperature profiles of the derivative weight and ion current corresponding to the loss of ions with a mass of 44 m/e (CO<sub>2</sub>) for the post-reaction catalyst after the hydrogenation of phenylacetylene at 70 °C.

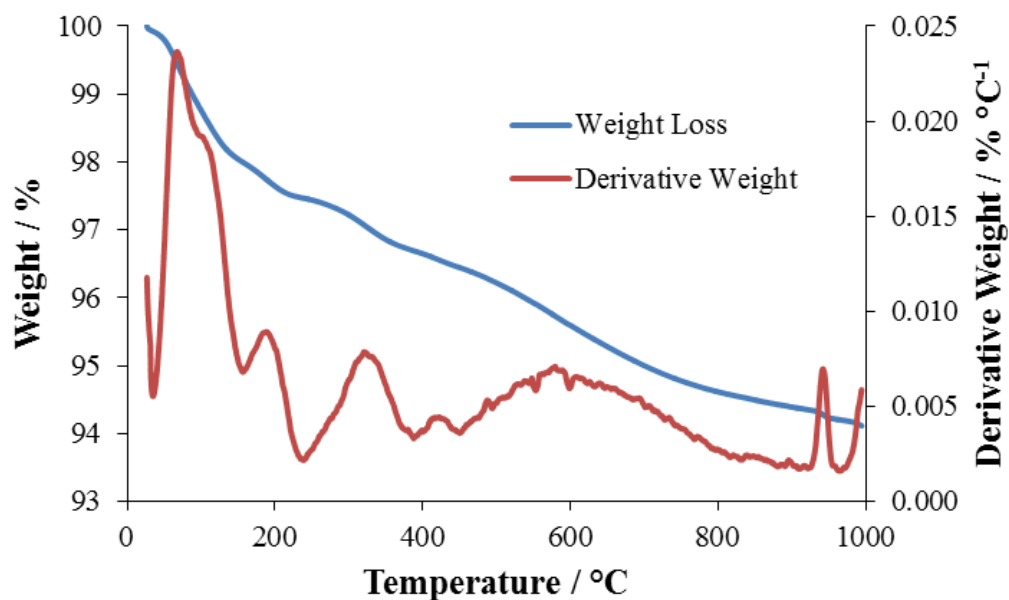


Figure 124 – Temperature profiles of the weight as a percentage and the derivative weight loss for the post-reaction catalyst after the deuteration of phenylacetylene at 50 °C.

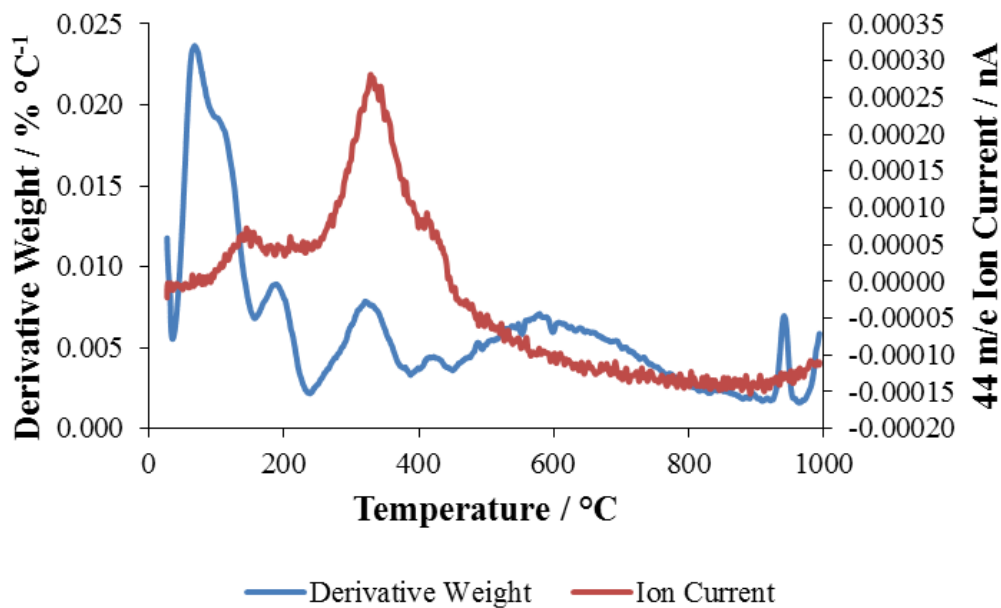


Figure 125 – Temperature profiles of the derivative weight and ion current corresponding to the loss of ions with a mass of 44 m/e ( $\text{CO}_2$ ) for the post-reaction catalyst after the deuteration of phenylacetylene at 50°C.

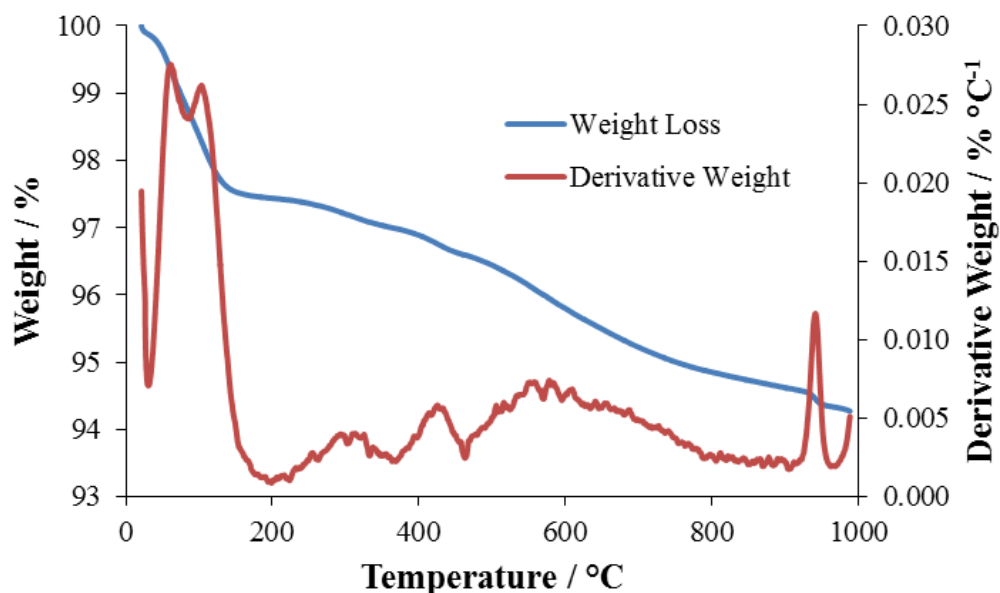
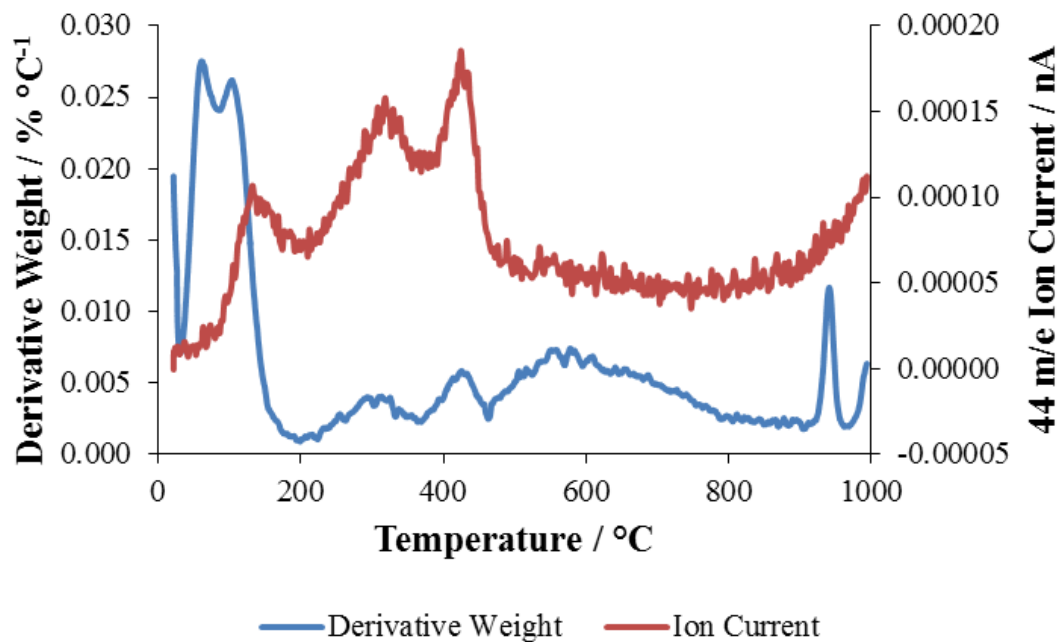


Figure 126 – Temperature profiles of the weight as a percentage and the derivative weight loss for the post-reaction catalyst after the deuteration of phenylacetylene at 70°C.



**Figure 127 – Temperature profiles of the derivative weight and ion current corresponding to the loss of ions with a mass of 44 m/e (CO<sub>2</sub>) for the post-reaction catalyst after the deuteration of phenylacetylene at 70°C.**

The results for catalysts after reactions involving styrene showed that the weight loss of the post-reaction catalyst was in the range of 5-9%, as can be seen in Figures 128, 130, 132 and 134, and three peaks were generally observed on the 44 m/e ion current plot, shown in Figures 129, 131, 133 and 135.

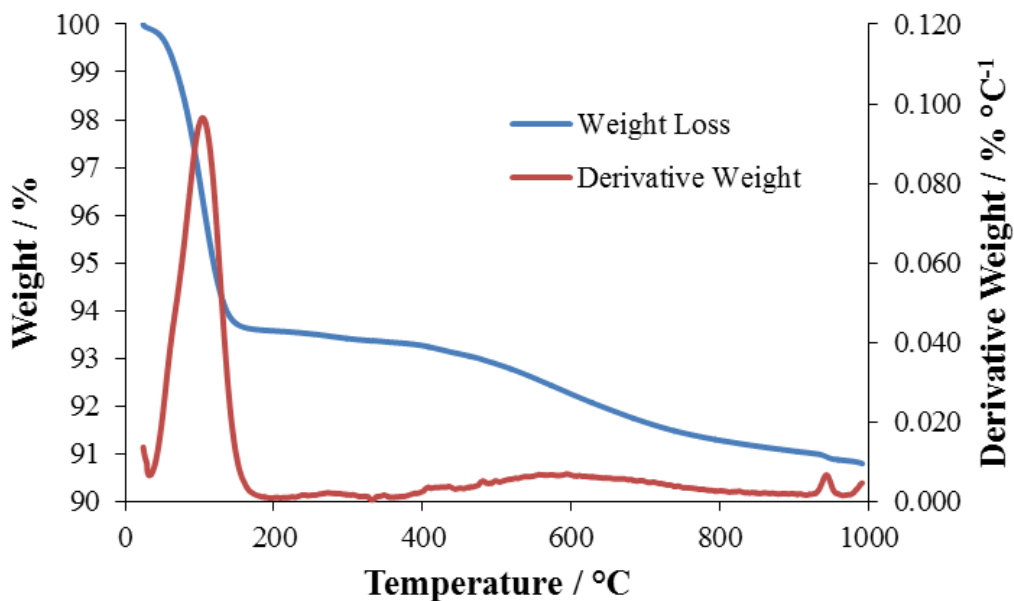


Figure 128 – Temperature profiles of the weight as a percentage and the derivative weight loss for the post-reaction catalyst after the hydrogenation of styrene at 50°C.

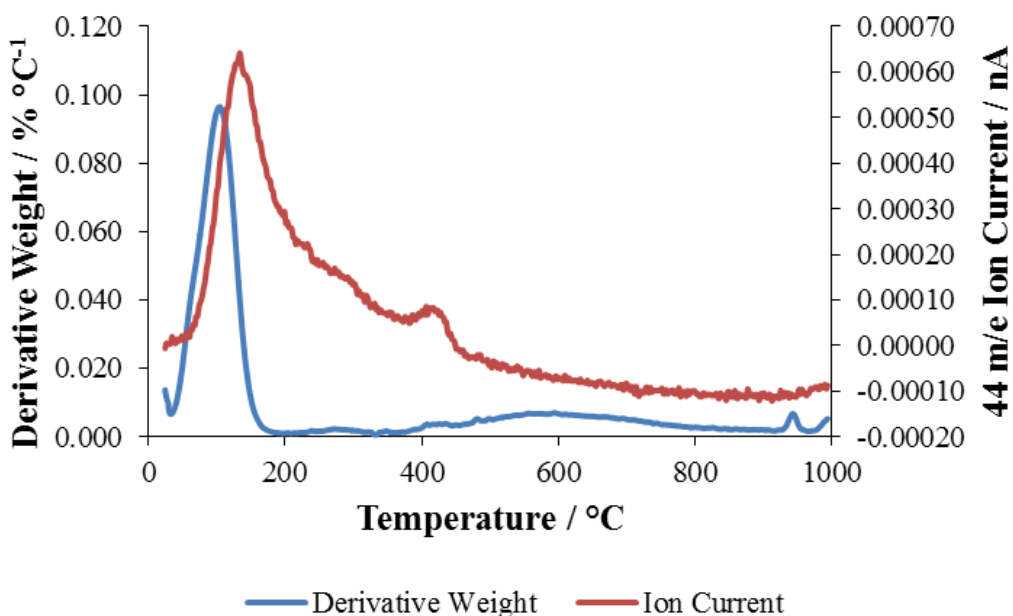


Figure 129 – Temperature profiles of the derivative weight and ion current corresponding to the loss of ions with a mass of 44 m/e ( $\text{CO}_2$ ) for the post-reaction catalyst after the hydrogenation of styrene at 50°C.

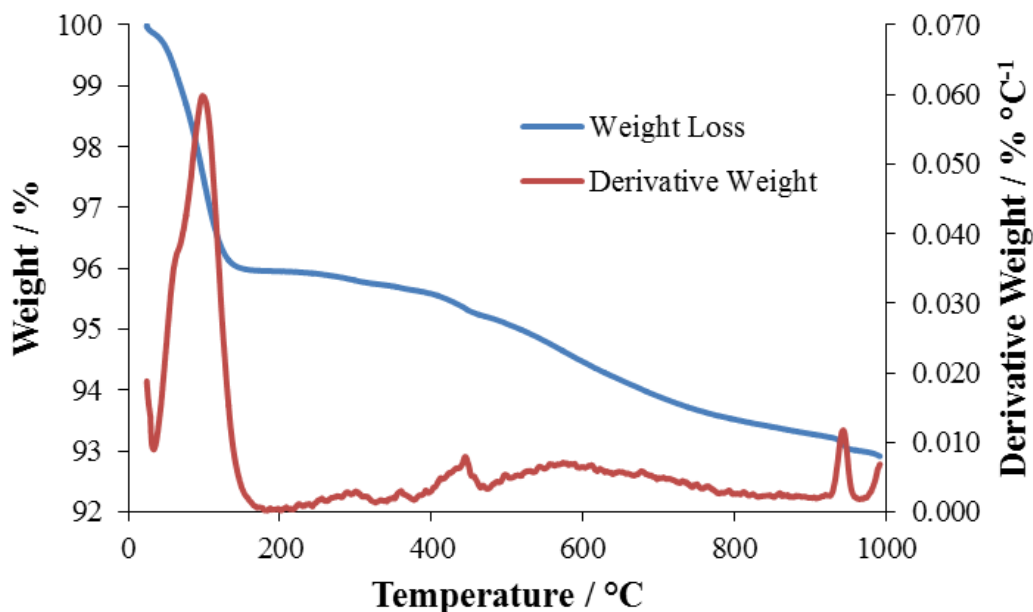


Figure 130 – Temperature profiles of the weight as a percentage and the derivative weight loss for the post-reaction catalyst after the hydrogenation of styrene at 70°C.

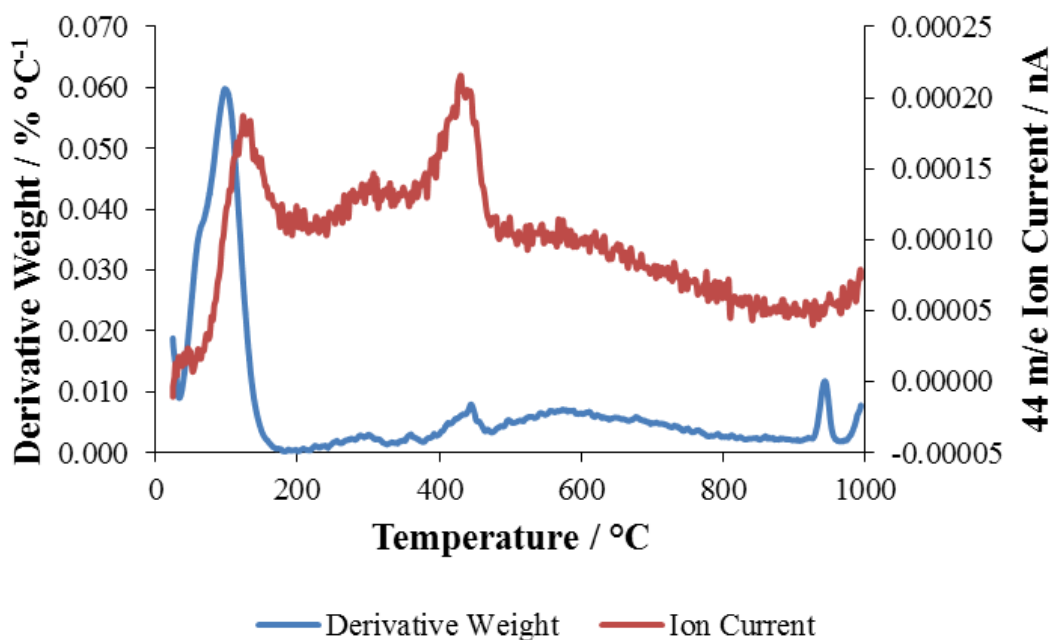


Figure 131 – Temperature profiles of the derivative weight and ion current corresponding to the loss of ions with a mass of 44 m/e ( $\text{CO}_2$ ) for the post-reaction catalyst after the hydrogenation of styrene at 70°C.

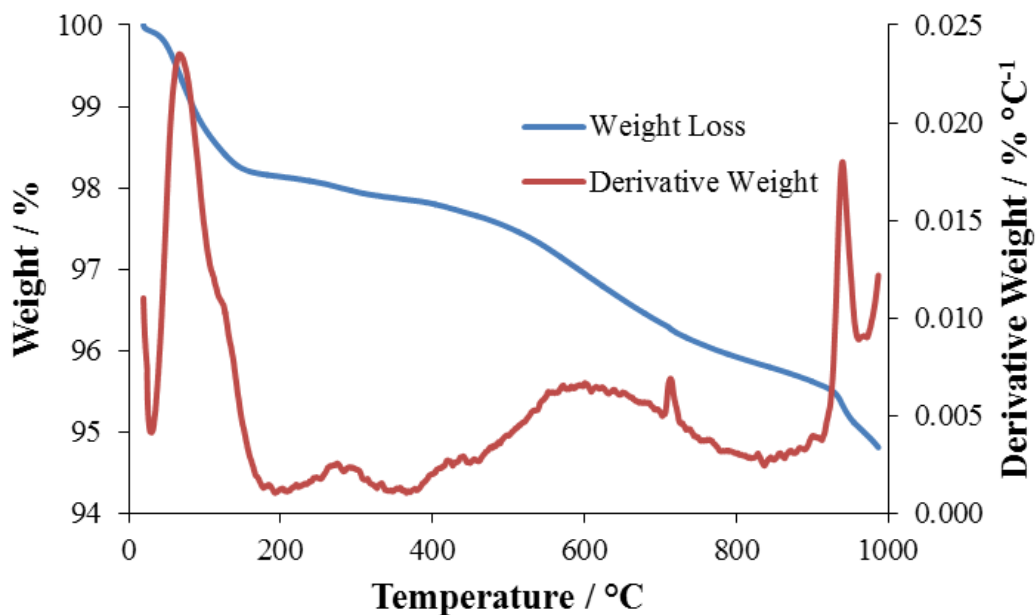


Figure 132 – Temperature profiles of the weight as a percentage and the derivative weight loss for the post-reaction catalyst after the deuteration of styrene at 50°C.

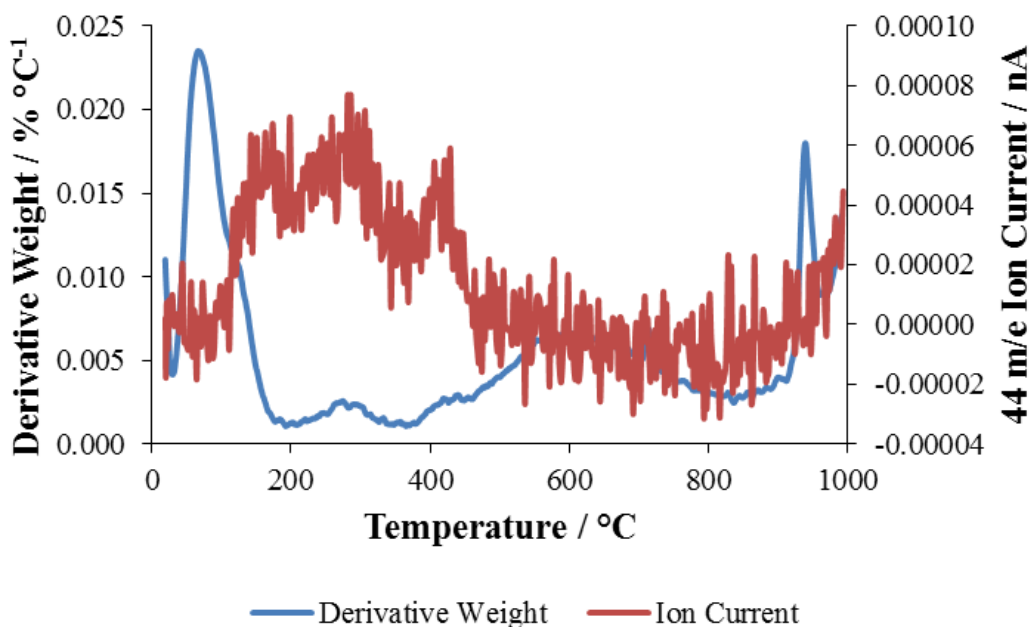


Figure 133 – Temperature profiles of the derivative weight and ion current corresponding to the loss of ions with a mass of 44 m/e ( $\text{CO}_2$ ) for the post-reaction catalyst after the deuteration of styrene at 50°C.

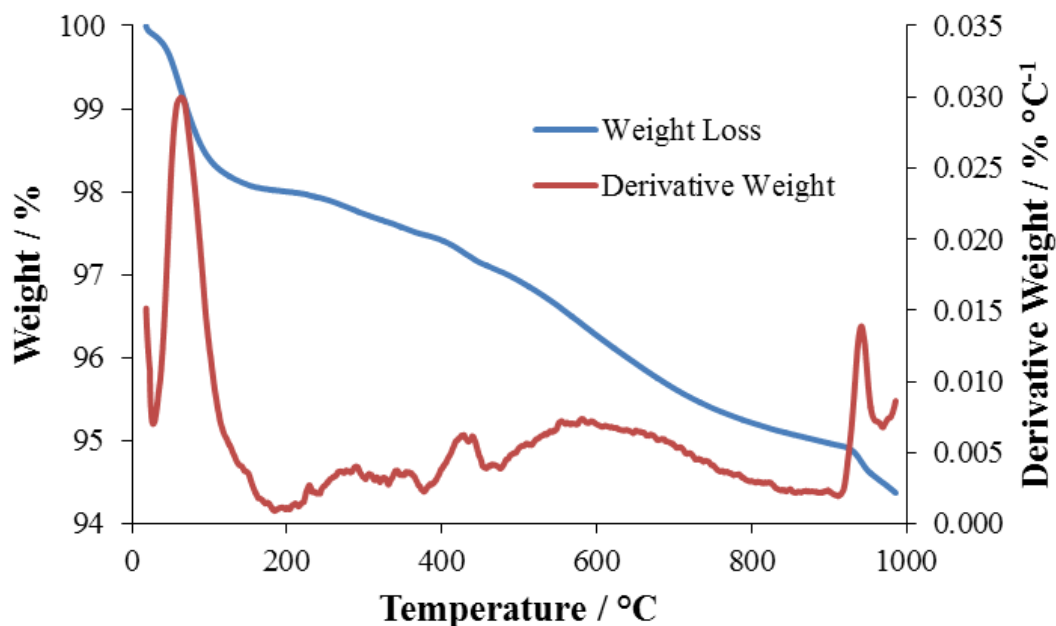


Figure 134 – Temperature profiles of the weight as a percentage and the derivative weight loss for the post-reaction catalyst after the deuteration of styrene at 70°C.

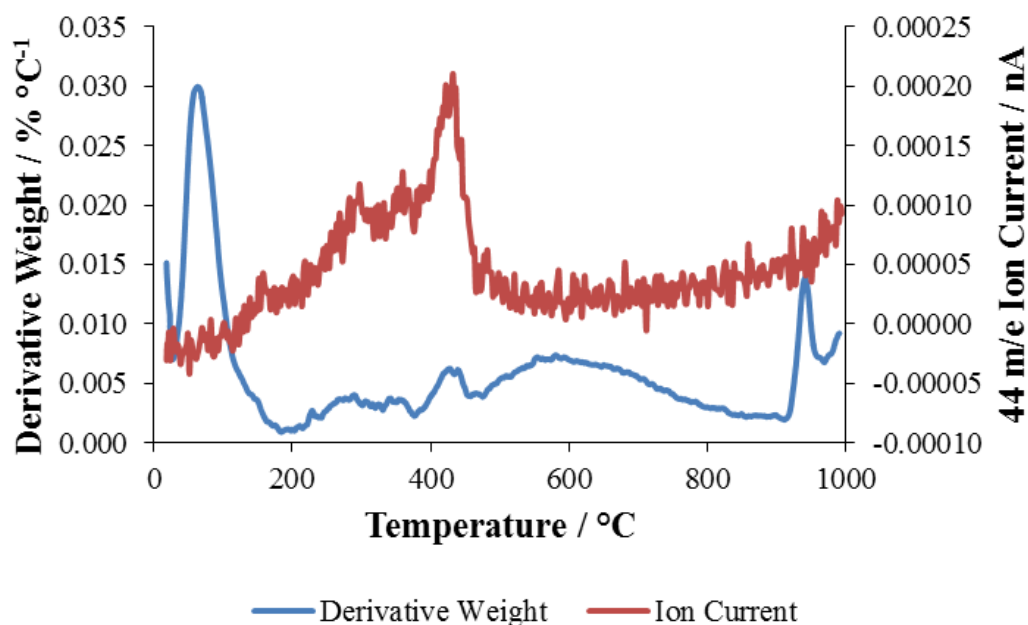
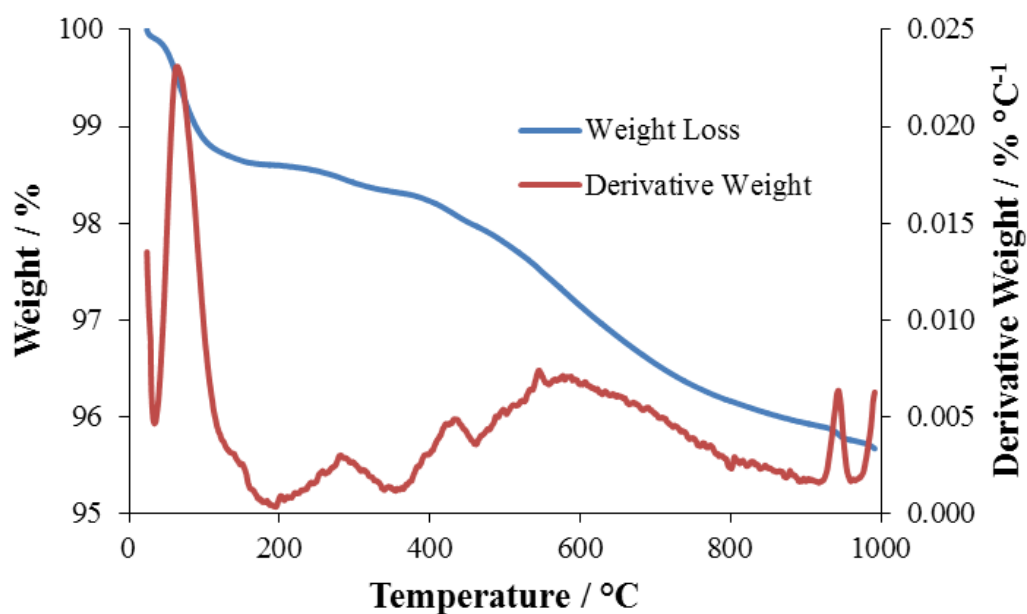


Figure 135 – Temperature profiles of the derivative weight and ion current corresponding to the loss of ions with a mass of 44 m/e ( $\text{CO}_2$ ) for the post-reaction catalyst after the deuteration of styrene at 70°C.

The results for catalysts after reactions involving styrene showed that the weight loss of the post-reaction catalyst was in the range of 4-6%, as can be seen in Figures 136, 138, 140 and 142, and three peaks were generally observed on the 44 m/e ion current plot, shown in Figures 137, 139, 141 and 143.



**Figure 136 – Temperature profiles of the weight as a percentage and the derivative weight loss for the post-reaction catalyst after the hydrogenation of 1-phenyl-1-propyne at 50°C.**

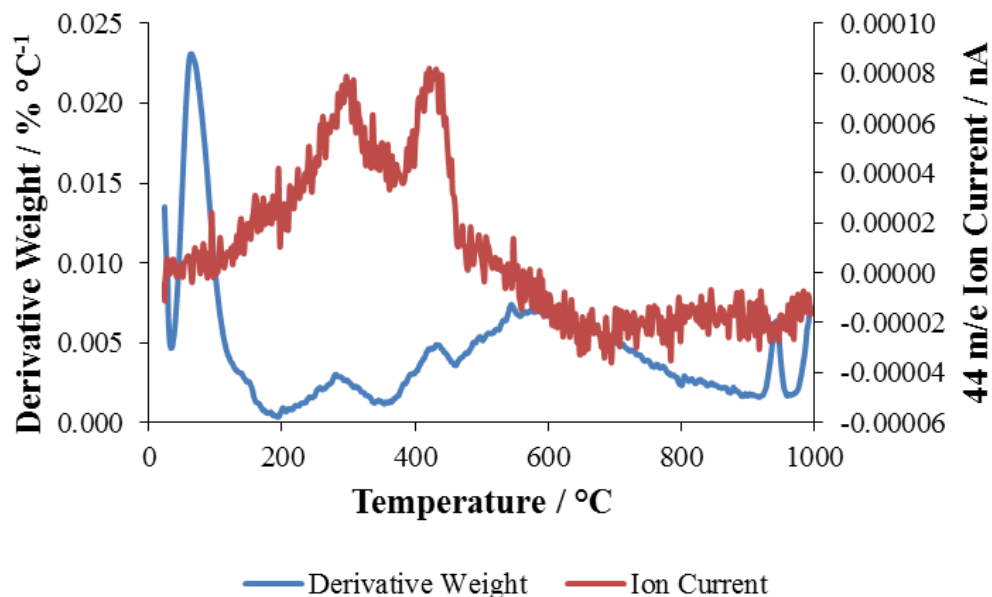


Figure 137 – Temperature profiles of the derivative weight and ion current corresponding to the loss of ions with a mass of 44 m/e ( $\text{CO}_2$ ) for the post-reaction catalyst after the hydrogenation of 1-phenyl-1-propyne at 50°C.

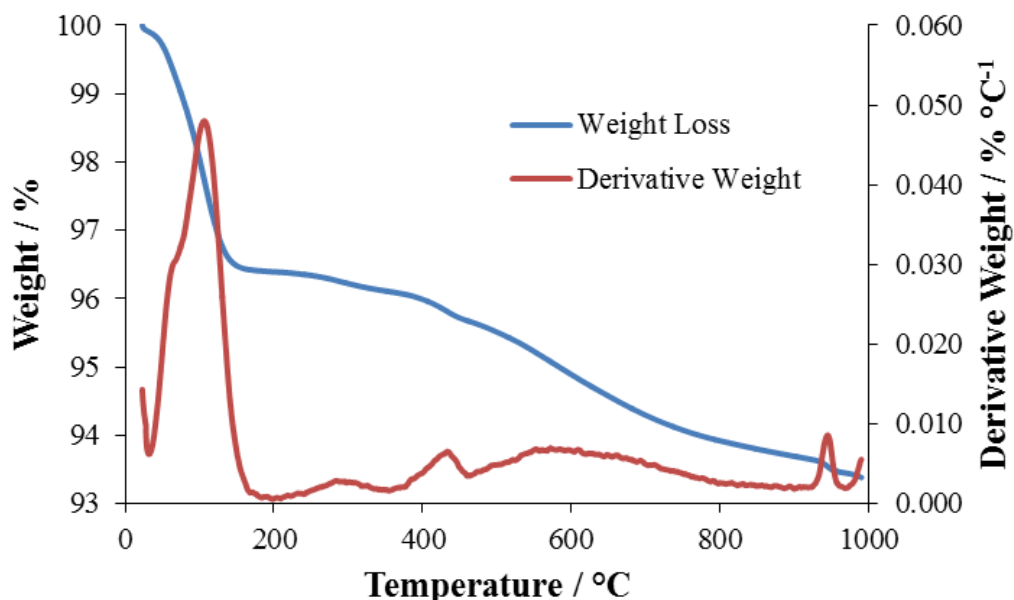
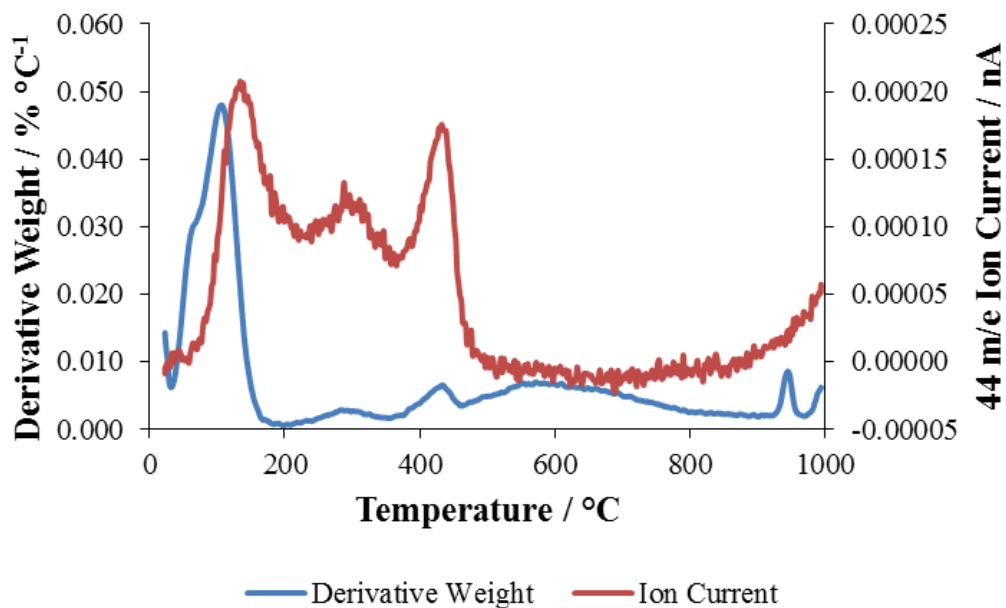
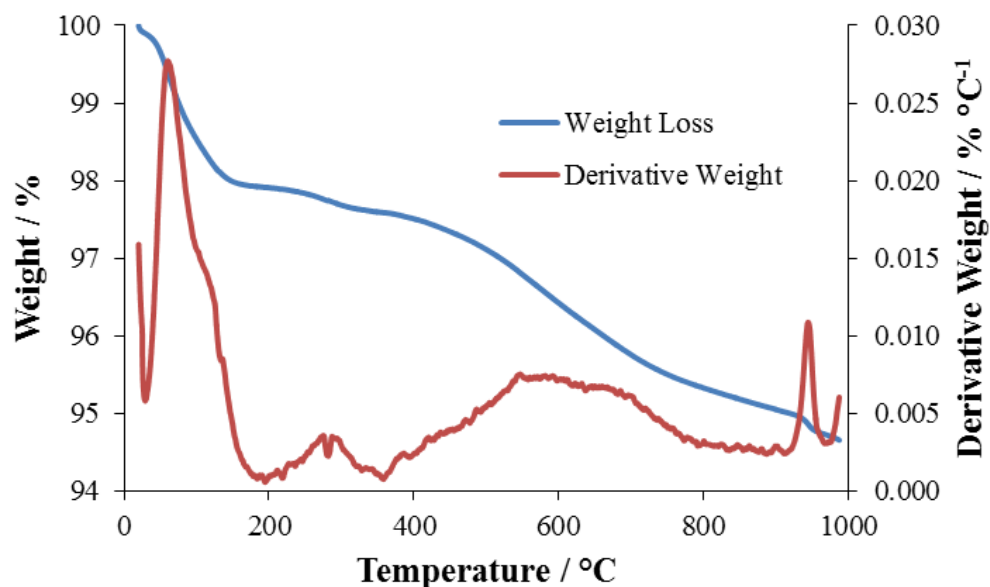


Figure 138 – Temperature profiles of the weight as a percentage and the derivative weight loss for the post-reaction catalyst after the hydrogenation of 1-phenyl-1-propyne at 70°C.



**Figure 139** – Temperature profiles of the derivative weight and ion current corresponding to the loss of ions with a mass of 44 m/e (CO<sub>2</sub>) for the post-reaction catalyst after the hydrogenation of 1-phenyl-1-propyne at 70°C.



**Figure 140** – Temperature profiles of the weight as a percentage and the derivative weight loss for the post-reaction catalyst after the deuteration of 1-phenyl-1-propyne at 50°C.

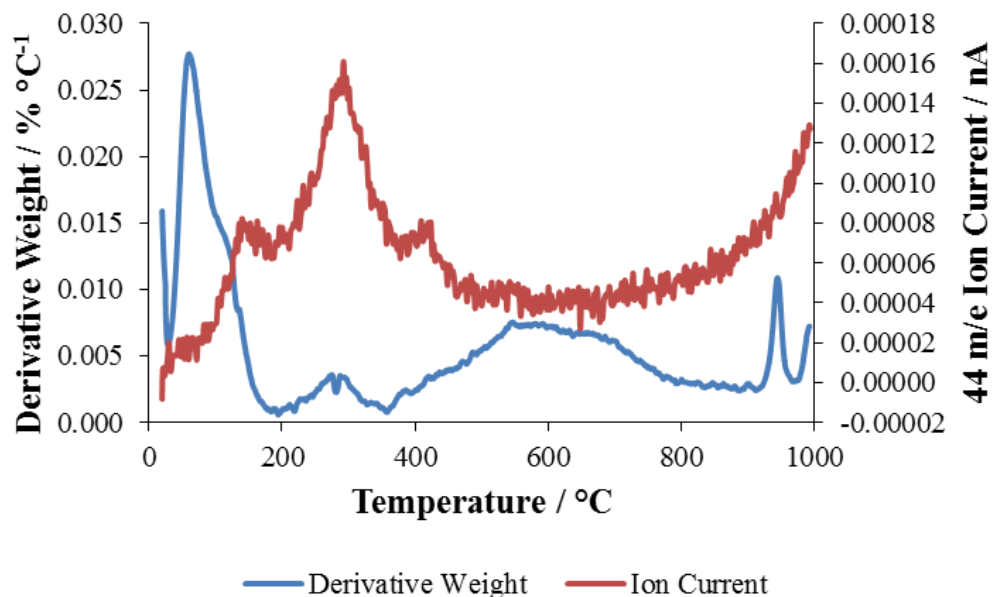


Figure 141 – Temperature profiles of the derivative weight and ion current corresponding to the loss of ions with a mass of 44 m/e ( $\text{CO}_2$ ) for the post-reaction catalyst after the deuteration of 1-phenyl-1-propyne at 50°C.

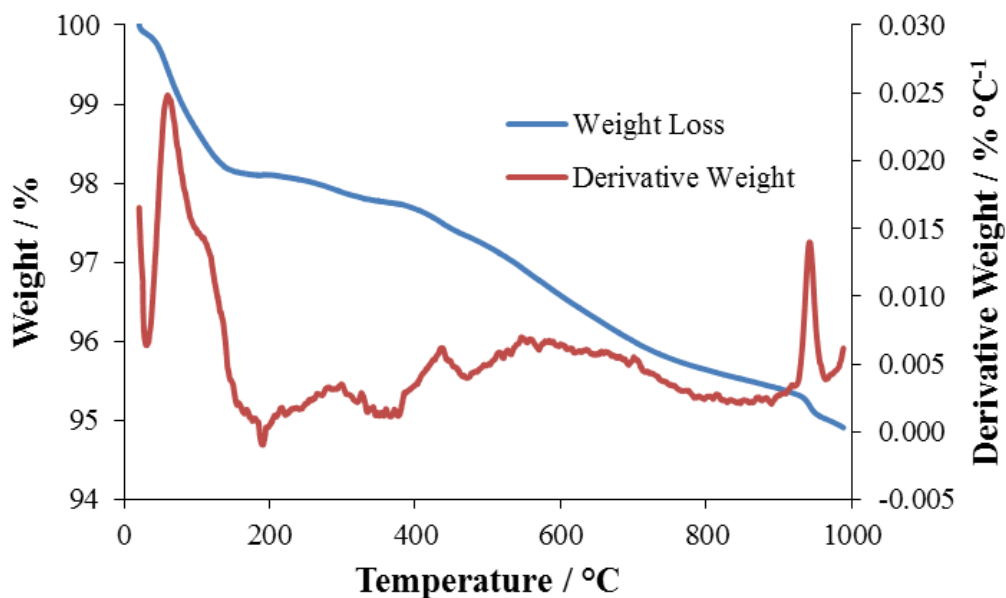
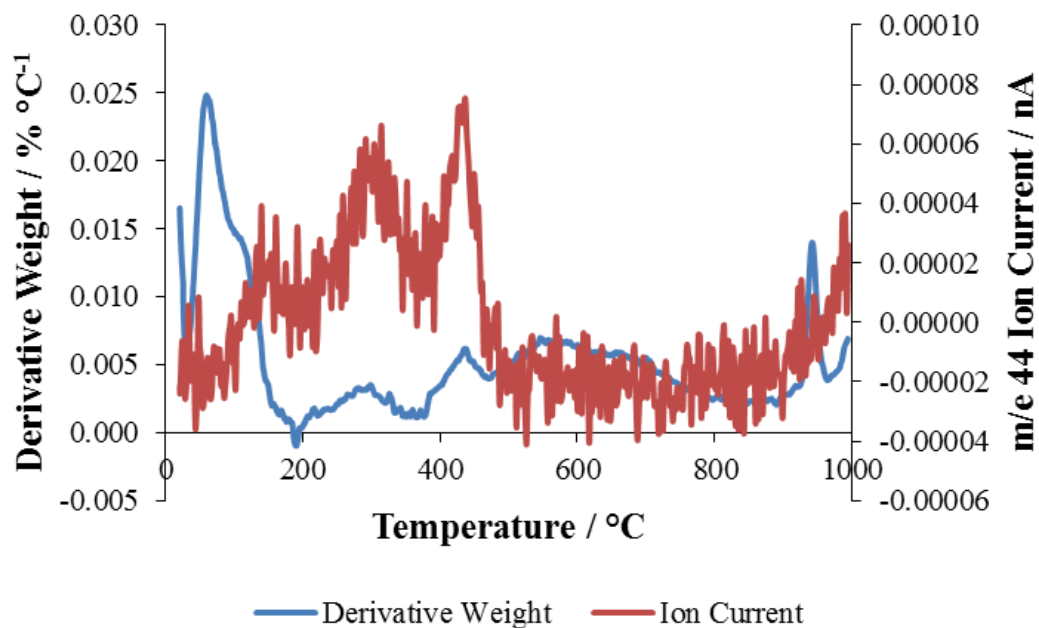


Figure 142 – Temperature profiles of the weight as a percentage and the derivative weight loss for the post-reaction catalyst after the deuteration of 1-phenyl-1-propyne at 70°C.



**Figure 143 – Temperature profiles of the derivative weight and ion current corresponding to the loss of ions with a mass of 44 m/e (CO<sub>2</sub>) for the post-reaction catalyst after the deuteration of 1-phenyl-1-propyne at 70°C.**

## 5 Discussion

### 5.1 Reactions

#### 5.1.1 Mass Transfer Limitation

The mass transfer limitation experiments showed that increasing the stirrer speed over 1000 rpm had no impact on the rate of reaction, as can be seen in Figures 144-145. From this, it can be concluded that the reactions were not mass transfer limited.

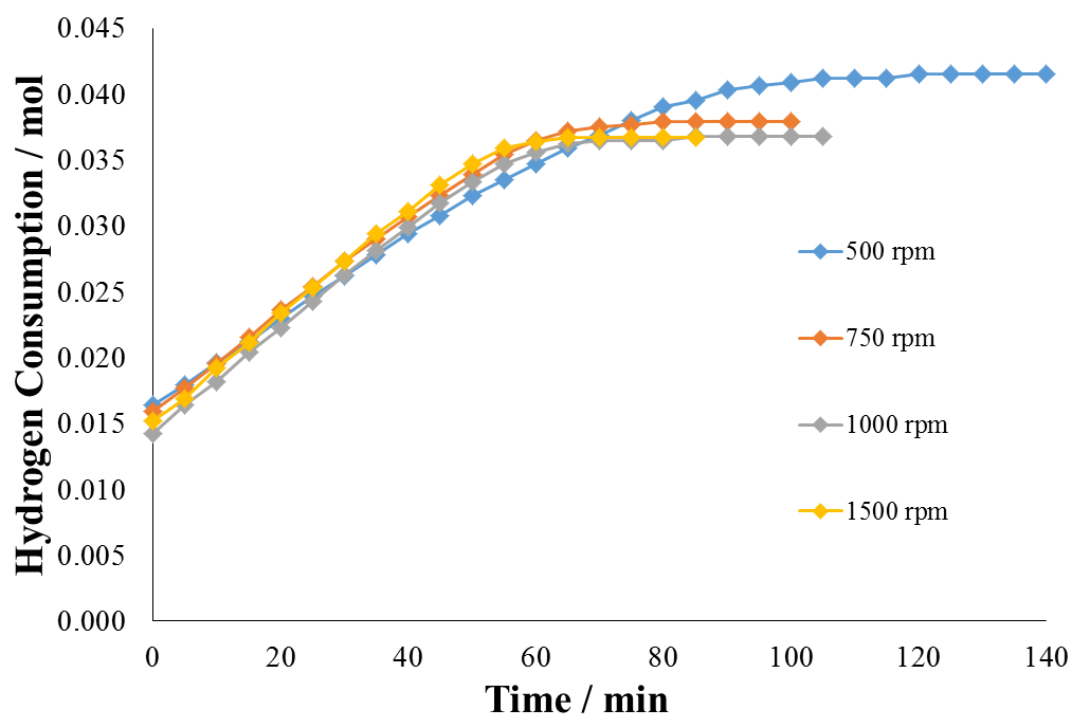
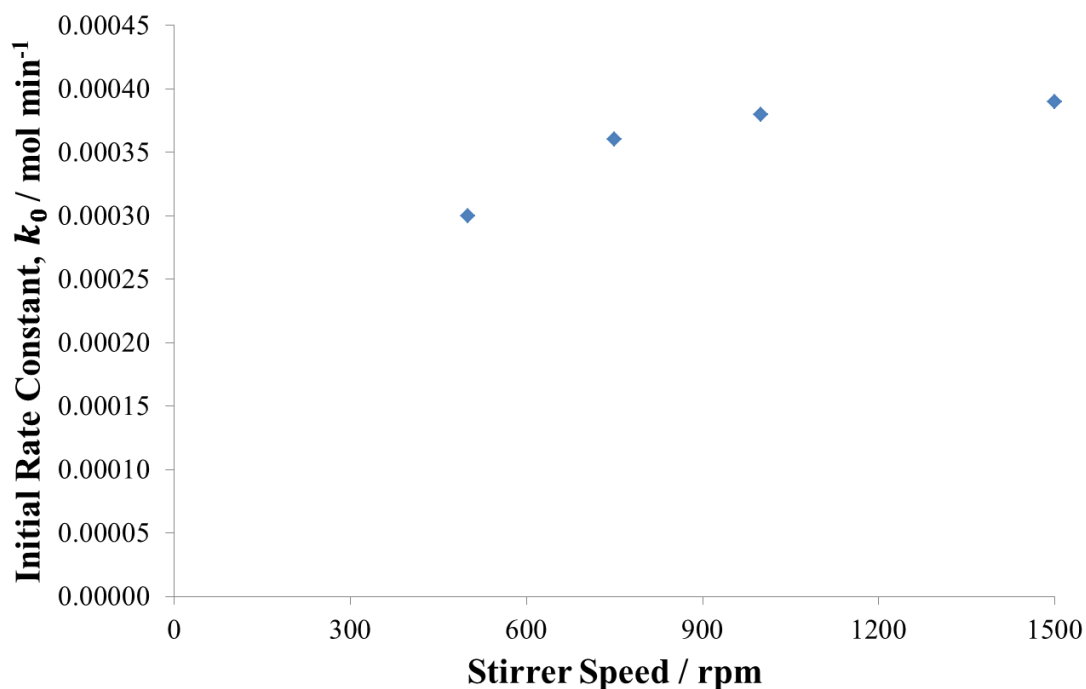


Figure 144 – A plot of hydrogen consumption against time at different stirrer speeds for the hydrogenation of phenylacetylene.



**Figure 145 – A plot of the initial rate constant against different stirrer speeds for the hydrogenation of phenylacetylene.**

The initial rate constant had clearly begun to plateau by 1000 rpm – the stirrer speed used for all reactions.

### 5.1.2 Temperature Dependence

The temperature dependence of the rates of hydrogenation allowed the activation energies to be calculated and provide some basic kinetic insights. The relative rates of hydrogenation of the different functionalities were considered and a relationship between the chain length of the substituent and the activation energy was found. The variation of the *cis/trans* ratio of  $\beta$ -methylstyrene with temperature in the hydrogenation cascade of 1-phenyl-1-propyne was also analysed, with the results suggesting a shift of the dominant reaction as temperature increases. The findings from

the temperature dependence form the basis of the project, showing the behaviour of the reactants under a range of relevant conditions.

The first noteworthy observation is that the rates of hydrogenation of different parts of the molecules are as follows:

Double Bond > Triple Bond > Aromatic Ring

The aromatic ring is the slowest due to the relatively large amounts of energy required to break aromaticity. The rate of double bond hydrogenation being faster than that of the triple bond, as demonstrated by Webb<sup>61</sup>, can be explained by the increased strength of adsorption of alkynes when compared with alkenes<sup>62</sup>.

The activation energies of the hydrogenation of phenylacetylene, ethylbenzene, 1-phenyl-1-propyne and propylbenzene were determined in Section 4.1.2 and are presented in Table 40 below.

**Table 40 – Calculated activation energies. The column labelled ‘EB (STY)’ denotes the activation energy of ethylbenzene hydrogenation when styrene was the initial reactant.**

Molecule	PA	EB (STY)	EB	PP	PB
$E_a / \text{kJ mol}^{-1}$	36.4	62.2	45.1	26.3	32.0

The hydrogenation of ethylbenzene occurs at a much faster rate than that of propylbenzene, whilst the hydrogenation reactions of phenylacetylene and 1-phenyl-1-propyne occur at similar rates. Steric factors and a greater strength of adsorption are likely reasons for the discrepancy in the rates of hydrogenation of the alkylbenzene molecules. The activation energy of phenylacetylene is greater than that of 1-phenyl-1-propyne, with the analogous alkybenzenes showing the same trend – the activation

energy of ethylbenzene is greater than that of propylbenzene. This suggests that the greater strength of adsorption of the longer chain molecules is leading to a more favourable reaction, with less energy required to reach the transition state. Alternatively, there could be different sites involved in the hydrogenation of propylbenzene and 1-phenyl-1-propyne, which have a greater impact in decreasing the activation energy than the sites involved in the hydrogenation of ethylbenzene and phenylacetylene.

The activation energy of the hydrogenation of ethylbenzene was significantly increased when observed as part of the cascade starting with styrene in comparison to the experiments where ethylbenzene was itself the initial reactant. This suggests that there is catalyst modification taking place during styrene hydrogenation which impacts the hydrogenation of ethylbenzene. From this, it can be postulated that both styrene and ethylbenzene hydrogenate at the same site.

The change in styrene mole fraction with temperature was not significant during the phenylacetylene hydrogenation cascade; lower temperatures simply prolonged the time taken to reach the maximum yield. This shows that the change in temperature affected the rates of phenylacetylene and styrene hydrogenation in similar proportions.

The alkene mole fraction variation with temperature was plotted in order to assess selectivity (Figures 146-148). The shapes of the profiles for a particular molecule generally resembled one other with temperature stretching them along the time axis.

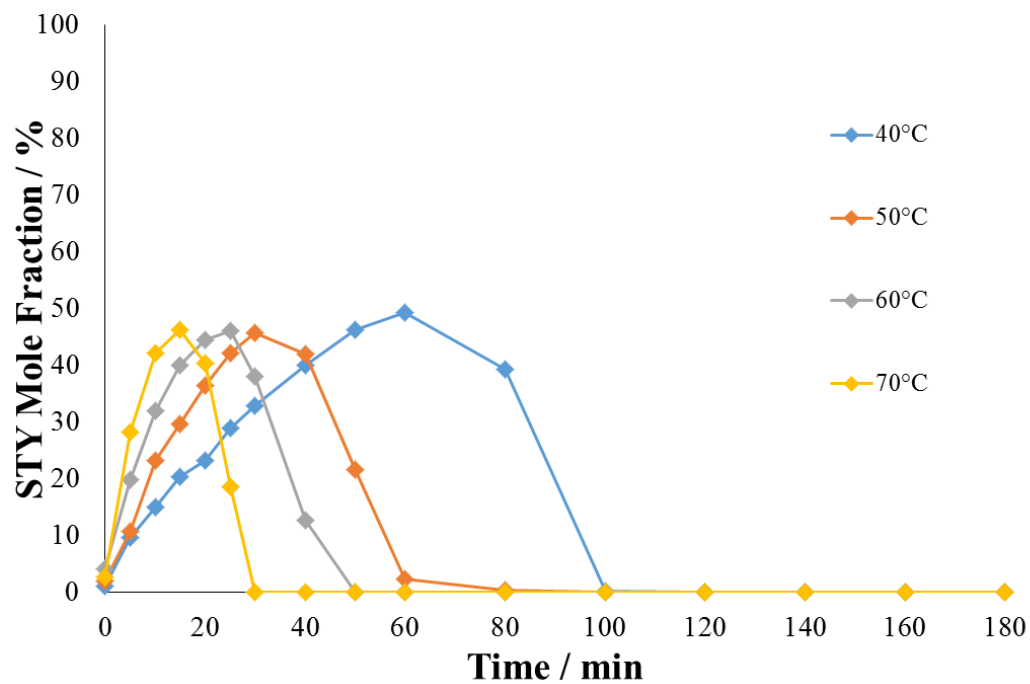


Figure 146 – Styrene mole fraction profiles at different temperatures during the hydrogenation of phenylacetylene.

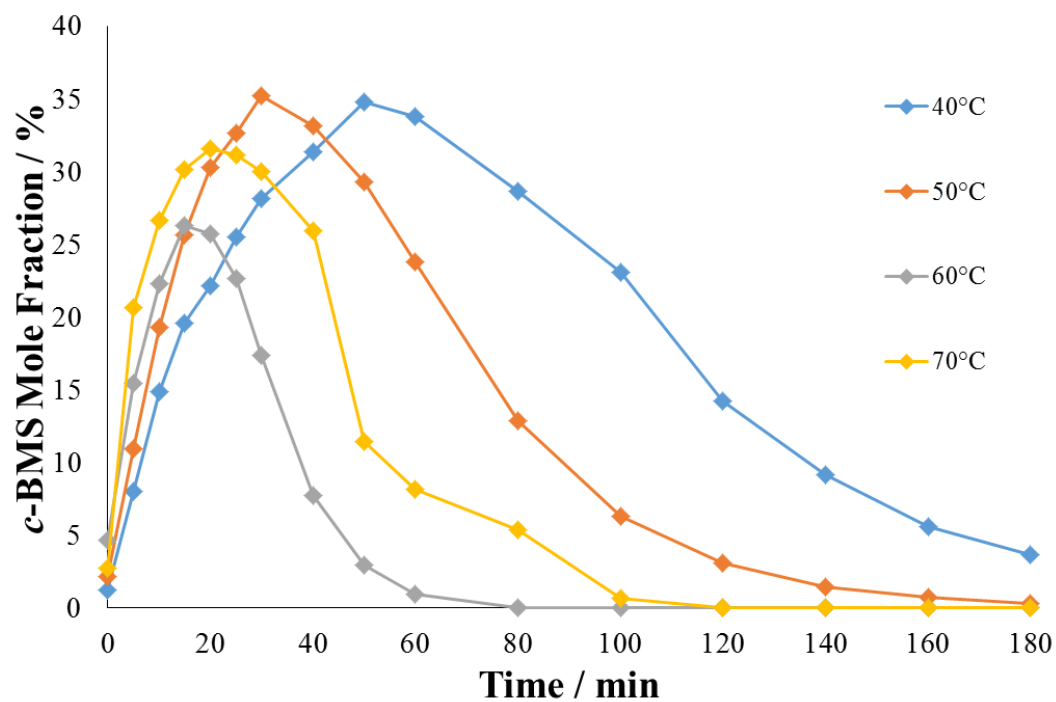
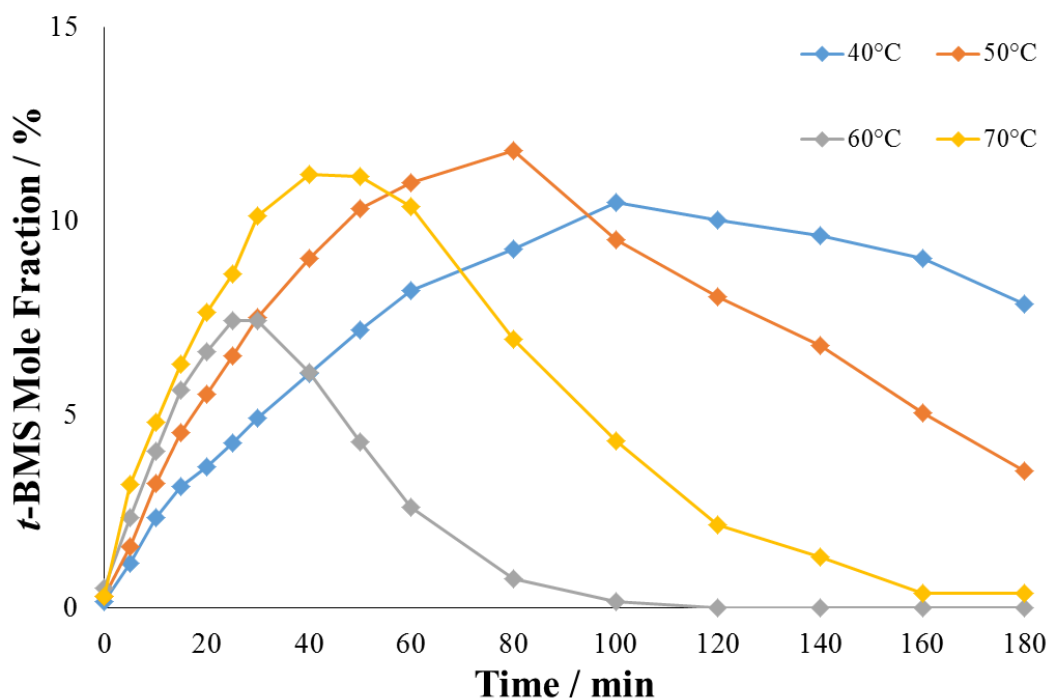


Figure 147 – *cis*- $\beta$ -Methylstyrene mole fraction profiles at different temperatures during the hydrogenation of 1-phenyl-1-propyne.



**Figure 148 – *trans*- $\beta$ -Methylstyrene mole fraction profiles at different temperatures during the hydrogenation of 1-phenyl-1-propyne.**

The change in styrene mole fraction with temperature was not significant during the phenylacetylene hydrogenation cascade; lower temperatures simply prolonged the time taken to reach the maximum yield. A similar trend was observed for both *cis*- and *trans*- $\beta$ -methylstyrene mole fraction with the exception of the profiles at 60°C. This could be due to 60°C being close to the temperature at which the transition from hydrogenation and isomerisation dominance occurs, however, if this was the case, the profile at 70°C should have a more extreme shift than the profile at 60°C and this is clearly not the case. The rate of hydrogenation of 1-phenyl-1-propyne and the remainder of the reaction cascade fit the expected trends, suggesting this anomaly is not the result of experimental error, but the explanation that this is solely due to the anomaly occurring at a transition temperature may not be the complete justification of these findings. Overall, these results show that the change in temperature affected the rates of alkyne and alkene hydrogenation in similar proportions.

A profile of the *cis/trans* ratio of  $\beta$ -methylstyrene was also produced for each temperature and is presented in Figure 149. The ratio decreased with time and typically decreased more slowly at higher temperatures, with the exception of the profile plotted for 60°C.

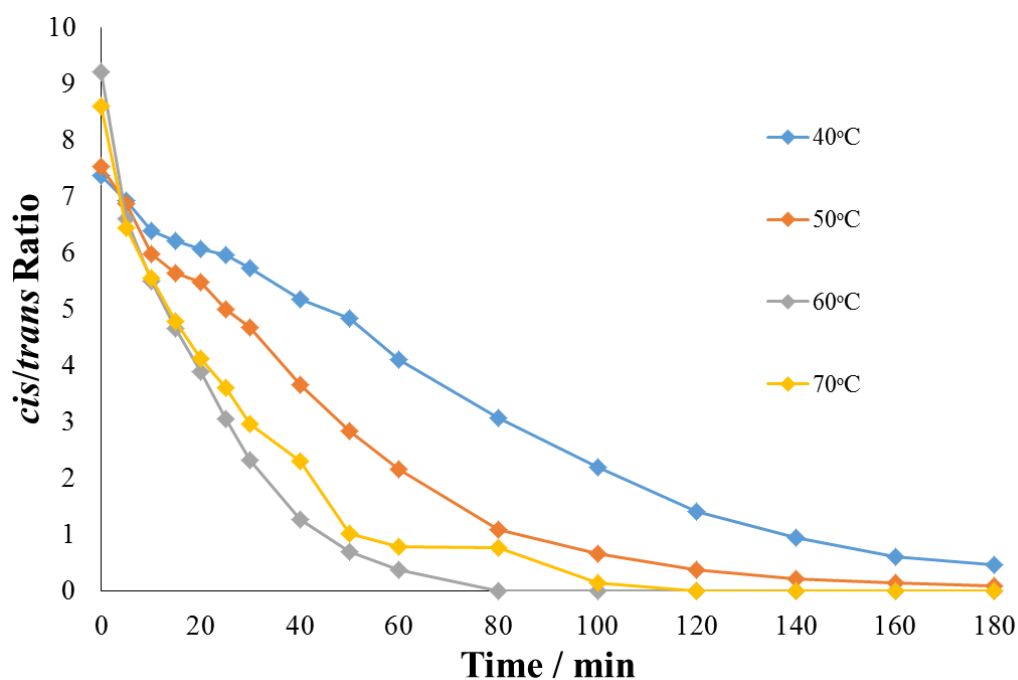


**Figure 149 – *cis/trans* ratio of  $\beta$ -methylstyrene during the hydrogenation of 1-phenyl-1-propyne at different temperatures.**

The initial *cis/trans* ratio of  $\beta$ -methylstyrene increases with temperature until a point between 60°C and 70°C. The rate of decrease of the *cis/trans* ratio also increases with temperature until a point between 60°C and 70°C. The results up to 60°C can be straightforwardly explained, as increasing the temperature increases the initial rate of hydrogenation of *cis*- $\beta$ -methylstyrene, as one would expect, and over time, isomerisation occurs to produce the *trans* isomer, as the *trans* isomer is the thermodynamic product. The change which occurs as the temperature nears 70°C is likely due to a change in reaction pathway, but it is impossible to make further conclusions without exploring the issue further.

The basic kinetic model for these reactions is now much clearer. These experiments have shown that, *ceteris parabus*, under the range of temperatures which will be used in this study, alkenes hydrogenate faster than alkynes, which in turn hydrogenate faster than aromatic rings. Moreover, the activation energy has been shown to decrease with increasing substituent chain length, suggesting that this is influenced by the strength of adsorption. These results are the framework against which results from more complex reactions will be compared; deviations from these results with changes to the conditions should improve understanding of the behaviour of unsaturated molecules and the rhodium/silica catalyst.

### 5.1.3 Reactions with Deuterium

The reactions with deuterium allowed for the calculation of the kinetic isotope effect, which is informative when considering the mechanism, and provided information about deuteration and exchange through  $^2\text{H}$  NMR analysis. The effect on ring hydrogenation was particularly striking and there was a systematic shift in the *cis/trans* ratio. These results reveal something of the nature of the rhodium catalyst and the sites which are active for the hydrogenation of different functional groups when compared with the results from hydrogenation using the  $^1\text{H}$  isotope.

For phenylacetylene hydrogenation at both 50°C and 70°C, a normal kinetic isotope effect is observed. This suggests that a bond to a hydrogen atom is involved in the rate determining step – most likely the second half-hydrogenation step, as proposed by Twigg<sup>14</sup>. For 1-phenyl-1-propyne, there is no significant kinetic isotope effect at 50°C, but there is a normal kinetic isotope effect at 70°C. This suggests that there is a change in reaction pathway between 50°C and 70°C, but more work would be required before a definitive conclusion could be made.

Reactions in deuterium had a considerable impact on the hydrogenation of the aromatic ring. Ring hydrogenation in the phenylacetylene cascade dropped to below detectable levels, as can be seen in Figures 150-151.

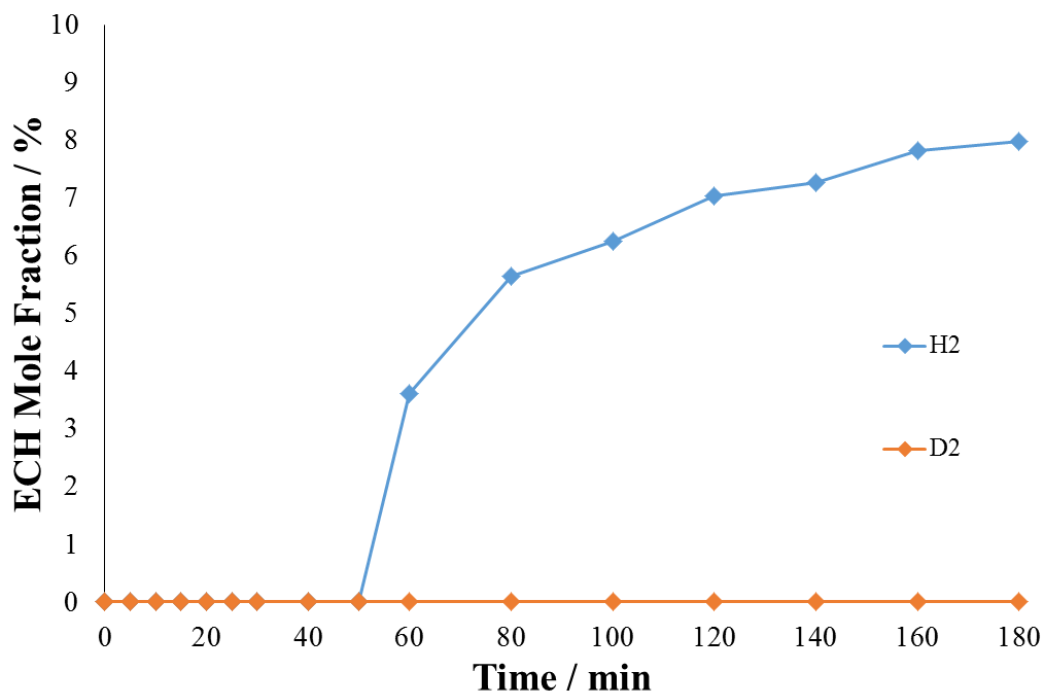


Figure 150 – A comparison of the ethylcyclohexane mole fraction profiles during the hydrogenation of phenylacetylene with hydrogen and deuterium at 50°C.

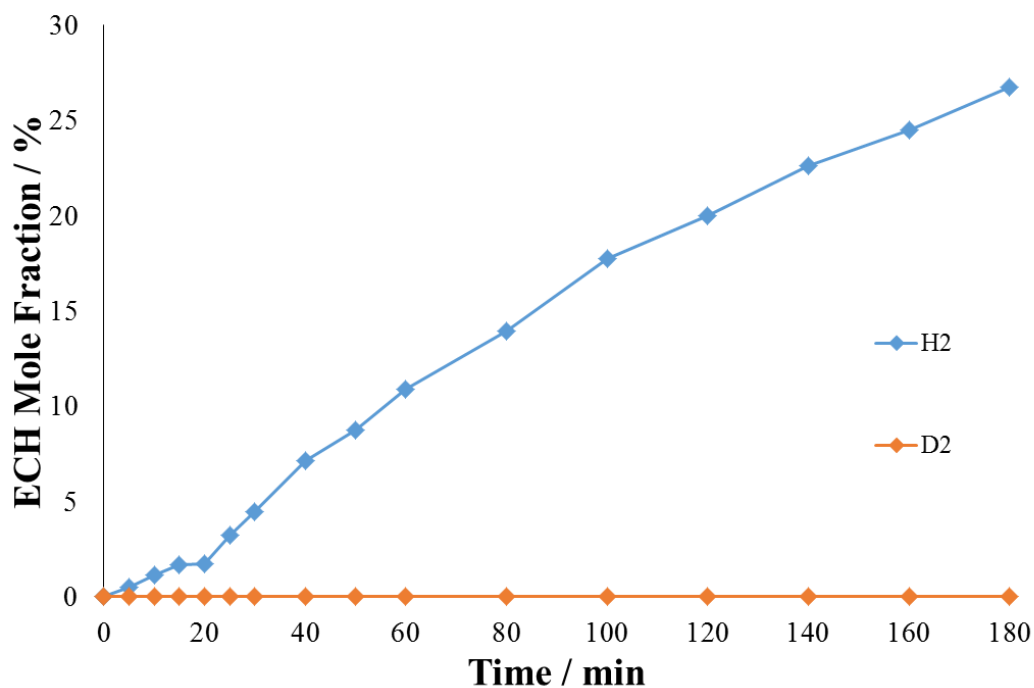


Figure 151 – A comparison of the ethylcyclohexane mole fraction profiles during the hydrogenation of phenylacetylene with hydrogen and deuterium at 70°C.

Ring hydrogenation in the 1-phenyl-1-propyne cascade was less affected, but did show a decrease at 70°C (Figures 152-153).

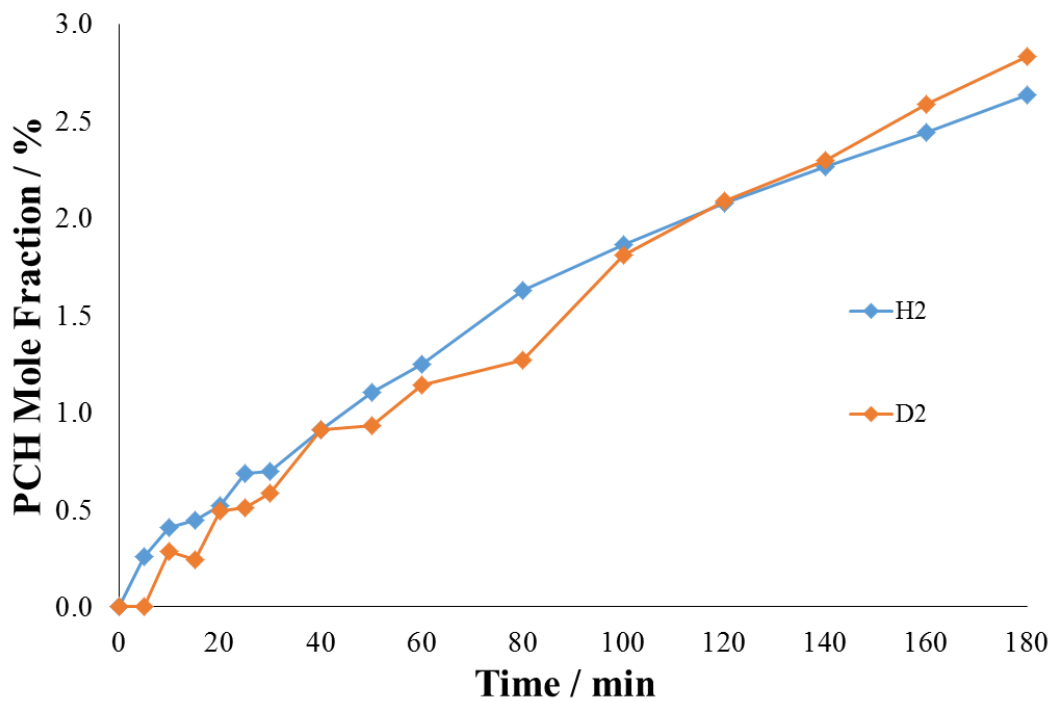
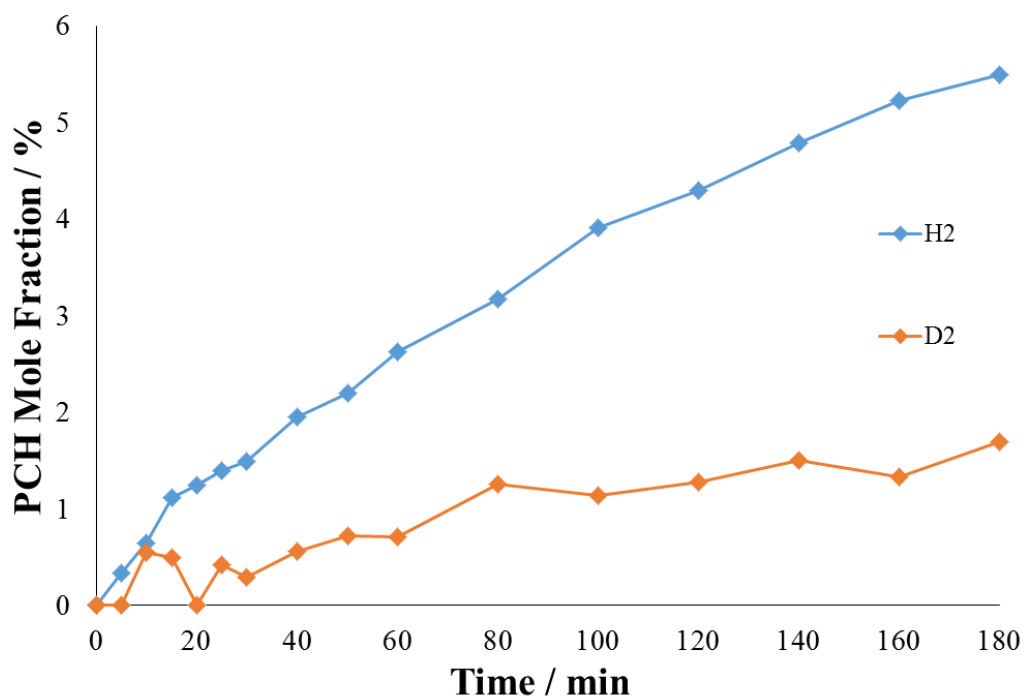
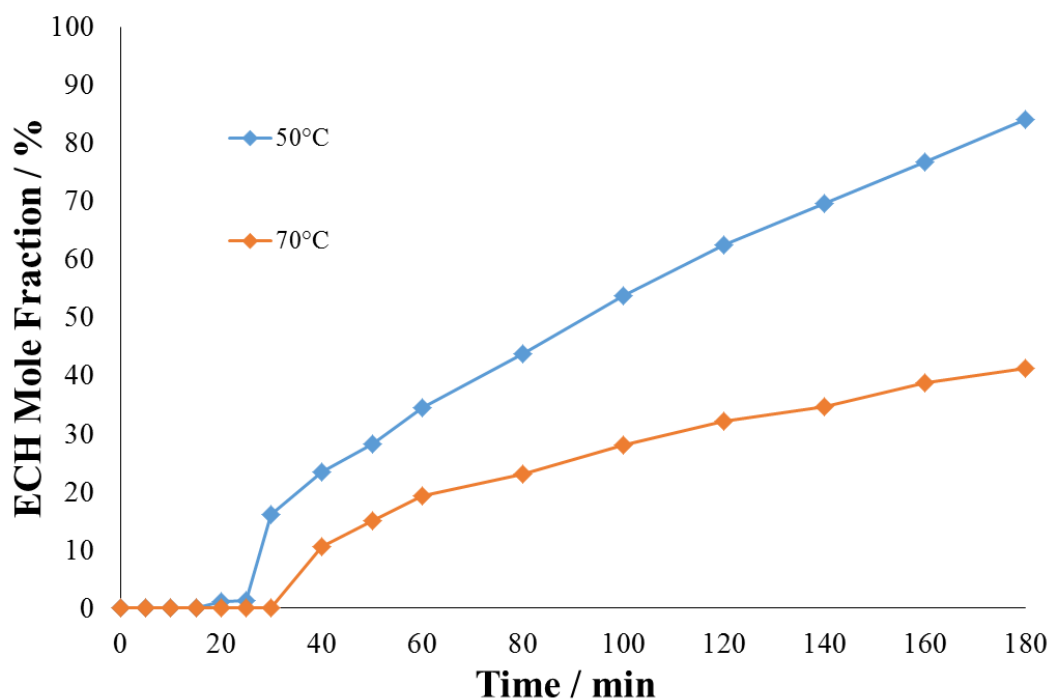


Figure 152 – A comparison of the propylcyclohexane mole fraction profiles during the hydrogenation of 1-phenyl-1-propyne with hydrogen and deuterium at 50°C.



**Figure 153 – A comparison of the propylcyclohexane mole fraction profiles during the hydrogenation of 1-phenyl-1-propyne with hydrogen and deuterium at 70°C.**

Another notable observation was that the rate of ethylcyclohexane production when the reaction cascade starts at styrene was faster at 50°C than 70°C in deuterium, as is shown in Figure 154. This is not expected when considering the Arrhenius equation, which assumes the order in each reactant to remain constant, however it is possible that varying the temperature is altering the order of the reactants, which is the probable cause of these observations.



**Figure 154** – A comparison of the conversion of styrene to (ethylbenzene to) ethylcyclohexane at 50°C and 70°C with 3 barg D<sub>2</sub>.

The lack of production of detectable levels of ethylcyclohexane after the deuteration of phenylacetylene suggests that the ring hydrogenation step involves subsurface hydrogen, as surface hydrogen would not be so drastically affected by the isotopic change as subsurface hydrogen, however the link between subsurface hydrogen and ring hydrogenation is not necessarily direct. The availability of subsurface hydrogen is clearly linked to the reaction of the alkyne, and that there are no such effects when styrene is hydrogenated – significant amounts of ethylcyclohexane are detected – presents the idea that the hydrogenation of phenylacetylene, which must occur at a different site to the hydrogenation of styrene, as was suggested by Bond, Dowden and Mackenzie<sup>22</sup>, is preventing hydrogen from entering the subsurface layer. If this is the case, then it provides evidence that the terminal alkyne of phenylacetylene is hydrogenating specifically on corner and edge sites, as these sites are known to be crucial for the diffusion of hydrogen into the subsurface layer<sup>27</sup>. The lack of subsurface hydrogen may lead to increased competition on the face sites, as species formed from the binding of alkyl and alkenyl chains to the surface do not desorb at a sufficient rate

and block sites which could form  $\pi$ -complex interactions with the aromatic ring. The effect of deuterium on the cascade previous to reaching ethylcyclohexane is particularly significant, as it is not only outweighing the inverse kinetic isotope effect reported from an earlier study in this laboratory<sup>60</sup>, but also decreasing the concentrations of ethylcyclohexane concentration to below detectable levels. The results of these experiments are conducive towards the theory that terminal alkynes hydrogenate on edge and corner sites, whereas alkenes and aromatic rings hydrogenate on the faces.

The decreased production of propylcyclohexane when 1-phenyl-1-propyne is deuterated can be ascribed to the normal kinetic isotope effect in the alkyne hydrogenation step, possibly combined with increased competition resulting from the alkene accessing a decreased reservoir of subsurface deuterium compared to what would be available if faster-diffusing hydrogen was used. The difference in behaviour with regards to alkylcyclohexane formation when compared with the phenylacetylene cascade may be partly attributed to the more significant inverse kinetic isotope effect associated with longer alkyl chains<sup>60</sup>. However this does not appear to cover the scale of the difference and a further factor which could be influencing the rate of ring deuteration is that the hydrogenation of the internal alkyne group does not take place on corner and edge sites, as with the terminal alkyne, but rather on terraced faces, meaning there is a less significant impact on the amount of deuterium which can access the subsurface. This lends itself to the prospect that terminal and internal alkynes undergo hydrogenation at different sites on a catalyst.

Mole fraction profiles, shown in Figures 155-160, were assessed to determine the effect of deuterium on alkene selectivity. The shape of the profile remained constant for each molecule, but was stretched along the axes with changing conditions.

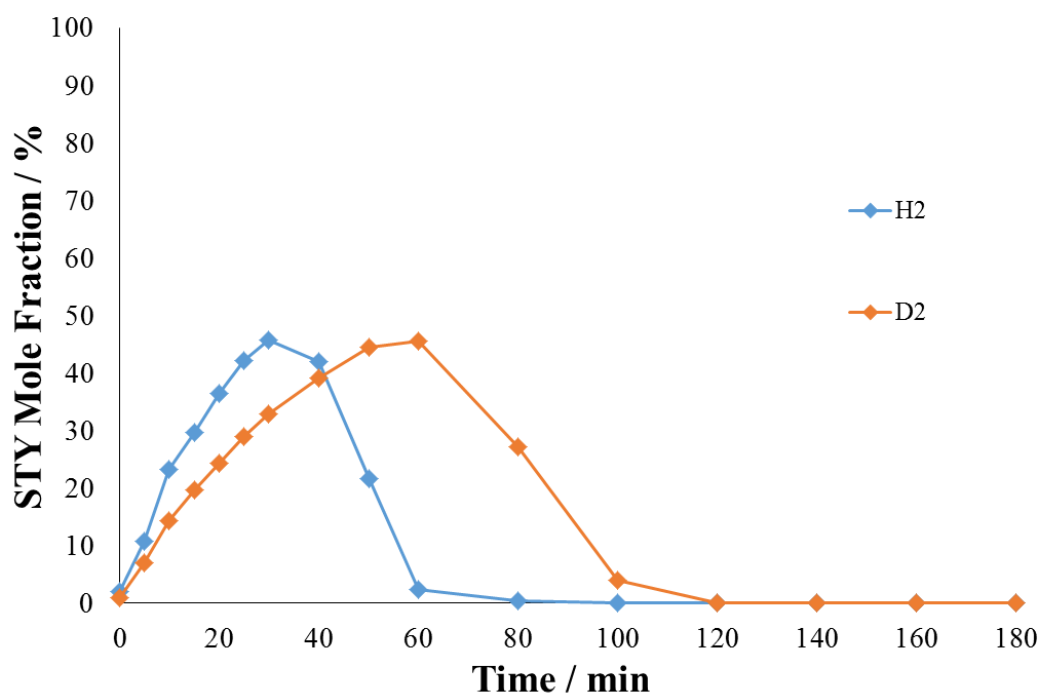


Figure 155 – A comparison of the styrene mole fraction profiles during the hydrogenation of phenylacetylene with hydrogen and deuterium at 50°C.

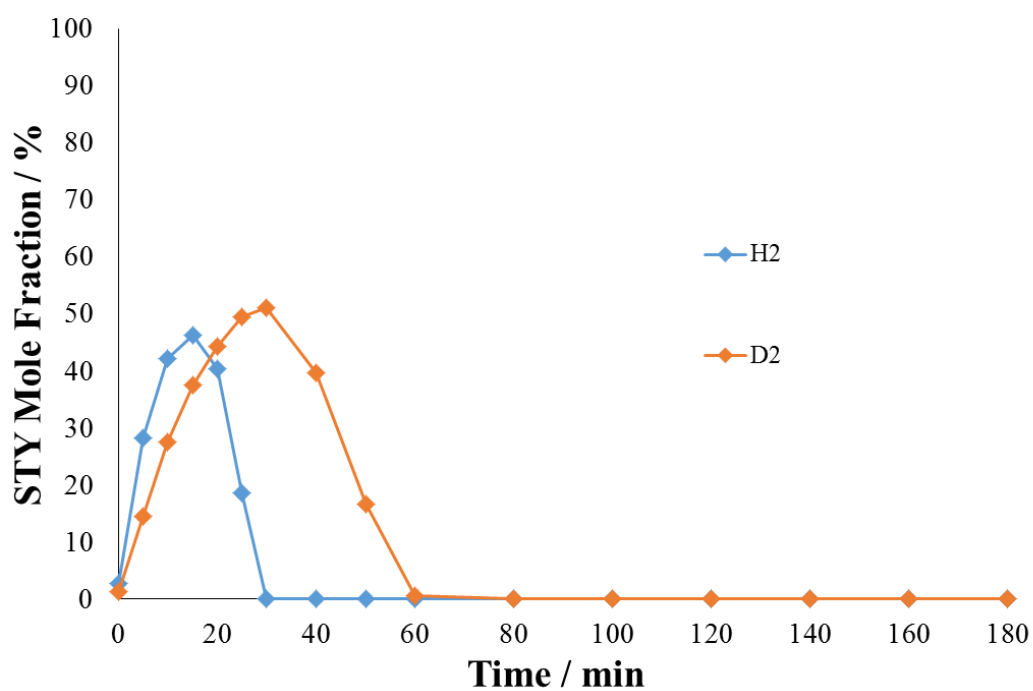


Figure 156 – A comparison of the styrene mole fraction profiles during the hydrogenation of phenylacetylene with hydrogen and deuterium at 70°C.

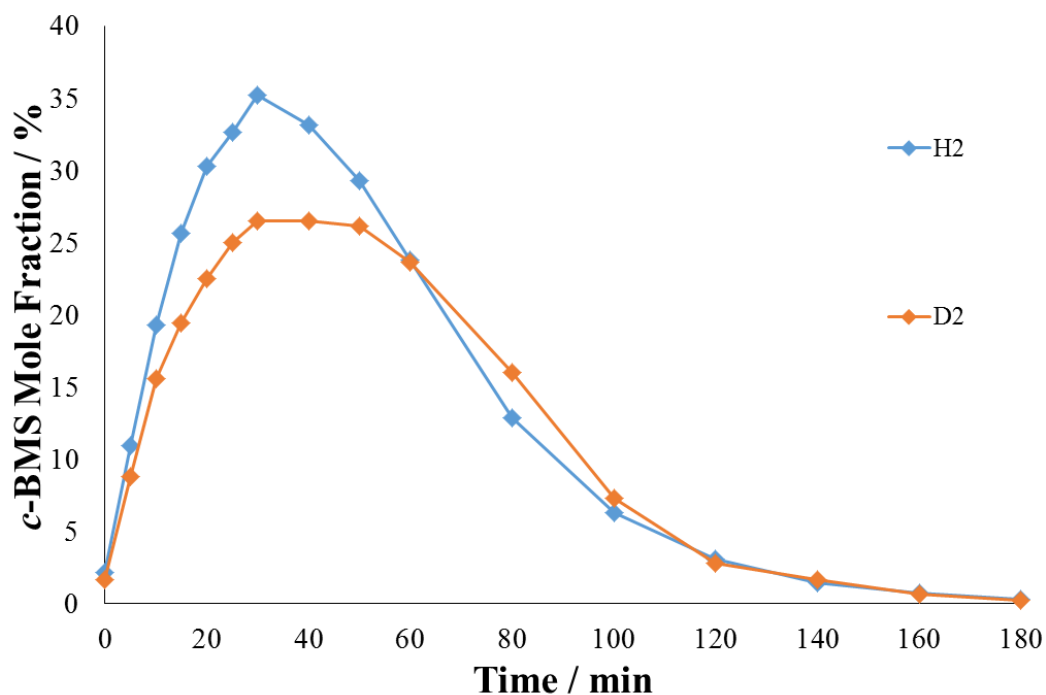


Figure 157 – A comparison of the *cis*- $\beta$ -methylstyrene mole fraction profiles during the hydrogenation of 1-phenyl-1-propyne with hydrogen and deuterium at 50°C.

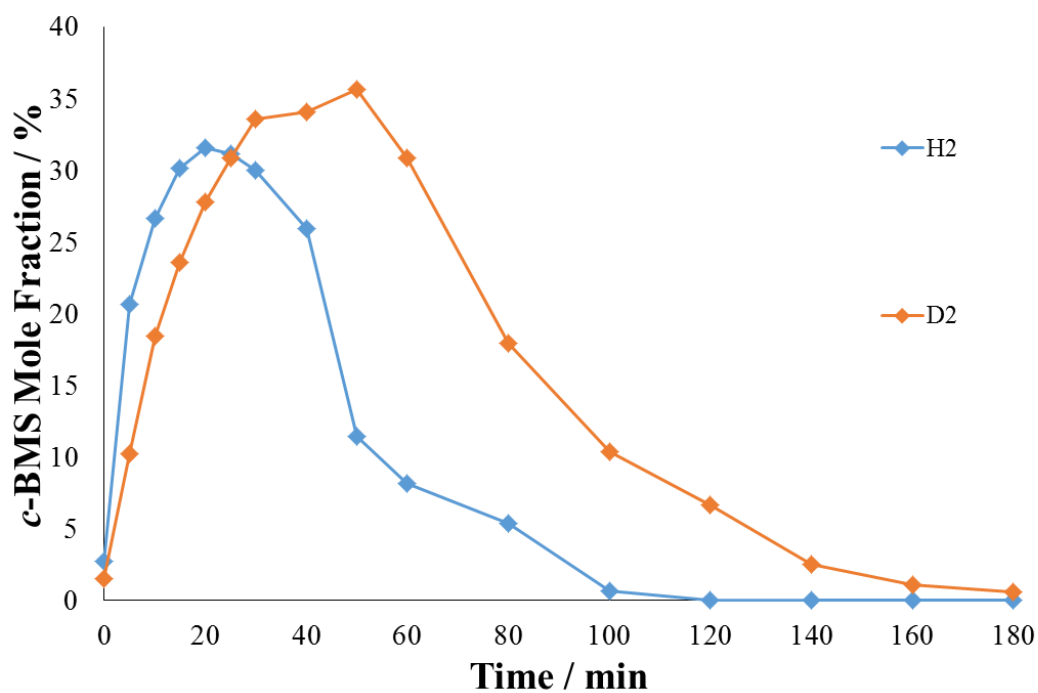


Figure 158 – A comparison of the *cis*- $\beta$ -methylstyrene mole fraction profiles during the hydrogenation of 1-phenyl-1-propyne with hydrogen and deuterium at 70°C.

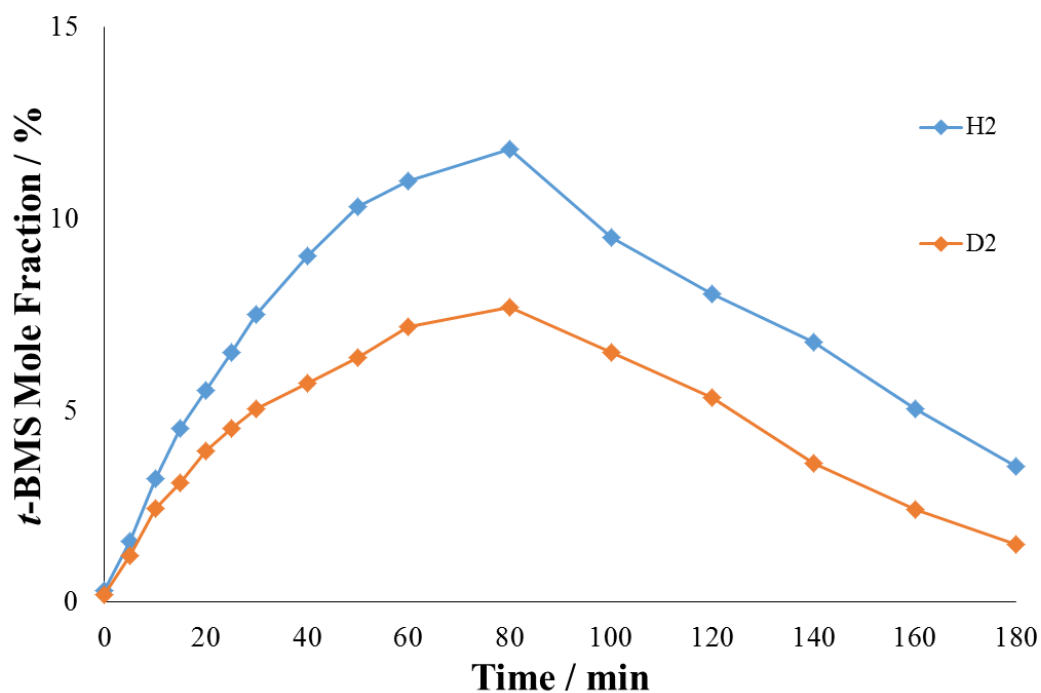


Figure 159 – A comparison of the *trans*- $\beta$ -methylstyrene mole fraction profiles during the hydrogenation of 1-phenyl-1-propyne with hydrogen and deuterium at 50°C.

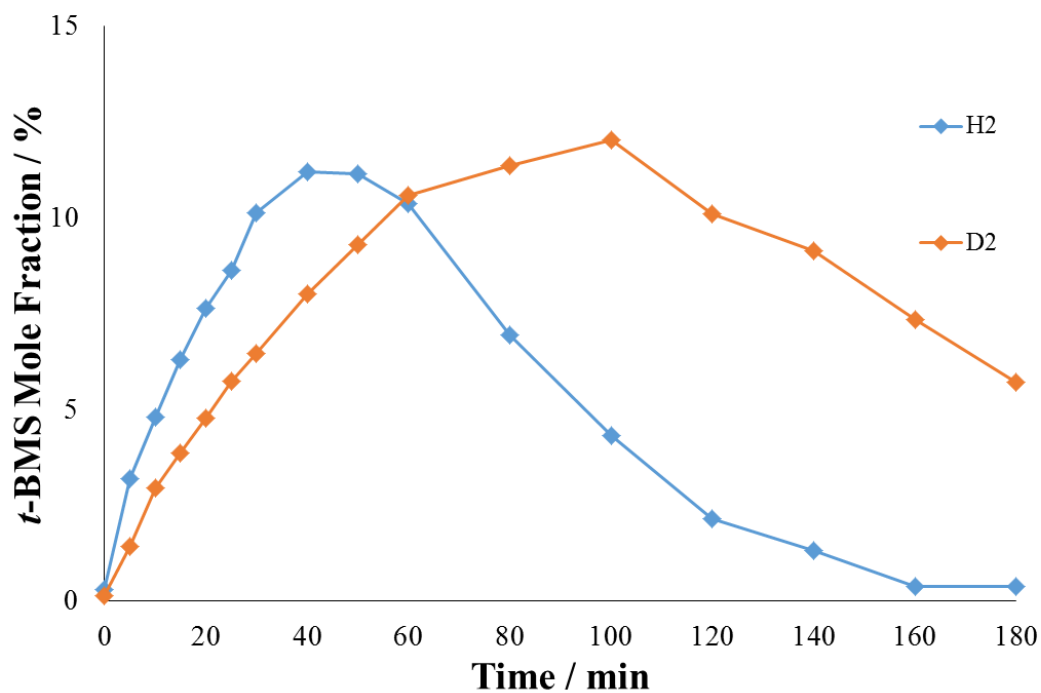


Figure 160 – A comparison of the *trans*- $\beta$ -methylstyrene mole fraction profiles during the hydrogenation of 1-phenyl-1-propyne with hydrogen and deuterium at 70°C.

The use of deuterium rather than hydrogen does not have a significant effect on the maximum styrene yield, again showing that changing the conditions does not have a notable impact on the relationship between phenylacetylene and styrene hydrogenation rates. At 50°C, deuterium does not shift the time at which the maxima of the *cis*- and *trans*- $\beta$ -methylstyrene mole fraction profiles appear, but does decrease the yield, suggesting that the rate of alkene hydrogenation is more strongly affected than the rate of alkyne hydrogenation by the change in isotope at this temperature. At 70°C, however, the deuterated product gives a greater mole fraction maximum for both *cis*- and *trans*- $\beta$ -methylstyrene and these maxima appear at a later time. This could be the result of  $\beta$ -methylstyrene isomerisation having a less significant kinetic isotope effect than hydrogenation and the impact of this becomes more prominent at 70°C.

Profiles of the *cis/trans* ratio of  $\beta$ -methylstyrene were also produced for the reactions with deuterium (Figures 161-162) and can be compared to those produced for reactions with hydrogen at the same temperature. The profiles were both the same shape, but the profiles produced from the deuteration had a slightly greater *cis/trans* ratio at each point.

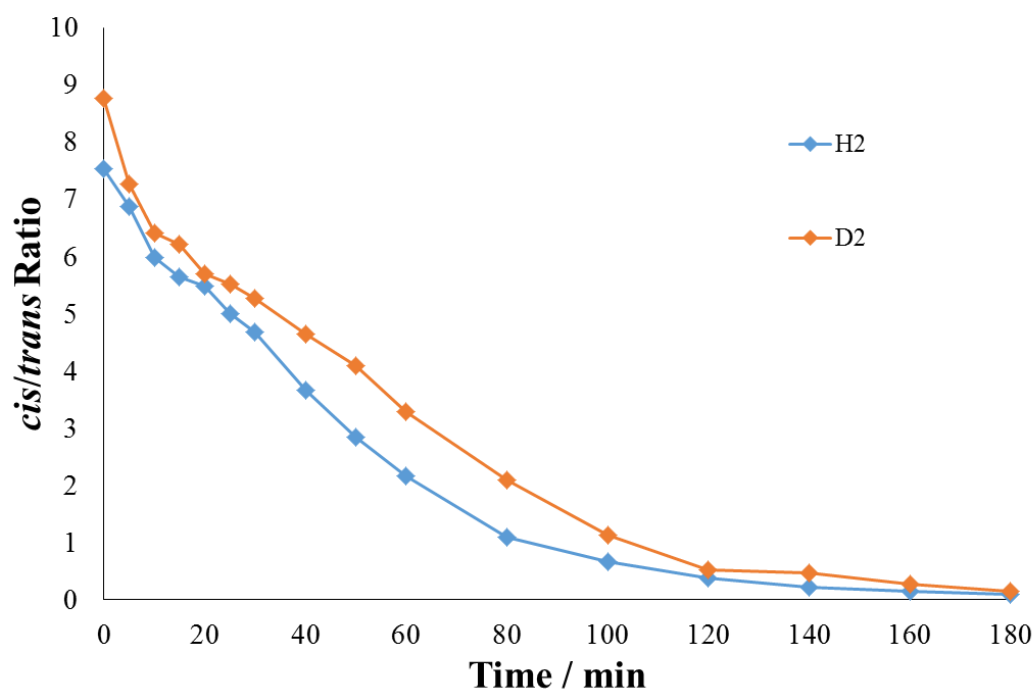


Figure 161 – *cis/trans* ratio of  $\beta$ -methylstyrene during the hydrogenation and deuteration of 1-phenyl-1-propyne at 50°C.

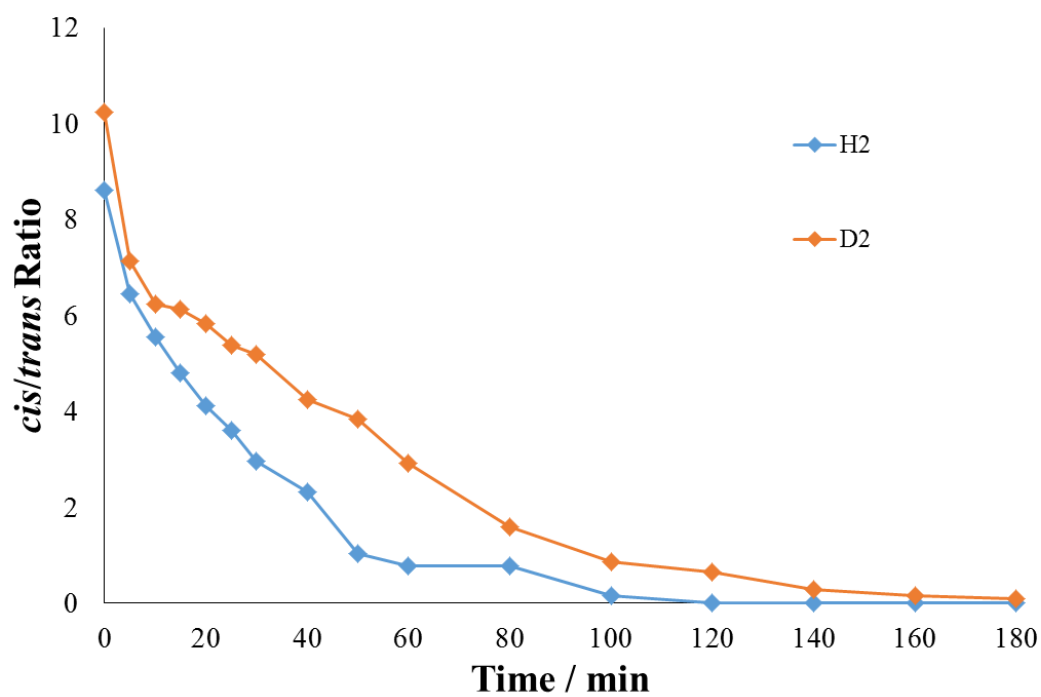


Figure 162 – *cis/trans* ratio of  $\beta$ -methylstyrene during the hydrogenation and deuteration of 1-phenyl-1-propyne at 70°C.

The *cis/trans* ratio is marginally increased by the use of deuterium rather than hydrogen until all the  $\beta$ -methylstyrene has reacted. This suggests that the kinetic isotope effect for 1-phenyl-1-propyne hydrogenation is more positive than the kinetic isotope effect for isomerisation.

The  $^2\text{H}$  NMR signals were compared across samples to assess how signals change with time and temperature; they are presented in Tables 41-43.

**Table 41 – A comparison of the relative intensities, normalised relative to the smallest peak, of each significant peak in the  $^2\text{H}$  NMR spectrum of a sample taken after 10, 40 and 180 minutes of phenylacetylene deuteration at 50°C and 70°C.**

Shift, $\delta$ / ppm	Temperature / °C					
	50			70		
	Time / min					
	10	40	180	10	40	180
7.6		1.1			1.0	
6.2 (solvent)	1.8	1.8	1.0	2.7	3.3	1.3
3.5 (solvent)		1.0	1.4		2.0	1.0
2.0 (solvent)	1.0	1.8	2.2	1.0	3.5	1.5

Most of the observable peaks are likely due to exchange with the solvent, although a peak at  $\delta = 7.6$  ppm can be seen at 40 minutes of both experiments. This peak is likely the result of an alkene deuteron. The alkane deuterons may not be detectable due to quadrupolar coupling broadening the peaks.

**Table 42 – A comparison of the relative intensities, normalised relative to the smallest peak, of each significant peak in the  $^2\text{H}$  NMR spectrum of a sample taken after 10, 40 and 180 minutes of styrene deuteration at 50°C and 70°C.**

Shift, $\delta$ / ppm	Temperature / °C					
	50			70		
	Time / min					
	10	40	180	10	40	180
5.7 (solvent)	2.6	5.6	9.9	1.5	4.0	4.7
3.0 (solvent)	1.0	1.9	1.0	1.0	2.7	1.5
2.1		1.0	2.9		1.0	1.0
1.6 (solvent)	2.4	4.6	4.9	2.6	5.7	3.0
1.3		1.3	4.4		1.1	1.4

In the  $^2\text{H}$  NMR spectra resulting from the deuteration of styrene, peaks at  $\delta = 2.1$  ppm and  $\delta = 1.3$  ppm are seen at 40 and 180 minutes and show deuterons at the CDH and CDH<sub>2</sub> groups, respectively, of the alkane.

**Table 43 – A comparison of the relative intensities, normalised relative to the smallest peak, of each significant peak in the  $^2\text{H}$  NMR spectrum of a sample taken after 10, 40 and 180 minutes of 1-phenyl-1-propyne deuteration at 50°C and 70°C. The first value for the shift is that given for the spectra of samples taken at 50°C and the second value for the shift is that given for the spectra of samples taken at 70°C.**

Shift, $\delta$ / ppm	Temperature / °C					
	50			70		
	Time / min					
	10	40	180	10	40	180
7.3/6.9		1.6		1.0	1.4	
6.7/6.2		1.2			1.1	
6.2/5.7 (solvent)	6.8	5.1	4.6	4.9	4.6	6.0
3.4/3.0 (solvent)	1.0	2.7	4.4	1.7	2.9	6.2
2.5/2.0	1.0	2.3	3.2	1.5	2.2	4.1
2.1/1.6 (solvent)	1.0	1.2	1.1	1.4	1.0	1.0
1.8/1.3		1.0	1.0		1.0	1.0

In the  $^2\text{H}$  NMR spectra resulting from the deuteration of 1-phenyl-1-propyne, peaks at  $\delta = 7.3/6.9$  ppm and  $\delta = 6.7/6.2$  ppm show alkene deuterons. Peaks at  $\delta = 2.5/2.0$  ppm and  $\delta = 1.8/1.3$  ppm show deuterons at the two  $\text{CD}_2$  groups, respectively, of the alkane.

It is notable that no exchange with aromatic protons is observed in any of the experiments. This suggests that there is an absence of  $\pi$  complex adsorption in these experiments, which partly explains the observed decrease in aromatic reactivity with deuterium in comparison to hydrogen.

The experiments with deuterium demonstrated kinetics which are consistent with a palladium-like model involving terminal alkynes hydrogenating at corner and edge sites and internal alkynes along with other unsaturated groups hydrogenating on terraced faces. They also provided evidence of a shift in reaction pathway in the 1-phenyl-1-propyne cascade between  $60^\circ\text{C}$  and  $70^\circ\text{C}$ . There appears to be little or no exchange with the aromatic ring before hydrogenation takes place and its hydrogenation is significantly affected by the change in hydrogen isotope, the substituent and, in some cases, the temperature.

#### 5.1.4 Competitive Reactions

Competitive hydrogenation was used to probe the kinetics of the studied reactions and further test ideas about hydrogenation sites and different types of hydrogen.

The reactions involving toluene- $\text{d}_8$  showed that aromatic molecules with larger substituents can completely prevent the chemical adsorption of aromatics with smaller substituents. This was seen in the complete inhibition of both the hydrogenation and exchange of toluene- $\text{d}_8$ , which remained at a constant concentration with a consistent  $^2\text{H}$  NMR spectrum throughout the hydrogenation of phenylacetylene and 1-phenyl-1-propyne. There may be some physical adsorption of toluene- $\text{d}_8$  during the hydrogenation of phenylacetylene, as the rate of phenylacetylene hydrogenation is decreased by a small amount, however the increase in rate of 1-phenyl-1-propyne hydrogenation when toluene- $\text{d}_8$  is present suggests that interactions between the aromatic rings are interfering with the rates of reactions<sup>48</sup>. This can be rationalised as

toluene donating electron density into the aromatic system of the adsorbed 1-phenyl-1-propyne, contributing to the breaking of the  $\pi$  bond.

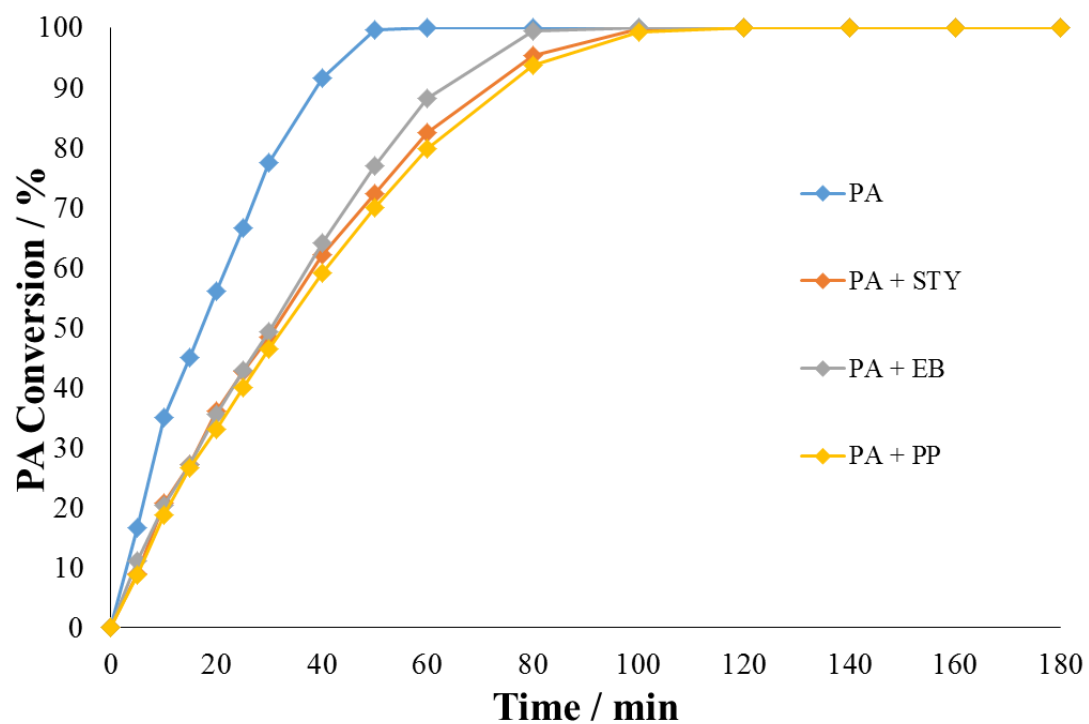


Figure 163 – A graph showing phenylacetylene conversion with no competition, in competition with styrene, in competition with ethylbenzene, and in competition with 1-phenyl-1-propyne, all at 50°C.

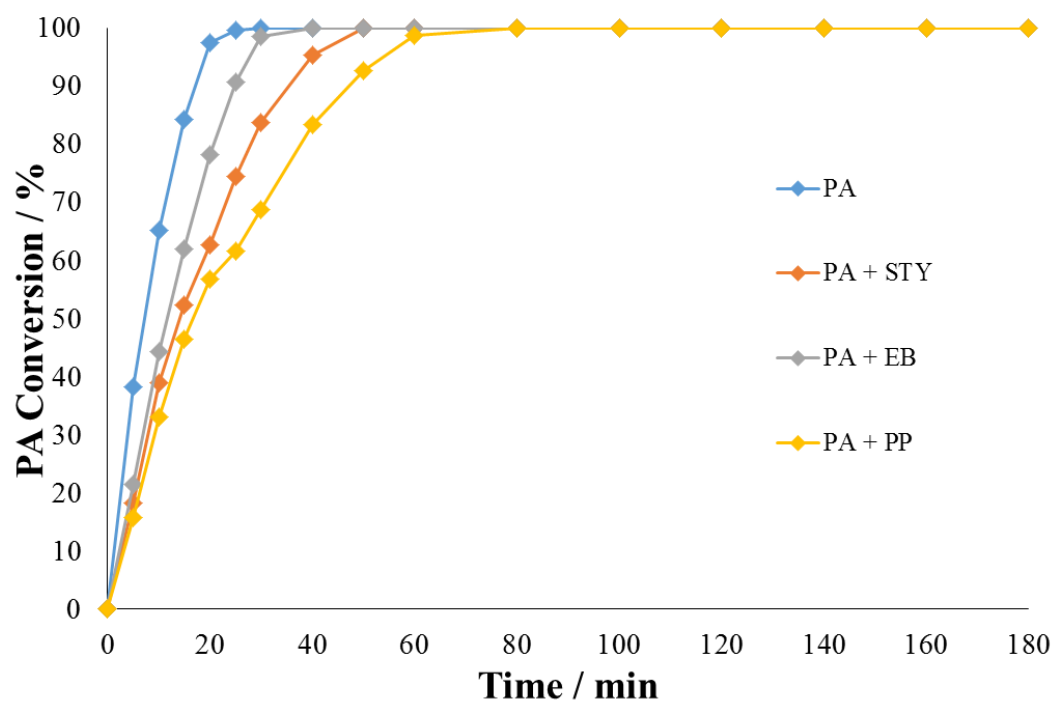
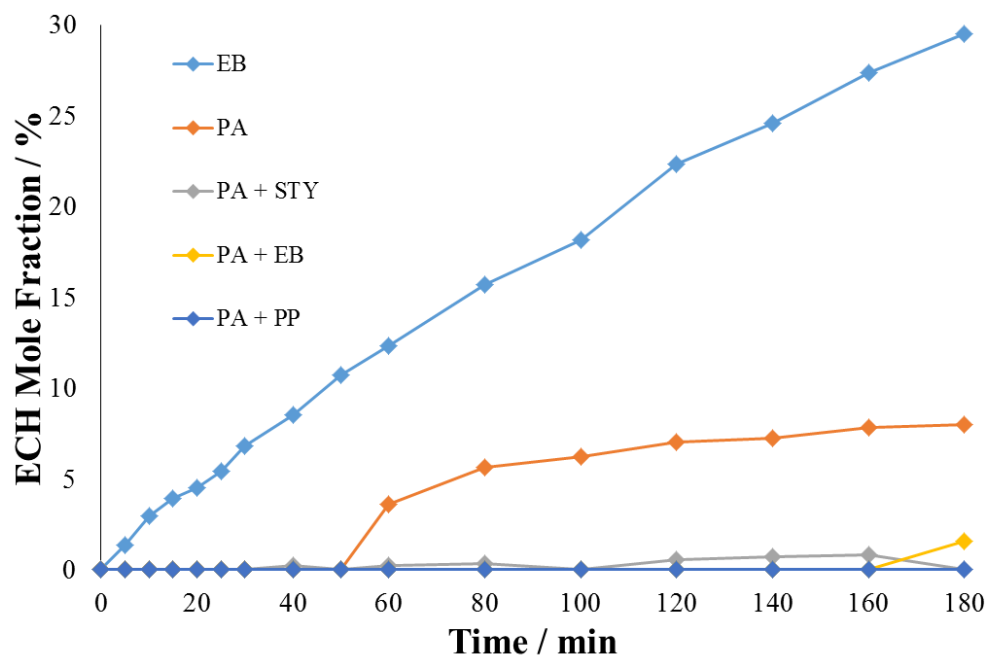
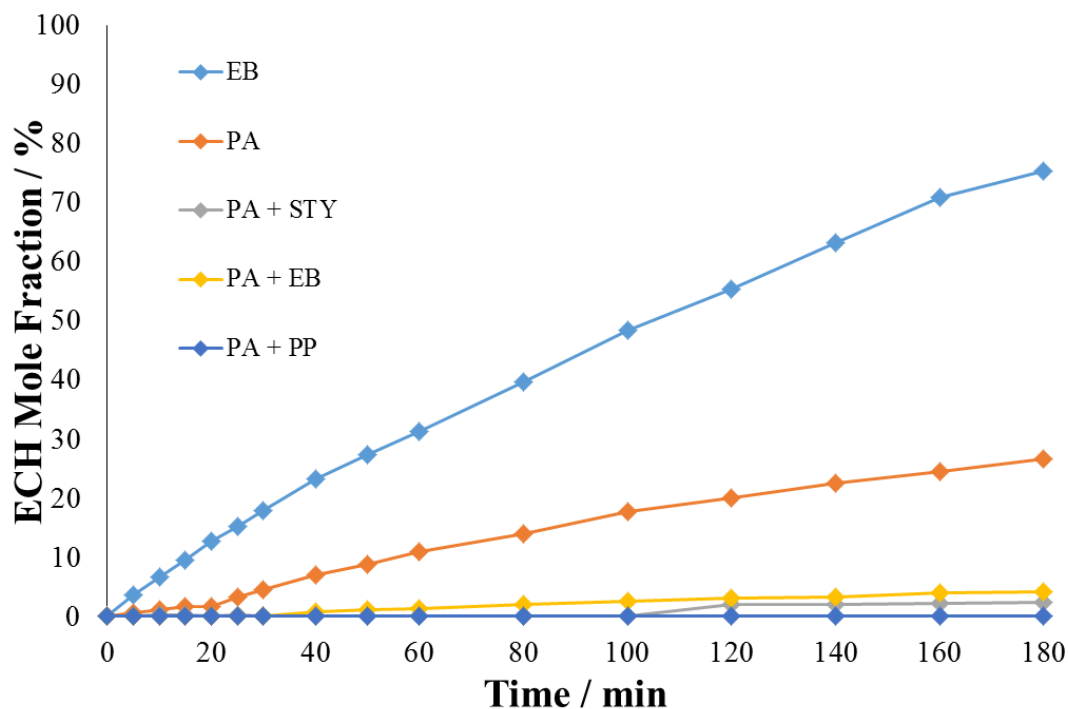


Figure 164 – A graph showing phenylacetylene conversion with no competition, in competition with styrene, in competition with ethylbenzene, and in competition with 1-phenyl-1-propyne, all at 70°C.



**Figure 165 – A graph showing ethylcyclohexane mole fraction from reactions of only phenylacetylene, only ethylbenzene, phenylacetylene and styrene, phenylacetylene and ethylbenzene, and phenylacetylene and 1-phenyl-1-propyne, all at 50°C. It should be noted that 100% ethylcyclohexane mole fraction in the competitive reactions would represent twice the number of moles of ethylcyclohexane as a 100% mole fraction in the other reactions.**



**Figure 166** – A graph showing ethylcyclohexane mole fraction from reactions of only phenylacetylene, only ethylbenzene, phenylacetylene and styrene, phenylacetylene and ethylbenzene, and phenylacetylene and 1-phenyl-1-propyne, all at 70°C. It should be noted that 100% ethylcyclohexane mole fraction in the competitive reactions would represent twice the number of moles of ethylcyclohexane as a 100% mole fraction in the other reactions.

When phenylacetylene is competitively hydrogenated with styrene or ethylbenzene, phenylacetylene conversion is minimally affected (Figures 163-164), but competitive reactions brought ethylcyclohexane yields to much lower, and in some cases, experimentally undetectable, levels (Figures 165-166). Starting the cascade from phenylacetylene also significantly decreased the ethylcyclohexane yield after 180 minutes when compared to starting with ethylbenzene. This could be the result of an increase in competition for active hydrogen species, caused by phenylacetylene preventing hydrogen from diffusing into the subsurface layer, which is known to cause a decrease in the rate of alkene hydrogenation. This effect then has implications for the steps further down the cascade, thus decreasing the rate of ring hydrogenation. The similarity in their effects on the reaction kinetics suggests that styrene and

ethylbenzene are occupying the same active sites, most likely sites on the terraced faces, as stated by Bond<sup>12</sup>.

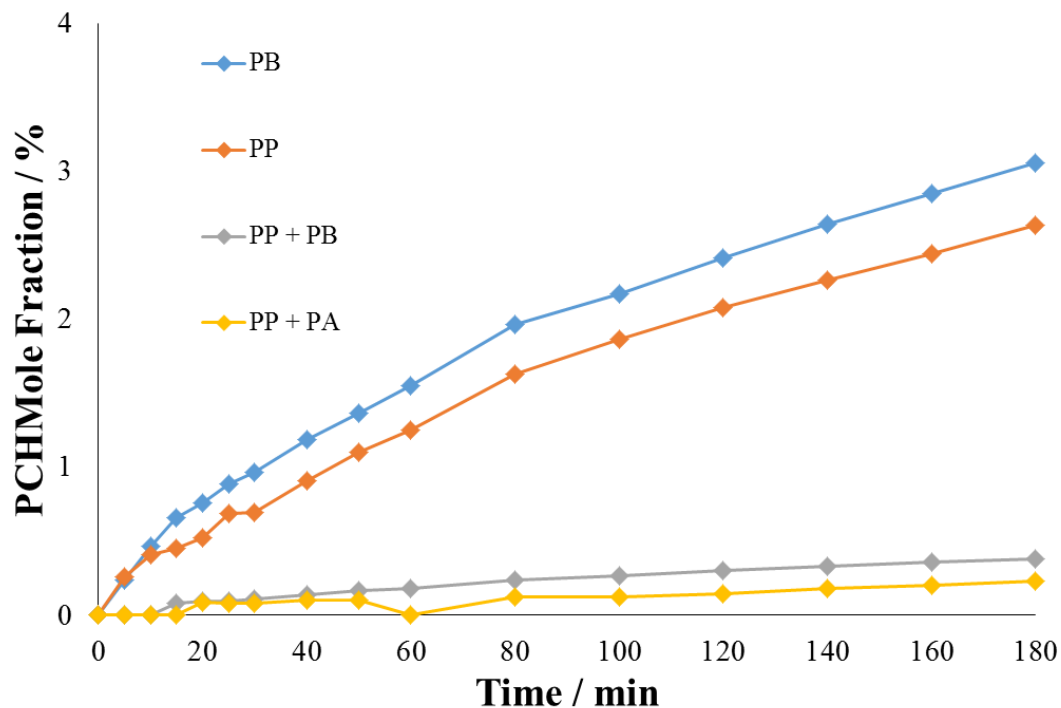


**Figure 167 – A graph showing propylcyclohexane mole fraction from reactions of only 1-phenyl-1-propyne, only propylbenzene, 1-phenyl-1-propyne and propylbenzene, and 1-phenyl-1-propyne and phenylacetylene, all at 50°C. It should be noted that 100% propylcyclohexane mole fraction in the competitive reactions would represent twice the number of moles of propylcyclohexane as a 100% mole fraction in the other reactions.**

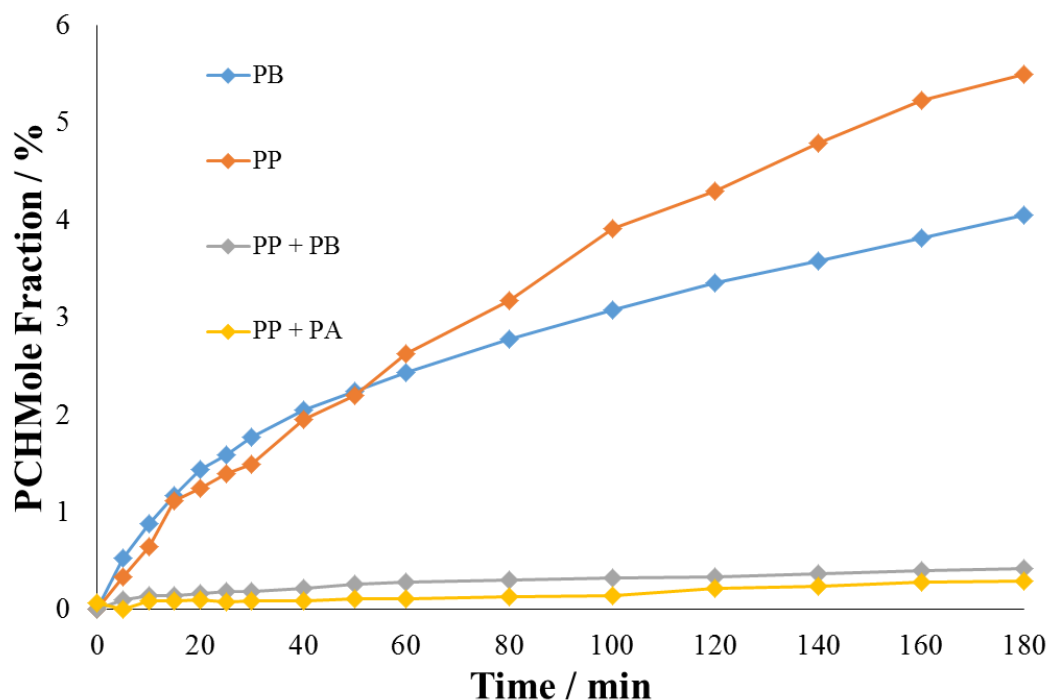


**Figure 168** – A graph showing propylcyclohexane mole fraction from reactions of only 1-phenyl-1-propyne, only propylbenzene, 1-phenyl-1-propyne and propylbenzene, and 1-phenyl-1-propyne and phenylacetylene, all at 70°C. It should be noted that 100% propylcyclohexane mole fraction in the competitive reactions would represent twice the number of moles of propylcyclohexane as a 100% mole fraction in the other reactions.

The competitive hydrogenation of propylbenzene and 1-phenyl-1-propyne does not significantly affect the initial rate of hydrogenation of 1-phenyl-1-propyne (Figures 169-170), but does show a large decrease in propylcyclohexane production over the 180 minutes, when compared with the hydrogenation of either propylbenzene or 1-phenyl-1-propyne alone (Figures 167-168). This is likely due a combination of the competition for sites for propylbenzene hydrogenation, as there are double the number of molecules in the cascade when compared to conditions in the non-competitive reactions, and the slow reaction of the molecules earlier in the cascade due to their competition for active sites with propylbenzene. The results fit the hypothesis that internal alkynes hydrogenate on face sites, as there appears to be direct competition between 1-phenyl-1-propyne, *cis*- and *trans*- $\beta$ -methylstyrene and propylbenzene.

The presence of 1-phenyl-1-propyne does not have a noteworthy impact on the hydrogenation of phenylacetylene, as is shown in Figures 163-164, but its hydrogenation is largely prevented until after the phenylacetylene has almost completely reacted, as can be seen in Figures 171-172. This does not necessitate direct competition between the two molecules however, as styrene is quickly produced from the hydrogenation of phenylacetylene. The maximum in styrene concentration occurs fractionally before substantial 1-phenyl-1-propyne hydrogenation is observed, so it is likely that it is the styrene which is outcompeting 1-phenyl-1-propyne for face sites. The availability of subsurface hydrogen appears to be decreased by the hydrogenation of the terminal alkene on the edge and corner sites, possibly providing a source of indirect competition, which, in tandem with the direct competition of the styrene, produces clearly observable results.

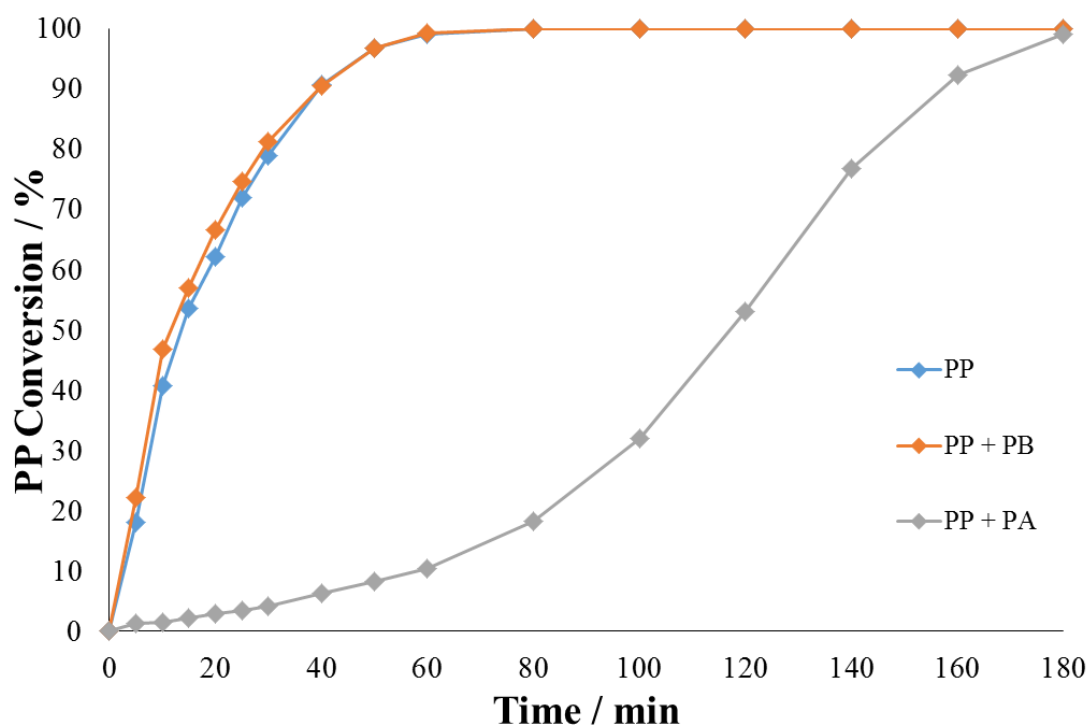


**Figure 169 - A graph showing 1-phenyl-1-propyne conversion with no competition, in competition with propylbenzene, and in competition with phenylacetylene, all at 50°C.**

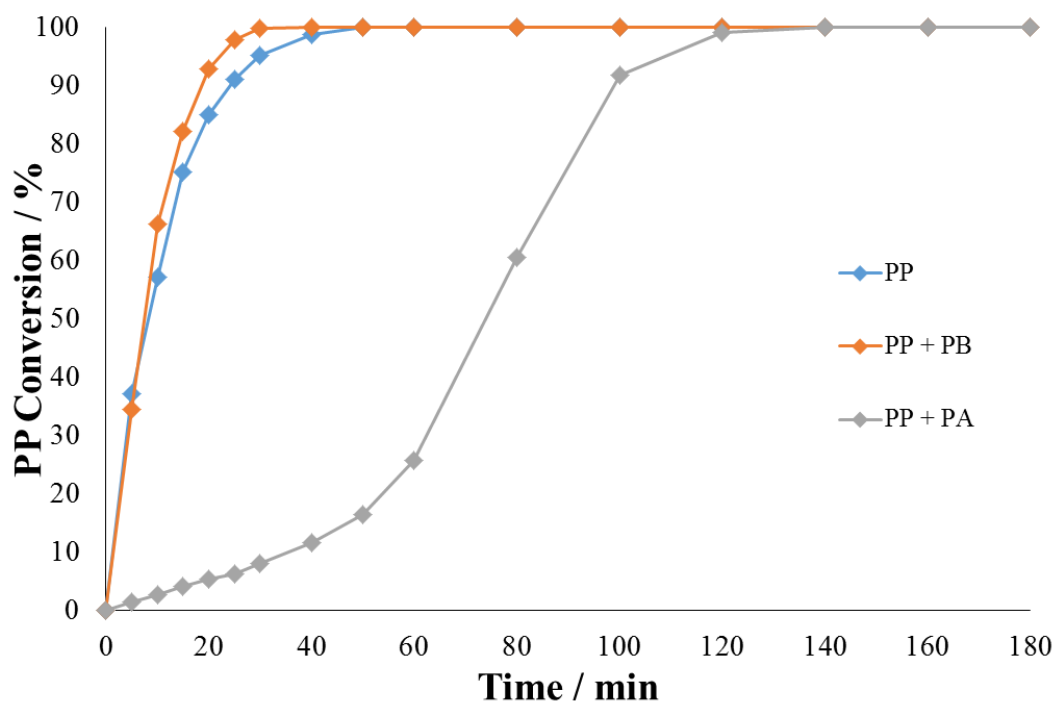


**Figure 170 - A graph showing 1-phenyl-1-propyne conversion with no competition, in competition with propylbenzene, and in competition with phenylacetylene, all at 70°C.**

The suppression of 1-phenyl-1-propyne hydrogenation can be seen to correlate with the presence of styrene. Once the styrene has reacted, the rate of 1-phenyl-1-propyne hydrogenation increases dramatically. This is demonstrated in Figures 171-172.

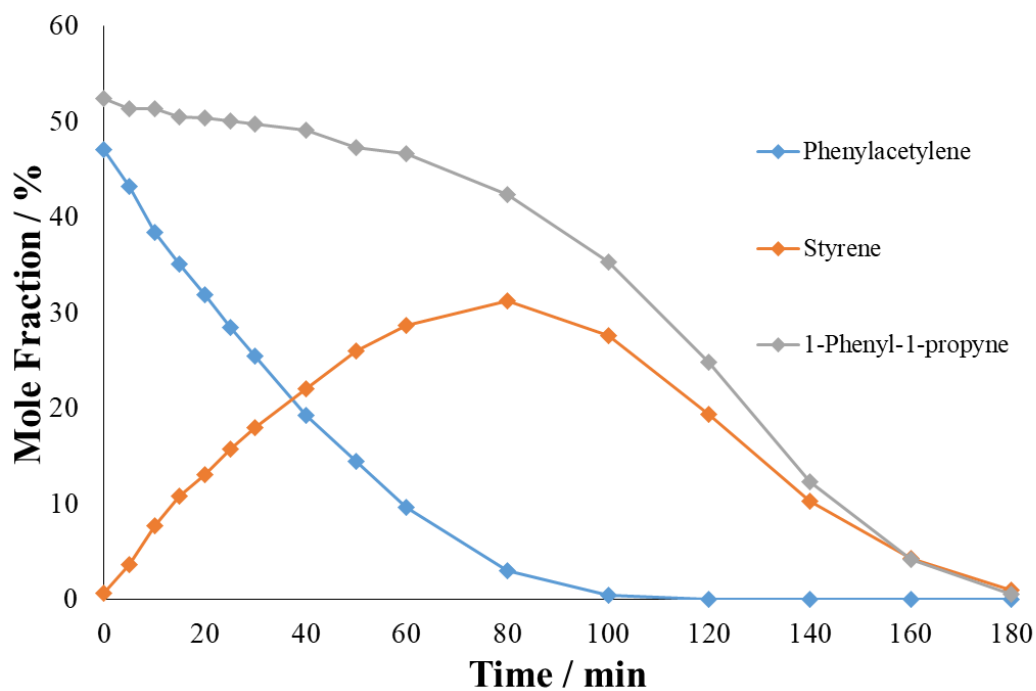


Figure 171 – A mole fraction profile for the competitive hydrogenation of phenylacetylene and 1-phenyl-1-propyne at 50°C.

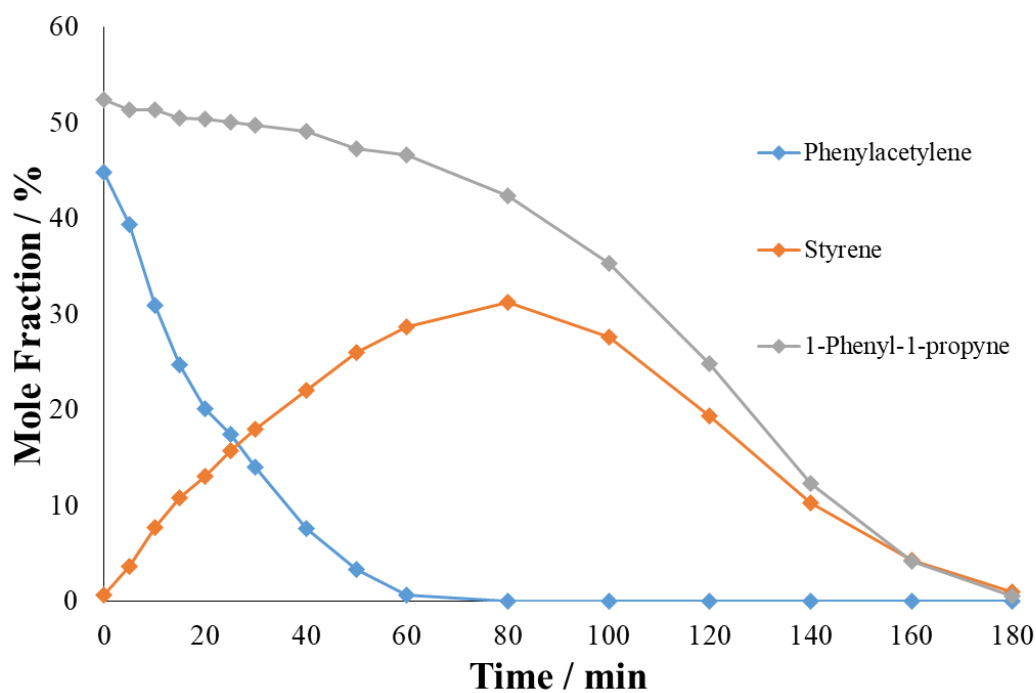


Figure 172 – A mole fraction profile for the competitive hydrogenation of phenylacetylene and 1-phenyl-1-propyne at 70°C.

Alkene mole fraction under different competitive conditions was considered in Figures 173-178.

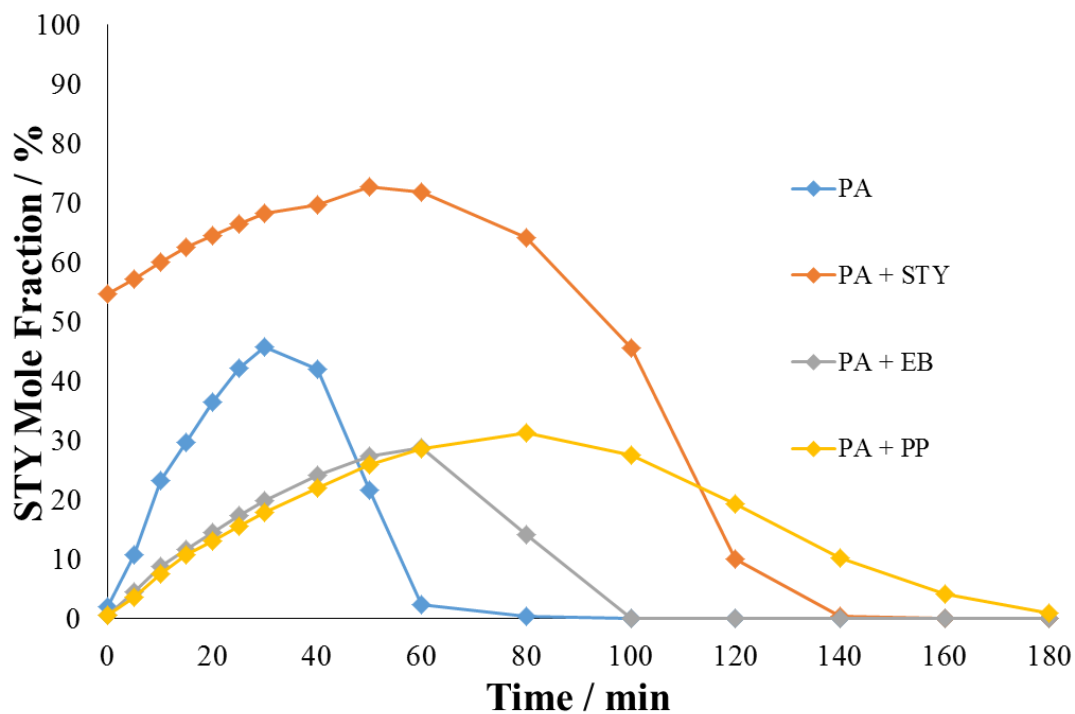


Figure 173 – A comparison of the styrene mole fraction profiles during the hydrogenation of phenylacetylene alone and of phenylacetylene in competition with styrene, ethylbenzene, and 1-phenyl-1-propyne at 50°C.

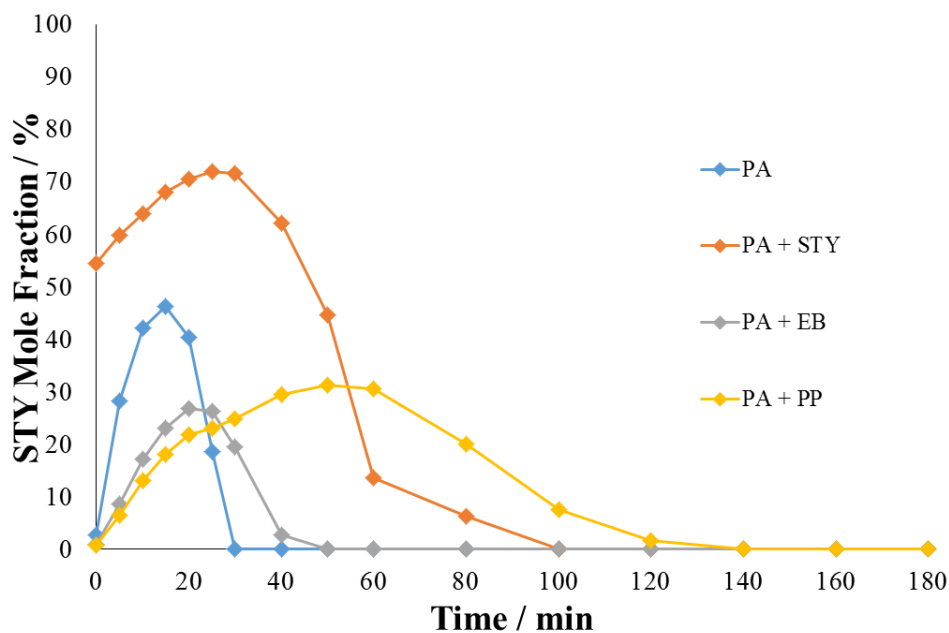


Figure 174 – A comparison of the styrene mole fraction profiles during the hydrogenation of phenylacetylene alone and of phenylacetylene in competition with styrene, ethylbenzene, and 1-phenyl-1-propyne at 70°C.

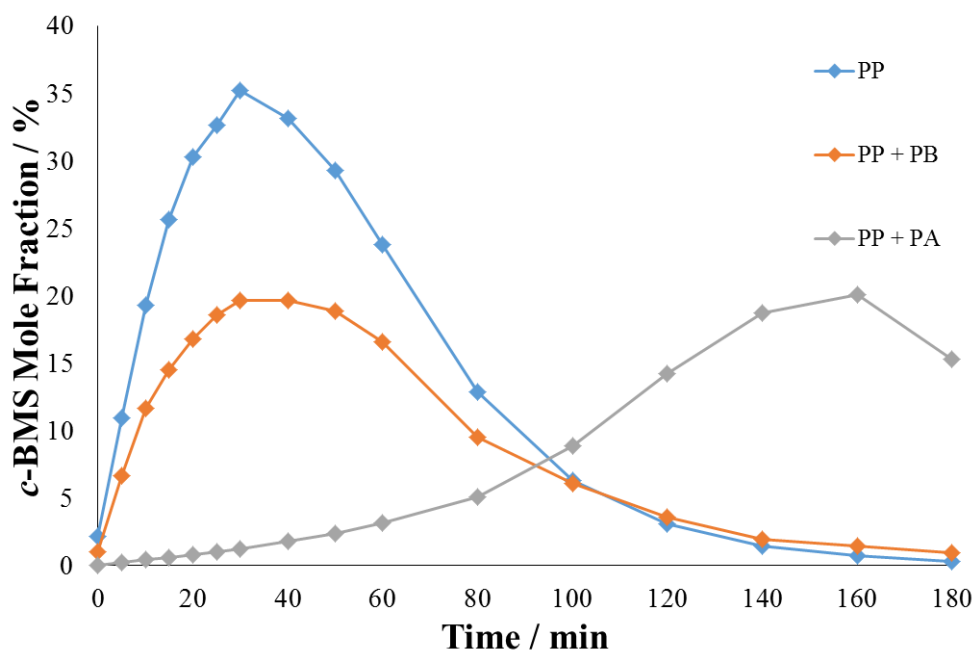


Figure 175 – A comparison of the *cis*- $\beta$ -methylstyrene mole fraction profiles during the hydrogenation of 1-phenyl-1-propyne alone and of 1-phenyl-1-propyne in competition with propylbenzene, and phenylacetylene at 50°C.

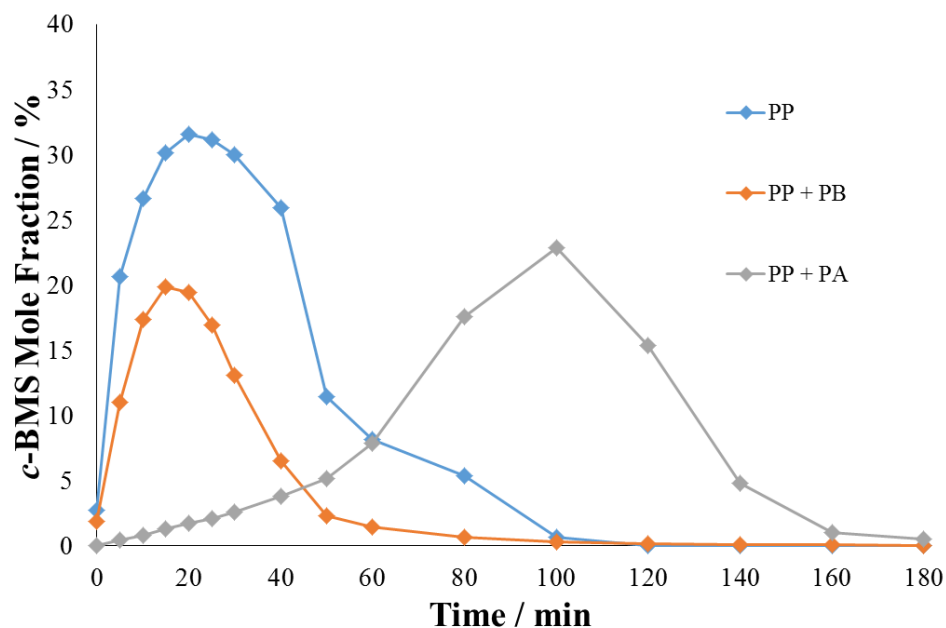


Figure 176 – A comparison of the *cis*- $\beta$ -methylstyrene mole fraction profiles during the hydrogenation of 1-phenyl-1-propyne alone and of 1-phenyl-1-propyne in competition with propylbenzene, and phenylacetylene at 70°C.

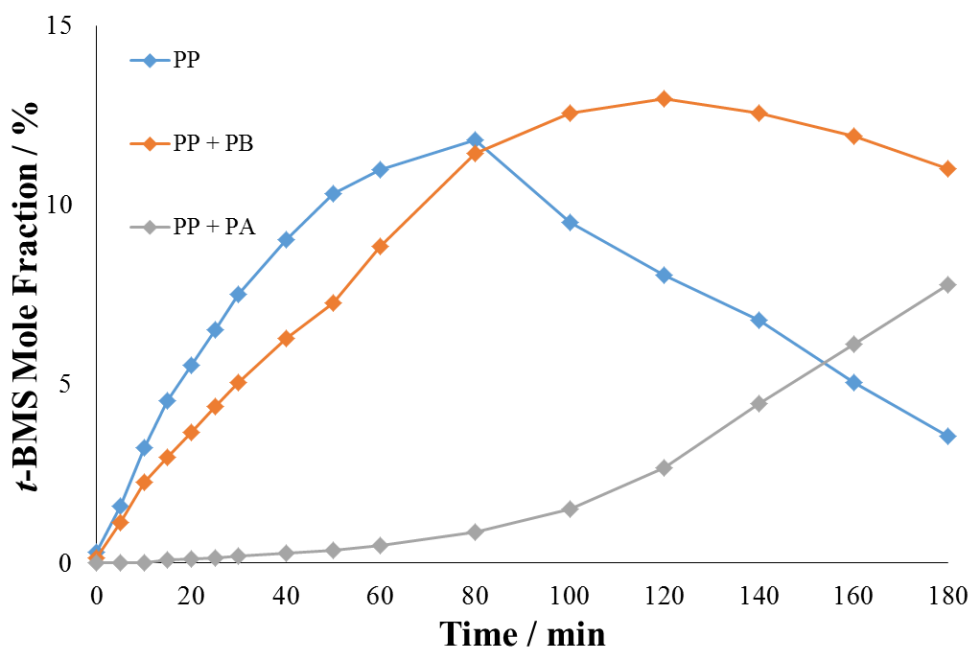
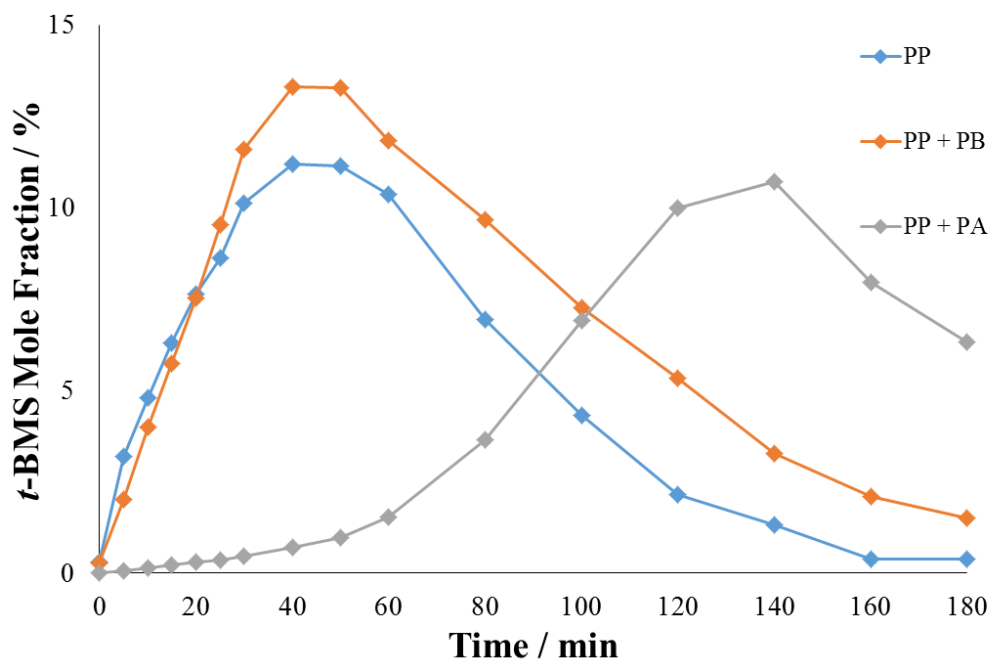


Figure 177 – A comparison of the *trans*- $\beta$ -methylstyrene mole fraction profiles during the hydrogenation of 1-phenyl-1-propyne alone and of 1-phenyl-1-propyne in competition with propylbenzene, and phenylacetylene at 50°C.



**Figure 178 – A comparison of the *trans*- $\beta$ -methylstyrene mole fraction profiles during the hydrogenation of 1-phenyl-1-propyne alone and of 1-phenyl-1-propyne in competition with propylbenzene, and phenylacetylene at 70°C.**

Competition was found to allow for an improved styrene yield (Figures 173-174), with the rate of phenylacetylene hydrogenation being hindered to a greater extent than styrene hydrogenation. This provides more evidence that the phenylacetylene triple bond is being hydrogenated at a different site to the other unsaturated functional groups, as it suggests that phenylacetylene faces a lack of direct competition and, thus, its hydrogenation is less hindered than that of styrene, which would appear to be directly competing with other species. These findings are in conjunction with a similar study carried out in this laboratory<sup>56</sup>, as well as the previous results in this study, in revealing kinetics which lead one to conclude that the position of the alkyne functional group influences that site at which it is hydrogenated.

It was difficult to draw conclusions from the reaction involving styrene as a competitive species, but the hydrogenation of phenylacetylene was slowed by its presence. It was found that competition with 1-phenyl-1-propyne enhanced the styrene yield more than competition with ethylbenzene, although both provided an

enhancement to styrene production when compared with the hydrogenation of just phenylacetylene. This may be the result of 1-phenyl-1-propyne and  $\beta$ -methylstyrene providing competition for subsurface hydrogen as well as sites, whereas ethylbenzene only competes for sites, as its hydrogenation requires surface hydrogen, a notion concluded from the poisoning effects of carbon laydown<sup>47</sup>. Another factor could be the longer chain length of the substituents in the 1-phenyl-1-propyne hydrogenation cascade causing them to bind more favourably than styrene<sup>50</sup>.

Selectivity to *cis*- $\beta$ -methylstyrene (Figures 175-176) appears to be temperature dependent. Improved selectivity towards the *trans* isomer under competition at both 50°C and 70°C (Figures 177-178) shows that there is competition for subsurface hydrogen, reducing the rate of hydrogenation and meaning that isomerisation is enhanced, as this requires surface hydrogen. These results seem to confirm the findings of Anderson *et al.*<sup>39</sup>, but the most interesting information arises when analysing the *cis/trans* ratio.

The *cis/trans* ratio of the  $\beta$ -methylstyrene isomers under competitive conditions was calculated and is displayed in Figures 179-180. Competition with propylbenzene decreased the *cis/trans* ratio by a small amount at each data point, but competition with phenylacetylene changed the overall shape of the profile significantly.

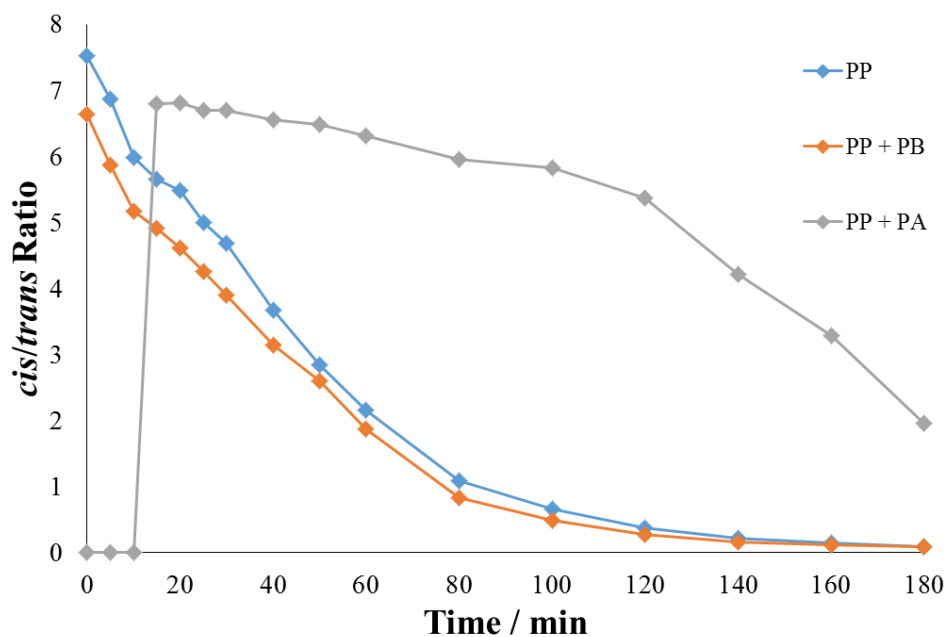


Figure 179 – *cis/trans* ratio of  $\beta$ -methylstyrene during the hydrogenation of 1-phenyl-1-propyne without competition, in competition with propylbenzene and in competition with phenylacetylene, at 50°C.

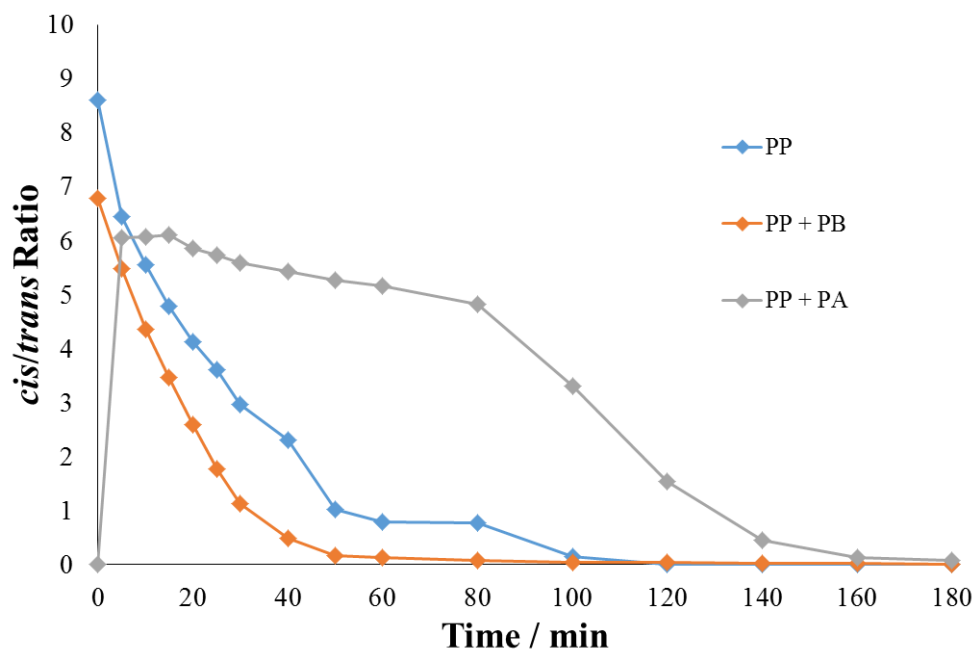


Figure 180 – *cis/trans* ratio of  $\beta$ -methylstyrene during the hydrogenation of 1-phenyl-1-propyne without competition, in competition with propylbenzene and in competition with phenylacetylene, at 70°C.

Competition with propylbenzene marginally decreases the *cis/trans* ratio of  $\beta$ -methylstyrene throughout the reaction, suggesting that the rate of isomerisation is increased relative to the rates of hydrogenation of the alkyne, the alkene or both. Competition with phenylacetylene decreases the rate at which the *cis/trans* ratio of  $\beta$ -methylstyrene decreases, suggesting phenylacetylene is inhibiting isomerisation, however all other results have suggested that phenylacetylene hydrogenation occurs at corner and edge sites, whereas studied reported in the literature have shown that internal alkenes undergo reactions on terraced faces<sup>39, 56</sup>. A possible explanation for this is that it is the styrene which is preventing isomerisation, as styrene appears to react at the same sites as  $\beta$ -methylstyrene, however this seems unlikely, as the extra methyl group would mean that  $\beta$ -methylstyrene would interact with the surface more strongly than styrene<sup>50</sup>, and thus would be expected to outcompete styrene.

Competitive reactions have shown that there is direct competition for active sites on the face of the catalyst from most of the molecules. This competition is dominated by molecules with longer chains and the clear exception is that phenylacetylene appears to be hydrogenated on the corner and edge sites. These conclusions have been drawn from the kinetics caused by interactions between the relevant molecules and the different species of hydrogen. Subsurface hydrogen appears to be playing a significant role in alkene and internal alkyne hydrogenation, with surface hydrogen being influential in ring hydrogenation and alkene isomerisation.

## 5.2 TGA

Thermogravimetric analysis was used to assess the carbon laydown on the post-reaction catalysts. There are generally three peaks observed on the ion current temperature profiles show that there are three different types of carbon on the post-reaction catalysts, as is shown in Table 44. The carbon which is oxidised at temperatures less than 200°C is likely due to organic molecules from the reaction which are trapped in the pores of the catalyst. The boiling points of the relevant molecules are between 125°C and 185°C, meaning these molecules are likely boiling, diffusing out of the pores and then being oxidised in the first observed peak. The other

two peaks show amorphous hydrocarbonaceous deposits of two varieties have been laid down on the catalyst surface during the reaction. There are, however, no graphitic species observed, which would be shown by peaks at higher temperatures.

**Table 44 – A comparison of the relative ion current peaks, normalised relative to the smallest peak in the spectrum, caused by carbon dioxide release from post-reaction catalysts.**

<b>Molecule</b>	<b>Temperature / °C</b>	<b>Hydrogen Isotope</b>	<b>Peak 1</b>	<b>Peak 2</b>	<b>Peak 3</b>
PA	50	<sup>1</sup> H	1.0	2.2	1.4
PA	70	<sup>1</sup> H	1.2	1.0	1.8
PA	50	<sup>2</sup> H	1.0	3.7	1.3
PA	70	<sup>2</sup> H	1.0	1.5	1.8
STY	50	<sup>1</sup> H	10.5	1.0	
STY	70	<sup>1</sup> H	1.3	1.0	1.5
STY	50	<sup>2</sup> H	1.2	1.4	1.0
STY	70	<sup>2</sup> H	1.0	1.2	1.9
PP	50	<sup>1</sup> H	1.0	1.9	1.9
PP	70	<sup>1</sup> H	1.5	1.0	1.2
PP	50	<sup>2</sup> H	1.1	2.1	1.0
PP	70	<sup>2</sup> H	1.0	1.6	1.8

## 6 Conclusions

The activation energies of the studied molecules inversely correlated the size of the substituent with the activation energy of hydrogenation, although the rate of hydrogenation was faster for molecules with smaller substituents. These are both likely to be linked to the greater strength of adsorption associated with larger substituents<sup>50</sup>.

Aromatic molecules with larger substituents are capable of completely inhibiting the chemical adsorption of aromatic molecules with smaller substituents onto the rhodium/silica catalyst under the conditions used. Competitive conditions can utilise this to improve selectivity, for example the presence of propylbenzene appeared to have the effect of inhibiting the hydrogenation of ethylbenzene once it had been produced from the phenylacetylene hydrogenation cascade.

Competition can also be used to improve the styrene yield. The initial rate of phenylacetylene hydrogenation did not change significantly under competitive conditions, however the rate of styrene hydrogenation was slowed by direct competition for active sites, meaning that a build-up of styrene was observed which was greater than the yield achieved when hydrogenating phenylacetylene alone.

The terminal alkyne group of phenylacetylene appeared to react at a different site to the other unsaturated groups, as its reactivity was largely unaffected by the presence of other molecules. Its hydrogenation affected the reaction of other molecules, suggesting that it was removing hydrogen from the system which would otherwise have diffused into the subsurface region. The combination of these findings leads to the conclusions that the terminal alkyne group was hydrogenating at edge and corner sites, aligning the results with those from other studies<sup>39, 56</sup>, and that rhodium's catalytic behaviour is similar to that of palladium in the sense that its capacity for hydrogen absorption into the subsurface region, as was discovered by Gorodetskii *et al.*<sup>30</sup>, allows for enhanced alkyne and alkene hydrogenation on the terraced faces.

## 7 Further Work

Whilst the results of the experiments presented in this thesis have generally fit a palladium-like model, there are some questions which remain unanswered. In order to fully understand the reactions of molecules with multiple unsaturated functionality over rhodium/silica, further research is required.

The *cis/trans* ratio profiles of  $\beta$ -methylstyrene around 60°C cannot be completely explained by the results of this study. The reaction pathway at different temperatures could be examined to assess whether a change in pathway causes the change in the trend of *cis/trans* ratio profiles. The effect of competition with phenylacetylene on the *cis/trans* ratio profiles could also be further examined, as the shape of these profiles differs from those under the other conditions employed during this study.

More research into the changes which the catalyst undergoes during the reaction could be carried out. The analysis of carbon laydown is an area which required particular attention and could reveal more about the effects of molecules on the cascades in which they are involved. Further to this point, catalyst deactivation could be measured by adding a fresh solution of substrate after 180 minutes. These experiments could also be used to further probe which active sites are deactivated by hydrogenating a different molecule to the one initially used over a post-reaction catalyst.

The interaction of aromatic systems could be further investigated spectroscopically to assess the effects, or lack thereof, of ‘ $\pi$ -stacking’ or other similar processes.

## 8 References

1. M. Bowker, *The Basis and Applications of Heterogeneous Catalysis*, Oxford University Press, 1998.
2. J. J. Berzelius, *Årsberättelse om framstegen i fysik och kemi*, Norstedt, 1835.
3. J. J. Bravo-Suárez, R. V. Chaudhari and B. Subramaniam, *Novel Materials for Catalysis and Fuels Processing*, American Chemical Society, Washington DC, 2013.
4. N. Cherkasov, A. J. Expósito and T. B. E. V. Rebrov, *React. Chem. Eng.*, 2019, **4**, 112-121.
5. P. Sabatier and J. B. Senderens, *Compt. Rend. Chimie*, 1901, **132**, 210.
6. S. D. Jackson and L. A. Shaw, *Appl. Catal., A*, 1996, **134**, 91-99.
7. K. Timmer, D. H. M. W. Thewissen, H. A. Meinema and E. J. Bulten, *Recl. Trav. Chim. Pays-Bas*, 1990, **109**, 87-92.
8. V. Mévellec, A. Nowicki, A. Roucoux, C. Dujardin, P. Granger, E. Payen and K. Philippot, *New. J. Chem.*, 2006, **30**.
9. S. A. Nikolaev, N. A. Permyakov, V. V. Smirnov, A. Y. Vasil'kov and S. N. Lanin, *Kinet. Catal.*, 2010, **51**, 305-309.
10. J. E. Lennard-Jones, *Trans. Faraday Soc.*, 1932, **28**, 333-359.
11. G. A. C. Diaz, PhD, Bay Area Environmental Research Institute, 2015.
12. G. C. Bond, *Metal-Catalysed Reactions of Hydrocarbons*, Springer, Boston, MA, 2005.
13. I. Horiuti and M. Polanyi, *Trans. Faraday Soc.*, 1934, **30**, 1164-1172.
14. G. H. Twigg, *Discuss. Faraday Soc.*, 1950, **8**, 152-159.
15. S. B. Mohsin, M. Trenary and H. J. Robota, *J. Phys. Chem.*, 1988, **92**, 5229-5233.
16. S. M. Davis, F. Zaera, B. E. Gordon and G. A. Somorjai, *J. Catal.*, 1985, **92**, 240-246.
17. P. S. Cremer, X. Su, Y. R. Shen and G. A. Somorjai, *J. Am. Chem. Soc.*, 1996, **118**.
18. H. Nakatsuji, M. Hada and T. Yonezawa, *Surf. Sci.*, 1987, **185**, 319-342.
19. W. T. McGown, C. Kemball and D. A. Whan, *J. Catal.*, 1978, **51**, 173-184.
20. S. LeViness, V. Nair and A. H. Weiss, *J. Mol. Catal.*, 1984, **25**, 131-140.
21. T. P. Beebe and J. T. Yates, *J. Phys. Chem.*, 1987, **91**, 254-257.

22. G. C. Bond, D. A. Dowden and N. Mackenzie, *Trans. Faraday Soc.*, 1958, **54**, 1537-1546.
23. J. Margitfalvi, L. Gucci and A. H. Weiss, *React. Kinet. Catal. Lett.*, 1980, **15**, 475-479.
24. A. S. Al-Ammar and G. Webb, *J. Chem. Soc., Faraday Trans. 1*, 1978, **74**.
25. A. S. Al-Ammar and G. Webb, *J. Chem. Soc., Faraday Trans. 1*, 1979, **75**, 1900-1911.
26. A. Borodziński and A. Gołębiowski, *Langmuir*, 1997, **13**, 883-887.
27. W. Ludwig, A. Savara, K.-H. Dostert and S. Schauer mann, *J. Catal.*, 2011, **284**, 148-156.
28. J. M. Nicol, J. J. Rush and R. D. Kelley, *Phys. Rev. B*, 1987, **36**, 9315(R).
29. M. G. Cattania, V. Penka, R. J. Behm, K. Christmann and G. Ertl, *Surf. Sci.*, 1983, **126**, 382-391.
30. V. V. Gorodetskii, B. E. Nieuwenhuys, W. M. H. Sachtler and G. K. Boreskov, *Surf. Sci.*, 1981, **108**, 225-234.
31. D. Teschner, J. Borsodi, A. Wootsch, Z. Révay, M. Hävecker, A. Knop-Gericke, S. D. Jackson and R. Schlögl, *Science*, 2008, **320**, 86-89.
32. S. D. Jackson and G. J. Kelly, *Current Topics in Catalysis*, 1997, **1**, 47-59.
33. F. Zaera and D. Chrysostomou, *Surf. Sci.*, 2000, **457**.
34. F. Zaera, *Acc. Chem. Res.*, 2009, **42**, 1152-1160.
35. F. Zaera and I. Lee, *Top. Catal.*, 2013, **56**, 1284-1298.
36. I. Lee, F. Delbecq, R. Morales, M. A. Albiter and F. Zaera, *Nat. Mater.*, 2009, **8**.
37. D. Teschner, E. Vass, M. Hävecker, S. Zafeiratos, P. Schnörch, H. Sauer, A. Knop-Gericke, R. Schlögl, M. Chamam, A. Wootsch, A. S. Canning, J. J. Gamman, S. D. Jackson, J. McGregor and L. F. Gladden, *J. Catal.*, 2006, **242**, 26-37.
38. J. McGregor and L. F. Gladden, *Appl. Catal., A*, 2008, **345**, 51-57.
39. J. A. Anderson, J. Mellor and R. P. K. Wells, *J. Catal.*, 2009, **261**, 208-216.
40. W. A. Sollich-Baumgartner and J. L. Garnett, *Adv. Catal.*, 1966, **16**, 95-121.
41. E. Crawford and C. Kemball, *Trans. Faraday Soc.*, 1962, **58**, 2452-2467.
42. J. J. Rooney, *J. Catal.*, 1963, **2**, 53-57.
43. M. C. Schönmaker-Stolk, J. W. Verwijs, J. A. Don and J. J. F. Scholten, *Appl. Catal.*, 1987, **29**, 73-90.

44. A. Stanislaus and B. H. Cooper, *Cat. Rev. - Sci. Eng.*, 1994, **36**, 75-123.
45. J. L. Garnett, *Cat. Rev. - Sci. Eng.*, 1972, **5**, 229-267.
46. X. Su, K. Y. Kung, J. Lahtinen, Y. R. Shen and G. A. Somorjai, *J. Mol. Catal. A: Chem.*, 1999, **141**, 9-19.
47. M. Viniegra, R. Gomez and R. D. Gonzalez, *J. Catal.*, 1988, **111**, 429-432.
48. C. R. Martinez and B. L. Iverson, *Chem. Sci.*, 2012, **3**, 2191-2201.
49. C. Minot and P. Gallezot, *J. Catal.*, 1990, **123**.
50. J. Völter, M. Hermann and K. Heise, *J. Catal.*, 1968, **12**, 307-313.
51. K. Heise and K. Wencke, *Z. Physik. Chem.*, 1968, **239**, 289-306.
52. G. Carturan, G. Facchin, G. Cocco, S. Enzo and G. Navazio, *J. Catal.*, 1982, **76**.
53. R. V. Chaudhari, R. Jaganathan and D. S. Kolhe, *Chem. Eng. Sci.*, 1986, **41**, 3073-3081.
54. J.-L. Pellegatta, C. Blandy, V. Collière, R. Choukroun, B. Chaudret, P. Cheng and K. Philippot, *J. Mol. Catal. Chem.*, 2002, **178**, 55-61.
55. C. A. Hamilton, S. D. Jackson, G. J. Kelly, R. Spence and D. d. Bruin, *Appl. Catal., A*, 2002, **237**, 201-209.
56. L. C. Begley, K. J. Kakanskas, A. Monaghan and S. D. Jackson, *Catal. Sci. Technol.*, 2012, **2**, 1287-1291.
57. A. J. Bennet, *Curr. Opin. Chem. Biol.*, 2012, **16**, 472-478.
58. K. J. Laidler, *Chemical Kinetics*, 3 edn., 1987.
59. R. Z. C. v. Meerten, A. Morales, J. Barbier and R. Maurel, *J. Catal.*, 1979, **58**, 43-51.
60. F. Alshehri, Ph.D Thesis, University of Glasgow, 2017.
61. G. Webb, in *Comprehensive Chemical Kinetics*, eds. C. H. Bamford and C. F. H. Tipper, Elsevier, Amsterdam, 1978, vol. 20, pp. 1-121.
62. J. A. Delgado, O. Benkirane, C. Claver, D. Curulla-Ferré and C. Godard, *Dalton Trans.*, 2017, **46**, 12381-12403.